Sheffield Hallam University

Design and Synthesis of Potential Novel Antibiotic Compounds Utilising Photoredox Catalysis

SLATER, Jack Eric

Available from the Sheffield Hallam University Research Archive (SHURA) at:

http://shura.shu.ac.uk/33228/

A Sheffield Hallam University thesis

Design and Synthesis of Potential Novel Antibiotic Compounds Utilising Photoredox Catalysis

Jack Eric Slater

A thesis submitted in partial fulfilment of the requirements of
Sheffield Hallam University
for the degree of Doctor of Philosophy

March 2023

Candidate Declaration

I hereby declare that:

1. I have not been enrolled for another award of the University, or other academic or professional organisation, whilst undertaking my research degree.

2. None of the material contained in the thesis has been used in any other submission for an academic award.

3. I am aware of and understand the University's policy on plagiarism and certify that this thesis is my own work. The use of all published or other sources of material consulted have been properly and fully acknowledged.

4. The work undertaken towards the thesis has been conducted in accordance with the SHU Principles of Integrity in Research and the SHU Research Ethics Policy.

5. The word count of the thesis is 37,000.

Name	*Jack Eric Slater*
Date	*March 2023*
Award	*PhD*
Faculty	*Health and Wellbeing*
Director(s) of Studies	*Dr. Daniel M. Allwood*

Abstract

The continued emergence of widespread antibiotic resistance over the prior several decades poses an increasingly severe worldwide challenge to public health. Several frontline antibiotic treatments are being rendered obsolete due to the advent of numerous bacterial resistance mechanisms, an issue further compounded by the lack of antibiotics currently residing within the antibacterial drug discovery pipeline that operate *via* previously unexploited mechanisms of action. There are numerous underlying issues that have propagated this unsavoury situation, some specific to antibiotic drug development and others that negatively impact the field of drug discovery as a whole. One of the latter issues centres around the implementation of high throughput target-based screening of suboptimal compound libraries for hit identification, and the narrow range of synthetic methodologies used to explore chemical space within such compound collections.

Dihydrodipicolinate synthase (DHDPS) constitutes a promising biomolecular target for novel antibiotic therapies due to its key role in the biosynthesis of essential amino acid L-lysine, a process widely specific to bacteria. Despite several prior campaigns and the development of micromolar potency inhibitors of DHDPS through target–based screening approaches, so far no compounds have been developed that display *in vitro* antibacterial activity in the subsequent phenotypic screens.

In silico screening constitutes an invaluable range of techniques used in the identification of potential hit compounds that has been implemented to great effect in numerous drug discovery campaigns, including the discovery of novel antibacterial compounds, often aiding in the design of more focused compound libraries for assessment *in vitro*.

Photoredox catalysis has emerged as a powerful synthetic tool for enabling access to previously unexplored regions of chemical space especially within medicinal chemistry contexts, facilitating highly chemoselective activation of reagents under benign reaction conditions. Sulfonylhydrazones are well established reagents within the field of organic synthesis capable of undergoing a myriad of transformations. Recent reports concerning the photocatalytic activation of hydrazone substrates to enable radical cyclisations served as the basis for the initial interest in developing related methodologies to generate desired compounds in the search for novel antibacterial agents.

In this thesis is described the design and synthesis of potential novel antibacterial compounds, initially utilising pharmacophore searches and qualitative *in silico* docking investigations to identify molecular scaffolds of interest as synthetic targets. The development of a novel photoredox reaction for the generation of sulfone hit structures from sulfonyl hydrazone starting materials is described, including exploration of the substrate scope and reaction mechanism studies. The synthesis of additional *in silico* derived hit structures is also described, as well as attempts made to expand the synthetic utility of the developed photocatalytic methodology. Initial evaluation of antibacterial activity of the compound collection is described including preliminary discussion of structure activity relationships as a foundation for the derivation of future work. The final chapter contains technical experimental details and characterisation data pertaining to the previously discussed work.

Table of Contents

Abbreviations and Symbols

ΔG	Change in free energy
(R)-	Rectus
(S)-	Sinister
[M+H$^+$]	Protonated molecular ion peak
1,2–DCE	Dichloroethane
Å	Angstroms
Ac	Acetyl
Arg	Arginine
ASAP	Atmospheric solids analysis probe
ATP	Adenosine triphosphate
ATR	Attenuated total reflection
Boc	*tert*-butyloxycarbonyl
Bu	Butyl
C	Celsius
CCDC	Cambridge crystallographic data centre
ClpP	ATP-dependent Clp protease proteolytic subunit
COSY	Correlation spectroscopy
CPCM	Conductor-like polarizable continuum
CSD	Cambridge structural database
D-	Dexter
DABCO	1,4-Diazabicyclo[2.2.2]octane
DEPT	Distortionless enhancement by polarisation transfer
dF(CF$_3$)ppy	2-(2,4-Difluorophenyl)-5-(trifluoromethyl)pyridine
DFT	Density functional theory
DHDPR	Dihydrodipicolinate reductase
DHDPS	Dihydrodipicolinate synthase
DMDO	Dimethyldioxirane
DMF	Dimethylformamide
DmgH	Dimethylglyoxime
DMSO	Dimethylsulfoxide
DNA	Deoxyribonucleic acid
DNB	Dinitrobenzene

7

dtbpy	4,4'-Di-*tert*-butyl-2,2'-bipyridine
E. coli	Escherichia coli
ECP	Effective core potential
Et	Ethyl
FabB	β-ketoacyl-synthase I
FabF	β-ketoacyl-synthase II
FabH	β-ketoacyl-synthase III
fac	Facial
FTIR	Fourier transform infra-red
FtsZ	Filament temperature sensitive mutant z
GOLD	Genetic optimisation for ligand docking
GTP	Guanosine triphosphate
HAT	Hydrogen atom transfer
HMBC	Heteronuclear multiple bond correlation
HMQC	Heteronuclear multiple quantum correlation
HOGA1	4-hydroxy-2-oxoglutarate aldolase 1
HPLC	High performance liquid chromatography
HRMS	High resolution mass spectrometry
HTS	High throughput screening
i–Pr	Isopropyl
IC_{50}	Half maximal inhibitory concentration
Ile	Isoleucine
J	Coupling constant(s)
K_i	Reversible inhibitor constant
$K_i{'}$	Inhibitory dissociation constant
K_i^{app}	Apparent dissociation constant
K_{ic}	Dissociation constant of enzyme inhibitor
K_{is}	Dissociation constant for competitive inhibition
L-	Laevus
LEDs	Light emitting diodes
Leu	Leucine
LigA	DNA ligase
LogP	Partition coefficient
LR	Linear response

8

Lys	Lysine
M	mol/L
m–	*meta*
m–CPBA	3-Chloroperoxybenzoic acid
M. tuberculosis	Mycobacterium tuberculosis
Me	Methyl
MeCN	Acetonitrile
MHz	Megahertz
MIC	Minimum inhibitory concentration
mL	Millilitre
mM	Millimolar
MMFF94s	Merck molecular force field 94 static
MP2	Moller-Plesset 2nd order perturbation theory
Ms	Mesyl
nm	Nanometre
nM	Nanomolar
NMR	Nuclear magnetic resonance
$^{\circ}$	Degrees
o–	*ortho*
OD_{600}	Optical density at 600 nm wavelength
ORCA	*ab initio* quantum chemistry program
p–	*para*
PDB	Protein data bank
pK_a	Acid dissociation constant
pK_{aH}	Conjugate acid dissociation constant
PMP	*para*–methoxyphenyl
PPh_3	Triphenylphosphine
ppm	Parts per million
ppy	2–phenylpyridine
psi	Pounds per square inch
Py	Pyridine
quant.	Quantitative
R_f	Retention factor
RI	Resolution of identity approximation

rpm	Revolutions per minute
rt	Room temperature
$Ru(bpy)_3^{2+}$	Tris(bipyridine)ruthenium
S. aureus	Staphylococcus aureus
SAR	Structure activity relationship
SET	Single electron transfer
S_N1	Substitution, nucleophilic, unimolecular
S_N2	Substituiton, nucleophilic, bimolecular
TEMPO	(2,2,6,6-Tetramethylpiperidin-1-yl)oxyl
Tf	Triflate
TFA	Trifluoroacetic acid
THF	Tetrahydrofuran
Thr	Threonine
TLC	Thin layer chromatography
TMK	Thymidylate kinase
Ts	Tosyl
TS	Transition state
Tyr	Tyrosine
TZVPP	Valence triple-zeta with two polarization function sets
UV	Ultraviolet
Val	Valine
ZINC	Zinc is not commercial
ZPE	Zero point energy
μL	Microlitre
μm	Micrometre
μM	Micromolar

Chapter 1

Introduction

1.1. Antibiotic Resistance: Challenges and Outlook

Antimicrobial resistance is an ongoing public health challenge estimated to be the underlying cause of between 700,000 and several million deaths per year worldwide, often at the hands of pathogenic infections once considered entirely treatable throughout the latter half of the 20th century, and the problem has been identified by both the World Economic Forum and the World Health Organisation as one of the gravest threats to human health in recent times.[1,2] The vast array of antimicrobial treatments uncovered in the 1950's-70's during the 'golden age' of antibiotic drug discovery have fallen prey to rapidly emerging resistance mechanisms, and subsequently no novel classes of antibiotics have been reported since 1987 (**Figure 1**). This prolonged lack of new anti-bacterial treatments within the drug discovery pipeline, alongside the diminishing efficacy of current frontline antibiotics and exacerbated further by the widespread clinical misuse and incorrect disposal of anti-bacterial drugs has led to serious concerns that the world may soon enter a post-antibiotic era.[3]
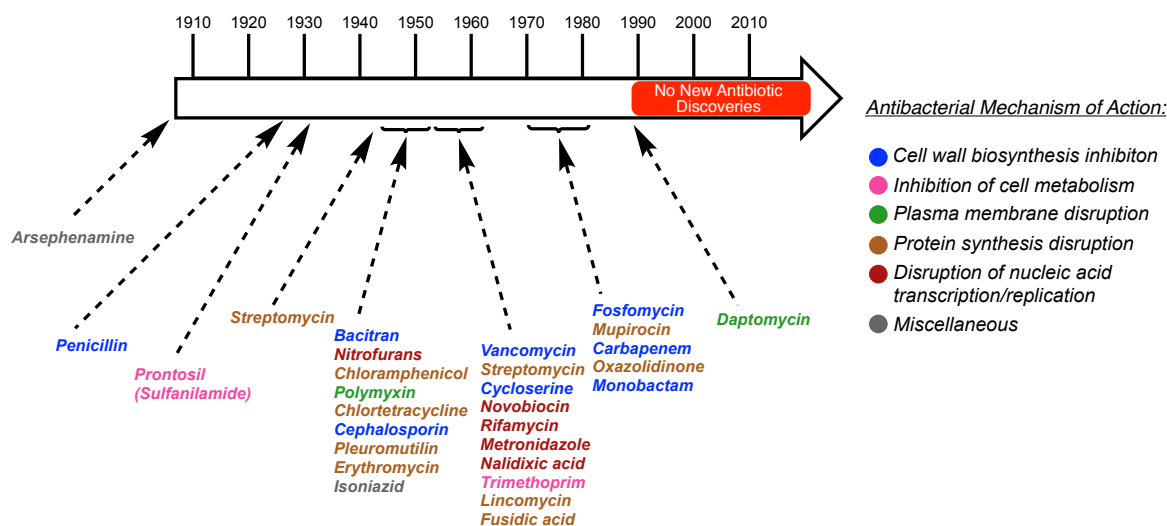
Figure 1. *Timeline showing the discovery of distinct classes of antibiotic treatments throughout the 20th century, colour-coded to indicate their general mechanism of action.*

Hence there is a significant need for antibiotics which operate *via* novel mechanisms of action in order to combat various multi-drug resistant strains while avoiding potential cross-resistance with older agents. The problems surrounding the issue of emerging antibiotic resistance are worsened by overarching concerns being faced within modern day drug discovery, as the rate at which novel drug candidates have been discovered has decreased significantly despite vast increases in research and development expenditure

within the pharmaceutical industry (**Figure 2**).[4–7] This decrease in efficiency can be attributed to various factors, one of notable concern is the approach adopted by pharmaceutical companies in the creation and employment of screening libraries.[8] The recognition of rising anti-bacterial resistance coincided with the advent of various technological and conceptual changes within the field of medicinal chemistry, which saw a general shift away from classical pharmacology towards more genomics-driven approaches involving target-based screening of vast compound libraries.[3]
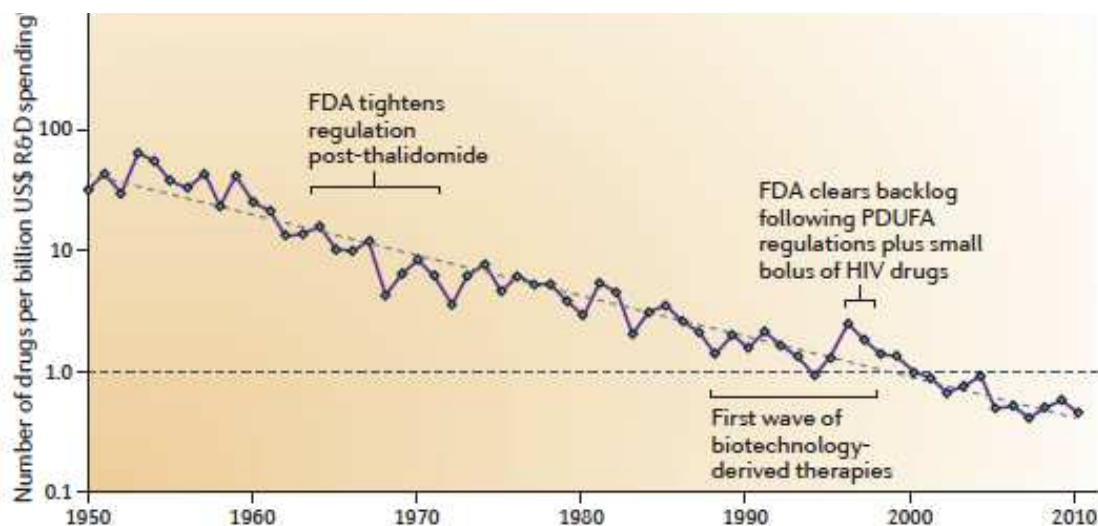
Figure 2. *Overall trend in drug research and development efficiency (inflation adjusted) showing the decline in the number of drugs approved by the US Food and Drug Administration (FDA) per billion US dollars spent on research and development. Reproduced from reference.[6]*

This resulted in the identification and validation of several promising novel antibiotic targets, subsequently followed by the discovery of numerous potent inhibitors courtesy of large scale high-throughput screening (HTS) campaigns, however most lead compounds ascertained in this manner proved unviable due to either a failure to show significant *in vitro* activity or were found to do so by engaging in non-specific modes of action.[9,10] The repeated failure of this drug discovery approach alongside financial and regulatory concerns led to the near abandonment of anti-bacterial research and development by large pharmaceutical companies in the mid 2000's. As concerns over rising antibiotic resistance intensified, several initiatives and agencies have been formed in order to incentivize a return to the field by the pharmaceutical sector in order to foster much needed progress.[11] Despite this renewed interest in the field successes remain scarce, to the authors knowledge within the last 20 years only 8 lead compounds that

operate *via* novel mechanisms of action have been developed which exhibit *in vivo* efficacy, and of these only two originated from hits obtained *via* target-based screening: the thymidylate kinase inhibitor TK-666, and adenosine-derived analogs targeting DNA ligase (**Table 1**, entry 1 & 2).[12,13] The remainder were predominantly derived through phenotypic screening of natural product mixtures produced by bacterial or fungal strains (**Table 1**, entry 4–8).[14–17]

Table 1. *Overview of novel antibiotic compounds possessing in vivo efficacy reported between 2000-2021.*

Entry	Name	Structure	Target	Source
1	TK666[12]	**1**	Thymidylate kinase (TMK)	Target-based drug discovery: Rationally designed small libraries of ligand-based thymine containing scaffolds
2	Adenosine analogue 4[13]	**2**	DNA ligase (LigA)	Target-based-drug discovery: HTS campaign and subsequent lead optimisation
3	PC190723[18]	**3**	Filamenting temperature sensitive mutant Z (FtsZ)	Fragment-based drug discovery: Phenotypic screen of 500 analogues derived from initial 3-methoxybenzamide fragment
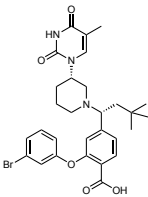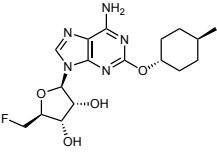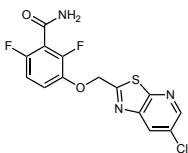
4	R207910[19]	 **4**	ATP synthase	Phenotypic drug discovery: Diarylquinoline lead compounds identified through whole-cell assays of a diverse chemical series.
5	Platensimycin[14]	 **5**	β-ketoacyl-synthase I/II (FabF/B)	Phenotypic drug discovery: Natural product extracted from *Streptomyces platensis* ferment
6	ADEP4[15]	 **6**	ATP-dependent Clp protease proteolytic subunit (ClpP)	Phenotypic drug discovery: Semi-synthetic derivative of natural product extracted from *Streptococcus hawaiiensis* ferment
7	Teixobactin[16]	 **7**	Lipid II/III (peptidoglycan biosynthesis)	Phenotypic drug discovery: Natural product extracted from uncultured *Eleftheria terrae* strains
8	Plectasin (1ZFU)[17,20]	 **8**	Lipid II (peptidoglycan biosynthesis)	Phenotypic drug discovery: Fungal defensin produced by *Pseudoplectania nigrella*
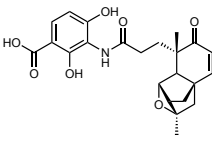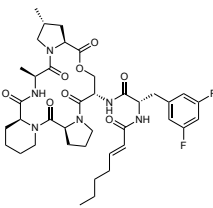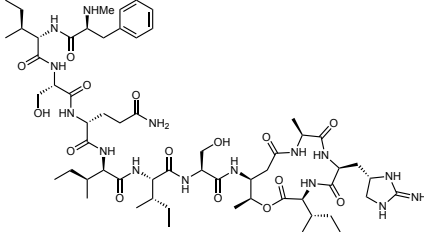
This highlights how ill-suited reverse pharmacology approaches are to antibacterial drug discovery, as inhibition of a particular target does not necessarily confer *in vitro* activity and furthermore such target-based assays are prone to false positives arising from non-specific interactions and promiscuous binding, leading to poor hit-to-lead conversion rates in the majority of HTS campaigns reported thus far.[10,21] Another major underlying concern pertains to the construction of compound libraries, as medicinal chemists continue to rely on a narrow selection of reactions for compound library synthesis leading to a lack of structural diversity.[22,23] This lack of chemical variety is aggravated by the fact that most commercial compound libraries are inherently biased towards mammalian targets which are more frequently the subject of prior investigations. Comparison of the physicochemical profiles of non-antibacterial drugs against antibiotics undergoing clinical trials revealed significant differences in both molecular weight and hydrophobicity, with broad-spectrum antibiotics being substantially more polar.[21,24] Furthermore compounds of the desired size, lipophilicity and possessing the polar surface area typical of antibacterial compounds were found to not be well-represented in most corporate screening collections. It is for these reasons that most of the more promising novel antimicrobial therapies continue to be derived from natural products, however this appears to be a dwindling resource in the search for new antibiotics as the majority of the compounds isolated from these sources are already known, and verification of duplicate structures is both time consuming and labour intensive.[3,25] Hence there is a considerable research-based drive towards the implementation of novel drug discovery and design approaches to attempt to improve the overall quality of hit and lead compounds obtained *via* initial screening processes, and further emphasis still on the development of practical synthetic methodologies for use in the creation of compounds of interest in order to facilitate access to unexplored regions of chemical space.

1.2. DHDPS: Structure, Function and Antibiotic Target

Dihydrodipicolinate synthase (DHDPS) is a lyase enzyme that is central to the biosynthesis pathway of L-lysine (**14**) in prokaryotes, a process crucial for bacterial survival due to the critical role of L-lysine as both a fundamental building block in bacterial protein synthesis and in the formation of crosslinks within the peptidoglycan cell wall.[26] DHDPS catalyses the reversible condensation reaction of L-aspartate-β-

semialdehyde (**10**) with pyruvate (**9**) to form 4-hydroxy-tetrahydrodipicolinic acid (**11**), the reaction mechanism commences with the condensation of pyruvate and a highly conserved lysine residue within the active site to form a Schiff base complex (**Scheme 1**).
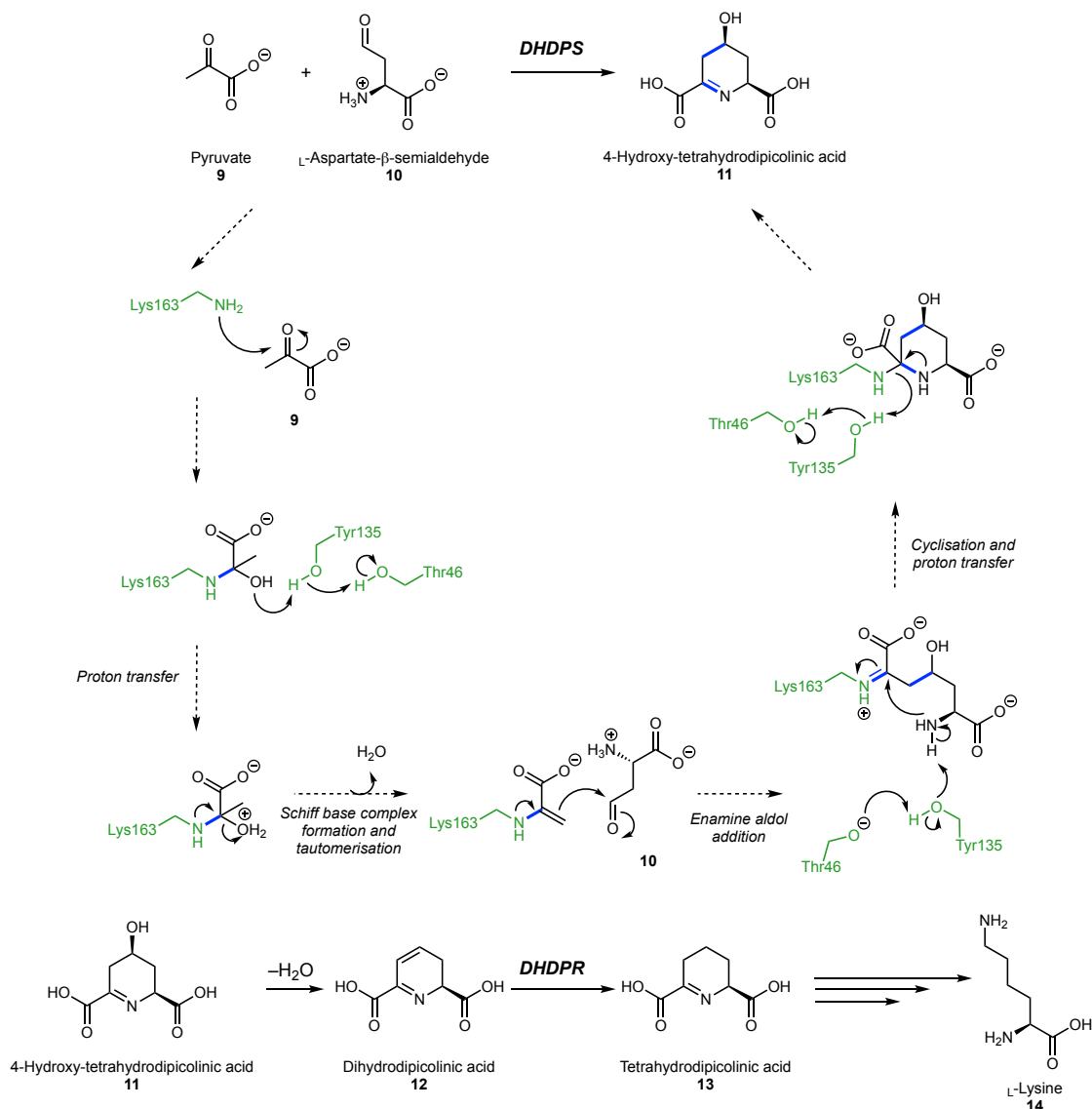
Scheme 1. *The biosynthetic pathway of L-lysine (**14**) in bacteria starting with the conversion of pyruvate (**9**) and L-aspartate-β-semialdehyde (**10**) into 4-hydroxytetrahydrodipicolinate (**11**) by dihydropicolinate synthase (DHDPS) showing the proposed catalytic mechanism for DHDPS. This is followed by dehydration to the dihydrodipicolinate (**12**) and reduction by dihydrodipicolinate reductase (DHDPR) to form tetrahydrodipicolinic acid (**13**). Some residues involved in the proton transfer chain omitted for clarity.*

This rate-limiting step is followed by tautomerisation to the enamine form and subsequent aldol-type addition to the substrate **10**. The final sequence involves nucleophilic attack at the lysine-bound pyruvate carbon by the aspartic amine accompanied by multiple proton

transfer steps to liberate the 4-hydroxy-tetrahydrodipicolinate product **11** alongside the unbound lysine residue.[26,27] This product is then believed to readily undergo dehydration before being reduced by dihydrodipicolinate reductase (DHDPR) to yield the corresponding dehydroxylated tetrahydrodipicolinate (**13**). At this point the fate of the substrate diverges to various species-dependent enzymatic pathways before reconverging at the final step whereby the biosynthesis of L-lysine is completed, hence the product of DHDPS- and subsequently that of DHDPR- is a key intermediate within this pathway as it serves as an exclusive substrate across several species for numerous enzymatic processes downfield of DHDPS and DHDPR.[28] Furthermore, gene knockout studies have shown that the DHDPS-encoding gene (*DapA*) is essential to survival for several gram-positive and gram-negative bacterial species including *S. aureus* and *E. coli*, therefore it is unsurprising that since its initial characterisation in 1965 DHDPS has invoked the interest of numerous efforts to establish its structure, mechanism and potential modes of inhibition.[26,29,30] DHDPS typically adopts a homotetrameric quaternary structure however recent studies suggest that a dimeric structure is the true active oligomer, with each subunit consisting of an α/β-barrel where the active site is located, and a C-terminus α-helix that contains several residues involved in tetramer binding and stabilization (**Figure 3**).[26,31–33] The allosteric site is located in the crevice formed between the two monomers that form the so-called 'tight' dimer interface, L-lysine can usually allosterically inhibit DHDPS at this site as part of a negative feedback loop in order to regulate the rate of L-lysine production.[34]
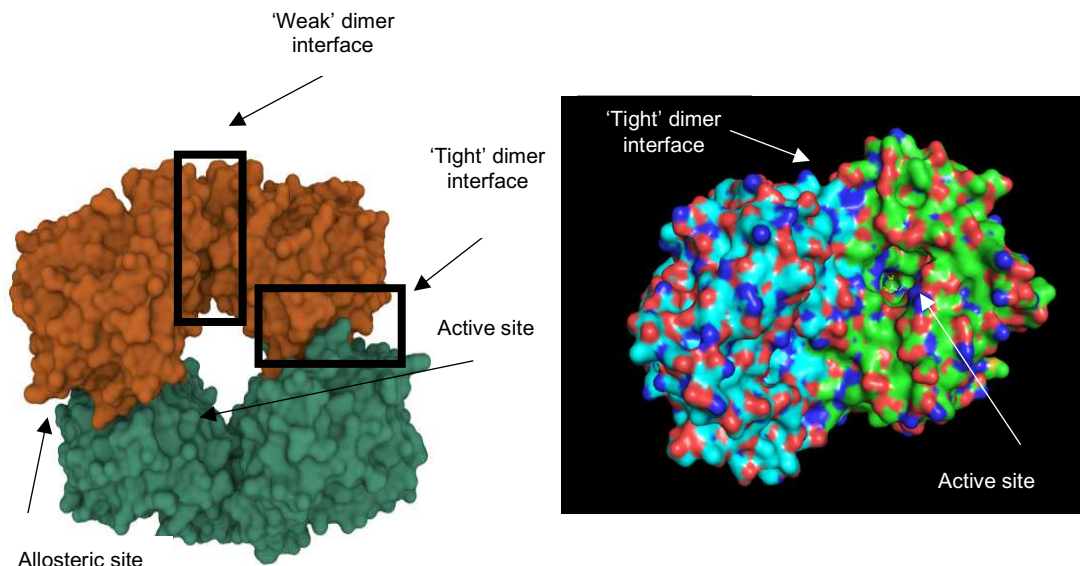
Figure 3. *(Left) Homotetrameric quaternary structure of E. coli DHDPS (PDB ID: 1YXC) with binding sites and oligomeric interactions labelled. (Right) S. aureus DHDPS dimer (PDB ID: 3DI1) showing exposed active site.*

The active site of DHDPS is highly conserved across bacterial species, centering around the key Lys163 residue (*S. aureus* numbering) which forms the Schiff base complex with pyruvate. This is accompanied by an Arg140 gatekeeping residue that facilitates entry of both pyruvate and L-aspartate-β-semialdehyde to the active site and a quintet of residues, namely Thr46, Thr47, Tyr108, Tyr109 and Tyr135 (*S. aureus* numbering) that encompass the active site and participate in shuttling protons to and from desired regions of the binding site for the multiple proton transfer steps (**Figure 4**).[30,33] This signature seven residue configuration is highly conserved and has been discerned in all wild type bacterial DHDPS sequences characterised to date, including more than 200 crystal structures from some 45 different bacterial species deposited to the Protein Data Bank (PDB).[26,30,35]
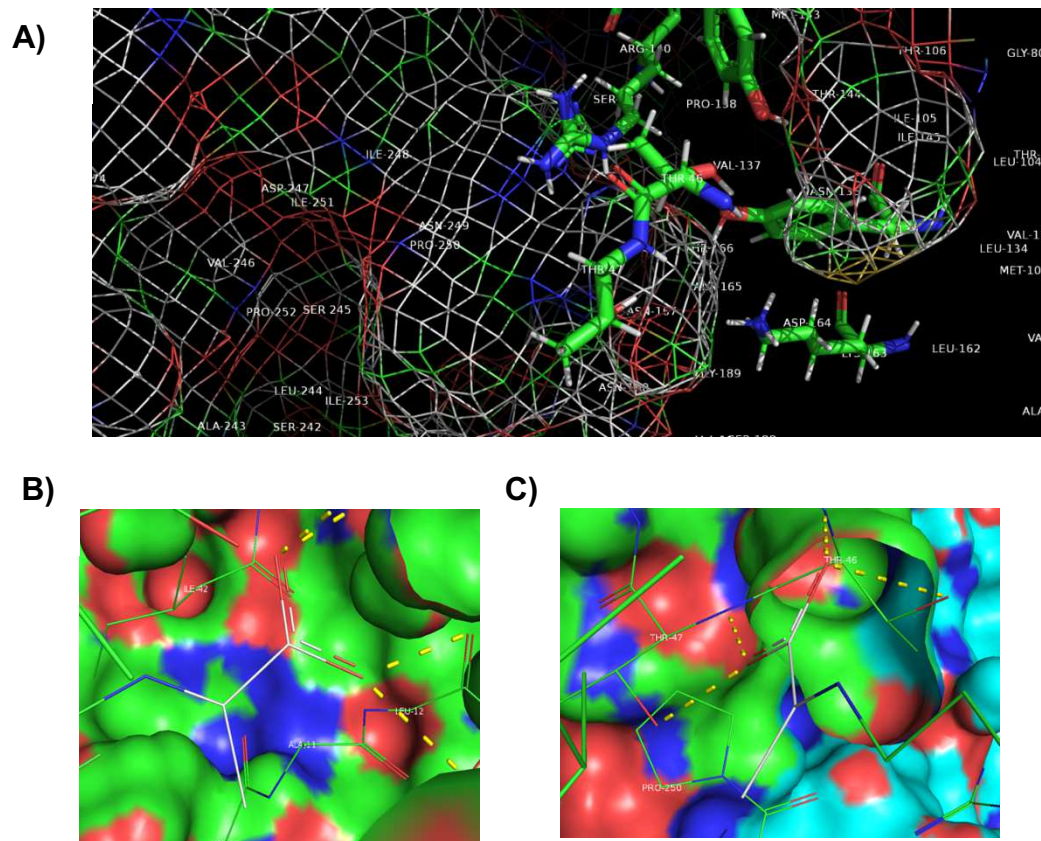
Figure 4. *Images of the active site of S. aureus DHDPS (PDB ID: 3DI1). A) Vacant active site with the conserved signature residues that encircle the binding site highlighted- (clockwise from centre) Arg140, Thr46, Tyr109, Tyr135, Lys163 and Thr47 (Tyr108 not shown). B) Image of pyruvate substrate bound to the DHDPS active site via condensation with the catalytically active Lys163 residue. C) Image of putative hydrogen-bonding interactions between bound pyruvate and Thr46/ Thr47 residues.*

Due to the absence of the L-lysine biosynthesis pathway in animals there are no known direct homologs of DHDPS present in humans, with the closest related enzyme being mitochondrial 4-hydroxy-2-oxoglutarate aldolase 1 (HOGA1) which despite being archaically described as a 'DHDPS-like' enzyme bears little resemblance in overall structure and function to DHDPS.[26,36,37] It is therefore likely that inhibitors of DHDPS would possess broad-spectrum antibacterial activity and display high levels of selectivity for the pathogen over the host. It has been postulated that antimicrobial treatments targeting DHDPS could be susceptible to resistance due to the target being the product of a single gene, implying that single mutations would result in structural variants of DHDPS impervious to inhibition with a minimal fitness cost being incurred by the mutant strains.[38] Despite these concerns the susceptibility of DHDPS inhibitors to resistance remains to be observed empirically and considering the essentiality of DHDPS' function alongside its highly conserved active site and the wealth of information available

concerning its structure, it remains a promising target for the development of novel broad spectrum antibiotic compounds.[26]

1.3. DHDPS Inhibitors

.

1.3.1. Substrate Inspired DHDPS Inhibitors

The earliest reports regarding DHDPS inhibitors largely focused on identifying pyruvate (**9**) analogues, with initial studies by Laber *et al.* identifying 3-bromopyruvate as a relatively ineffective reversible inhibitor of *E. coli* DHDPS (**Figure 5**).[39] Several other 3-substituted derivatives were screened including 3-fluoropyruvate (**15**), however it was not until the emergence of reports several years later by Karsten *et al.* that it was identified *via* more robust quantitative DHDPS-DHDPR coupled enzyme assays as a reasonable DHDPS inhibitor.[40] α-Ketopimelic acid (**16**) is another α–keto acid that has been investigated several times as a potential DHDPS inhibitor, however it was not until 2016 that its half maximal inhibitory concentration (IC$_{50}$) was elucidated alongside that of the derivate **17** as part of a focused library of α-ketopimelic acid structural analogues, with both compounds displaying micromolar potencies against *M. tuberculosis* DHDPS.

Pyruvate
9
K$_{ic}$: 54 μM *E. coli*

3-Fluoropyruvate
15
K$_{is}$ (**9**): 0.22 mM *E. coli*

α-Ketopimelic acid
16
IC$_{50}$: 21 μM *M. tuberculosis*

α-Hydroxypimelic acid
17
IC$_{50}$: 31 μM *M. tuberculosis*
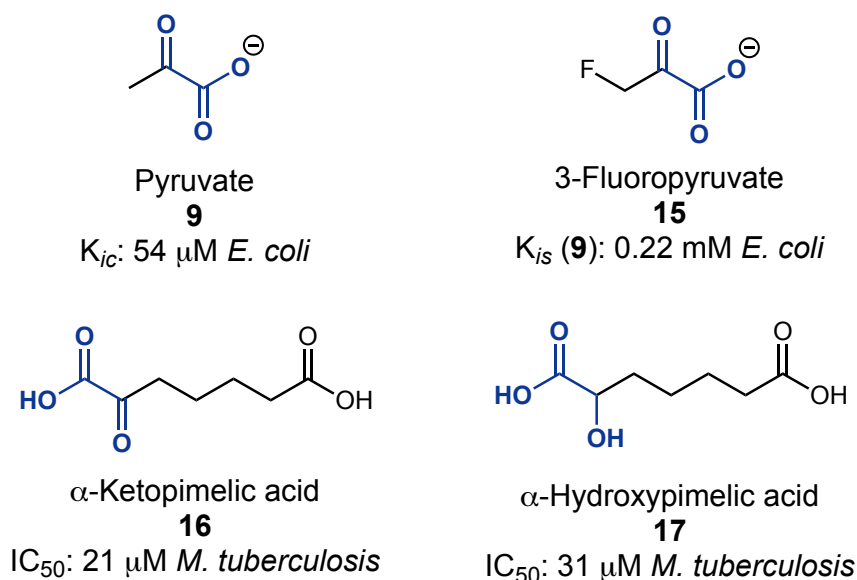
Figure 5. *Known inhibitors of DHDPS (**15-17**) structurally inspired by the substrate pyruvate (**9**) and their corresponding inhibitory concentrations and dissociation constants. Functional groups highlighted to indicate their importance in binding to the DHDPS active site and their structural analogy to substrate **9** (K$_{ic}$= defined as 'dissociation constant of enzyme inhibitor'. K$_{is}$= defined as 'dissociation constant for competitive inhibition').[26, 39-41]*

Further co-crystallisation studies confirmed that **16** binds to the same pocket within the active site as pyruvate (**Figure 6**).[41]
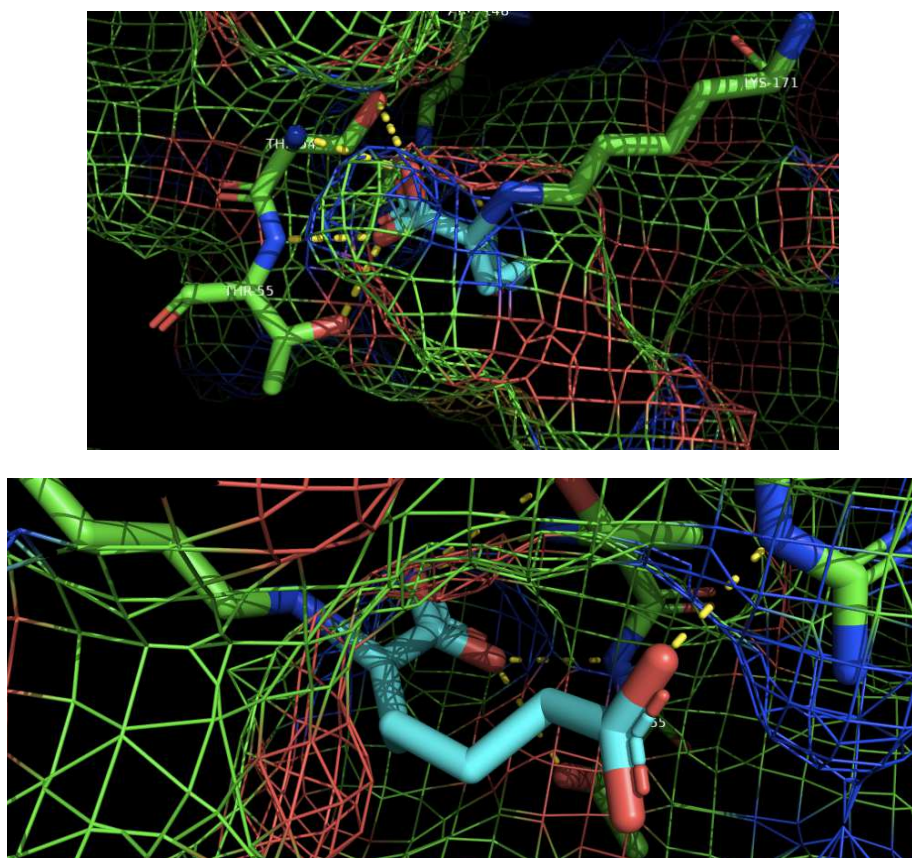
Figure 6. *Crystal structure of M. tuberculosis DHDPS (green) with established inhibitor α−ketopimelic acid **16** (blue) bound to the active site showing binding interactions to key residues Lys171, Thr54, Thr55 and Arg148 (M. tuberculosis numbering). Dashed yellow lines indicate intermolecular polar contacts (PDB ID: 5J5D.[41]*

Analysis of the crystallographic data for **16** indicates the presence of binding interactions similar to those exhibited by the native pyruvate substrate. The carboxylate group of the 1,2-dicarbonyl framework engages in hydrogen bonding interactions with the two threonine residues (Thr54 and Thr55, *M. tuberculosis* numbering) that form part of the highly conserved active site configuration, in a manner analogous to that observed for pyruvate. Furthermore the ketone group of **16** engages in Schiff base formation with the key Lys171 residue (*M. tuberculosis* numbering), and the presence of this binding motif likely underpins the increased potency of **16** in comparison to analogue **17**. The distinguishing binding feature of **16** as a DHDPS ligand is its engagement with the gatekeeper arginine residue (Arg148, *M. tuberculosis* numbering). The hydrogen bonding interaction between the terminal carboxylate of **16** and the protonated guanidinium

moiety of Arg148 likely confers additional stability upon occupation of the active site, and in conjunction with the other engagements of key active site residues there is clear evidence that **16** is capable of disrupting DHDPS function *via* competitive inhibition. However attempts to further develop derivatives of α-ketopimelic acids such as **16** and **17** that possess improved efficacy have so far been unsuccessful. This is due to a particularly narrow SAR observed when assessing the inhibitory activity of related keto acids. Even relatively minor structural changes such as single carbon increases or decreases in chain length, introduction of carboxylic acid bioisosteres or the introduction of additional hydrogen-bonding groups towards the centre of the carbon chain, all resulted in significant reductions of inhibitory activity.
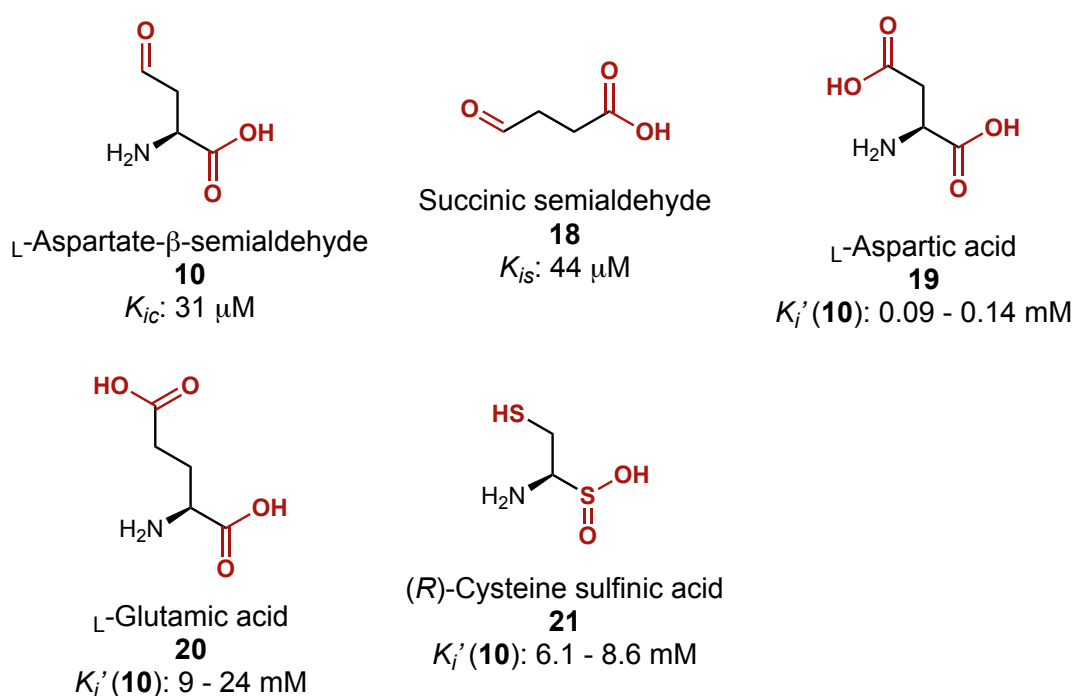
Figure 7. *Reported inhibitors of DHDPS (**18-21**) developed from ʟ-aspartate-β-semialdehyde **10** and their experimentally determined dissociation constants against E. coli DHDPS. Functional groups highlighted to indicate their role in binding to the active site and their structural analogy to substrate **10** (K_{ic}= defined as 'dissociation constant of enzyme inhibitor'. K_{is}= defined as 'dissociation constant for competitive inhibition'. K_i'= defined as 'the inhibitory dissociation constant').[26, 40, 42]*

The alternate aspartate semialdehyde substrate (**10**) has also proven to be a source of inspiration for the development of novel DHDPS inhibitors, with structurally related derivatives such as the succinic aldehyde **18** displaying dissociation constants comparative to those obtained for ʟ-aspartate-β-semialdehyde, suggesting that the amino

group plays only a minor role in binding to the DHDPS active site (**Figure 7**).[40] L-Aspartic acid (**19**) was interestingly found to be a mixed inhibitor of *E. coli* DHDPS with significantly reduced inhibitory activity relative to the aldehyde equivalent. Furthermore, within the same study multiple compounds with hydrogen-bonding bioisosteres mimicking the hydrate form of semialdehyde **10** were tested utilising the DHDPS-DHDPR coupled assay, whereby L-glutamic acid (**20**) and *R*-cysteine-sulfinic acid (**21**) were identified as uncompetitive DHDPS inhibitors possessing inhibitory dissociation constants within the millimolar range.[42] Despite this several other hydrate-based analogues such as L-asparagine and *S*-methylcysteine were found to lack inhibitory activity.

1.3.2. Lysine Derived Allosteric Inhibitors

Interest in allosteric inhibitors of DHDPS has increased substantially over time due to the lack of success of the initial substrate-mimetic approaches in divining efficacious inhibitors, as well as the potential to develop antibiotics possessing a narrower spectrum of activity. This is possible due to the greater amount of structural variation within the DHDPS allosteric site between different bacterial species compared to the active site, signified by the disparity in IC_{50} values obtained for L-lysine (**14**) against *E. coli* DHDPS and *M. tuberculosis* DHDPS respectively (**Figure 8**). Indeed, despite the supposed role of L-lysine in the feedback control of DHDPS activity surprisingly not all bacterial DHDPS enzymes are subject to allosteric inhibition, believed to arise from a lack of glutamic or histidine residues at position 56 (*E. coli* numbering) deemed crucial for the binding of L-lysine within the allosteric cleft. To the authors knowledge only two L-lysine analogues have been tested for inhibitory activity so far, the first being thialysine (**22**) reported by Karsten *et al*. which was found to display millimolar potency against *E. coli* DHDPS through co-operative inhibition of the allosteric site whereby two ligands simultaneously occupy the binding pocket, in a manner similar to L-lysine itself.[40] Based on this observed mode of inhibition, Skovpen *et al.* developed the ethylene bridged bis-lysine dimer **23** which exhibited sub-micromolar inhibitory concentrations and was found to bind across the 'tight' dimer interface according to crystallographic studies.[43] The development of further allosteric DHDPS inhibitors remains a promising approach towards the discovery of novel antibacterial compounds, however such agents are likely

to exhibit a restricted spectrum of activity considering the varying role of allosteric DHDPS inhibition across bacterial species.
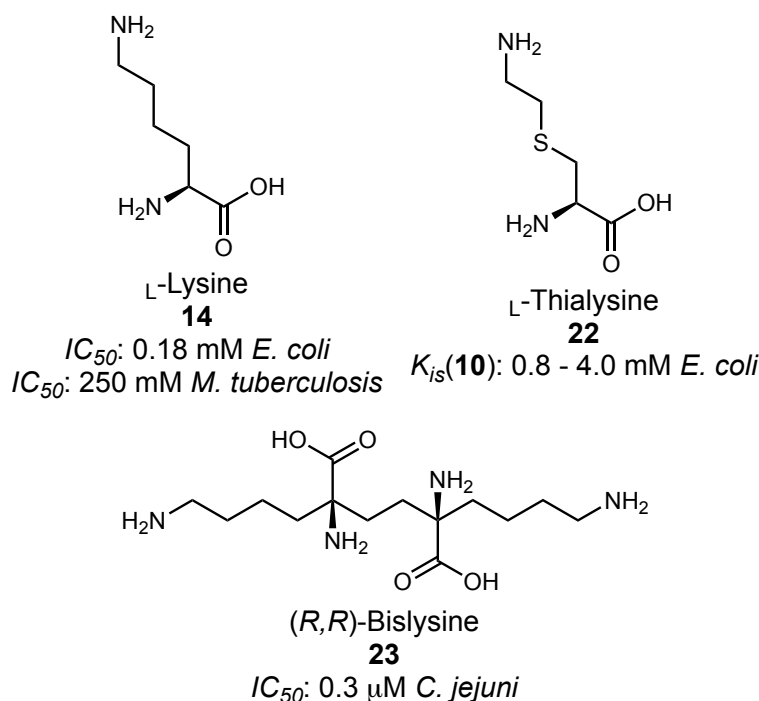
Figure 8. *Reported allosteric inhibitors of DHDPS L-lysine (14), L-thialysine (22) and (R,R)-bislysine (23) and their corresponding inhibitory concentrations and dissociation constants (K_{is}= defined as 'dissociation constant for competitive inhibition').*[26, 40, 43]

1.3.3. Dipicolinate Scaffolds as DHDPS Inhibitors

The majority of DHDPS inhibitors reported to date are biomimetic analogues of the dipicolinic acid products (**11**, **12** and **13**) of the DHDPS and DHDPR pathway, as these heterocyclic scaffolds inherently confer more 'drug-like' properties arising from the hydrogen-bonding capabilities of their functional groups embedded within a conformationally rigid structure, while further allowing for trivial exploration of structure-activity relationships around a central ring.[26,44] Initial attempts by Couper *et al.* to capitalise on this approach oversaw the construction of over thirty pyridine and piperidine analogues, such as dipicolinic acid (**24**) which was found to inhibit *E. coli* DHDPS at micromolar levels (**Figure 9**).[45] Oxidation of **24** to the corresponding N-oxide (**25**) resulted in a derivative exhibiting twice the potency and a similar improvement was

seen for the di-imidate **26**. The corresponding dipicolinate methyl ester (**27**) also demonstrated reasonable activity possessing an IC_{50} of 0.7 mM, and additional derivatives possessing carboxylic acid bioisosteres such as dicyanopyridine **28** and the ditetrazole **29** were also seen to attain micromolar potency. The series of piperidine analogues showed little to no inhibitory activity towards DHDPS and a proceeding report by the same author identified two isopthalate derivatives as potential inhibitors, tetrahydroisopthalic acid (**30**) which was identified as a comparatively weak inhibitor with an IC_{50} of 15 mM, and isopthalic acid (**31**) that interestingly demonstrated competitive inhibition of DHDPS with relatively high potency.[42] This observation highlights the importance of the degree of saturation in optimising ligand-protein intermolecular interactions within the DHDPS active site, highlighting an apparent preference for unsaturated ring scaffolds.
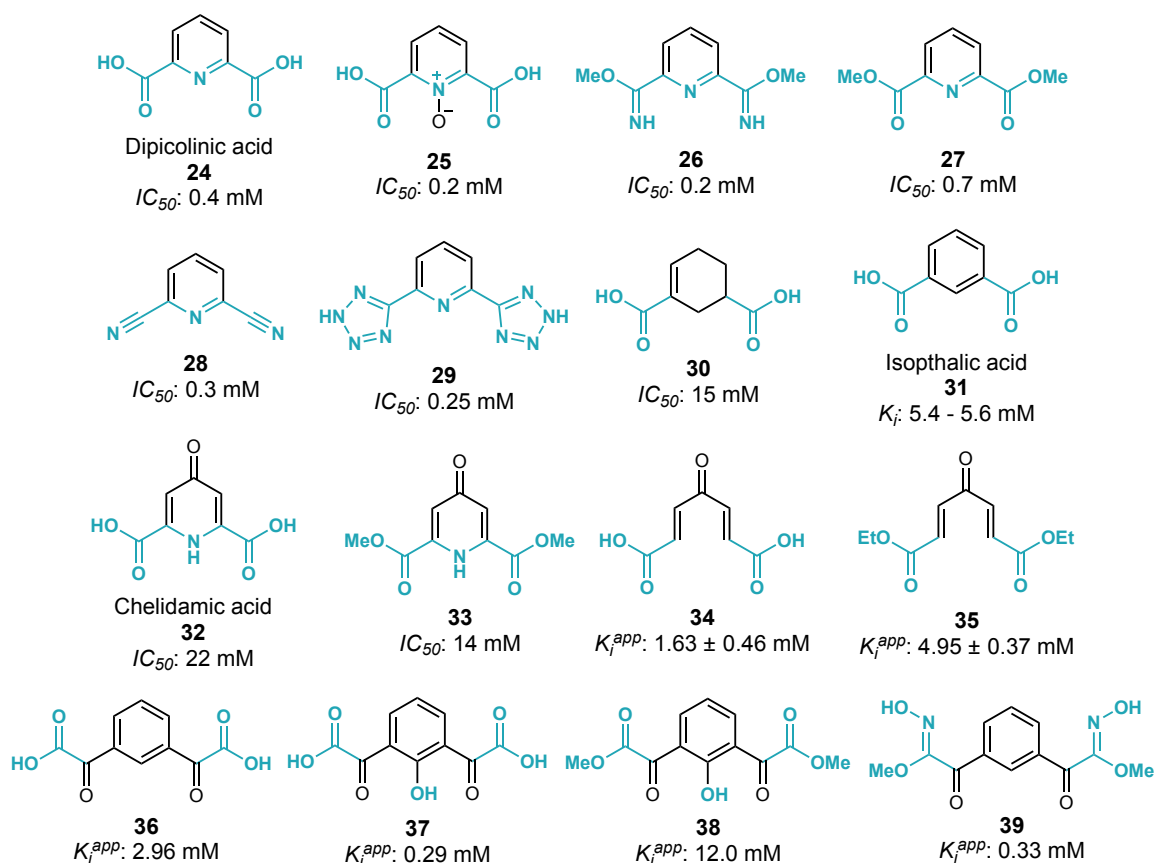
Figure 9. *Inhibitors of DHDPS based on the structure of the cyclic enzymatic product 4-hydroxytetrahydropicolinate (**14**) and their experimentally determined inhibitory concentrations and dissociation constants obtained against E. coli DHDPS. Includes analogues of dipicolinic acid (**24-29**), isopthalic acid (**30, 31**), chelidamic acid (**32, 33**), irreversible inhibitors (**34, 35**) and bis-keto acids (**36-39**). Functional groups highlighted to indicate their role in binding to the DHDPS active site and structural analogy to the parent compound dipicolinic acid. (K_i= defined as 'the reversible inhibitor constant'. K_i^{app}= defined as 'the apparent dissociation constant').[26, 42, 45-48]*

26

Structural variants of chelidamic acid (**32**) such as the methyl ester **33** were identified by Turner *et al.* as inhibitors of DHDPS after screening of a heterocyclic compound library.[46] Expanding on this work, further reports by the same author identified α/β–unsaturated diene **34** and its corresponding ethyl ester **35** as non-reversible DHDPS inhibitors, based on the enzyme-bound acyclic condensation intermediate formed between pyruvate and L-aspartate-β-semialdehyde.[47] These Michael acceptors undergo consecutive nucleophilic attacks from the key Lys163 residue (*S. aureus* numbering) resulting in occupation of the active site by a covalently bound piperidinone adduct. More recently a series of bisketo-acids based on the acyclic pyruvate-aspartate complex have been reported, starting from the diglyoxylate **36** which displayed moderate inhibitory activity.[48] The incorporation of a phenolic moiety (**37**) saw an almost ten-fold increase in potency, however the corresponding di-methyl ester **38** demonstrated considerably reduced activity against DHDPS compared to the starting compound. Interestingly however replacement of the phenol group with ketoxime functionalities led to a restoration of activity for the di-ester with derivative **39** obtaining an apparent dissociation constant (K_i^{app}) of 0.33 mM. Furthermore, kinetic and mass-spectrometry analysis of the inhibitors **36-39** ascertained the prevalence of a slow-tight binding mode of inhibition. This behaviour exemplifies the need for dual hydrogen-bonding arrays within the core ligand scaffold in order to facilitate high-affinity binding to the DHDPS active site.

Despite the considerable progress made so far in identifying effective DHDPS inhibitors possessing low millimolar to micromolar potency through the utilisation of robust enzymatic assays, none of the candidate structures uncovered through these biomimetic ligand-based drug design strategies discussed above have demonstrated *in vitro* antibiotic activity. This detail highlights both the need for different approaches to be employed towards the design of potential antibacterial compounds- in particular those targeting novel antibiotic targets such as DHDPS- as well as the disadvantages ubiquitous to target-based screening in identifying hits for lead development within antimicrobial drug discovery. Circumvention of these key issues is required in order to develop novel molecular scaffolds endowed with improved *in vitro* antibacterial activity, target selectivity and less constrained structure-activity relationships.

1.4. In Silico Screening for Drug Discovery

Since the advent of the new millennium several computational tools have been developed for the study of various aspects of pharmacology. Virtual ligand screening- the process of scoring/ranking molecules from large chemical libraries based on binding interactions with the biomolecular target observed _in silico_- has become an established methodology across various stages of drug discovery programs, as it enables rational drug design through virtual diagnosis of structure-activity relationships.[49,50] Numerous strategies based upon _in silico_ modelling of ligand-protein interactions have been employed, the vast majority of which can be accomplished utilising standard computers in combination with free to access software and virtual libraries, making such approaches relatively inexpensive compared to equivalent experimental high-throughput screening methods (HTS).[51] Nevertheless virtual ligand screening has made valuable contributions towards the development of several successful drugs, typically identifying novel pharmacophores through either ligand-based or target-based approaches, followed by organic synthesis efforts and _in vitro_ testing.[52]

In recent years the application of _in silico_ docking procedures towards antibacterial drug discovery has uncovered several promising lead compounds through screening against validated targets. A range of 2,4-dihydroxyphenylthiazoles (**40**) were identified as potent inhibitors of DNA gyrase B by Brvar _et al._ following ligand-based screening of a pharmacophore generated from previously established inhibitors, and more recently a series of virtual screening campaigns accompanied by molecular dynamic simulations identified a range of dicarboxylic acids (**41**) possessing inhibitory activity against various bacterial Mur ligase enzymes involved in peptidoglycan synthesis (**Figure 10**).[53,54] However, despite obtaining micro-molar levels of potency against the desired targets, in both cases the authors did not report any _in vitro_ anti-bacterial activity regarding the analogues tested. Thus the use of phenotypic screening in tandem with virtual screening procedures has become increasingly common in order to more efficiently ascertain potential antibacterial activity, for example the quinuclidine derivative **42** was uncovered through employment of iterative cycles of target-based _in silico_ screening of natural product libraries against the guanosine triphosphate (GTP) binding site of FtsZ, with both assay-based inhibitory activity and _in vitro_ antibacterial activity of derivatives evaluated and utilised throughout the several rounds of lead compound design.[55] Another example

of this approach was reported by Sun *et al.* whereby a series of piperazine derivatives were computationally assessed for their binding affinity to the active site of β-ketoacyl-synthase III (FabH), a key enzyme in the bacterial fatty acid biosynthesis pathway.[56] Once potentially effective FabH inhibitors had been identified through this molecular docking procedure, they were synthesised and tested for antibacterial activity *in vitro* which established compound **43** as the most potent derivative across several bacterial species. Ensuing experiments deduced the inhibitory activity of **43** against FabH alongside several structurally related analogues, however these lead compound derivatives were only subjected to such target-based assays after their *in vitro* antibiotic activity had been established through phenotypic screening.
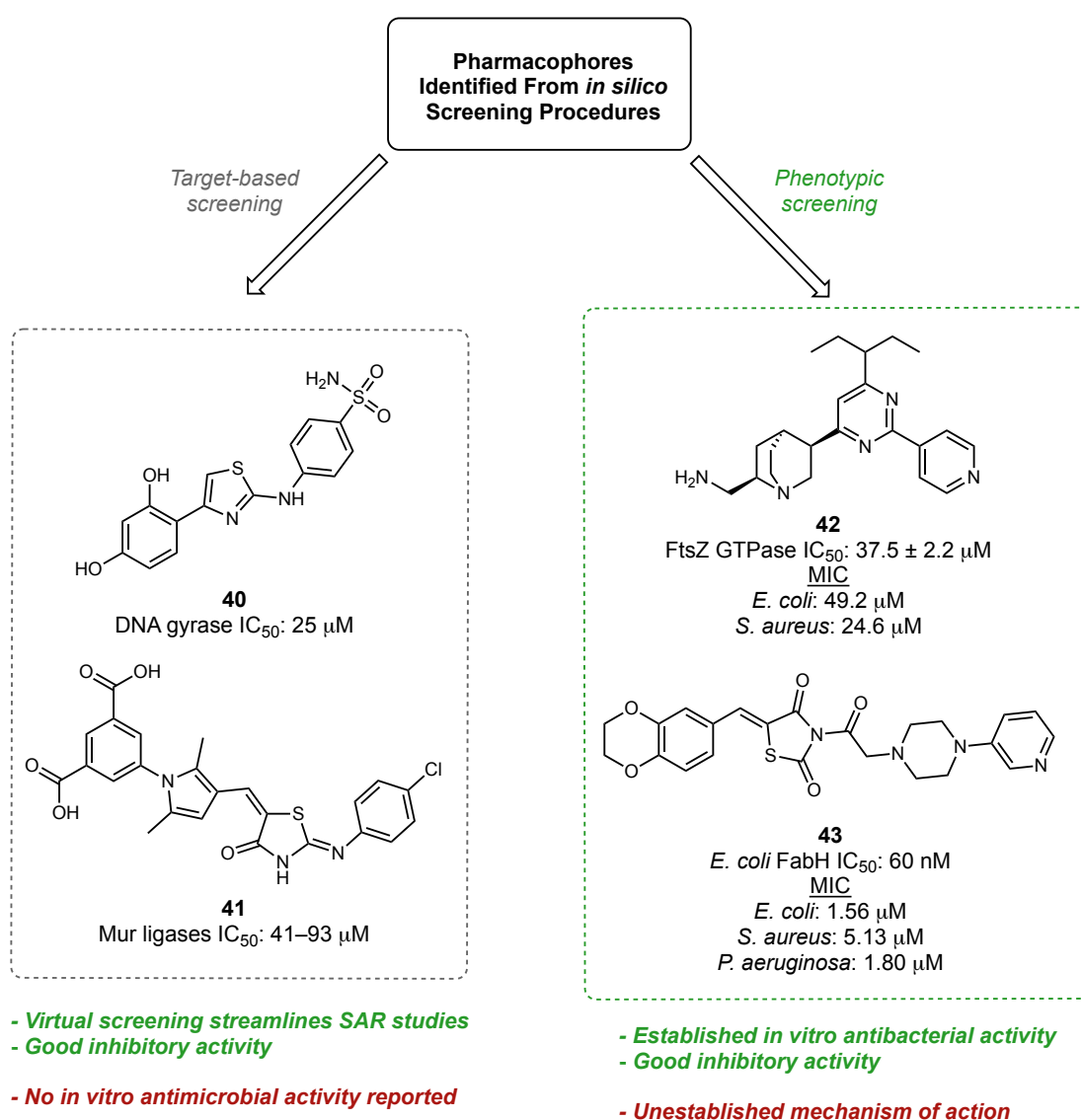
Figure 10. *Recent examples of novel anti-bacterial lead compounds identified via virtual ligand screening processes against validated targets, coupled with subsequent target-based screening (**40**, **41**) and phenotypic screening (**42**, **43**) methods to establish in vitro activity.*[52-56]

Due to the considerable amount of structural information available concerning the DHDPS enzyme supported by the availability of numerous high-resolution crystal structures, several virtual screening efforts have been undertaken to identify novel inhibitors. The earliest to the authors knowledge was performed by Garg *et al*. and identified several lead structures as potential inhibitors of the *M. tuberculosis* DHDPS (PDB ID: 1XXX) active site through *in silico* screening of over 8000 molecules derived from three sources- a combinatorial library of pyruvate analogues, compounds within the national cancer institute and PubChem libraries containing pyruvate substructures (**44**, **45**) and known anti-infective compounds (**46**)- all subsequently filtered according to Lipinski's rule of five (**Figure 11**).[57,58] Lead compounds **44** and **45** were predicted to engage in the anticipated polar interactions with the key Lys171 residue (*M. tuberculosis* numbering) in a fashion similar to the pyruvate substrate, while the anti-infective cefmetazole **46** formed comparable intermolecular interactions between its carboxylic acid moiety and Lys171 as well as additional polar contacts between the adjacent tetrazole group and an aspartic residue (Asp196). The authors also noted that the majority of the hits identified *via* the virtual screening process were characterised by high levels of aromaticity and multiple functional groups capable of engaging in dominant hydrogen-bonding interactions with the key Lys171 residue. A proceeding report by Rehman *et al.* also established several analogues of **46** as potential inhibitors of *M. tuberculosis* DHDPS through a similar pharmacophore driven virtual screening approach of both PubChem and natural product libraries against the DHDPS active site, with the carboxylic acid and tetrazole groups once again playing a key role in the supposed virtual ligand-protein binding.[59]

Molecular docking studies performed by Singh *et al.* also identified several isonicotinate esters (**47**) as potential inhibitors with promising binding affinities calculated for the *M. tuberculosis* DHDPS active site, and several of the top docking hits engaged in promising binding interactions with the gate-keeper Arg148 residue (*M. tuberculosis* numbering).[60] These derivatives were selected as structural analogues of 2-methylheptyl isonicotinate, a secondary metabolite isolated from *Streptomyces* strains displaying potent *in vitro* antimicrobial activity particularly against *M. tuberculosis*.[61] Although these *in silico* screening results imply that 2-methylheptyl isonicotinate functions as an inhibitor of

DHDPS its mechanism of action remains unknown, and furthermore none of the compounds identified as potential lead structures *via* virtual ligand screening against DHDPS as discussed above have yet been evaluated in reality for actual inhibitory activity or otherwise.
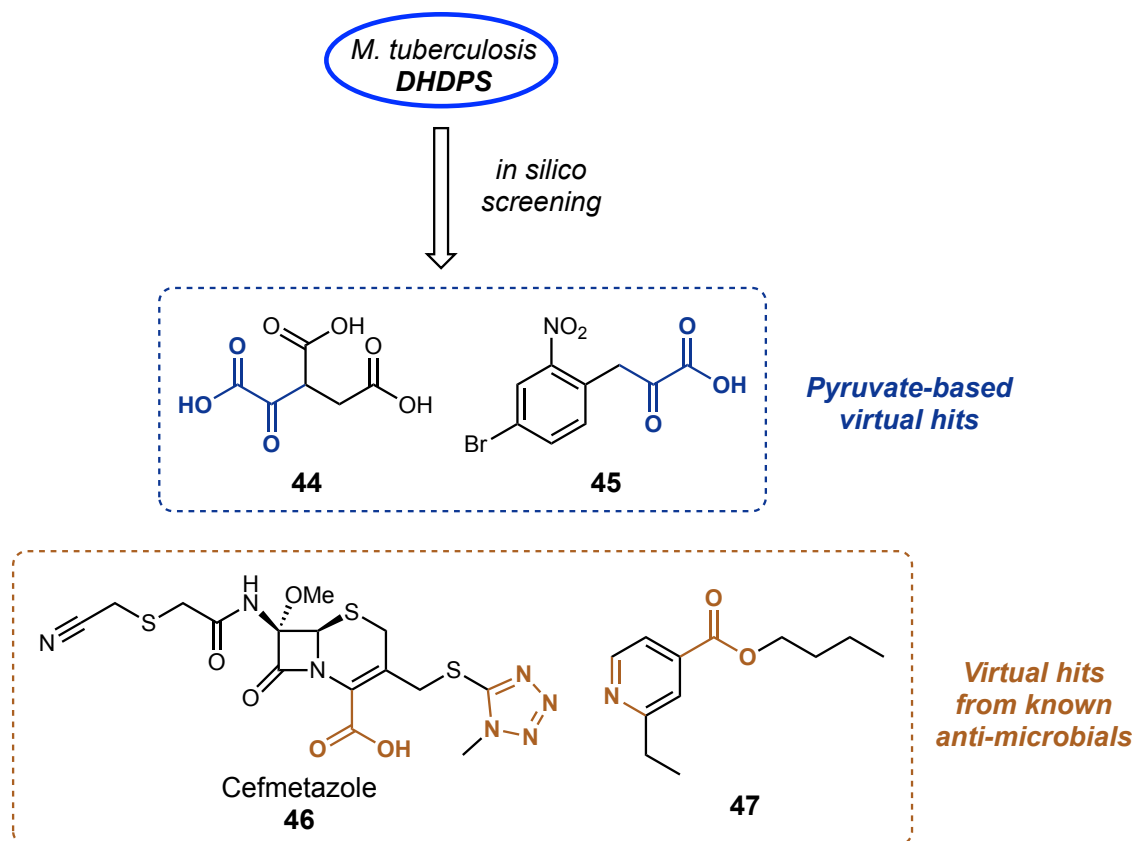
Figure 11. *Virtual 'hits' identified via in silico screening of various compound libraries against the active site of M. tuberculosis DHDPS (PDB ID: 1XXX). Compounds **44** and **45** were uncovered through pharmacophore searches based on the pyruvate substrate and subsequent docking to the DHDPS active site. Cefmetazole (**46**) was identified as the most promising candidate out of a screened library of known anti-infectives. Several derivatives of the known antimicrobial 2-methylheptyl isonicotinate such as **47** were also recognised as potential DHDPS inhibitors following in silico screening efforts (highlighted regions indicate key functional groups involved in DHDPS active site binding according to virtual docking calculations).* [56-59]

1.5. Photoredox Catalysis

1.5.1. Background and Development of Photoredox Catalysis

The development of new reactions that permit facile access to desirable regions of chemical space is one of the most considerable challenges within the field of drug design. Despite a seemingly endless influx of novel synthetic methodologies over the years, medicinal chemists continue to rely on a narrow selection of procedures with only ten modes of reactivity accounting for almost two-thirds of all reactions performed.[23,62] Although such a restricted approach is obviously detrimental to the structural diversity of chemical libraries and the overall drug discovery process, it is borne out of the necessity for robust synthetic methodologies that exhibit high levels of chemoselectivity and functional group tolerance in order to be applied effectively across a broad scope of substrates.[63,64] Over the course of the past decade photoredox catalysis has emerged as a powerful approach within the field of organic synthesis allowing for unconventional modes of chemical bond activation and construction through employing catalytic amounts of photosensitizers, usually as either organic dyes or transition-metal complexes such as the commonly used tris(bipyridine)ruthenium **48** ($Ru(bpy)_3^{2+}$), allowing photons of visible light to be efficiently harnessed as an energy source for chemical transformations (**Figure 12**).[65–67]
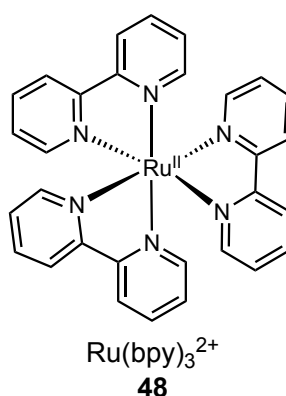
$Ru(bpy)_3^{2+}$
48

Figure 12. *Structure of tris(bipyridine)ruthenium(II) complex **48** ($Ru(bpy)_3^{2+}$) a commonly employed photocatalyst for visible light promoted photoredox transformations.*[65–67]

The initial reports by D.W.C MacMillan, Tehshik P. Yoon and Corey J. Stephenson exemplified the diverse range of transformations and high levels of reaction control that could be achieved using photocatalysts such as Ru(bpy)$_3^{2+}$ (**Scheme 2**).[68–70] Through synergy with previously established asymmetric organocatalytic methodologies, MacMillan's lab were able to couple the enamine formed from the condensation of enolisable aldehydes **49** and chiral imidazolidinone **51** with electron-deficient alkyl bromides (**50**) to afford the corresponding α-alkylated aldehydes **52** in fair to excellent yields and high enantioselectivity under exceedingly mild reaction conditions. The report by Yoon entailed the use of sunlight as a photon source as opposed to more conventional artificial light sources, in combination with lewis acids to activate enone starting materials **53** and generate ring-fused cyclobutanes **54** in fair to excellent yields and with high levels of diastereoselectivity, forming four stereocentres in one step. The following year Stephenson reported the photocatalytic reductive dehalogenation of pyrolloindoline **55** to derivative **56** alongside a diverse array of other brominated substrates, all proceeding in good to excellent yields with no observed racemisation.
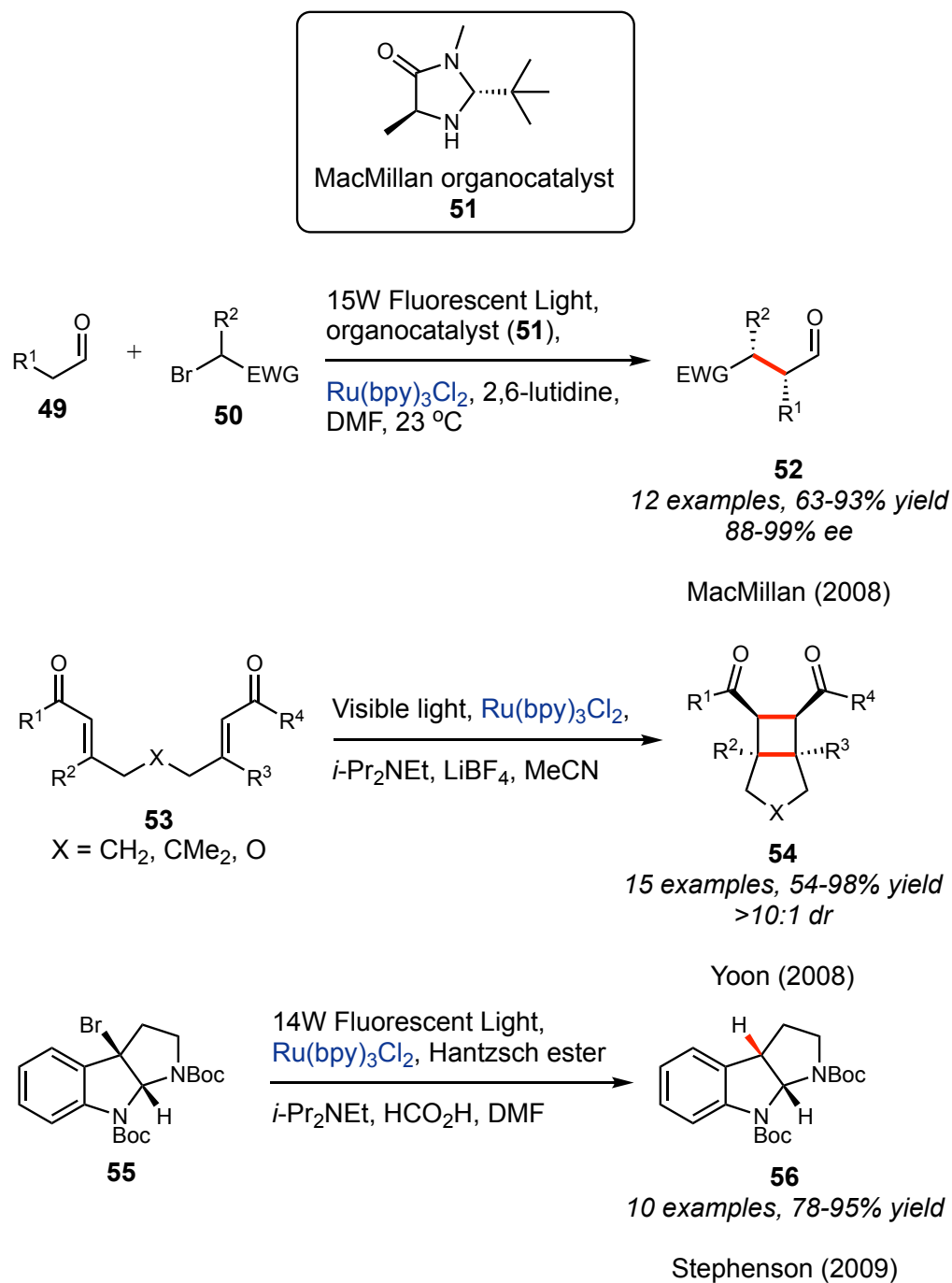
Scheme 2. *Seminal examples of organic synthesis procedures utilising photosensitizers reported by the groups of David W.C Macmillan, Tehshik P. Yoon and Corey J. Stephenson. Entailing novel visible light promoted transformations and giving birth to the field of photoredox catalysis.[68–70]*

Such photochemical processes commence with absorption of a suitable wavelength of light by the photocatalyst ($h\nu_A$) leading to the formation of an excited singlet state, in the case of **48** this involves excitation of a single electron to a higher-energy ligand anti-bonding (π^*) orbital forming **48a** (**Figure 13**).[71,72] This step is generally followed by

34

either relaxation to the ground state *via* fluorescence (hv_F) or intersystem-crossing (ISC) to an excited triplet state (**48b**). This triplet form constitutes a relatively long-lived excited state (~1100 ns) due to the spin-forbidden nature of the relaxation pathway which requires emission of a photon through phosphorecence (hv_P) and inversion of the excited electron's spin in order to return to the ground state. The triplet excited state of $Ru(bpy)_3^{2+}$ possesses more potent redox capabilities compared to the ground state due to its ability to engage in intermolecular quenching (**k_q**) *via* outer-sphere single-electron transfer (SET) processes, as metal-to-ligand charge transfer (MLCT) and consequent tunnelling of the excited electron facilitates the single-electron reduction of organic substrates. In turn the formation of a hole within the low energy *d*-orbital allows for single-electron oxidation to occur, concomitantly restoring the $Ru(bpy)_3^{2+}$ photocatalyst to its original ground state.
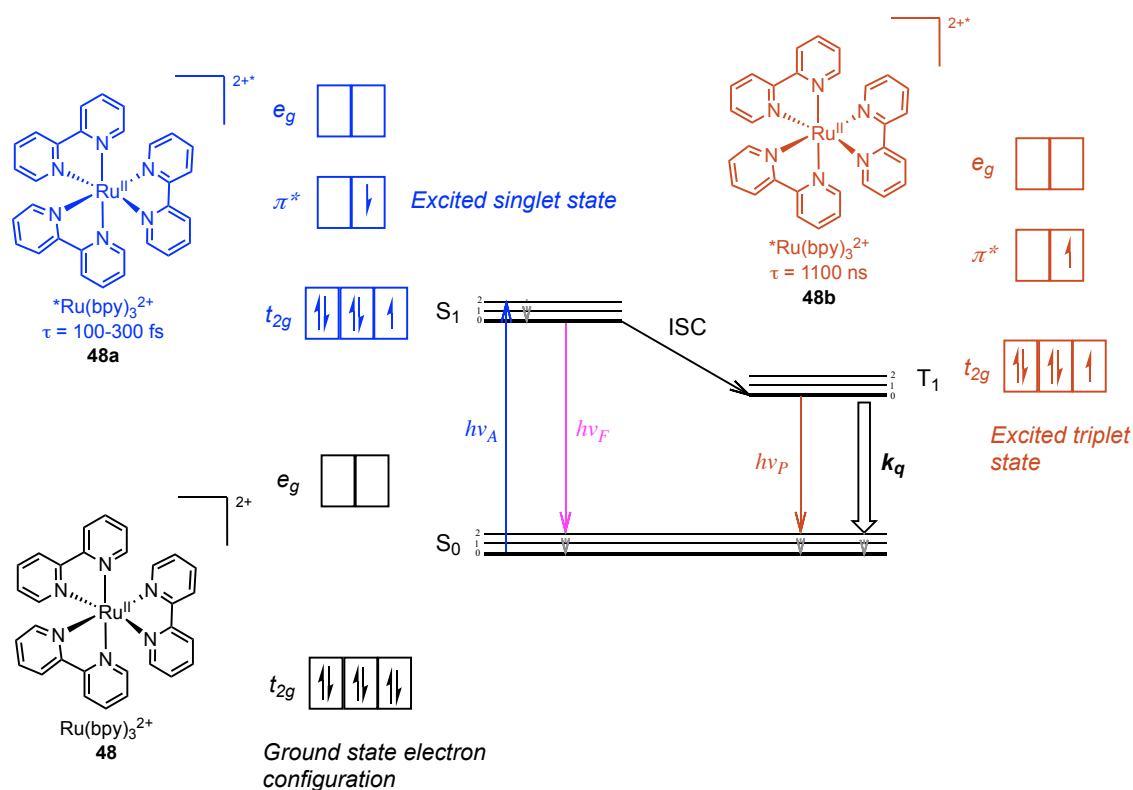
Figure 13. *Jablonski diagram showing the main photophysical outcomes of photocatalyst (**48**) excitation by visible light, starting with photon absorption (hv_A) generating the singlet excited state **48a**. Intersystem crossing (ISC) leads to formation of a long-lived triplet state (**48b**) capable of engaging in single-electron transfer (SET) processes with organic substrates (k_q) with reformation of the ground state photocatalyst. Other decay pathways include fluorescence (hv_F) from the S_1 state and phosphorescence (hv_P) from the T_1 state whereby a return to the ground state is accompanied by emission of an appropriate wavelength of light.*[71,72]

As the rate of SET to and from the photocatalyst depends largely on the relative difference in reduction or oxidation potentials between the photocatalyst and the functional groups present within the reactants, high levels of chemoselectivity can be achieved through judicious choice of photocatalyst and optimisation of reaction conditions, thus minimising potential side reactions. Furthermore, photoredox procedures are typically carried out efficiently under mild reaction conditions at room temperature and in the absence of high-energy ultra-violet (UV) light, enabling greater functional group tolerance in comparison to respectively less efficient thermal or UV promoted reactions.[67,73,74] Considering the inherent advantages of photoredox catalysis several visible-light promoted reaction manifolds have been developed and applied towards the synthesis of known pharmaceuticals and natural products, often facilitating unique synthetic disconnections and functionalisation of highly-decorated molecular scaffolds for the purposes of SAR exploration.[75–77] Indeed the popularity of photoredox catalysis as a field of study continues to grow, and the past thirteen years has seen a proliferation of reports concerning the development of photocatalytic reaction methodologies and their application to synthetic obstacles, highlighting the remaining potential for noteworthy synthetic discoveries (**Figure 14**).
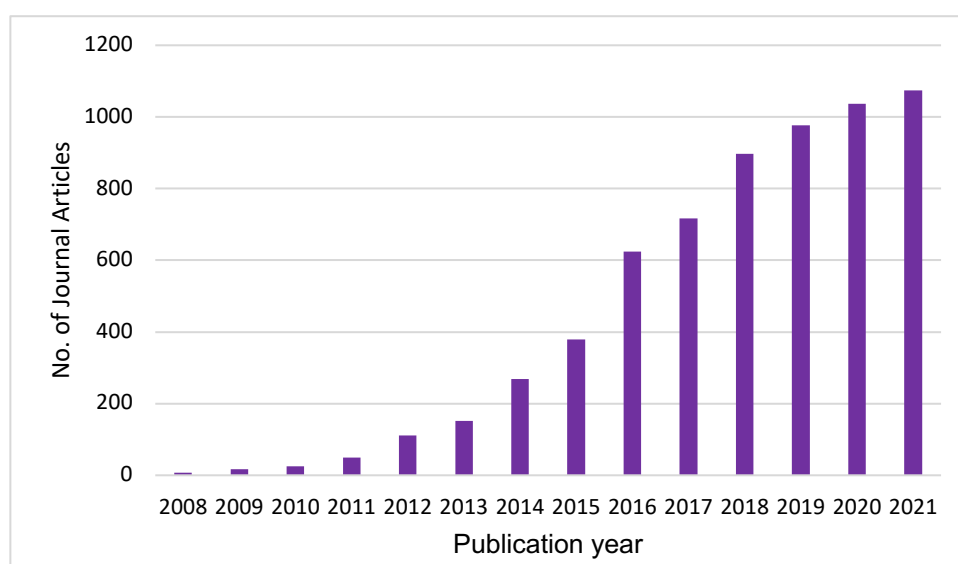
Figure 14. *Journal articles published from 2008-2021 found containing the concept 'photoredox catalysis' according to a CAS SciFinder literature search.*

1.5.2. Sulfonyl Hydrazones

Sulfonyl hydrazones are well established and versatile reagents within organic synthesis that have been utilised in a broad range of synthetic transformations, most notably as bench-stable carbenoid precursors (**61**) which can be easily obtained *via* condensation of sulfonyl-hydrazides (**58**) with the desired ketone or aldehyde starting material **57** (**Scheme 3**).[78] Typically under basic conditions sulfonyl-hydrazones enable umpolung modes of reactivity, acting as d^1 synthons capable of engaging in reactions with electrophilic coupling partners (**65**), and furthermore have also been shown to partake in various forms of cyclisation reactions to generate medicinally relevant pyrazole heterocycles (**67**).[79–83] Although they allow for straightforward approaches towards the formation of both carbon-carbon and carbon-heteroatom bonds, one of the main drawbacks to the usage of sulfonyl hydrazones is the need for elevated temperatures in the presence of strong bases in order to achieve sufficient activation and reaction progress.[84–87]
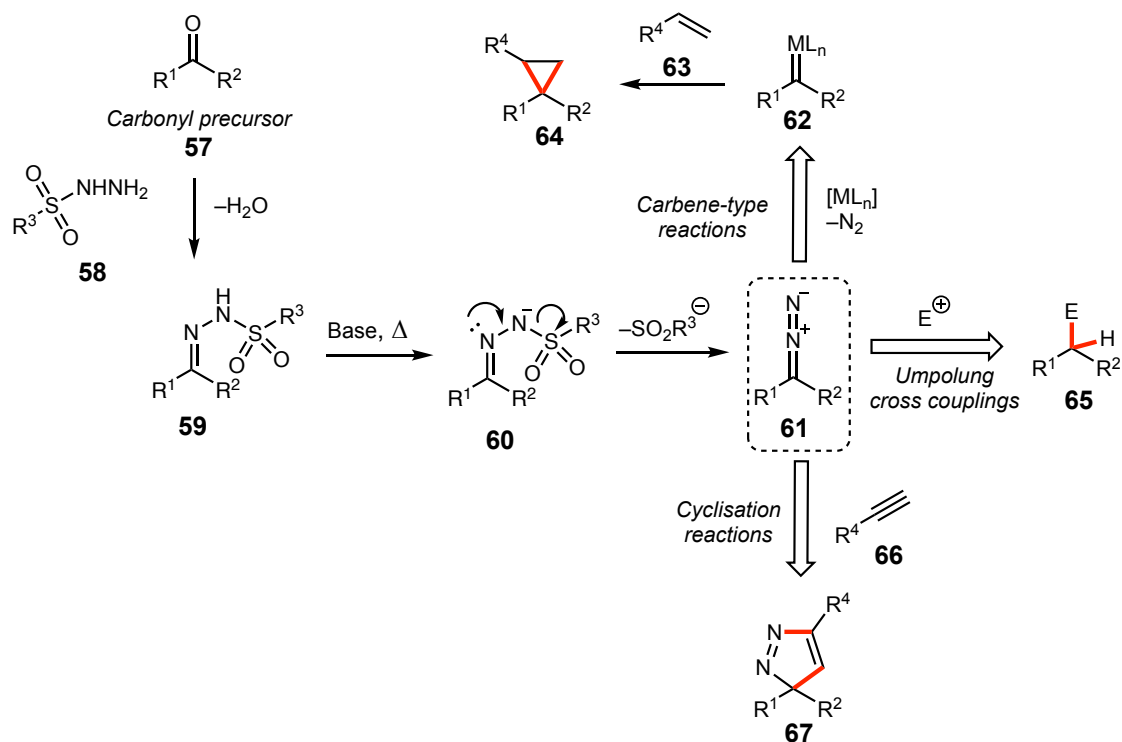
Scheme 3. *Overview of general modes of reactivity accessible utilising sulfonyl hydrazone reagents (**59**) derived from carbonyl precursors, predominantly occurring through diazo intermediate **61**. This includes transition metal carbene (**62**) mediated transformations such as alkene cyclopropanation, cross coupling reactions with electrophiles forming sp³-carbon centres (**65**), and cyclisation reactions to form nitrogen-containing rings such as spirocycle **67**.[78-87]*

1.5.3. Photocatalytic Transformations of Sulfonyl Hydrazones

In recent years several photocatalytic methods employing sulfonyl hydrazone substrates have been disclosed, utilizing $Ru(bpy)_3^{2+}$ as a single-electron oxidant of their deprotonated form in an attempt to facilitate the generation of hydrazonyl radical species under relatively mild reaction conditions. This also side-steps the constraints of established activation modes for sulfonyl hydrazones enabling access to previously unexploitable chemical transformations. In the initial reported cases the resulting nitrogen-centred radicals engage in intra-molecular cyclisations to form numerous atypical heterocyclic structures, and as opposed to earlier photoredox-based methods blue LEDs are employed as photon sources due to being relatively inexpensive as well as being able to generate a narrower spectrum of light in comparison to regular fluorescent bulbs, avoiding potential interference from unwanted side reactions.[88,89] An initial report by Hu

et al. established the ability of allyl tosylhydrazones **69** to undergo 5-exo-trig cyclisation to form the corresponding 5-methyldihydropyrazoles **70** in fair to very good yields (**Scheme 4**).[90] A proceeding report by the same authors found that the addition of stochiometric amounts of TEMPO alongside introduction of a geminal aryl ring to the alkene substituent (**71**) was able to significantly alter the favoured reaction pathway, leading to preferential formation of the 6-endo cyclisation products (**72**) in good to excellent yields.[91] DFT studies accompanied by mechanistic experiments suggested the electron-withdrawing nature of the aromatic ring leads to preferred formation of a benzyl radical intermediate, resulting in radical attack at the terminal end of the alkene. A report by Zhao *et al.* established the construction of fused dihydropyrazole benzylsultam rings (**74**) in poor to good yields from β,γ–unsaturated tosylhydrazones **73**, featuring the utilization of a cobalt co-catalyst which serves as an oxidant for the Ru(bpy)$_3^{2+}$ photocatalyst.[92] Furthermore the presence of an α-dimethyl moiety was found to be necessary for the observed reactivity, enabling kinetic acceleration of the radical addition steps *via* angle compression. Despite constituting significant milestones of progress within the field the overall applicability of these methodologies is restricted by the intra-molecular nature of the cyclisations, as well as the need for highly engineered substrates to ensure adoption of the desired reaction pathway.
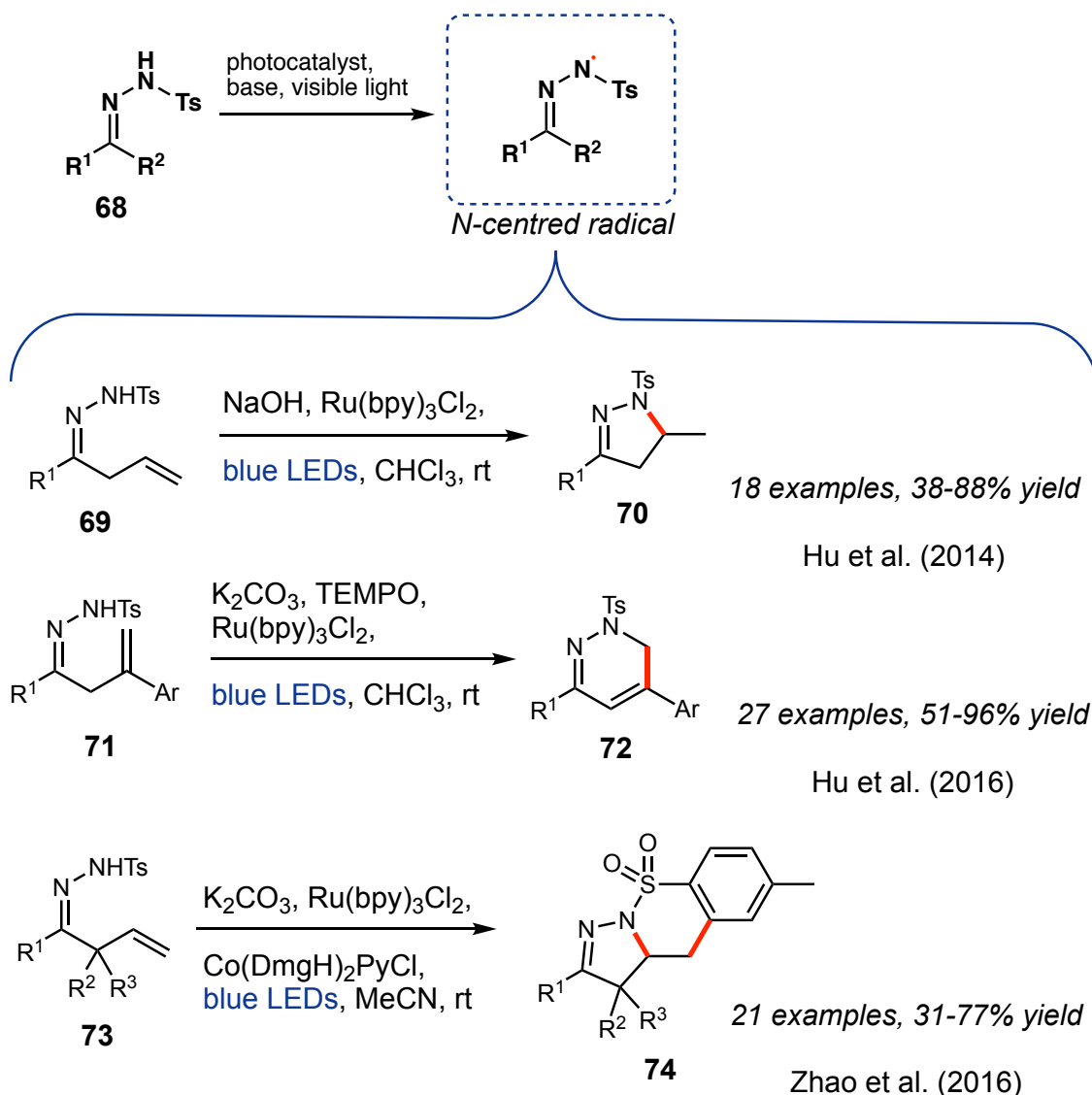
Scheme 4. *Earliest examples of photoredox transformations involving sulfonyl hydrazone substrates, employing photocatalyst Ru(bpy)₃²⁺ to generate nitrogen-centred radicals capable of engaging in intramolecular cyclisation reactions forming pyrazole (70), pyridazine (72) and fused sultam (74) heterocycles.*[90-92]

A subsequent report by Parisotto *et al.* was distinct in determining the first instance of photocatalytic rearrangement reactions utilising α,β-unsaturated sulfonyl hydrazones **75** under previously established photoredox conditions to generate allylic sulfones **76** (**Scheme 5**).[93] The proposed reaction mechanism entailed delocalization of the hydrazonyl radical spin density across the conjugated system, followed by a concerted 1,5-shift of the sulfonyl group with expulsion of nitrogen gas and finally hydrogen atom abstraction from the solvent, as implied by deuterium labelling studies. This constituted

a novel mode of reactivity regarding Ru(bpy)$_3$$^{2+}$ catalysed photochemical transformations of sulfonyl hydrazones, underlining the potential utility of enabling direct functionalisation of the hydrazonyl carbon under mild reaction conditions. However, despite extensive optimisation efforts only poor yields could be obtained across a relatively limited substrate scope.
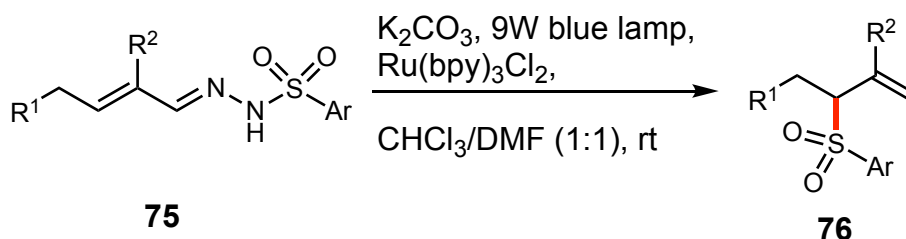
11 examples, 30-46% yield

S. Parisotto et al. (2017)

Scheme 5. *Photocatalytic generation of allyl sulfones **76** from α,β-unsaturated sulfonyl hydrazone precursors (**75**) proceeding with poor to fair yields.*[93]

A recent report by Burkhard Konig's research group expands on this approach, utilizing a third generation heteroleptic iridium photocatalyst (**79**) to enable coupling of tosylhydrazones **77** with sulfur-centred radicals derived from thiols **78**, followed by trapping with model electrophiles carbon dioxide or aldehydes (**81**) to generate the difunctionalised products **80** and **82** correspondingly in high yields at room temperature (**Scheme 6**).[94] Within the same publication the authors described the photocatalytic conversion of tosylhydrazones into geminal difluoro-alkenes **84** utilizing trifluoromethylsulfonate (**83**) as a –CF$_2$ source, proceeding in poor to good yields. Such reaction types represent an ideal approach towards organic synthesis efforts within medicinal chemistry contexts whereby multiple synthetic pathways can be accessed *via* a single mode of chemical activation, while reaction progress remains unobstructed under relatively benign conditions and occurs with the required levels of chemoselectivity to facilitate the construction and decoration of a diverse range of molecular scaffolds.

79
[Ir(dFCF₃ppy)₂dtbbpy]PF₆
photocatalyst

77 + **78** → **80**
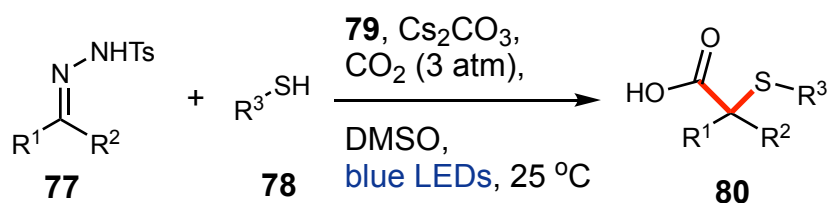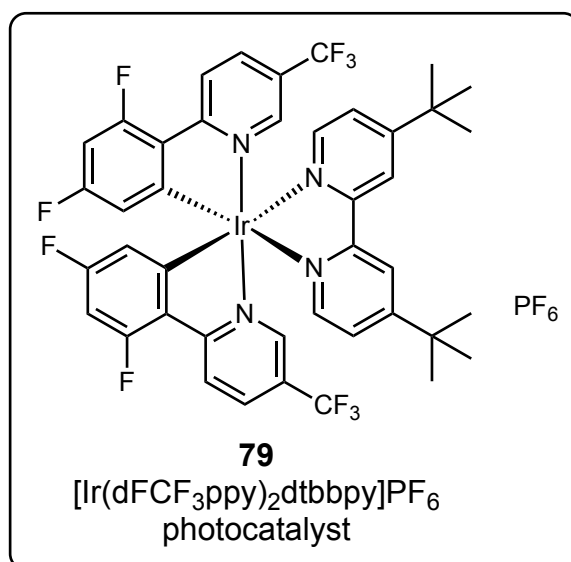
43 examples, 34-82% yield

77 + **78** + **81** → **82**

15 examples, 26-78% yield

77 + **83** → **84**

30 examples, 30-77% yield

Wang et al. (2020)

Scheme 6. *Photoredox transformations of sulfonyl hydrazones (77) catalysed by iridium complex 79 allowing for difunctionalisation of the hydrazonyl carbon centre via multicomponent coupling reactions with thiols 78 and carbonyl electrophiles such as CO₂ and aldehydes (81). Analogous conditions employed alongside trifluoromethanesulfinate 83 enable straightforward access to geminal difluoroalkenes 84.*[94]

1.6. Summary and Project Aims

As a persistent and significant challenge to public health, antibiotic resistance is an issue that requires a wide range of solutions to address the numerous and often distal underlying causes. The discovery of novel antibiotic compounds that operate *via* previously unencountered mechanisms of action is a major component in overcoming the existing devices of evolved resistance as such discoveries allow for the circumvention of over-exploited microbial biomolecular targets and synthetic pathways, and ultimately enable the replenishment of increasingly ineffective frontline treatments. Despite the early promise of HTS and similar assay-based drug discovery approaches, it has become clear that such methodologies are ill-suited to identifying suitable anti-bacterial hit and lead structures for development due to their distinct susceptibility towards false-positive results. Therefore efforts to uncover novel antibiotics have been forced to rely on approaches more akin to classical pharmacological methods, including the phenotypic screening of natural product libraries and rationally designed drug candidates.

DHDPS is considered one of the most promising antibiotic targets identified in recent times due to its highly conserved active site, essentiality of function, ubiquity across bacterial species and well characterised protein structure. Despite numerous preliminary drug design efforts no DHDPS inhibitors exhibiting *in vitro* anti-bacterial activity have yet been identified, despite several compound classes based upon endogenous ligand structures frequently obtaining high levels of potency when assessed *via* enzyme-based assays. In addition to rationally designed DHDPS inhibitors based upon the substrate and product scaffolds, limited efforts have been made to identify novel molecular architectures through virtual docking studies in order to efficiently assess unexplored pharmacophores *in silico* for potential affinity towards the DHDPS active site. However, these virtually derived hits are yet to be tested for *in vitro* activity and the practicality of such *in silico* screening methods when applied in isolation remains restricted.

Another major problem that has hampered the practice of drug discovery can be found in the lack of structural diversity present within the vast majority of commercial compound libraries, a principal factor behind the prolongation or outright failure of hit identification and lead optimisation efforts. This lack of structural variation has arisen through the continued reliance by medicinal chemists on a narrow spectrum of reaction types in order

to ensure efficient and robust assembly of target compound sets, often to the detriment of scaffold diversity and complexity. Photoredox catalysis has emerged over the preceding fifteen years as a powerful approach towards facilitating unconventional bond formations difficult to achieve through conventional methods of kinetic and thermodynamic control. Indeed there are numerous examples of photocatalytic approaches being applied towards the synthesis and late stage functionalisation of drug candidates and natural products alike, with practical yields often obtained due to the highly chemoselective nature of photoredox functional group activations and otherwise mild reaction conditions. This demonstrates the capability of photocatalytic methodologies to streamline synthetic routes and overcome persisting challenges regarding compound library assembly.

It was envisaged that *in silico* screening of virtual compound libraries against the DHDPS active site would enable the identification of novel molecular scaffolds capable of engaging in unprecedented modes of binding, with potential inhibitory activity arising from the supposed affinity for the DHDPS active site. Photoredox catalysis methodologies could be developed and employed alongside more conventional synthetic procedures to generate focused libraries of target molecules identified *via* virtual docking procedures. Determination of the *in vitro* antibacterial activity of the selected compounds can be accomplished utilising routine minimum inhibitory concentration (MIC) protocols to reliably ascertain potential hits *via* phenotypic screening. The SAR's of desirably performing compounds can then be explored *in silico* through continued virtual screening of various structural derivatives, allowing further identification of potential DHDPS inhibitors as target compounds for synthesis and *in vitro* testing. This cyclic feature of the overall drug discovery approach enables the potential continuous development of lead compounds and synthetic methodologies (**Figure 15**).
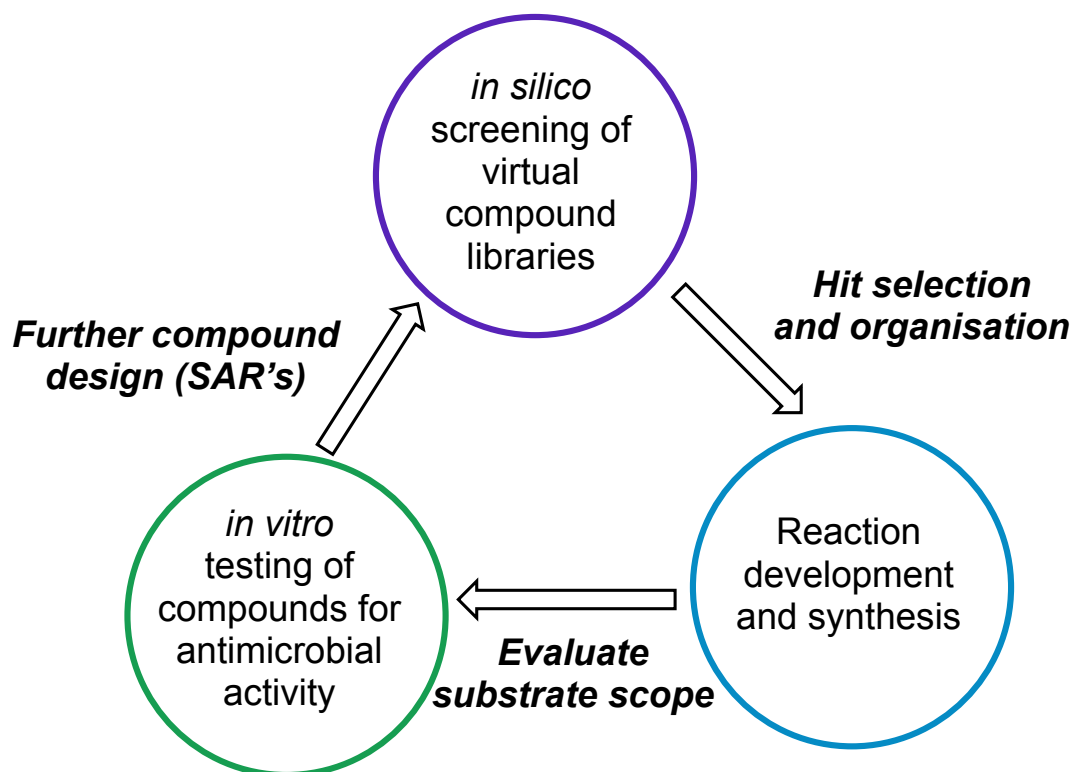
Figure 15. *General overview of the distinct stages of the proposed drug discovery approach, commencing with in silico screening of virtual compound libraries against a validated antibacterial target (DHDPS), followed by reaction optimisation and synthesis of virtual 'hits' and finally determination of their antibacterial activity in vitro. Derivatives of promising candidates identified via phenotypic screening can be assessed in silico to refine structure-activity relationships (SAR's) and thus provide further target compounds for synthesis and biological testing as part of an iterative, cyclic process.*

Chapter 2

Results and Discussion

2.1. In Silico Docking Studies

Pharmacophore models were constructed *in silico* based on structural features of the endogenous ligand pyruvate (**9**) and previously reported inhibitors of desirable potency including picolinate derivative **25** and bis-keto acid **37**. Selected directional and point features derived from the reference structures were then used to generate individual pharmacophore outlines (**Figure 16**).[95] The features were selected based on their

9

25   **37**
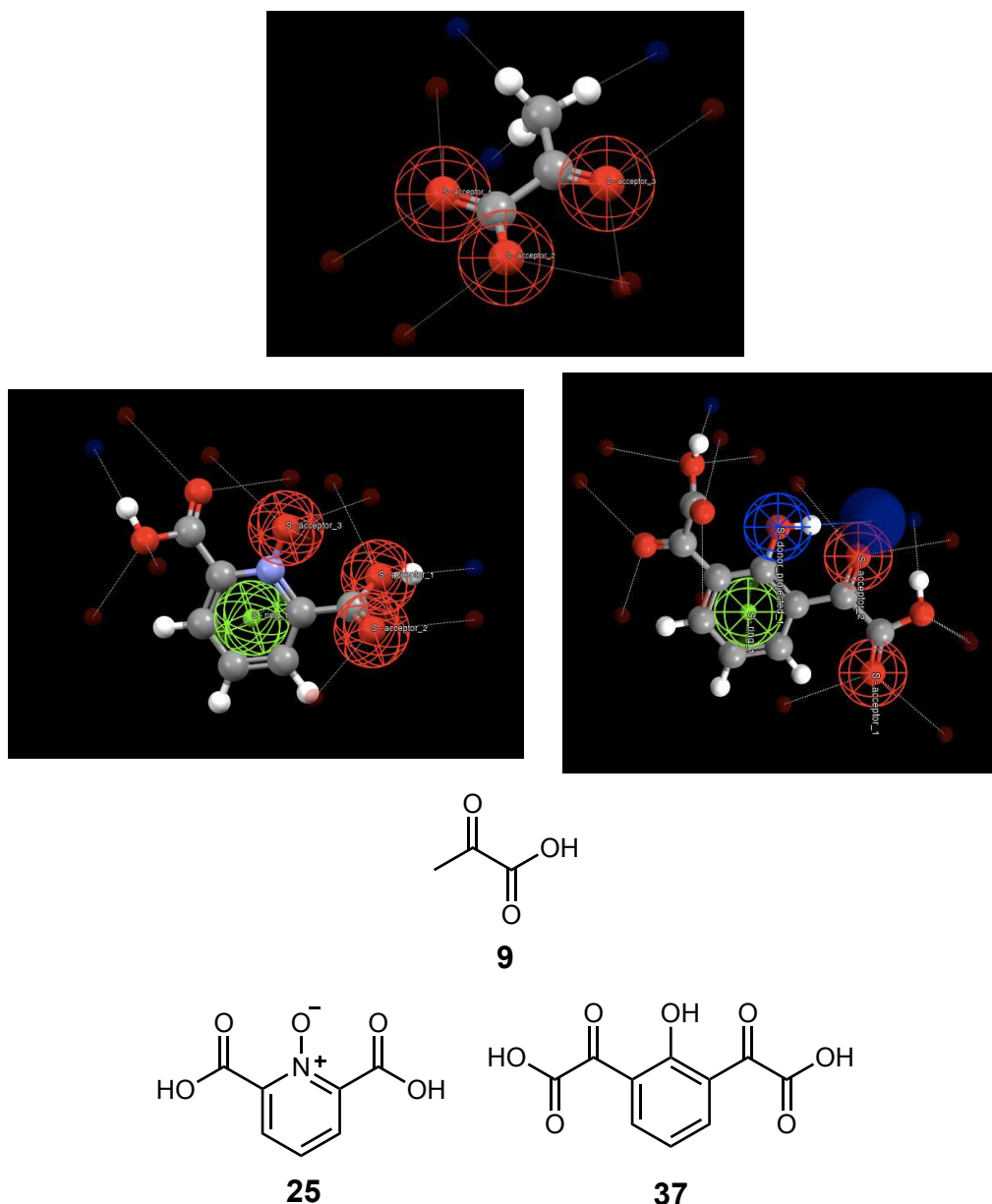
Figure 16. *Pharmacophore profiles derived from reference structures pyruvate (top) alongside previously reported inhibitors dipicolinic acid N-oxide 25 (left) and keto-acid derivative 37 (right) constructed principally of hydrogen-bond acceptor/donor features (constructed using CSD-Crossminer).[95]*

contribution towards enabling occupation of the DHDPS active site as determined in previous reports.[26,46,48]

These pharmacophore profiles were subsequently screened against the ZINC database of commercially available compounds (200–400 molecular weight, –1–3.5 logP) filtered to ensure low reactivity, encompassing some ~250,000,000 structures.[96] An additional pharmacophore based search was performed again transcribing structural features derived from the aforementioned reference structures, this time using ZINCPharmer in order to perform a less restricted search of the ZINC database across a wider range of molecular weights (100-500) and logP (–1–5) values (**Figure 17**).[97]
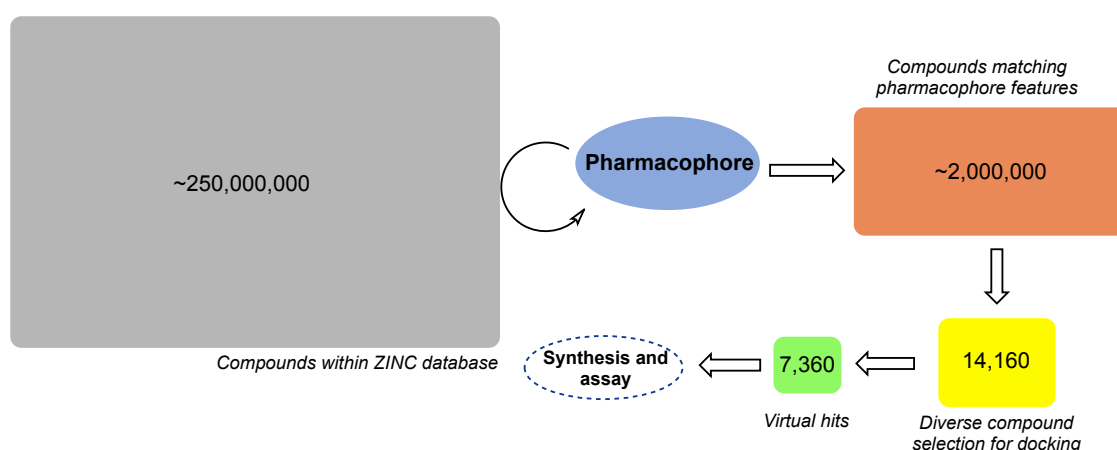
Figure 17. *General workflow diagram of compound selection via in silico guided identification of candidate structures for synthesis and in vitro screening.*

In total over 2,000,000 compounds were found to completely match the derived pharmacophores, therefore the clustering of molecular scaffolds based on relative structural similarity and subsequent selection of diverse compound sets was required in order to reduce the number of compounds to be assessed *in silico* to a manageable cohort of representative structures. In total 14,160 compounds were selected for virtual docking against a computational model of the resolved crystal structure of *S. aureus* DHDPS active site (PDB ID: 3DI1). This specific variant was chosen due to the prevalence of *S. aureus* bacterial strains in routine minimum inhibitory concentration (MIC) testing, the presence of endogenous pyruvate ligand cocrystals allowing intuitive location of the active site, as well as the relative simplicity of the protein's native dimeric quaternary structure compared to the more common tetramer aggregates available *via* the PDB crystallographic database.[33,35,98]

Upon identification of the desired docking site, a 10 Å radius cavity around the bound pyruvate substrate was defined as the area in which to attempt ligand docking. The pyruvate molecule was extracted leaving an unoccupied binding site, and all ligands were subjected to conformation energy minimisation prior to docking using a random low energy bias algorithim employing initial torsions derived from integrated crystallographic data (**Figure 18**).[99] Throughout the docking process no constraints were imposed on ligand flexibility, allowing for the assessment of multiple conformers for each individual ligand. A certain degree of flexibility was also afforded to the DHDPS protein including the active site, whereby amino acid side chains and the heteroatom–hydrogen bonds of Ser, Thr, Tyr and Lys residue side chains were afforded complete rotational and torsional freedom enabling them to adopt approximated optimal positions for engaging in hydrogen bonding interactions with docked ligands. A key limitation of the virtual screening process is that the protein backbone is treated as a rigid system, with no conformational freedom given to the various amide linkages forming the primary amino acid sequence. Although likely reducing the accuracy of the *in silico* model in predicting the overall structural layout of the protein, such an impediment is necessary to reduce the computational complexity of the calculations and is therefore included by default in the majority of high volume docking studies.[100]
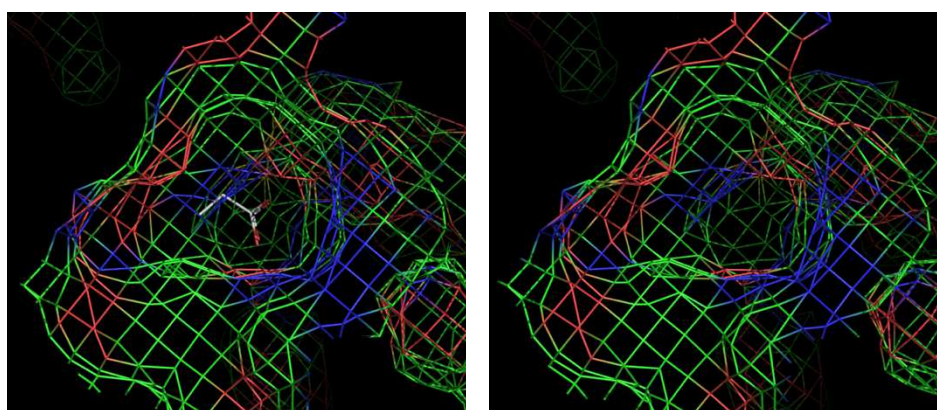
Figure 18. *In silico extraction of pyruvate (white) from the active site of S. aureus DHDPS in preparation of the virtual docking site (radius: 10Å).*

Ten docking poses per structure were selected for evaluation of potential binding affinity to the active site, and structures of known inhibitors **25** and **37** were screened against the selected docking site alongside the virtual library for reference in the qualitative assessment of *in silico* binding abilities (**Figure 19**).[101,102] The fitness functions employed (ChemPLP and Goldscore) in the scoring of ligands are constructed of various calculated energy terms that incorporate empirical parameters such as hydrogen bond energies, atomic radii and polarisability, torsion potentials for specific bond types and hydrogen bond directionalities based on predefined geometries.[102,103] Although some of these parameter inputs such as hydrogen bond energies are initially derived from binding affinity data, it is important to state that the scoring functions used are optimised towards the prediction of ligand binding poses and are inherently dimensionless. Therefore the docking results cannot be interpreted directly as estimations of binding affinities or energies, only as predictions of ligand-protein docking poses. The scoring functions therefore only provide a framework to assess the qualities of predicted ligand-protein interactions in relation to one another.

Qualitatively good binding modes were observed for compounds capable of engaging in reasonable hydrogen-bonding interactions with the key Lys163 residue, as well as additional polar interactions with nearby Thr46, Thr47, Tyr135 and Arg140 residues. Compounds which exhibited solely poor binding ability were discarded and not investigated further, and from the initial 14,160 compounds screened 7,360 were identified as virtual hits.
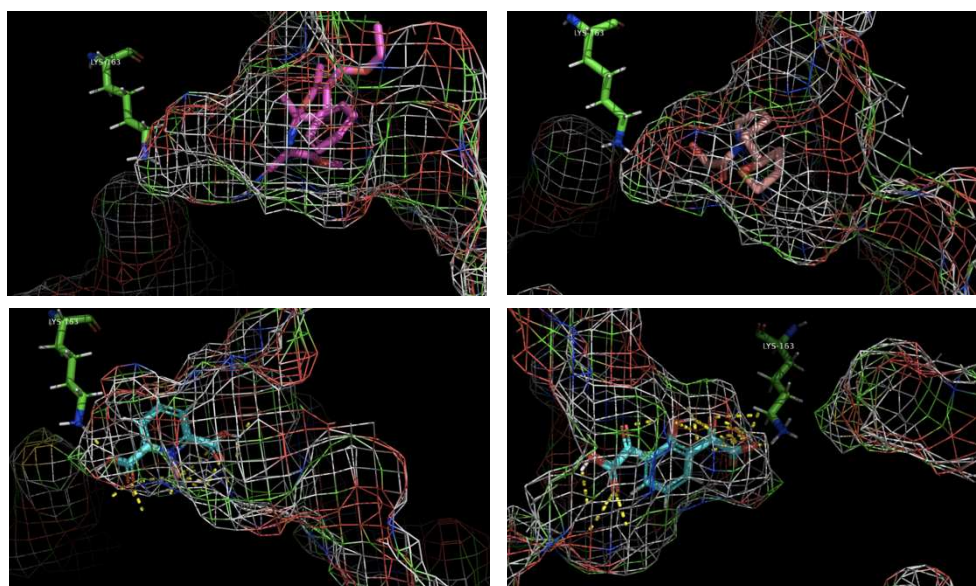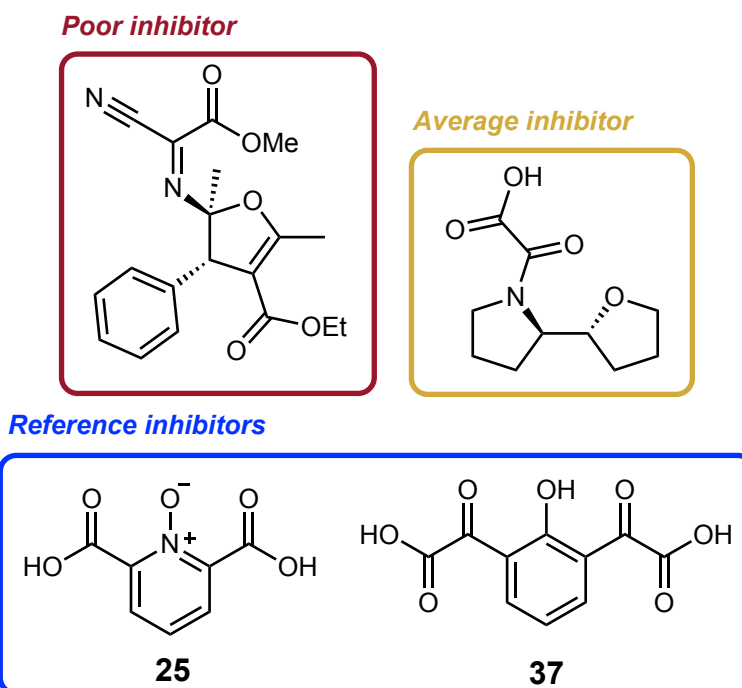
Figure 19. *Examples of qualitative determination of ligand binding affinity obtained from analysis of virtual docking results; poor binding (top left), average binding (top right), and good binding demonstrated by known inhibitors **25** (bottom left), and **37** (bottom right) for reference (dashed lines indicate potential ligand-protein polar contacts).*

A relatively diverse range of molecular scaffolds adorned with various functional groups were recognised as being congruent with promising *in silico* binding affinity, furthermore several were identified as re-occurring motifs bestowed with potential complementation of the hydrogen-bonding networks enclosed within the active site. Numerous factors were considered in deciding on which hit structures to pursue, starting with evaluation of the functional groups present and their relevance within a medicinal chemistry context.

Structures containing motifs known to frequently engage in non-specific interactions with biological targets or impart broad cytotoxic activity were disregarded, due to the likelihood of misleading results arising from the subsequent *in vitro* assays. Compounds bearing unusual functional groups not typically utilised within drug discovery programs were also disregarded due to the potential unexpected negative influences on molecular stability and behaviour under assay conditions.

Despite possessing a core scaffold which satisfied the pharmacophore requirements employed, several of the hit structures also contained significant fragments that were not observed to engage with the DHDPS binding site in any of the docking poses investigated. This trait was especially prominent at increased molecular weights, therefore selection preference was given to lower molecular weight compounds that displayed greater binding efficiency in fitting the pharmacophore profile and occupying the DHDPS active site with minimal unnecessary structural features present. The possible synthetic routes towards hit structures were also considered, with preference given to compounds that could be obtained *via* straightforward transformations. More elaborate targets were considered only when justified by demonstration of superior binding interactions in the absence of simpler analogues. The main principle on which hit compounds were evaluated was the presence of unifying chemical moieties, that consistently resulted in favourable docking poses. This is exemplified by the presence of several hit structures possessing similar molecular scaffolds, and comparable hydrogen bonding groups capable of engaging with the key residues within the DHDPS active site. Considering the efforts taken to ensure structural diversity within the sampled compound libraries, such recurring structural features are likely significant in facilitating effective binding to the active site. Therefore pursuing hit compounds belonging to a group with shared structural features harbours considerable potential regarding the design of effective DHDPS inhibitors.

Numerous sulfonyl group bearing structures were found to demonstrate inhibitory potential *in silico*, as evidence by several examples of methylphenyl sulfones intimating polar interactions with the key Lys163 residue whereby the hydrogen bond accepting dioxide moiety effectively mimics the binding conduct of the carboxylic acid groups of reference structures pyruvate, **25** and **37** (**Figure 20**).
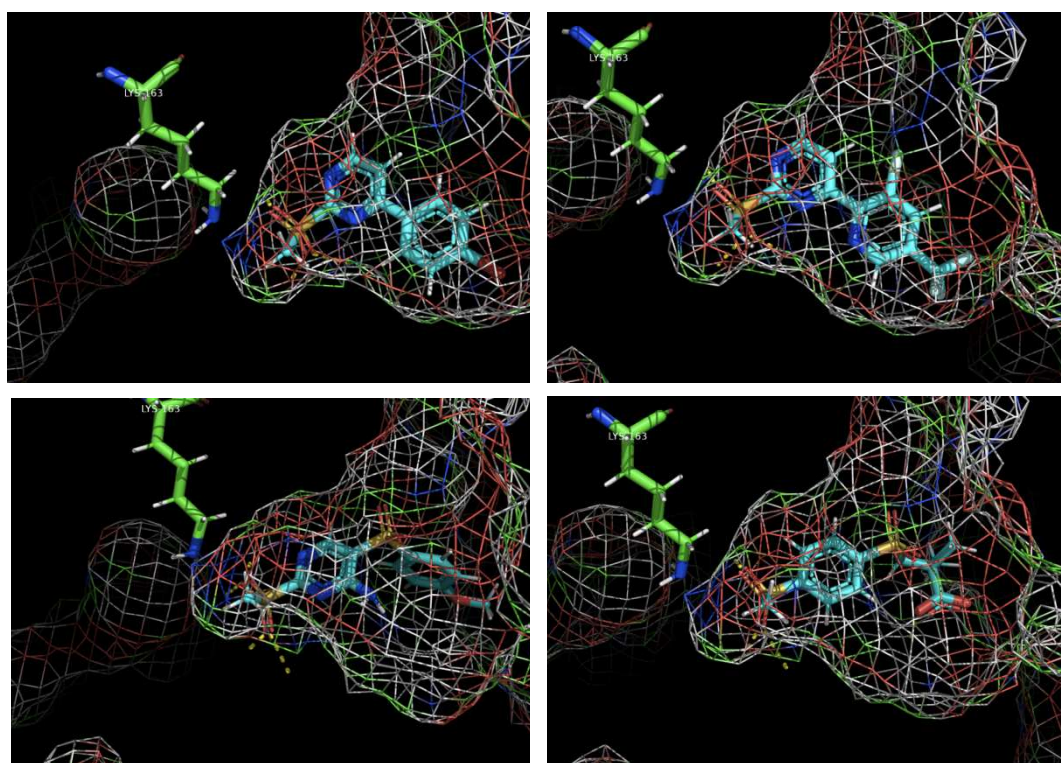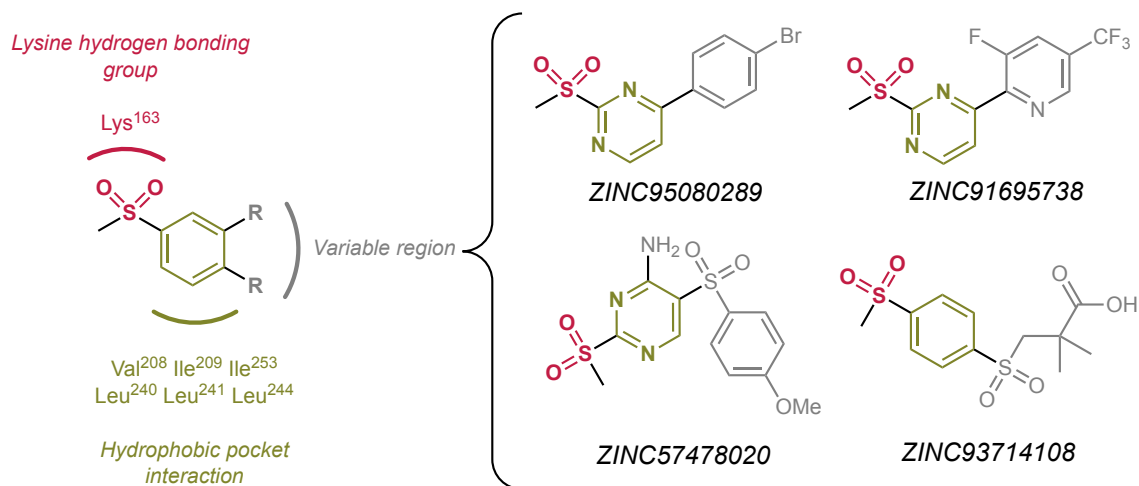
Figure 20. *Virtual docking procedure generated models of sulfone derivatives ZINC95080289 (top left), ZINC91695738 (top right), ZINC57478020 (bottom left) and ZINC93714108 (bottom right) within the S. aureus DHDPS binding site, and their corresponding skeletal structures showing shared features of the molecular scaffold. Dashed lines indicate supposed polar interactions with nearby residues, including the key Lys163 residue highlighted as a skeletal structure.*

In addition to the desired intermolecular hydrogen bonding of the sulfonyl moiety, in several cases such as ZINC95080289 and ZINC91695738 the adjoining aromatic rings were found to occupy a hydrophobic pocket beside the substrate binding region constructed of residues Val208, Ile209, Ile253, Leu240, Leu241 and Leu244. To the authors knowledge significant binding to this hydrophobic region has not been observed with any previously reported DHDPS inhibitors *in vitro* or in any preceding virtual

docking studies, indicating that the virtual interactions observed within the hydrophobic pocket could potentially constitute a novel binding mode that could be exploited in the design of further hit and lead candidates.
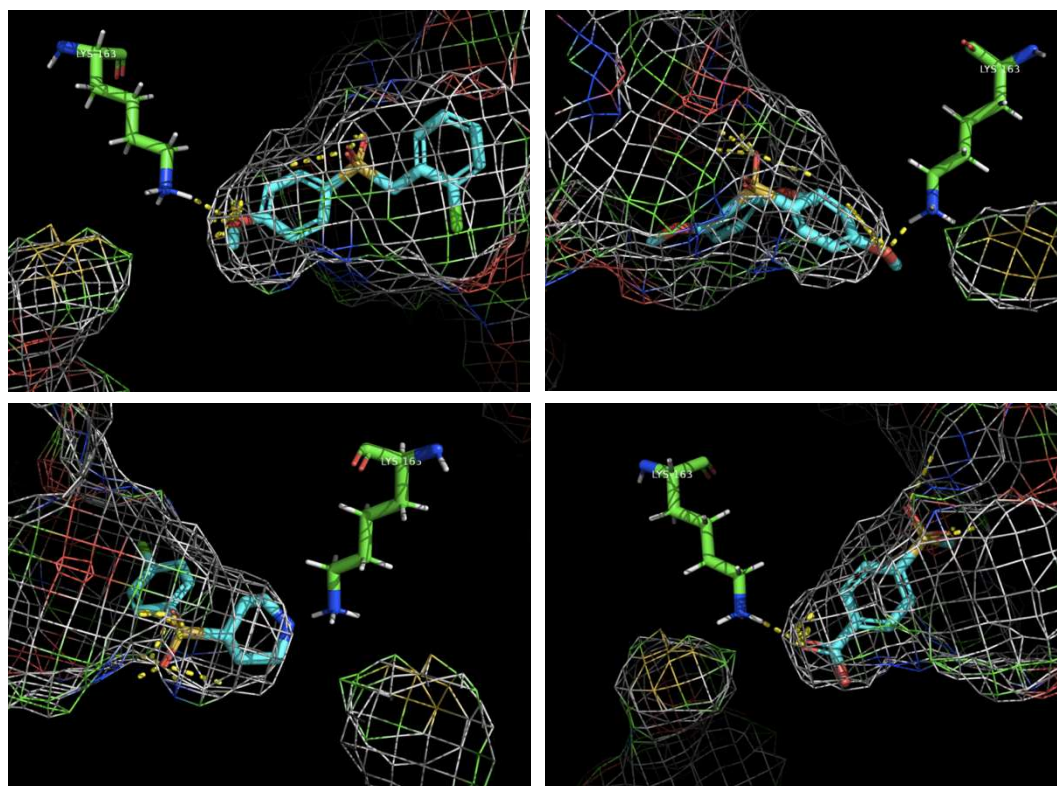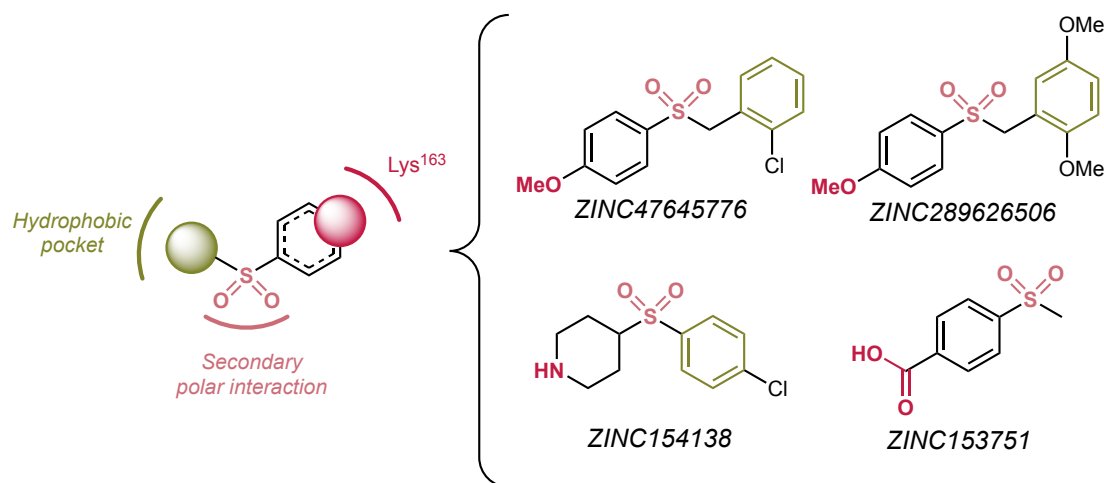
Figure 21. *Results of virtual docking studies showing suspected binding interactions of additional sulfone derivatives ZINC47645776 (top left), ZINC289626506 (top right), ZINC154138 (bottom left) and ZINC153751 (bottom right) within the DHDPS binding site, alongside the ligand skeletal structures and pharmacophore overview. Polar interactions indicated by dashed lines, skeletal form of Lys163 residue shown.*

Several additional sulfone derivatives were also found to exhibit high potential binding affinities *in silico,* whereby the sulfonyl group engages in secondary binding interactions with outer regions of the binding site such as *p*-methoxy derivatives ZINC47645776 and ZINC289626506 (**Figure 21**). Alongside the supplemental binding interactions provided by the sulfonyl moiety with either the Asp191 or Arg140 residues, the *para* positioned methyl ether group appears ideally placed to engage in desirable hydrogen-bonding interactions with the Lys163 residue and furthermore the distal aromatic ring is capable of associating with the previously described hydrophobic pocket. Similar binding modes were identified in the case of ZINC154138 in which a secondary amine group was found to readily engage in polar interactions with Lys163, and comparably with compound ZINC153751 whereby the key interactions of the benzoic acid group with the Lys163 residue are complemented by additional hydrogen-bonding interactions between the *para* situated sulfonyl moiety and the highly conserved Arg140 gatekeeper residue.

Comparably, sulfonamides such as ZINC20223890 were also capable of utilising the sulfonyl moiety to engage in supposed auxiliary binding interactions within the active site, supplementing the crucial intermolecular bonding between the cyclic ketone and Lys163 residue (**Figure 22**). Furthermore numerous carbonyl group-bearing virtual hits were identified as capable of engaging in auspicious polar interactions with the all-important Lys163 residue, rather unsurprisingly given their reputation as exemplary hydrogen-bond acceptors and their prolific appearance within the pharmacophore reference structures.[104] Ketones and α-keto esters such as ZINC259808968 and ZINC28295599 exhibited promising carbonyl-Lys163 polar interactions, the latter candidate in particular demonstrated considerable promise as a potential inhibitor due to the ester carbonyl also engaging with the nearby highly conserved Tyr135 residue. Furthermore the ketone and methyl ether groups flanking either side of the ester carbonyl were seen to engage in intermolecular bonding with the key Arg140 and Thr47 residues respectively, while the *p*–methoxy group contributes additional bonding interactions *via* association with the nearby Asn190 residue. Isatin derivatives such as ZINC71483382 bearing multiple carbonyl groups were also found to be pertinent *in silico* inhibitors, displaying apparent hydrogen-bonding interactions with the key Lys163, Tyr135 and Arg140 residues once again.
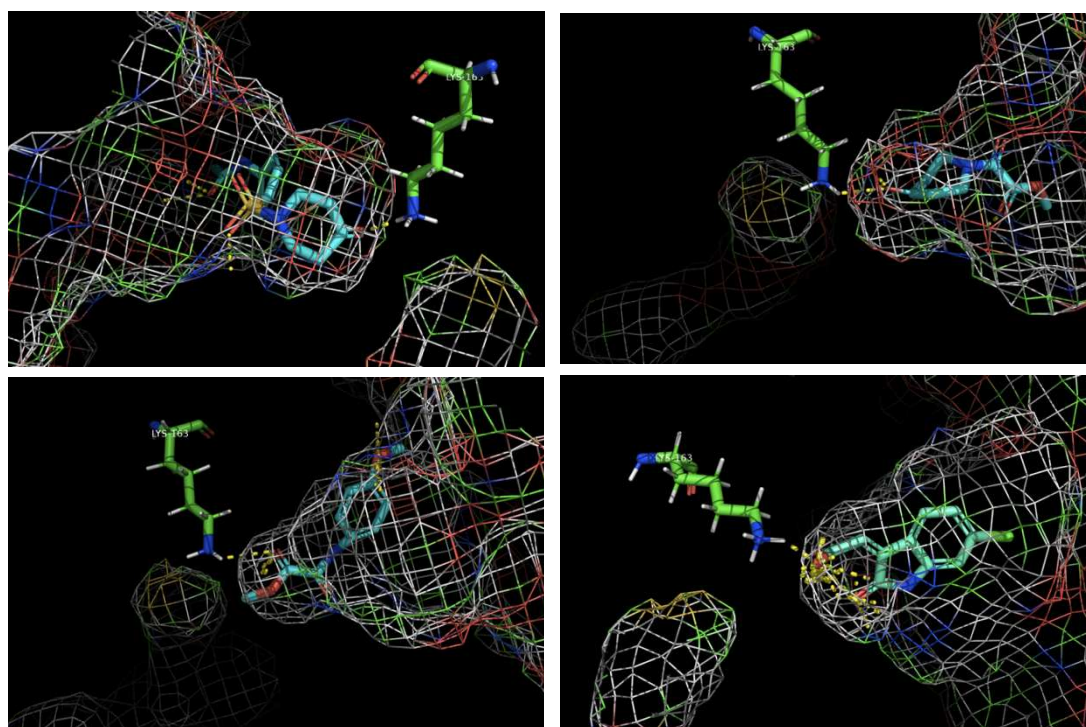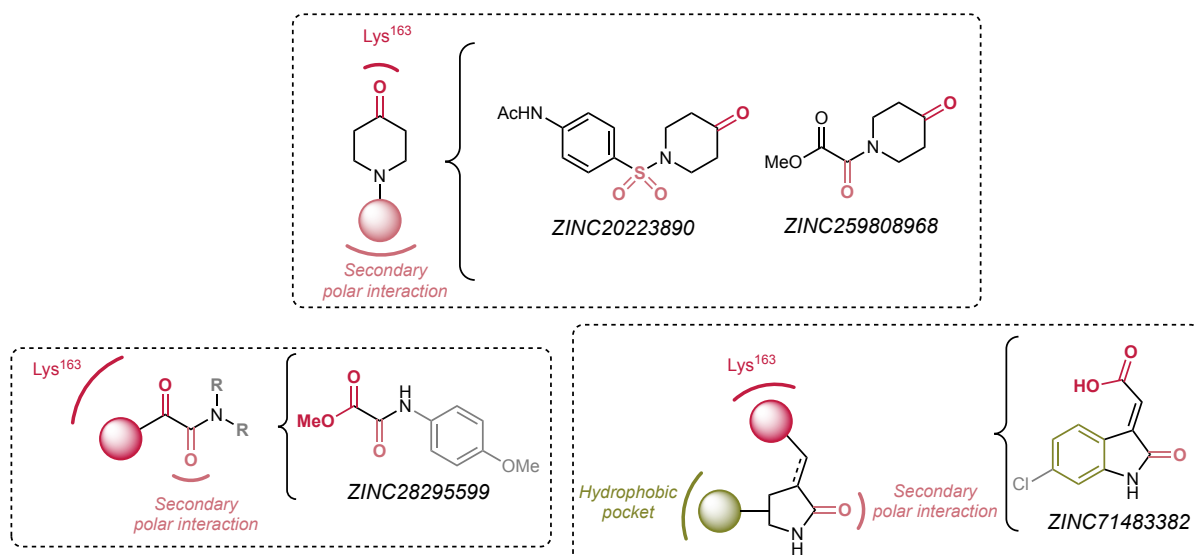
Figure 22. *Virtual docking results showing presumed occupation of the DHDPS binding site by sulfonamide ZINC20223890 (top left), α-keto esters ZINC259808968 (top right), ZINC28295599 (bottom left), and isatin ZINC71483382 (bottom right) alongside the skeletal structures of the ligands and overviews of their representative molecular scaffolds. Supposed polar interactions indicated by dashed lines, skeletal form of Lys163 residue shown.*

Hydrazones constituted another recurring molecular scaffold, typically bearing hydrogen-bond accepting groups present within the aforementioned virtual hit structures, such as methyl esters and carboxylic acids in the case of ZINC490675521 and ZINC72370081 respectively (**Figure 23**). The 1,3-dihydroxybenzyl dimer ZINC2666610 also demonstrated effective *in silico* inhibitory activity *via* intermolecular bonding between

Lys163 and the phenolic moiety, while the hydrazonyl backbone engaged in polar interactions with alternate residues adjacent to the active site.
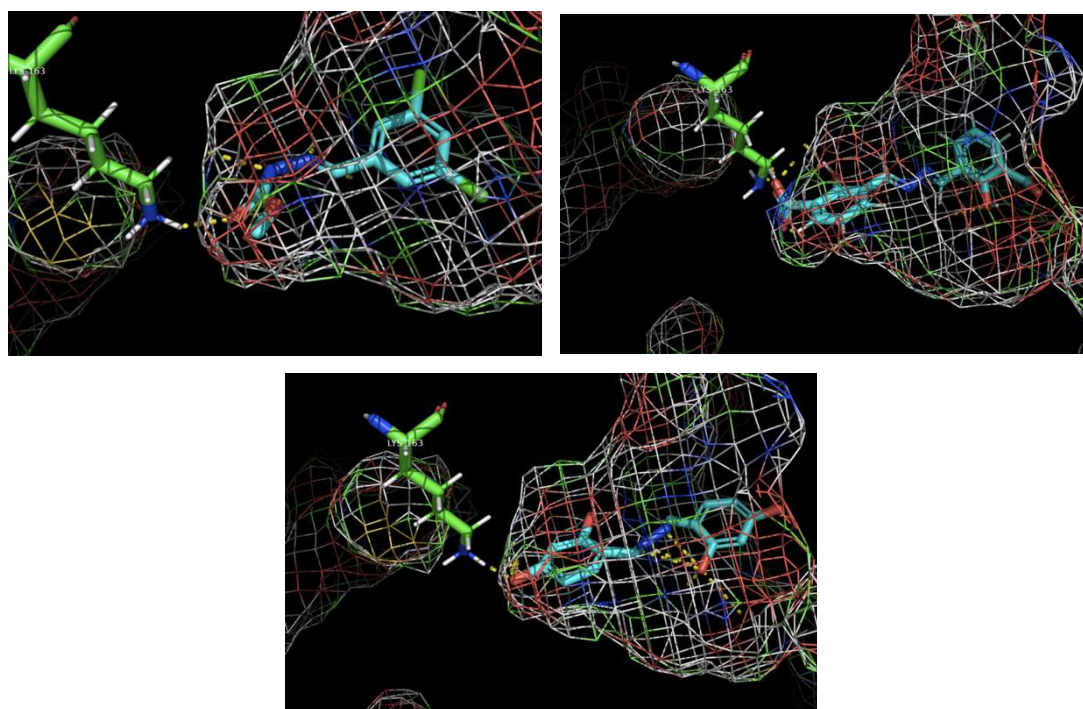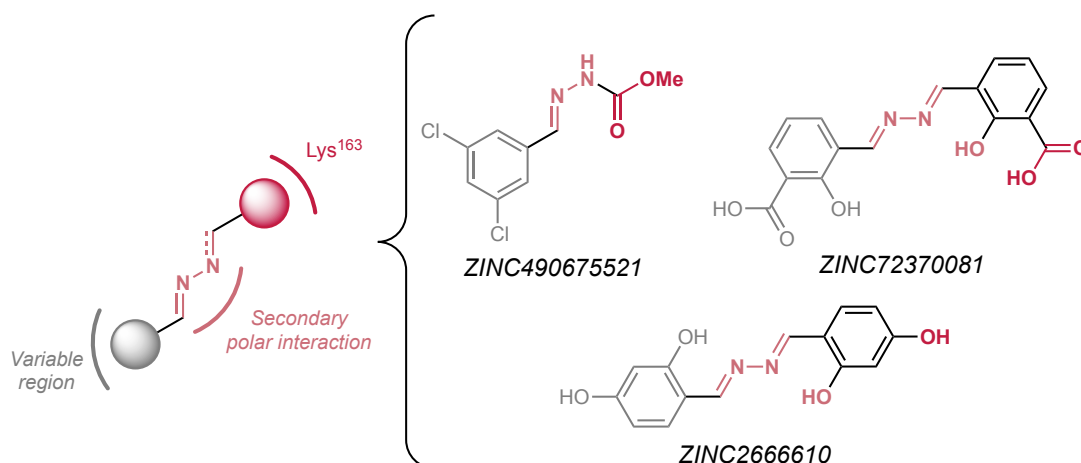
Figure 23. *Virtual docking results showing hydrazone derivatives ZINC490675521 (top left), ZINC72370081 (top right) and ZINC2666610 (centre) within the DHDPS active site alongside an overview of the ligand structures. Supposed polar interactions are indicated by dashed lines, Lys163 residue highlighted in its skeletal form.*

Several tetrazole derivatives were found to indicate promising binding potential, as non-classical bioisosteres of carboxylic acids it appears that such tetrazole rings are ideally suited for engaging in polar interactions with the key Lys163 residue (**Figure 24**). The

fused bicyclic core of ZINC94726762 facilitates seemingly effective occupation of the active site despite being devoid of additional bonding features, whereas derivative ZINC825594726 benefits from the supplemental interaction between its tallow alkyl chain and the established hydrophobic pocket.
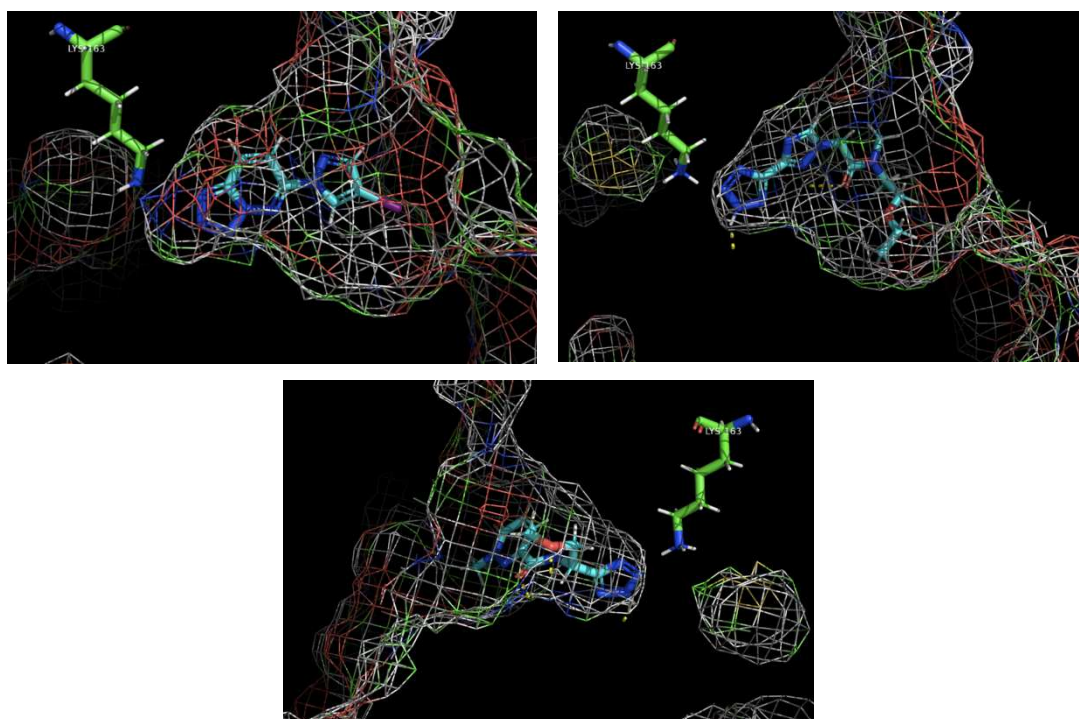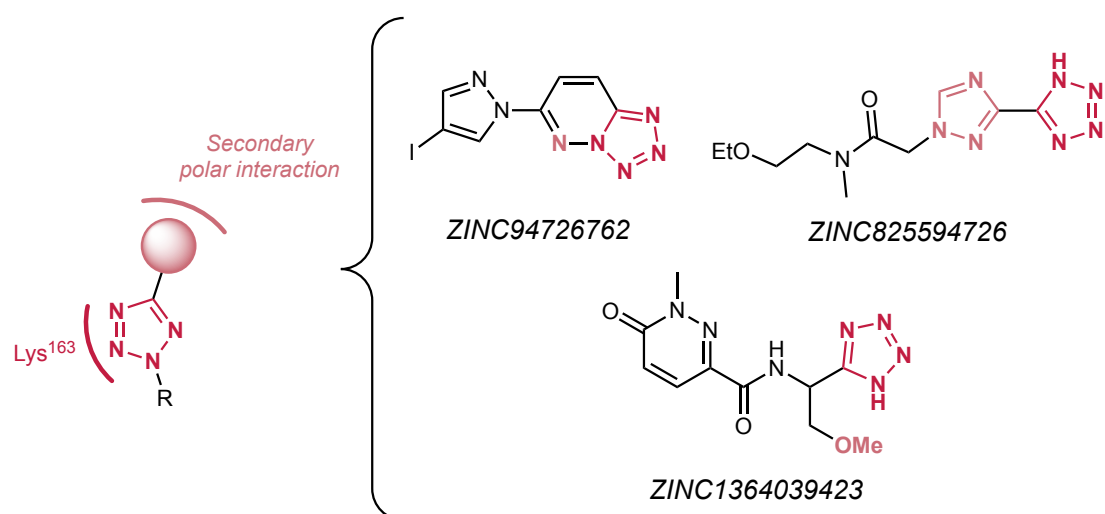
Figure 24. *Virtual docking results showing tetrazole derivatives ZINC94726762 (top left), ZINC825594726 (top right), ZINC1364039423 (centre) occupying the DHDPS active site, with the key Lys163 residue highlighted in its skeletal form. An overview of the skeletal structures is also shown with key pharmacophore features highlighted.*

Furthermore, the last example ZINC1364039423 features encouraging secondary polar interactions between a β-methoxy group and the Tyr135 residue resulting in a bonding array similar in arrangement to that of cefmetazole (**46**) identified as a virtual hit in prior *in silico* studies.[59] The secondary polar interactions are further complemented by a less prominent yet still contributory occupation of the hydrophobic pocket by the pyradizinone ring, accentuating two complementary potential routes for lead development. The discussed qualitative determination of potential inhibitory activity based on the *in silico* ligand screening efforts, facilitated the construction of generic structural outlines for the targets of initial synthetic efforts *via* identification of recurring intermolecular bonding motifs as well as the combination and truncation of prospective molecular scaffolds (**Figure 25**).
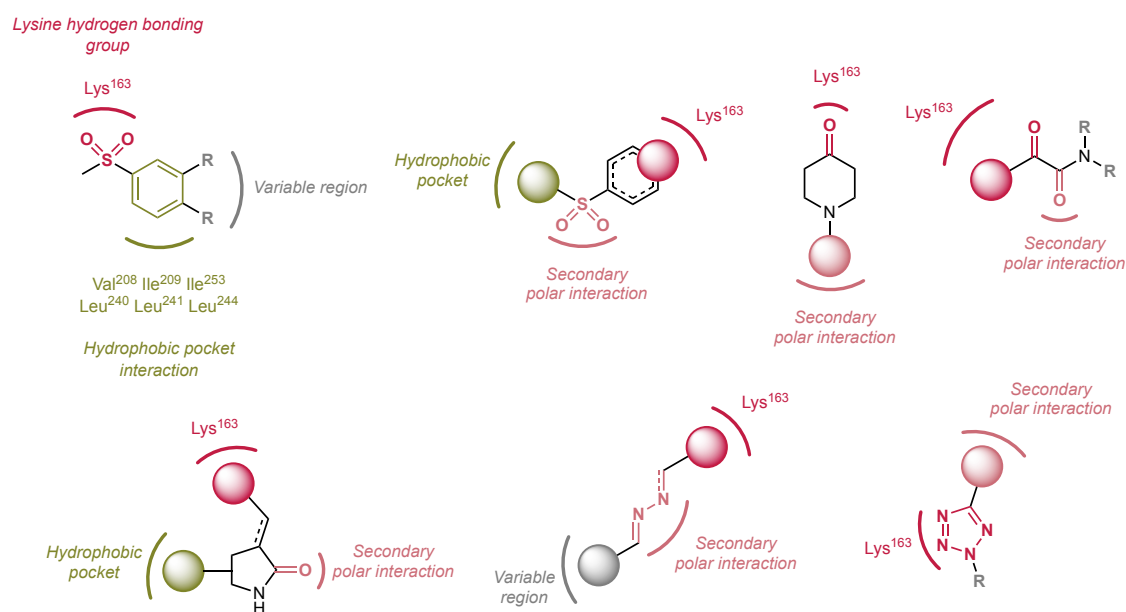
Figure 25. *Overview of molecular scaffolds identified as promising templates for lead compound design via virtual docking efforts, with expected potential antibacterial activity based on binding interactions within the DHDPS active site determined in silico.*

2.2.   Synthesis of Sulfones

2.2.1. Prior Synthetic Routes to Sulfones

Sulfones in their own right are considered a highly important class of compounds that see extensive usage both as versatile intermediates in organic synthesis and as a valuable molecular scaffold within various medicinal chemistry contexts, including the field of antimicrobial drug discovery (**Figure 26**).[105–110]
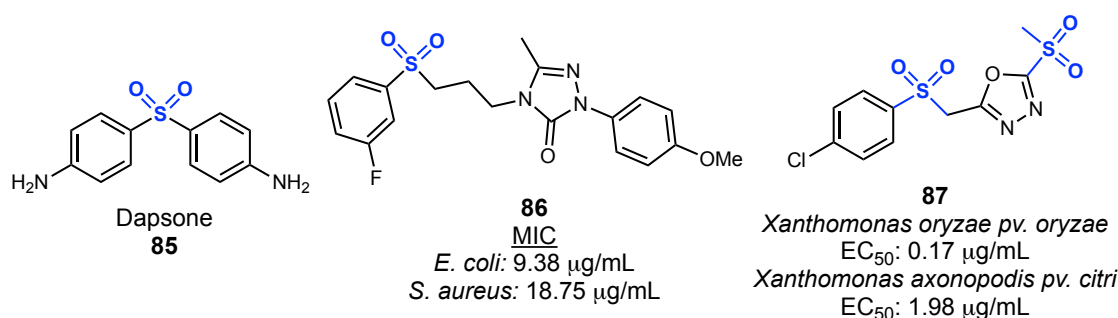
Figure 26. *Medicinally relevant examples of sulfone-based antimicrobial scaffolds including established antibiotic Dapsone (85) alongside recently discovered antibacterial agents 86 and 87.*

The majority of reactions involving sulfone substrates fall into one of two categories, depending on the reactivity of the adjacent carbon centre. The electron-withdrawing sulfonyl moiety is capable of facilitating deprotonation of the adjacent carbon centre under basic conditions enabling electrophilic attack of the stabilised α-carbanion, while conversely acting as a leaving group in other cases leading to nucleophilic substitution of the adjacent carbon centre. In limited cases these alternate reaction types can occur consecutively allowing for difunctionalisation of a single carbon centre, however with the exception of tertiary substituted carbons or conjugated substrates sufficiently activated towards nucleophilic attack, the α-carbanion based reaction pathways tend to predominate and thus constitute the majority of reported sulfone transformations. Alongside their propensity for engaging in dual modes of reactivity, the often crystalline and bench-stable nature of sulfone derivatives ensures trivial handling and purification.[111–115]

The oxidation of sulfides to form the corresponding sulfone product is a well-explored transformation for which several reagents have been discovered, with hydrogen peroxide and *m*-CPBA being particularly popular choices (**Scheme 7**). This approach has been successfully employed towards the synthesis of several medicinally-relevant compound libraries targeting a variety of disease states.[116–118] However despite such progress the majority of examples remain limited in scope due to the incompatibility of starting materials that possess oxidation sensitive functional groups.
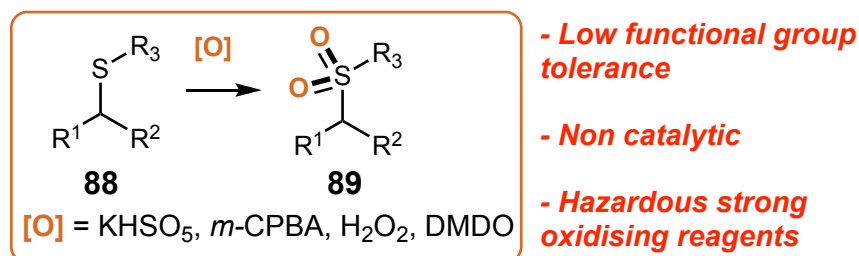
Scheme 7. *Traditional approach towards the synthesis of sulfones **89** via oxidation of corresponding sulfides **88**.*

Furthermore, super-stochiometric quantities of the oxidant are also typically required to afford the desired sulfones in high-yields in order to avoid formation of incomplete oxidation products such as sulfoxides. This negatively impacts the efficiency, atom economy, and ultimate environmental suitability of this approach, highlighting the necessity for more sustainable approaches towards the synthesis of sulfonylated compounds.[119–121] Another more general drawback regarding the application of this approach in organic synthesis is the need to form the C–S bond before subsequent oxidation to render the desired sulfone.[122] This not only requires the employment of
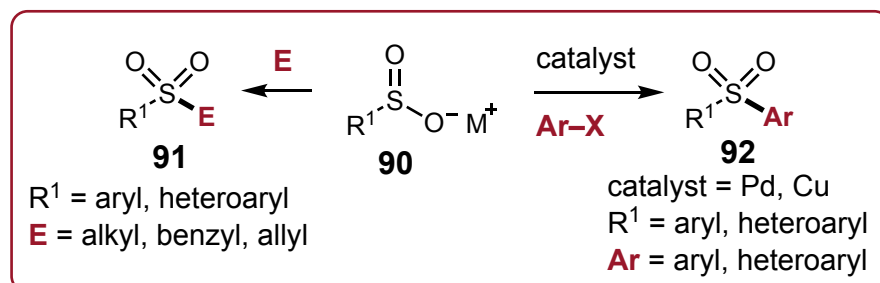
Scheme 8. *General approach towards the synthesis of sulfones **91** and **92** from sulfinate salt starting materials (**90**).*

odious and potentially toxic thiols as part of the synthetic process but also has a significant detrimental impact on the overall redox economy of the proposed synthetic route, imposing yet further restrictions on the practicality of this method.

Sulfinate salts are highly useful starting materials that have historically been employed in the synthesis of numerous classes of sulfur-containing compounds.[106] Furthermore, the development of bench-stable and crystalline SO_2 surrogate reagents has contributed to an ongoing revival in sulfinate salt chemistry by provision of more convenient reaction protocols.[123,124] The coupling of sulfinate salts (**90**) with carbon-based electrophiles remains one of the most common synthetic approaches towards sulfones **91** (**Scheme 8**). Further examples are available which showcase the utility of sulfinate salts as precursors to diaryl-sulfones (**92**) through transition-metal catalysed cross-coupling with aryl halides, and more recently *via* analogous metal-free couplings with diaryliodonium salts [125–129] Regarding the construction of $C(sp^3)$–SO_2 bonds however, possibilities remain restricted as only sufficiently activated alkyl-halides such as α-halogenated carbonyl compounds and benzyl bromides can typically undergo nucleophilic substitution.[130–132] Furthermore, the majority of sulfinate salt starting materials are generated *via* introduction of organometallic reagents to an appropriate SO_2 source generating stochiometric amounts of potentially hazardous metal waste in the process, they are also susceptible to unwanted oxidation forming non-reactive sulfonates.[106,133]

The employment of sulfonyl halides as electrophilic sulfur(VI) sources represents a substantial collection of reactions underpinning a wide-range of transformations.[134,135] The synthesis of sulfones and sulfonamides from sulfonyl halide starting materials is well-documented and provides methods complementary to those involving sulfinate salts, furthermore sulfonyl halides can be obtained by direct halogenation of the corresponding sulfinate salts- often *in situ*- allowing straightforward access to umpolung modes of reactivity.[106,123]

Scheme 9. *The coupling of sulfonyl halides (**93**) with carbon-centred nucleophiles including boronic acids and electron-rich aromatic coupling partners to generate sulfones **92** and **94**.*

Although the disconnection of sulfones *via* the coupling of readily attainable carbanion equivalents with sulfonyl halides appears to be a trivial one, the conventional non-catalytic employment of organometallic reagents is typically low yielding due to side reactions (**Scheme 9**).[136] In the majority of cases, the use of highly toxic organo-stannanes or difficult to prepare sulfonyl fluorides is necessary to obtain decent yields.[137–139] Lewis acid promoted Friedel-Crafts reactions constitute a direct alternative approach to aryl-sulfones, however a mixture of *ortho-* and *para*-substitution products are frequently obtained.[140–142] Several transition-metal catalysed approaches have been recently reported such as the cross coupling of sulfonyl chlorides with commercially available boronic acids, as well as more atom-efficient and regioselective C–H functionalisation processes.[143,144] Despite the clear progress, these methods remain united in their limitations as they require elevated reaction temperatures and are confined in their scope to the synthesis of electron-rich diaryl sulfones.

2.2.2. Photocatalytic Routes Towards Sulfones

The surge of photoredox catalysis procedures reported since the initial findings published over a decade ago has seen the emergence of a vast wealth of visible-light promoted synthetic methodologies capable of facilitating troublesome bond formations.[74,75,145] The recent development of photocatalytic sulfonylation reactions has endowed many of these aforementioned benefits towards the synthesis of sulfones. Notably permitting the construction of previously difficult $C(sp^3)$–SO_2 bonds utilising commercially available alkene (**96**) and alkyne (**97**) starting materials which readily undergo radical addition with a variety of sulfonyl sources (**Scheme 10**).[146–155]

R^1 = aryl, heteroaryl, alkyl
LG = M[+], DABCO, -NHNH$_2$, -OAr, -Cl, -CF$_3$
R^2 = H, aryl, heteroaryl, alkyl
R^3/R^4 = H, aryl, heteroaryl, alkyl
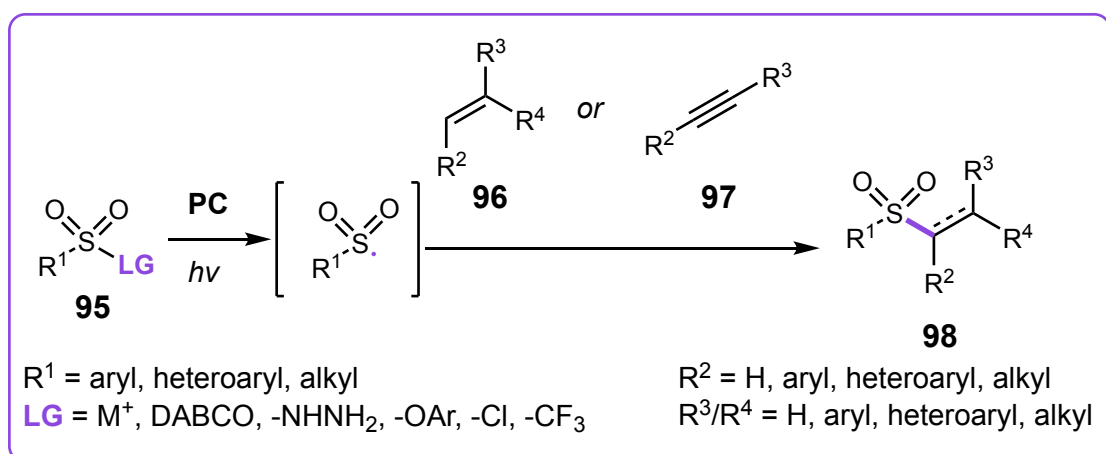
- Low temperatures and mild reaction conditions

- Wide range of efficient and non-toxic photocatalysts

- Straightforward construction of $C(sp^3)$–SO_2 bonds

Scheme 10. *General summary of photocatalytic sulfonylation procedures enabling access to sulfone scaffolds **98** via Giese-type addition of in-situ generated sulfonyl radicals from precursors **95** to alkene (**96**) and alkyne (**97**) coupling partners.*

Sulfonyl-hydrazones are highly versatile synthetic precursors that can be prepared readily from the corresponding commercially available ketones and aldehydes.[84] Previous procedures detailing the synthesis of sulfones from corresponding sulfonyl-hydrazones employ various transition-metal catalysts, proceeding *via* suspected diazo intermediates. This transformation was first reported by Zhang *et al.* employing a Ru(II) porphyrin-based catalyst, despite obtaining good yields at relatively low temperatures the reaction

is hampered by a narrow substrate scope and requires the use of highly toxic benzene as solvent under optimal conditions.[156] Later work by the groups of Barluenga and Yu were able to considerably expand the substrate scope of this procedure utilising $FeCl_3$ and CuI as catalysts respectively. However Barluenga's procedure requires the use of pyrophoric ethylmagnesium bromide as base, and furthermore both methods require high temperatures in order to furnish respectable yields of sulfones **100** (**Scheme 11**).[157,158]

Transition metal catalysed rearrangements:

14 examples, 40-76% yield

J. Barluenga et al. (2011)

$FeCl_3$ (cat.), EtMgBr, dioxane, 110 ºC

CuI (cat.), K_2CO_3, dioxane, 110 ºC

16 examples, 46-90% yield

X.W. Feng et al. (2010)

Photocatalytic rearrangement:

K_2CO_3, 9W blue lamp, $Ru(bpy)_3Cl_2$, $CHCl_3$/DMF (1:1), rt

11 examples, 30-46% yield

S. Parisotto et al. (2017)
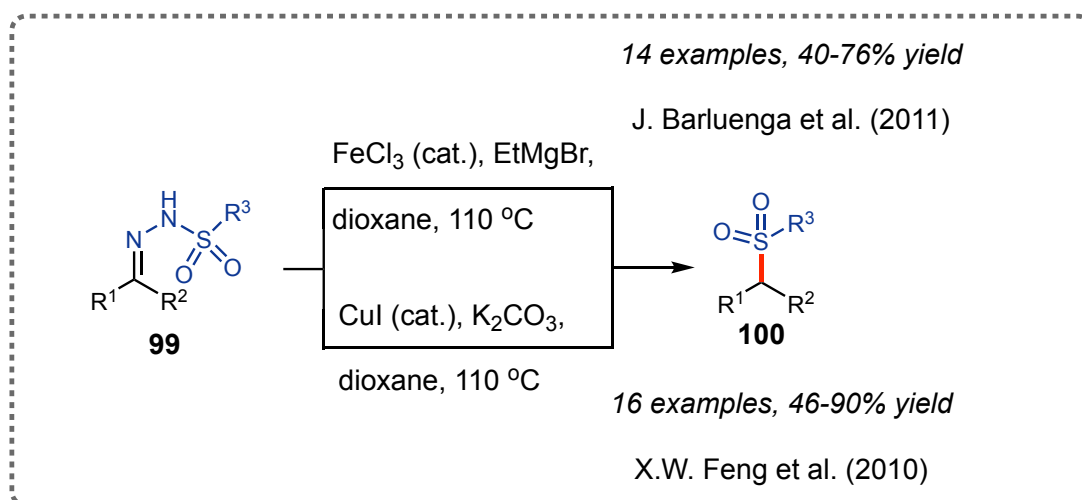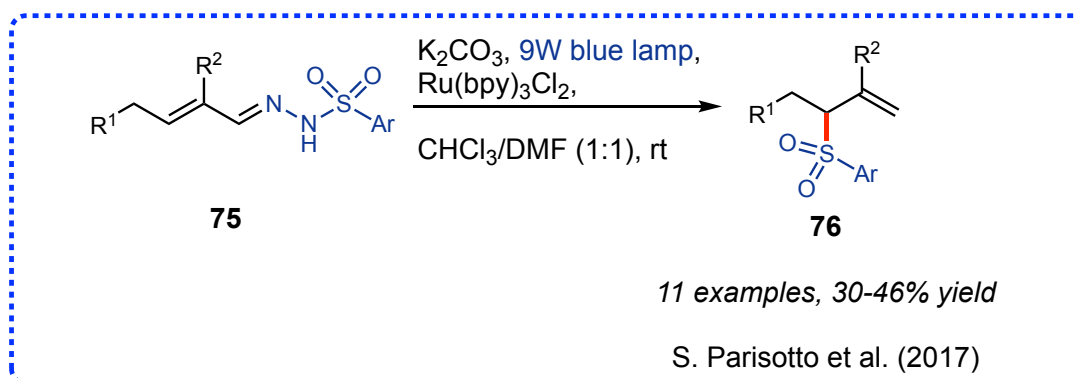
Scheme 11. *(Top) selected examples of sulfonyl-hydrazones (**99**) as precursors to sulfones (**100**) in transition metal catalysed rearrangement reactions. (Bottom) photocatalytic synthesis of α,β-unsaturated sulfones **76** from conjugated sulfonyl-hydrazone systems (**75**).*

More recently, photoredox-mediated single-electron transfer (SET) activation of hydrazone substrates has been explored as a means of accessing radical modes of reactivity alternate yet complementary to previously established heterolytic bond forming procedures, utilising considerably milder conditions and reagents. It was envisioned that

such photocatalysis methodologies could facilitate the formation of sulfones from sulfonyl-hydrazones under relatively mild conditions through some form of hydrazonyl radical rearrangement proceeded by expulsion of nitrogen and subsequent reincorporation of the sulfonyl moiety. The singular previously highlighted example by Parisotto *et al.* demonstrates this type of process, whereby α,β-unsaturated sulfonyl-hydrazones **75** were transformed into the corresponding allylic sulfones **76** *via* a suspected 1,5-radical shift under photoredox conditions.[93] Despite demonstrating the synthetic capability of such visible-light mediated approaches towards the construction of $C(sp^3)–SO_2$ bonds, the reaction exhibits poor yields of the desired sulfone products across a narrow scope of substrates.

2.2.3. *Photocatalytic Reaction Development*

Considering the promising performance of several aromatic sulfone derivatives noted throughout the *in silico* screening process (ZINC95080289, ZINC91695738, ZINC57478020, ZINC93714108, ZINC47645776, ZINC289626506, ZINC154138 and ZINC153751) the potential transformation of appropriate sulfonyl hydrazones into the corresponding sulfones utilising photocatalytic methodology was an appealing strategy for the generation of potential antibacterial compounds in a concise 3-step synthetic approach from commercially available starting materials (**Figure 27**).
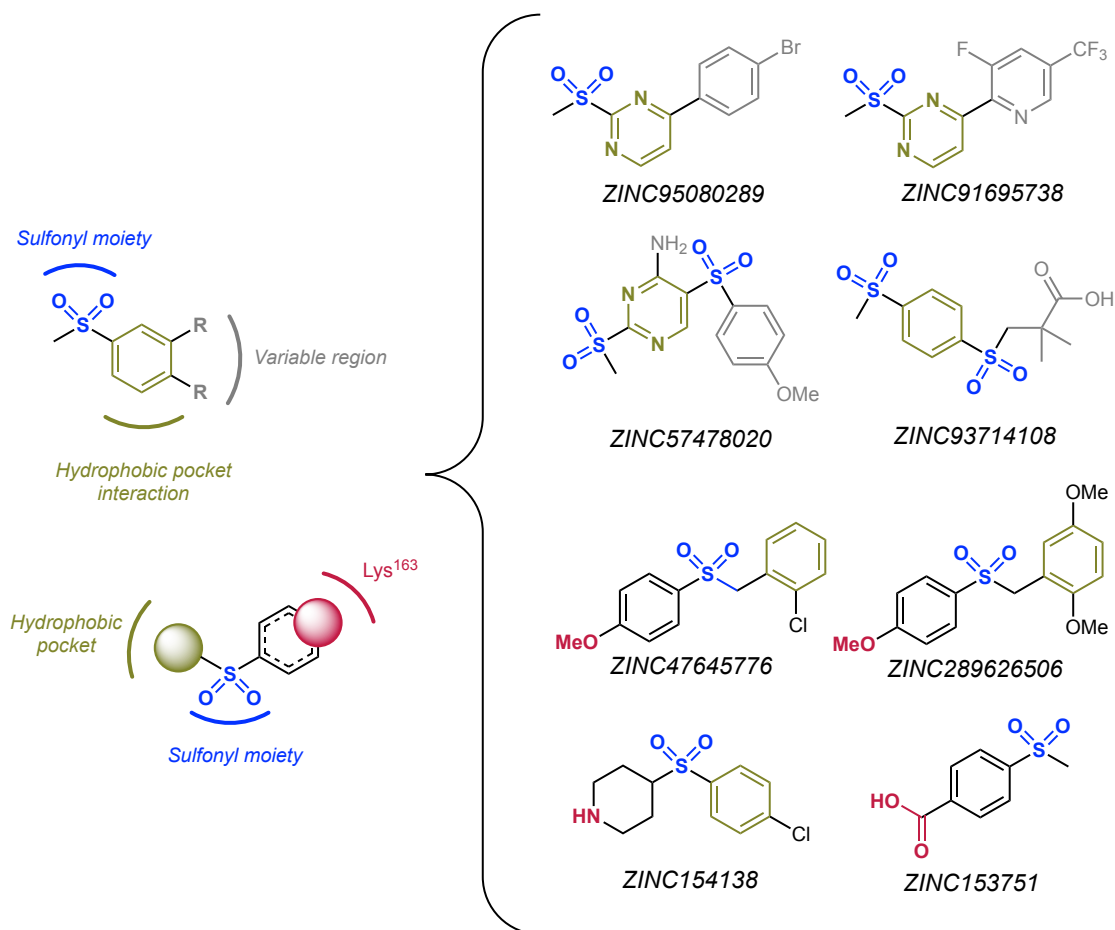
Figure 27. *Structures of aromatic sulfones ZINC95080289, ZINC91695738, ZINC57478020, ZINC93714108, ZINC47645776, ZINC289626506, ZINC154138 and ZINC153751 identified as hits via the in silico screening process, alongside overviews of the parent pharmacophores with the sulfonyl moieties highlighted in blue.*

Herein the synthesis of benzyl sulfone scaffolds from bench-stable and trivial to prepare sulfonyl-hydrazone starting materials is reported. This transformation is suspected to occur *via* an unprecedented photoredox-mediated radical rearrangement. The desired products were obtained in good to quantitative yields and the reaction displayed satisfactory functional group tolerance. Control experiments established the imperative role of base, photocatalyst and light as reaction components and further mechanistic studies were conducted to inform the proposed reaction mechanism, which suggests the reaction proceeds in a highly efficient and atom-economical manner through a key photoredox catalysed hydrogen atom transfer (HAT) propagation step.

2.2.4. _Photocatalytic Reaction Optimisation_

To commence the investigations, phenyl tosylhydrazone **101a**, caesium carbonate, 1,4-dinitrobenzene and Ru(bpy)$_3$Cl$_2$·6H$_2$O photocatalyst were irradiated with blue light (LEDs, ~470 nm) at 38 °C in dichloromethane overnight. Purification of the obtained crude product by flash column chromatography led to the recovery of sulfone **102a** in 16% yield (**Table 2**, entry 1). Other chlorinated solvents gave equally poor yields, and the employment of protic solvents gave only trace yields of the desired product (**Table 2**, entry 2–7). With the exception of tetrahydrofuran (THF), improved yields were obtained utilising polar aprotic solvents in particular dimethylformamide (DMF) which furnished the product **2a** in 39% yield (**Table 2**, entry 8–11). A subsequent screen of oxidants found that only dinitrobenzene derivatives afforded the desired sulfone in observable yields (**Table 2**, entry 12–16). 1,4-Dinitrobenzene initially offered the most promise as an oxidant, as expected due to its greater reduction potential and faster quenching rate for Ru(bpy)$_3^{2+}$ compared to the _ortho_ and _meta_ isomers.[159] However, the propensity for 1,4-dinitrobenzene to undergo nucleophilic aromatic substitution was deemed a potential liability capable of hindering catalytic turnover and propagating unwanted side reactions. 1,3-Dinitrobenzene was therefore selected moving forward with the hopes of facilitating more straightforward reaction optimisation.[160]

Table 2. *Optimisation of reaction conditions for photoredox catalysed rearrangement of tosylhydrazone **101a** to sulfone **102a**[a]*
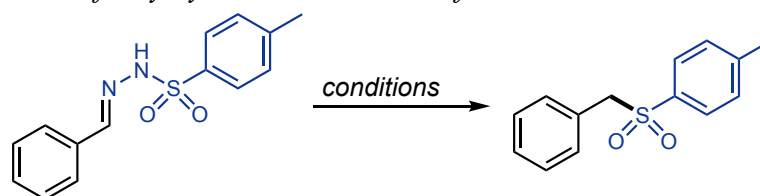
Entry	Solvent	Base	Oxidant	Yield (%)[b]
1	CH$_2$Cl$_2$	Cs$_2$CO$_3$ (1.5 equiv)	1,4-DNB	16[c]
2	CHCl$_3$	Cs$_2$CO$_3$ (1.5 equiv)	1,4-DNB	20
3	1,2-DCE	Cs$_2$CO$_3$ (1.5 equiv)	1,4-DNB	17
4	MeOH	Cs$_2$CO$_3$ (1.5 equiv)	1,4-DNB	trace
5	EtOH	Cs$_2$CO$_3$ (1.5 equiv)	1,4-DNB	trace
6	*i*-PrOH	Cs$_2$CO$_3$ (1.5 equiv)	1,4-DNB	trace
7	H$_2$O	Cs$_2$CO$_3$ (1.5 equiv)	1,4-DNB	trace
8	1,4-dioxane	Cs$_2$CO$_3$ (1.5 equiv)	1,4-DNB	30
9	THF	Cs$_2$CO$_3$ (1.5 equiv)	1,4-DNB	10
10	MeCN	Cs$_2$CO$_3$ (1.5 equiv)	1,4-DNB	26
11	DMF	Cs$_2$CO$_3$ (1.5 equiv)	1,4-DNB	39
12	DMF	Cs$_2$CO$_3$ (1.5 equiv)	1,2-DNB	14
13	DMF	Cs$_2$CO$_3$ (1.5 equiv)	1,3-DNB	17
14	DMF	Cs$_2$CO$_3$ (1.5 equiv)	CBr$_4$	trace
15	DMF	Cs$_2$CO$_3$ (1.5 equiv)	CCl$_3$Br	trace
16	DMF	Cs$_2$CO$_3$ (1.5 equiv)	CHI$_3$	trace
17	DMF	K$_2$CO$_3$ (1.5 equiv)	1,3-DNB	44
18	DMF	KHCO$_3$ (1.5 equiv)	1,3-DNB	67
19	DMF	NaHCO$_3$ (1.5 equiv)	1,3-DNB	58
20	DMF	CsHCO$_3$ (1.5 equiv)	1,3-DNB	66
21	DMF	NaOH (1.5 equiv)	1,3-DNB	trace
22	DMF	CsOH·H$_2$O (1.5 equiv)	1,3-DNB	40
23	DMF	CsOAc (1.5 equiv)	1,3-DNB	52
24	DMF	KOAc (1.5 equiv)	1,3-DNB	46
25	DMF	NaOAc (1.5 equiv)	1,3-DNB	59
26	DMF	NaOPiv (1.5 equiv)	1,3-DNB	68
27	DMF	KOPiv (1.5 equiv)	1,3-DNB	71
28	DMF	CsOPiv (1.5 equiv)	1,3-DNB	66
29	DMF	CsTFA (1.5 equiv)	1,3-DNB	trace
30	DMF	CsF (1.5 equiv)	1,3-DNB	73
31	DMF	CsCl (1.5 equiv)	1,3-DNB	trace
32	DMF	CsBr (1.5 equiv)	1,3-DNB	trace
33	DMF	CsI (1.5 equiv)	1,3-DNB	trace
34	DMF	CsF (2.0 equiv)	1,3-DNB	88
35	**DMF**	**CsF (2.0 equiv)**	**–**	**94**
36	DMF	–	–	0
37[d]	DMF	CsF (2.0 equiv)	–	0
38[e]	DMF	CsF (2.0 equiv)	–	0
39[f]	DMF	CsF (2.0 equiv)	–	88
40[g]	DMF	CsF (2.0 equiv)	–	61

[a] *Reaction conditions:* **101a** *(0.25 mmol), Ru(bpy)₃Cl₂·6H₂O (2.5 μmol), base, oxidant (0.375 mmol) sealed tube under inert atmosphere, degassed solvent (5 mL) added dropwise, 38 °C, blue LEDs (~470 nm), 20 hrs.* [b] *Yields determined by ¹H NMR (±5%) unless stated otherwise.* [c] *Isolated yield.* [d] *No photocatalyst.* [e] *Reaction conducted in darkness.* [f] *Non-degassed DMF.* [g] *Reaction performed in air.*

An extensive screen of potential bases was performed as previous reactions of sulfonyl-hydrazones have demonstrated the substantial importance of both the base pK_{aH} and metal counter-ion in facilitating reaction success.[83] The use of hydrogen carbonate bases led to moderate improvements in yield compared to the corresponding carbonates (**Table 2**, entry 17–20). Conversely however, the employment of higher pK_{aH} bases such as caesium and sodium hydroxide resulted in poorer yields (**Table 2**, entry 21 & 22). With this observation in mind it was postulated that relatively weaker bases would provide improved yields, hence numerous acetate and pivalate alkali metal salts were evaluated for their impact on reaction performance (**Table 2**, entry 23–28). Pleasingly, fair to good yields were obtained using the latter-mentioned bases rising to 71% in the case of potassium pivalate. A further improvement was observed utilising caesium fluoride providing the desired sulfone in 73% yield. However considerably weaker bases such as caesium iodide, bromide, chloride and trifluoroacetate salts resulted in only trace amounts of product being obtained, likely due to their inability to deprotonate the hydrazone starting material (**Table 2**, entry 29–33).

Increasing the stochiometric amount of caesium fluoride led to a further improvement in yield, and with seemingly optimal conditions achieved the focus shifted to the undertaking of control experiments (**Table 2**, entry 34). Surprisingly, it was found that exclusion of the dinitrobenzene oxidant afforded the product in 94% yield proving to be superior to all previous endeavours, however the remaining control experiments proceeded as expected establishing the need for base, photocatalyst and light to achieve reaction success (**Table 2**, entry 35–38). The reaction was carried out using non-degassed solvent and in the presence of air respectively, both resulted in decreased yields and thus discounting the potential involvement of oxygen as a surreptitious oxidant of the Ru(bpy)$_3^{2+}$ photocatalyst (**Table 2**, entry 39 & 40).

A small screen of different photocatalysts was undertaken to determine the possibility of developing tandem protocols to attain improved generality regarding reaction conditions. Disappointingly, the employment of Ir(ppy)$_3$ (**103**) under the established conditions led to only trace amounts of sulfone product, with the majority of starting material **101a** remaining unconsumed (**Table 3**, entry 2). Furthermore, the utilisation of established organic photoredox catalysts such as Eosin Y (**104**) and Rose Bengal (**105**) under either

blue or green light irradiation resulted in no observable conversion of the tosylhydrazone substrate (**Table 3**, entry 3–5).

Table 3. *Effect of photocatalyst choice on the conversion of **101a** to sulfone **102a** with structures of Ir(ppy)₃ (**103**), Eosin Y (**104**) and Rose Bengal (**105**) shown.*

CsF (2.0 equiv),
Photocatalyst (1.0 mol%),

DMF, 38 °C, 20 hrs,
Blue LEDs (~470 nm)

101a **102a**
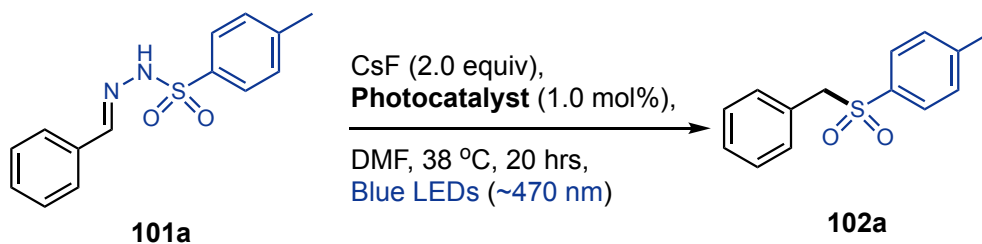
Entry	Photocatalyst	Yield (%)[a]
1	Ru(bpy)₃Cl₂.6H₂O	94
2	Ir(ppy)₃	Trace
3	Eosin Y	No conversion
4[b]	Eosin Y	No conversion
5[b]	Rose Bengal	No conversion

[a] Yields determined by ¹H NMR (±5%). [b] Irradiated with green LEDs (~525 nm).

fac-Ir(ppy)₃
103

Eosin Y
104

Rose Bengal
105
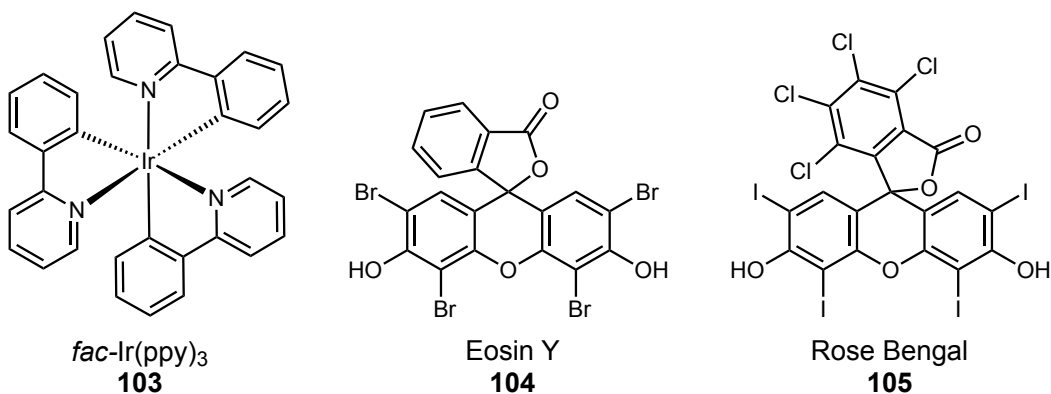
Lastly, the employment of alternative fluoride ion sources and their consequent impact on reaction yield was investigated. With the exception of caesium fluoride and potassium fluoride dihydrate, no reaction was seen to occur in the presence of other alkali and transition metal fluorides most likely due to their poor solubility in organic solvents (**Table 4**, entry 1–6). However, the use of an entirely organic fluoride source in the form of TBAF was found to provide the desired product in reasonable yield (**Table 4**, entry 7).

Table 4. *Influence of fluoride counter-cation on the yield of sulfone product **102a***

XF$_n$ (2.0 equiv),
Ru(bpy)$_3$Cl$_2$·6H$_2$O (1.0 mol%),

DMF, 38 °C, 20 hrs,
Blue LEDs (~470 nm)

101a

102a
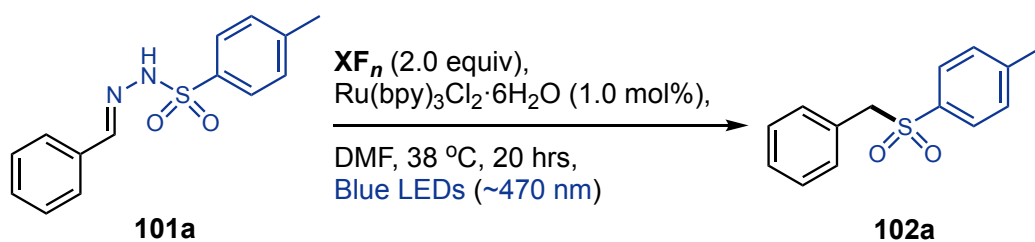
entry	fluoride source	yield (%)[a]
1	LiF	0
2	NaF	0
3	KF·2H$_2$O	79
4	**CsF**	**94**
5	AgF$_2$	0
6	ZnF$_2$	0
7	TBAF[b]	40

[a] *Yields determined by ^{1}H NMR (±5%).* [b] *Tetra-butylammonium fluoride added dropwise (0.5 mL) as 1.0 M THF solution.*

2.2.5. *Photocatalytic Reaction Substrate Scope*

With optimised reaction conditions in hand, the scope of the transformation was explored beginning with the sulfonyl segment of the starting material. Previously reported reactions of sulfonyl-hydrazones have illustrated the impact of electronic and steric effects arising from adjacent moieties, and their subsequent influence over the sulfonyl group as important factors in dictating the reaction pathway and consequent reaction rate.[82,84,157] *Para*-substituted phenyl rings possessing weak electron donating or withdrawing groups and strong electron donating groups were shown to be well tolerated and the desired sulfones were obtained in good to quantitative yields (**102a—102c, 102i**) with the notable exception of the *para*-acetamide derivative (**102d**) which was afforded in considerably lower yield (**Scheme 12**). As a comparatively more hydrophilic product, this anomaly could be due to ill-suited workup and purification conditions despite best attempts to render them optimal. Alternatively the reduced yield could arise from the ability of amides to undergo competing photoredox catalysed transformations.[161]

A substrate bearing a relatively electron rich heterocyclic thiophene group led to isolation of the desired product (**102ea**) in reasonable yield after purification, alongside an additional debrominated sulfone side product (**102eb**) in 20% yield. Furthermore, both cyclopropyl and methyl sulfonyl derivatives (**102f, 102g**) were obtained in very good yields despite the propensity for unwanted side reactions such as nucleophilic ring opening, deprotonation and nucleophilic substitution to occur under the relatively basic reaction conditions. In employing the *para*-nitrosulfonyl substrate only trace amounts of product (**102h**) were obtained as part of a complex mixture of products. This dramatic reduction in yield is likely due to the aforementioned interferences arising between nitro-aromatic species and the $Ru(bpy)_3^{2+}$ photocatalyst.[159]
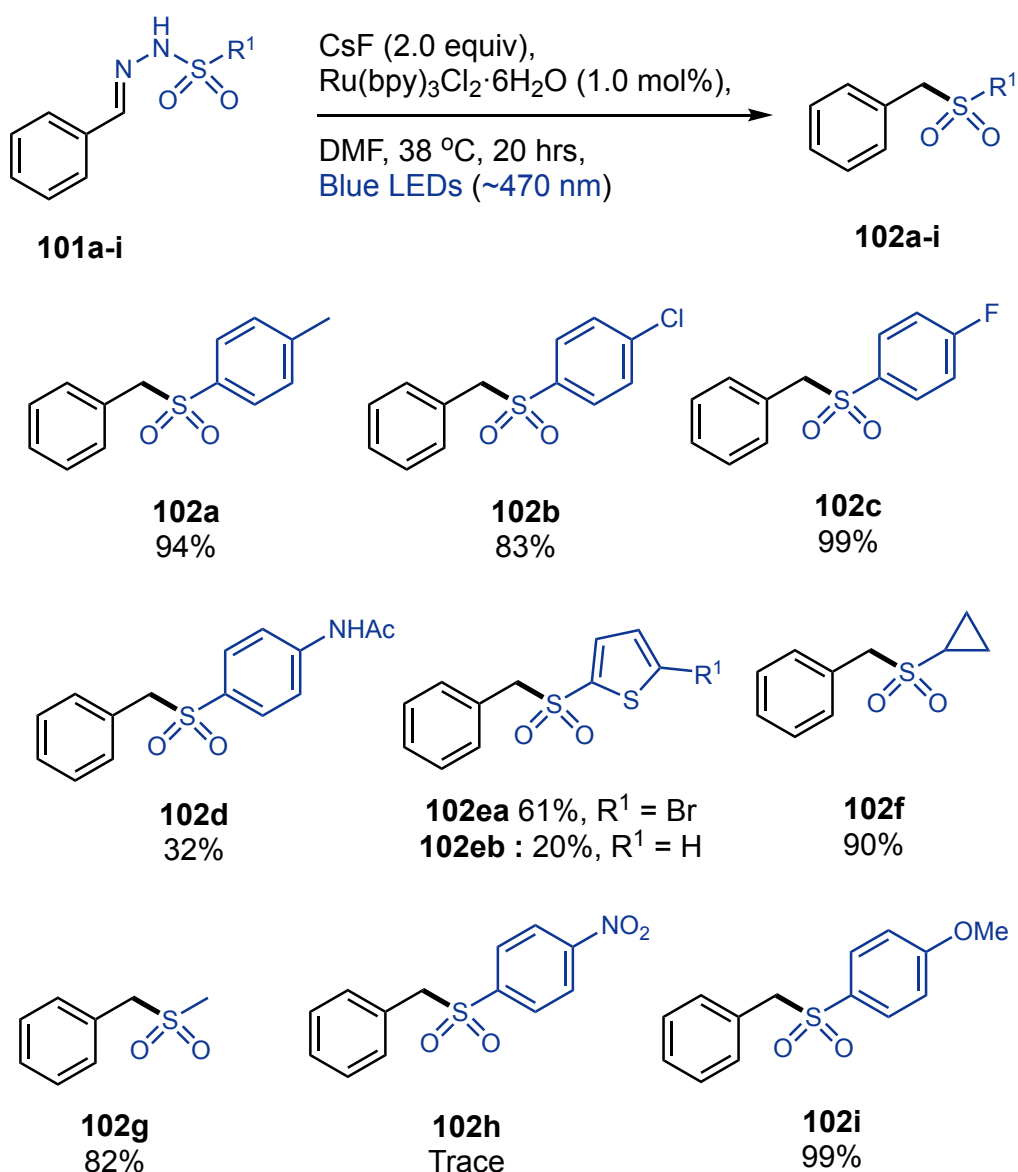
Scheme 12. *Isolated yields of phenylmethyl sulfones (**102a-i**) from the corresponding sulfonyl-hydrazone substrates (**101a-i**).*

Given the impressive yield achieved with the *para*-methoxyphenyl derivative (**102i**) and the ease of synthesis associated with such hydrazones it was adopted as the model sulfonyl group for substrate scope exploration around the *N*-benzylidene fragment of the molecule. Pleasingly the reaction was seen to tolerate a wide variety of *para*-substituted substrates comprised of both electron-rich (**102j**) and relatively electron poor (**102k, 102s**) ring systems, with the desired sulfones isolated in good to quantitative yields (**Scheme 13**). High yields were also obtained for *para*-halogenated species, (**102l, 102n, 102r**) noteworthy functional handles for allowing further structural elaboration. Similarly, *ortho*-substituted sulfones (**102m, 102o–102q**) were obtained in good to excellent yields, despite the increased obtrusion of steric hindrance. Despite these

74

successes there were several cases in which the reaction was determined to be non-viable, as aromatic substrates bearing strong electron donating groups, (**102t, 102u**) heterocyclic (**102v**) and non-aromatic substrates (**102w**) all provided the desired product in only trace amounts when employed. It was speculated that such sensitivity to electronic effects pointed towards the involvement of a carbon-centred benzylic radical reaction intermediate, which would be expected to be sensitive to substituent instigated mesomeric effects. Electron donating groups would be anticipated to destabilise benzylic radical species by interfering with unpaired electron delocalisation throughout the aromatic ring. For similar reasons the proposed radical intermediate would also account for the lack of reactivity observed for non-aromatic substrates, as the unconjugated aliphatic radical is likely to be significantly less stable in comparison to derivatives possessing adjacent electron-withdrawing π systems.
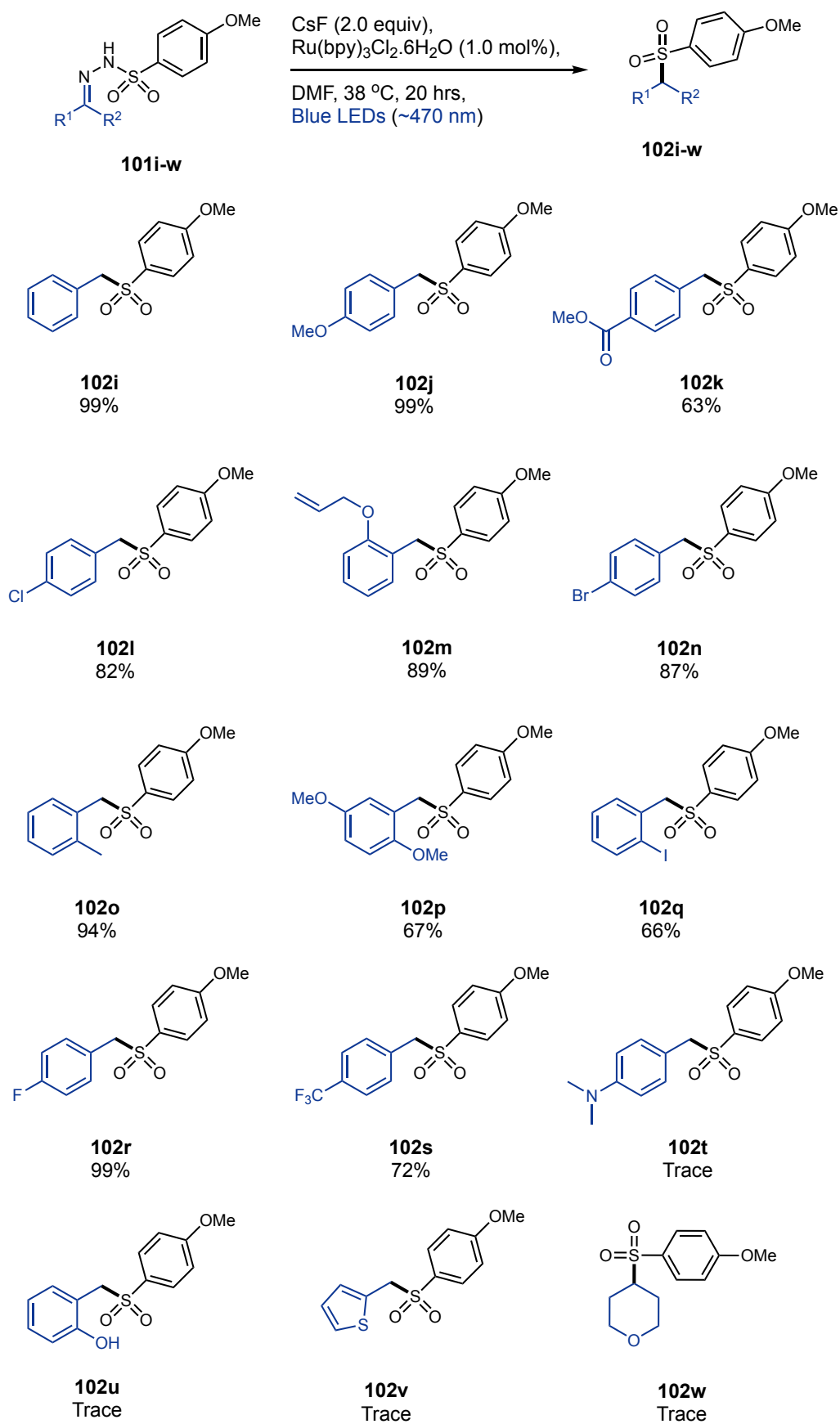
Scheme 13. *Isolated yields of sulfones **102i-w** obtained from various 4-methoxyphenyl-sulfonyl hydrazone starting materials.*

2.3. *Mechanistic Studies of Photoredox Catalysed Sulfone Synthesis*

2.3.1. *Radical Trap Experiments*

Given both the novel nature of the reaction and the relatively narrow substrate scope demonstrated, it was decided to investigate the reaction mechanism in order to ascertain potential approaches towards improving the reaction in future studies. Firstly, radical trapping studies utilising TEMPO (**106**) and diphenyl disulfide (**107**) were undertaken in an effort to isolate reactive intermediates, however both attempts yielded complex mixtures of products from which no clear hydrazone derivatives could be identified. However it was clear from the NMR spectra obtained that formation of sulfone product was completely inhibited, suggesting the presence of a radical mechanism (**Scheme 14**).
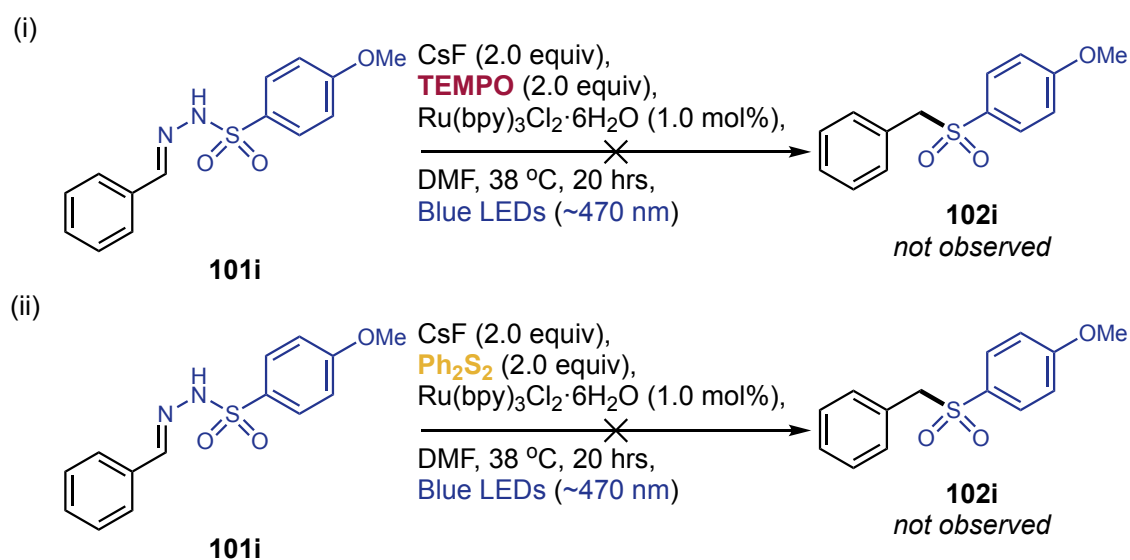
Scheme 14. *Radical trapping experiments of sulfonyl-hydrazone 101i utilising (i) TEMPO (106) and (ii) diphenyl disulfide (107) reagents.*

Both radical traps **106** and **107** have been employed previously in the investigation of photocatalytic reaction mechanisms, as they are relatively stable reagents and not reported to undergo degradation or engage in catalyst poisoning under typical photoredox conditions.[65,162] TEMPO (**106**) can be redox active and participate in competitive modes

of reactivity especially with the excited states of photocatalysts, however there are numerous reported examples of it being employed successfully to identify photocatalytic reaction intermediates.[89,162] Although the isolation and characterisation of radical trap adducts formed over the course of a reaction is preferable in determining underlying mechanistic details, numerous prior reports state the absence of anticipated reaction products in the presence of such trapping reagents as sufficient evidence to imply the presence of a radical mechanism.[163–165]

2.3.2. *Deuterium Labelling Study*

Next efforts were made to uncover details concerning formation of the benzylic sp^3-carbon centre. It was originally suspected that saturation ensued *via* a hydrogen atom transfer (HAT) step occurring between a photocatalytically generated carbon-centred hydrazonyl radical and the DMF solvent. Several prior examples highlight the ability of DMF and related solvents to act as hydrogen atom donors under photoredox conditions, as the multitude of relatively labile hydrogens capable of undergoing radical cleavage makes it an ideal participant for HAT processes.[88] This proposition was tested by performing the reaction employing deuterated DMF-d_7 as solvent, surprisingly no deuterium incorporation into the final sulfone product of hydrazone **101i** was observed by ^1H NMR analysis, signified by the absence of both the expected 1H integral value corresponding to the lone benzylic hydrogen and a 1:1:1 triplet splitting pattern indicative of J_{HD} coupling (**Scheme 15**).
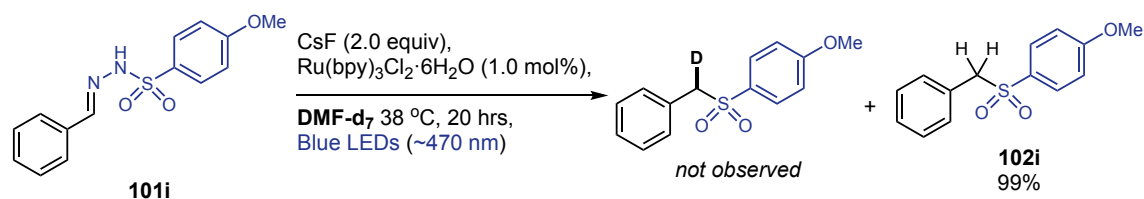
Scheme 15. *Isolated yield of sulfone products obtained from the reaction of sulfonyl-hydrazone **101i** in the presence of deuterated DMF solvent.*

2.3.3. Nucleophilic Cross-over Study

With the radical character of the reaction established, the focus shifted towards uncovering the mechanistic aspects concerning incorporation of the sulfonyl moiety. A nucleophilic cross-over experiment was performed in which two sulfonyl-hydrazone substrates bearing distinct functional groups on both the benzylic and sulfonyl ring portions of the molecules (**101r, 101x**) were subjected to the reaction conditions together (**Scheme 16**).
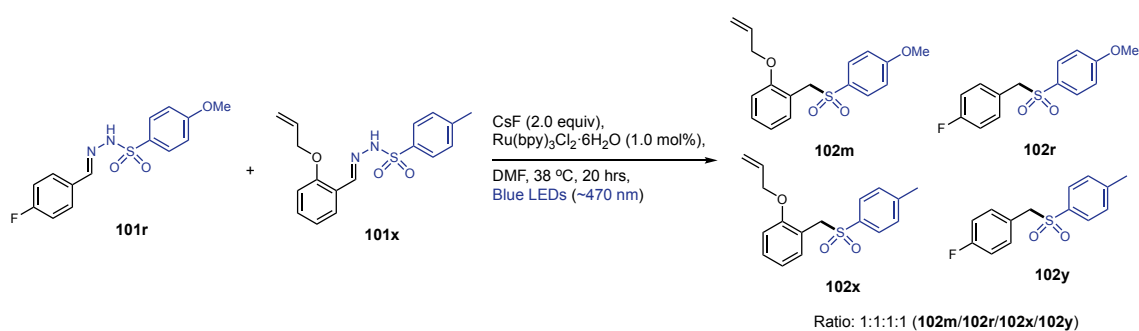
Scheme 16. *Relative yields of sulfone products* **102m**, **102r**, **102x** *and* **102y** *derived from binary mixture of sulfonyl-hydrazone substrates* **101r** *and* **101x**.

Crossover of the sulfonyl groups was clearly observed by ^{1}H NMR analysis of the crude product mixture due to the even distribution of sulfones detected, with four readily distinguishable methyl peaks at 2.37 (**102x**), 2.41 (**102y**), 3.81 (**102m**) and 3.85 (**102r**) δ/ppm possessing near identical values of integration (**Scheme 17**). Furthermore, close inspection of the spectrum in the 4.2–4.5 δ/ppm range shows the presence of four distinct albeit overlapping benzylic sulfone peaks. Such product distribution suggests the presence of an open transition state likely in the form of a step-wise S_N1 type reaction, as opposed to a concerted process whereby the expulsion of nitrogen gas and sulfonyl addition take place in a coordinated manner. This finding also complements the observed pattern of reactivity, as stabilisation of the benzylic cation in aromatic substrates *via* resonance is likely to further increase the feasibility of the preceding dissociation step.
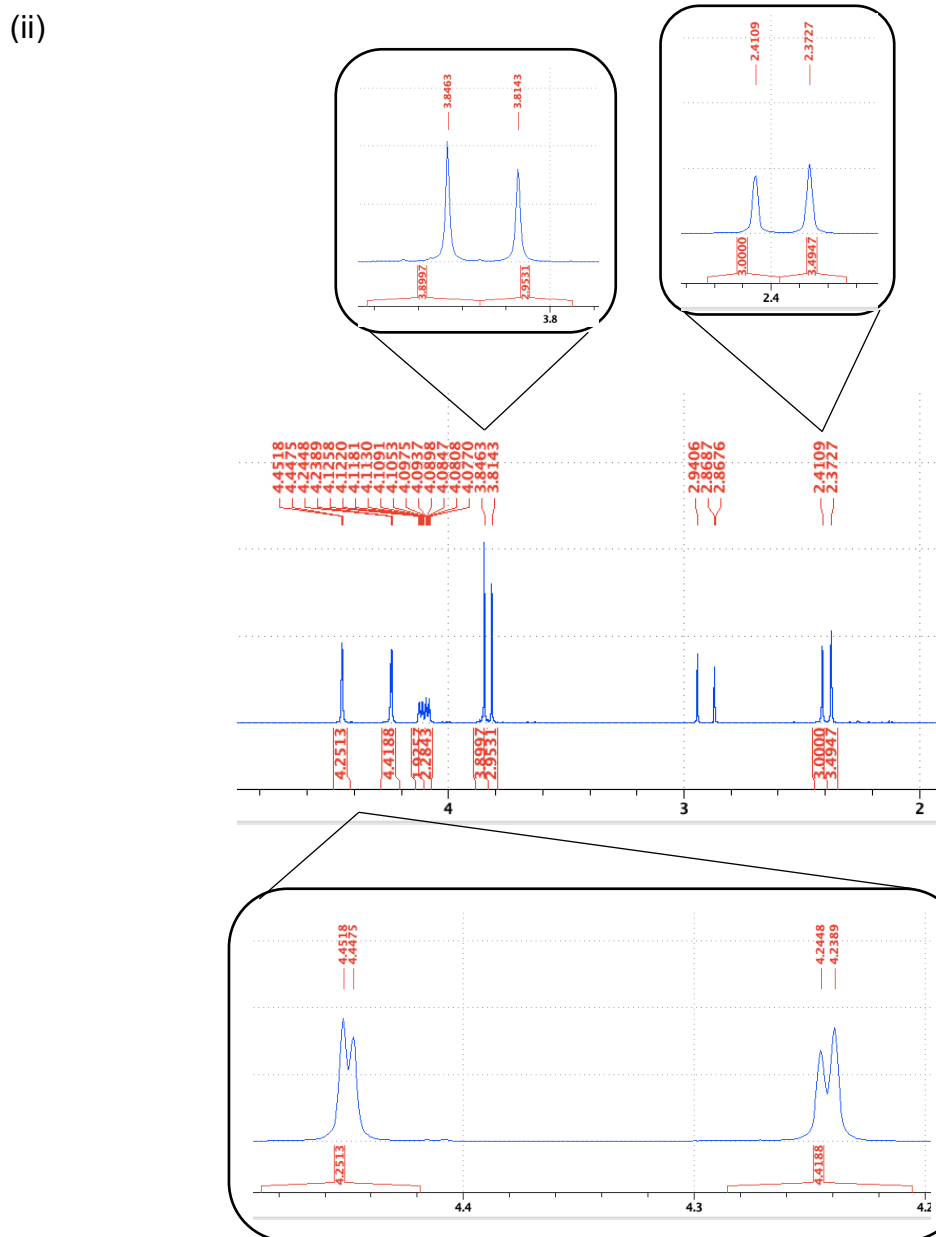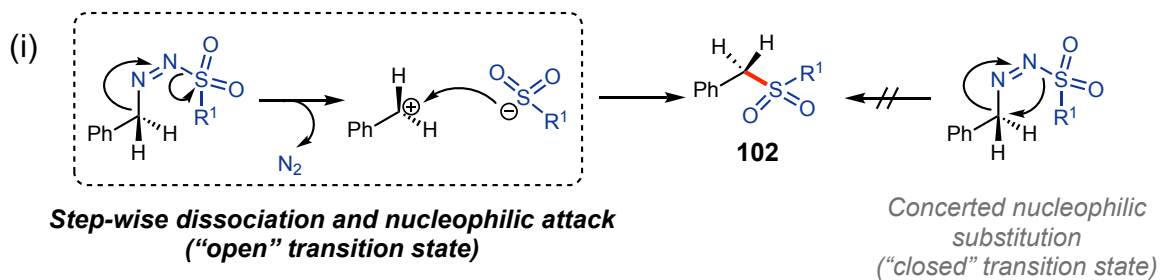
Scheme 17. *(i) Comparison of the suspected open transition state operating in the formation of sulfones **102** and the alternative concerted mechanism (closed transition state). (ii) ^1H NMR spectrum of the product mixture obtained from the reaction of **101r** and **101x** showing stoichiometrically equivalent formation of sulfone products **102m**, **102r**, **102x** and **102y** supporting operation of an open transition state.*

2.3.4. _Time Dependent ^{1}H NMR Reaction Monitoring_

In an attempt to discern further details regarding the mechanism, the reaction of substrate **101a** was monitored by ^{1}H NMR at various timepoints between periods of irradiation in order to identify potential intermediates. Comparison of the spectra clearly displays formation of the desired product (**102a**) denoted by the emergence of a singlet peak at 2.43 δ/ppm within 2-5 minutes of the initial irradiation, and the ensuing increase in intensity of the peak witnessed thereafter (**Figure 28**).
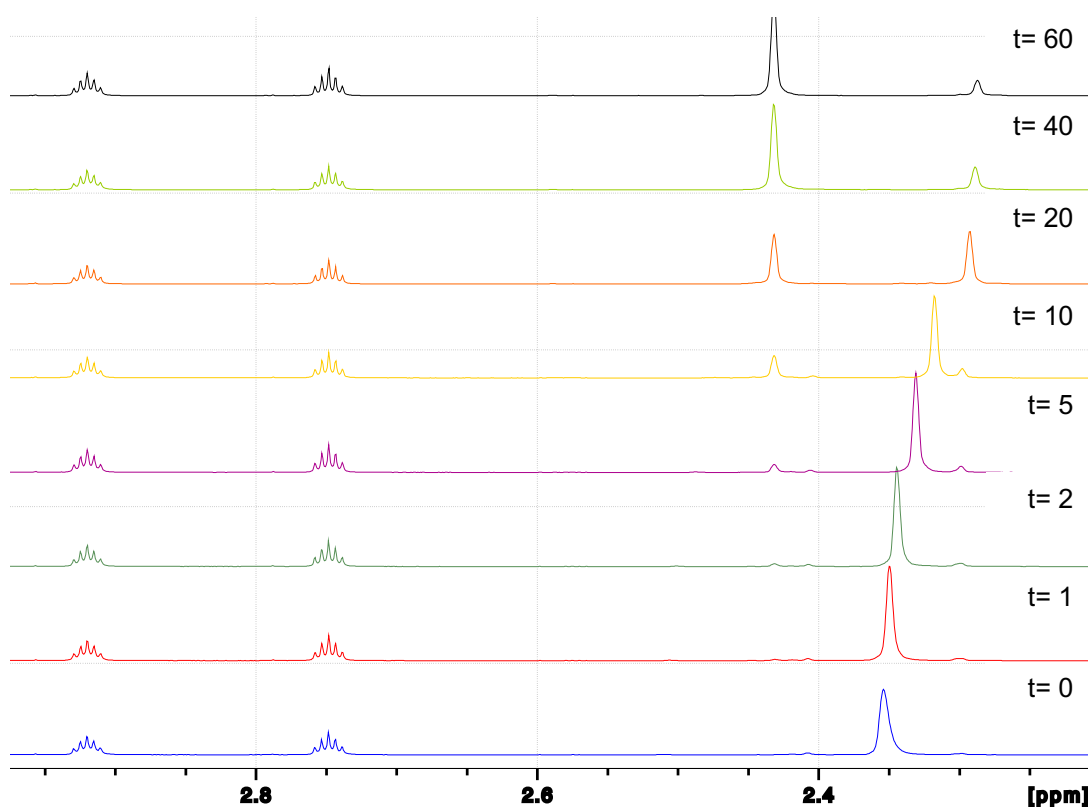
Figure 28. _^{1}H NMR collated spectra of reaction monitoring experiment utilising substrate **101a**. ^{1}H NMR performed at 38 °C and spectra collected at time (mins) stated in top right corners, reaction conditions: 0.025 mmol **101a**, CsF (2.0 equiv), Ru(bpy)$_3$Cl$_2$·6H$_2$O (1.0 mol%), DMF-d$_7$ (0.5 mL), blue LEDs (~470 nm), 38 °C, sealed NMR tube; 2.25–2.95 ppm region showing starting material peaks (**101a**), product **102a** and sulfonyl anion intermediate peaks alongside trace DMF peaks._

The singlet peak at 2.35 δ/ppm, corresponding to the methyl group of the tosyl-hydrazone starting material underwent a steady decline in intensity as expected, however the peak was also subjected to a significant upfield shift to ~2.29 δ/ppm over the course of the reaction. It is suspected that this change corresponds to the dissociation of the sulfonyl group leading to formation of a proposed sulfonyl anion intermediate _via_ cleavage of the

N–S bond. The transfer of electron density from the former bonding orbital to the sulfur centre is anticipated to result in alleviation of the electron withdrawing effects acting upon the *para*-situated methyl group, relative to the parent sulfonyl-hydrazone.
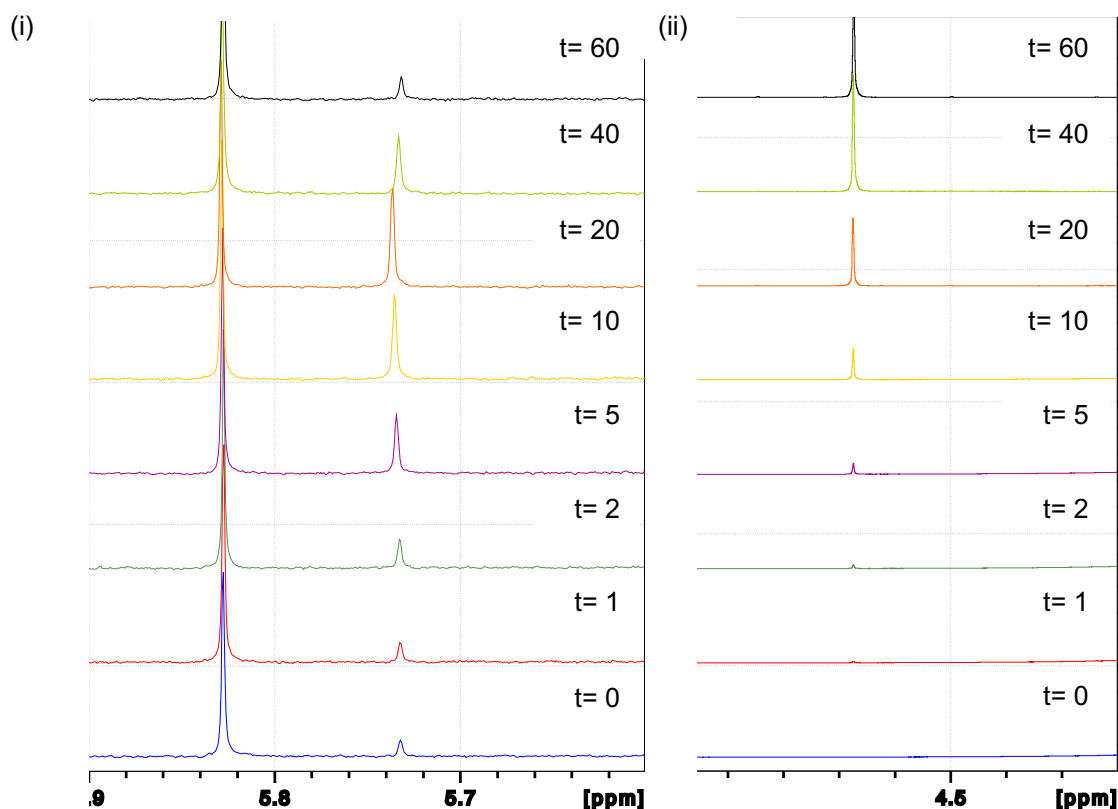
Figure 29. *¹H NMR collated spectra of reaction monitoring experiment utilising substrate **101a**. ¹H NMR performed at 38 °C and spectra collected at time (mins) stated in top right corners, reaction conditions: 0.025 mmol **101a**, CsF (2.0 equiv), Ru(bpy)₃Cl₂·6H₂O (1.0 mol%), DMF-d₇ (0.5 mL), blue LEDs (~470 nm), 38 °C, sealed NMR tube (i) 5.62–5.88 ppm region showing proposed diazonium cation intermediate peak at 5.76 δ/ppm the adjacent 5.83 δ/ppm peak did not change in intensity throughout the observed reaction period, (ii) 4.20–4.90 δ/ppm region showing the peak at 4.76 δ/ppm corresponding to the a-sulfonyl CH₂ of product **102a** (the intensities/scaling of (i) and (ii) is not equilibrated).*

Formation of the desired sulfone product over the course of the observed reaction timescale was confirmed by the steady emergence of the singlet peak at 4.76 δ/ppm (**Figure 29**). Examination of the spectra at higher relative intensities led to the discernment of a singlet peak at 5.76 δ/ppm, which was seen to increase in magnitude before receding at the 40-minute mark. Considering the relatively low concentration and regressive nature of the peak in question as well as its absence from the spectra of the starting material and sulfone product, alongside the caveat that it was only observed when the reaction was monitored under stringent anaerobic conditions this suggests that it

corresponds to a somewhat unstable reaction intermediate. Several phenyl-diazo compounds have been observed to exhibit benzylic resonance peaks within the 4–7 δ/ppm region of proton NMR spectra, therefore it is suspected that the observed singlet peak at 5.76 δ/ppm corresponds to a diazo intermediate formed after dissociation of the sulfonyl moiety.[166–171]

2.3.5. *DFT Calculations and Proposed Reaction Mechanism*

Density functional theory (DFT) calculations of the rearrangement of **101i** were undertaken in an attempt to further uncover details pertaining to the reaction mechanism.[172,173] Deprotonation of the sulfonyl-hydrazone starting material (**D**) by caesium fluoride and subsequent single-electron oxidation by $Ru(bpy)_3^{2+}$, generating the N-centred radical species **F** was determined to occur feasibly as suspected (**Figure 30**). The next step entailed dissociation of the *p*-methoxysulfonyl anion, with stabilisation of the resultant diazo π-radical (**G**) *via* conjugation alongside entropic compensation arising from molecular fragmentation enabling progression along the reaction co-ordinate. Resonance transition of the radical to the benzylic carbon centre leads to formation of intermediate **H** which partakes in the HAT step involving the starting material **D**, represented by the rate-determining transition state **TS$_{H-I}$** situated at the apex of the computed potential energy surface. Procession from this relatively high-energy transition state by way of unstable diazo cation **I** occurs with concomitant generation of the rate determining intermediate radical **F**, resulting in propagation of a supposed chain mechanism. Decomposition of intermediate **I** to form benzyl cation **J** with expulsion of nitrogen was calculated to proceed in a highly exergonic manner ($\Delta G = -33.0$ kcal mol^{-1}). A similar case was conceived for the final step involving nucleophilic attack of the sulfonyl anion with a further sharp decrease in potential energy ($\Delta G = -51.3$ kcal mol^{-1}), it has previously been shown that the relative stability of sulfones facilitates their selective generation *via* C–S bond formation over the corresponding sulfinic ester functional isomer (C–O bond formation).[157,174,175]
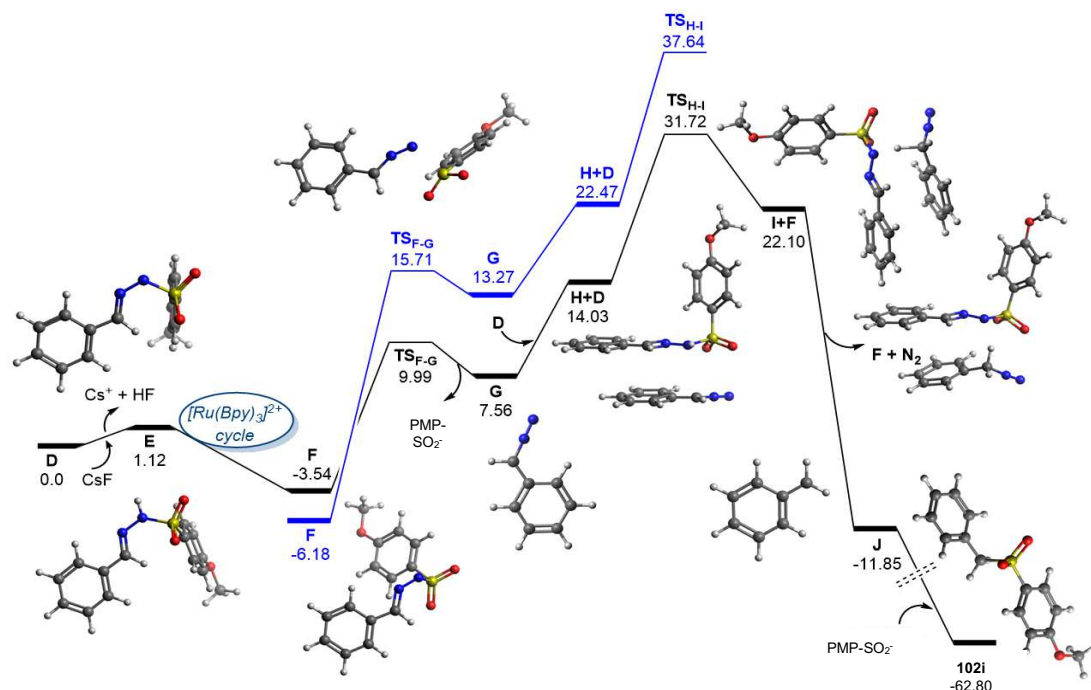
Figure 30. *DFT computed reaction profile for the transformation of sulfonyl-hydrazone **101i** (**D**) into sulfone **102i** with the energy level of species **D** taken as a reference (0.0 kcal mol⁻¹), blue line denotes DFT computed potential energy levels of sulfonyl-hydrazone **101w**.[166, 167]*

Calculations involving non-stabilised derivative **101w** (blue line, **Figure 27**) revealed that the expected hydrazonyl radical species **F** was relatively stable compared to the corresponding intermediate for model substrate **101i**. However, the potential energy gap from this rate determining intermediate to the **TS$_{F-G}$** state was significantly greater in relation to substrate **101w** (**101i** F–TS$_{F-G}$ ΔG = +13.5 kcal mol⁻¹, **101w** F–TS$_{F-G}$ ΔG = +21.9 kcal mol⁻¹). Proceeding directly from this transition state with the formation of intermediate **G** was determined to occur with a similar relative increase in stabilisation for both substrates (**TS$_{F-G}$–G** ΔG = –2.4 kcal mol⁻¹). Despite this the dissociation product of **101w** remains considerably more unstable occupying a potential energy level +5.7 kcal mol⁻¹ higher in comparison to the de-sulfonylated **101i** intermediate. Resonance transition to species **H** and introduction of starting material **D** is predicted to lead to a further unfavourable increase in relative potential energy (**101i** F–H+D ΔG = +17.6 kcal mol⁻¹, **101w** F–H+D ΔG = +28.7 kcal mol⁻¹), and approaching the key HAT transfer transition state (**TS$_{H-I}$**) it becomes apparent that the overall energy span of the reaction profile for **101w** from intermediate **F** is considerably greater compared to the equivalent term for

substrate **101i** (**101i** F–TS$_{H-I}$ ΔG = +35.3 kcal mol^{-1}, **101w** F–TS$_{H-I}$ ΔG = +43.8 kcal mol^{-1}).
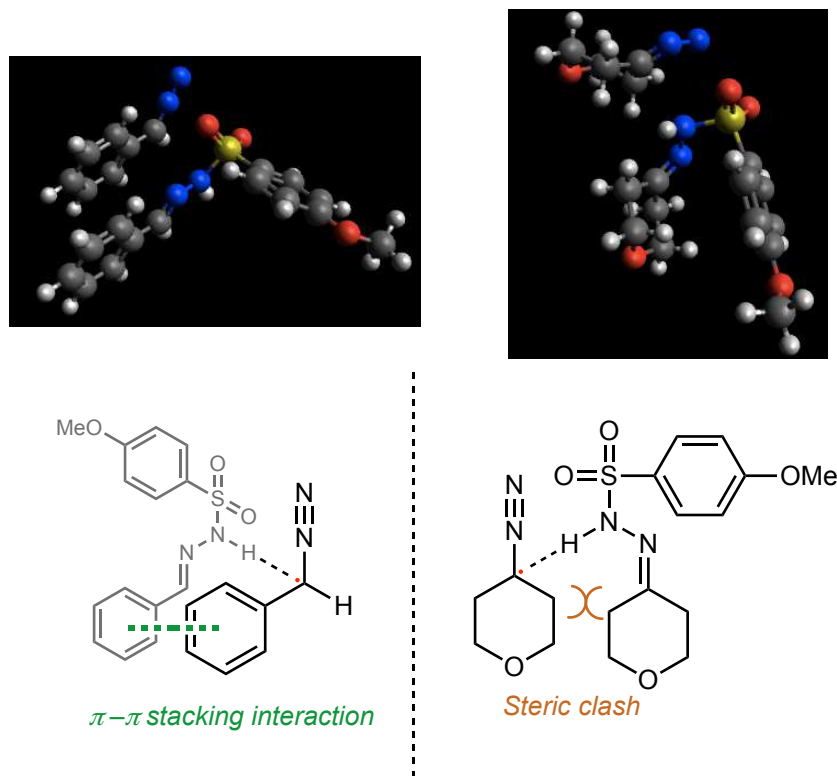
Figure 31. *Comparison of DFT computed intermediate* **TS$_{H-I}$** *for substrate* **101i** *(left) showing the proposed stabilising π–π stacking interaction, and that of substrate* **101w** *(right) showing the expected steric congestion around the carbon-centred radical .[166, 167]*

A direct comparison of the computed **TS$_{H-I}$** transition states for substrates **101i** and **101w** provides clear insights regarding the differences in reaction feasibility (**Figure 31**). For substrate **101i** the key HAT step appears to be facilitated by a stabilising intermolecular π–π stacking interaction between intermediate **H** and starting material **D**, denoted by the staggered alignment of their respective aromatic rings. The presence of such interactions is likely to reduce the relative energy level of the ensuing **TS$_{H-I}$** transition state, enabling more efficient HAT to occur for benzylic sulfonyl-hydrazone substrates in comparison to non-aromatic substrates. By contrast the equivalent transition state for derivative **101w** shows significant steric repulsion between the two tetrahydropyran rings, preventing engagement of the carbon centre of intermediate **H** with the –NH group of species **D**. This steric congestion is likely to be the cause of a considerable potential energy barrier preventing association of the two reaction intermediates, thus hindering the propensity of the HAT step to take place under the investigated conditions. This combination of steric

85

and electronic effects that impact the overall relative energy level of the TS_{H-I} transition state, and consequently the efficiency of the HAT step are likely responsible for the observed converse behaviour of aromatic substrates in comparison to non-aromatic derivatives.

.

The presence of such energetically unfavourable reaction states interceding the rate determining intermediate (**F**) and rate determining transition state (**TS$_{H-I}$**) has been proposed to inhibit reaction progress in accordance with the energetic span approximation.[176] Therefore the relative lack of stabilising electronic effects that lower the potential energy level of **TS$_{F-G}$** and intermediate **G** enabling dissociation of the sulfonyl group is believed to contribute to the observed deficient reactivity of certain electron-rich sulfonyl-hydrazone derivatives such as **101t**, **101u** and **101w**. Supplementary redox potential calculations also identified intermediate **G** as sufficiently electron deficient to oxidise the $[Ru(bpy)_3]^+$ photocatalytic species. This behaviour could foreseeably provide a route for regeneration of the ground state photocatalyst, in accordance with reports of similar diazo compounds engaging in oxidative quenching of excited state ruthenium photocatalysts.[177,178]

Taking into consideration the results obtained from both the mechanistic experiments and DFT studies performed, a mechanism for the reaction in question can be tentatively proposed (**Scheme 18**). Starting from sulfonyl-hydrazone **D**, deprotonation and subsequent SET oxidation by the excited state $[Ru(bpy)_3]^{2+*}$ photocatalyst **B** leads to formation of N-centred hydrazonyl radical **F**. Fragmentation of this reactive intermediate leads to the generation of a sulfonyl anion alongside a suspected diazo radical **G**, of which the resonance form **H** partakes in a key HAT propagating step involving a second molecule of the starting material **D**, generating a highly reactive diazonium species **I** with concomitant reformation of hydrazonyl radical **F**. It is believed that the transient species observed *via* ^{1}H NMR (~5.76 δ/ppm) corresponds to intermediate **G** given its greater relative stability compared to **I** however the exact identity of the species that the observed peaks represent remains unclear. The intermediate **I** then rapidly fragments with the expulsion of nitrogen gas leaving benzyl cation **J**, which readily engages in a straightforward S_N1 type reaction with the previously formed sulfonyl anion to generate the final product **102**. The sulfone is likely also accessible by a secondary pathway, involving the SET reduction of intermediate **G** which both completes the photocatalytic

cycle and generates diazo species **K**, which *via* deprotonation of the start material **D** also leads to formation of the key intermediate **I** from which point the reaction pathway proceeds identically to the first.
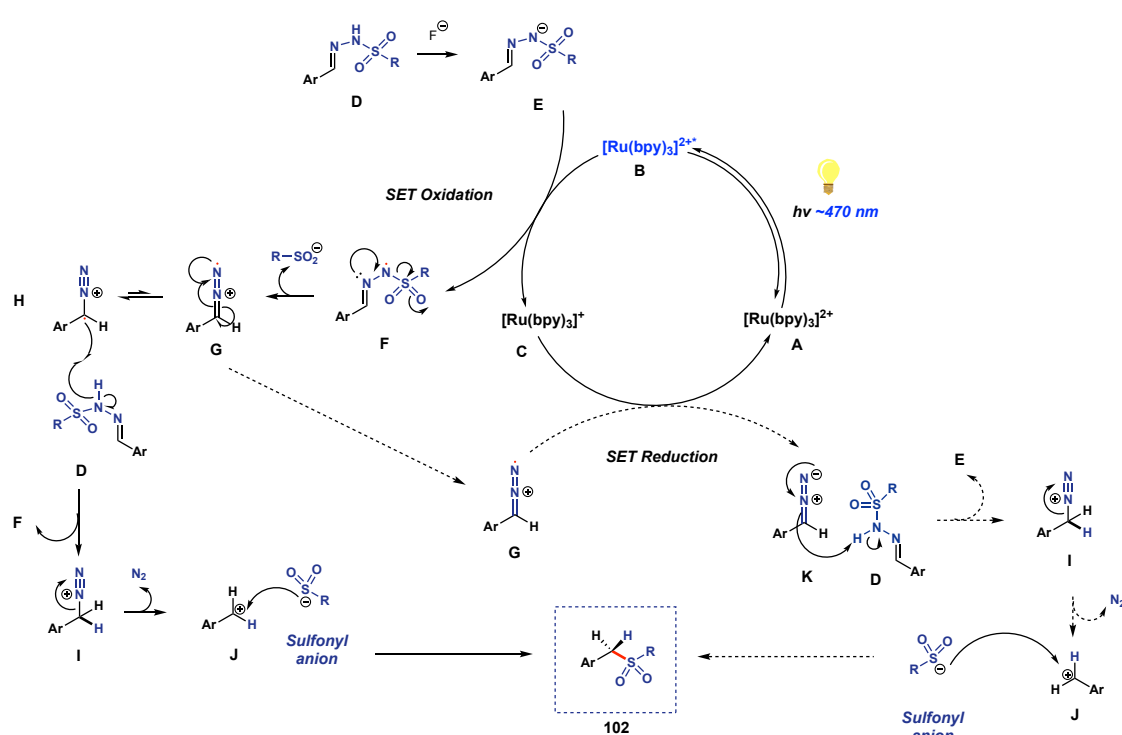
Scheme 18. *Proposed reaction mechanism of base promoted photocatalytic conversion of sulfonyl-hydrazones into sulfones (**102**) via key diazo radical species **G**, and the subsequent rate determining HAT step between the resonance form **H** and another molecule of starting material (**D**) to generate unstable diazo cation **I** which goes on to form the sulfone product.*

2.4.   Reaction Development Summary

In summation, the discovery and optimisation of a novel photoredox catalysed reaction is reported which allows for the facile conversion of bench-stable aromatic sulfonyl-hydrazones into the corresponding sulfones in good yields and under mild reaction conditions. In doing so this procedure exhibits various advantages over previously reported methodologies, which traditionally rely on harsh reaction conditions including high temperatures, strong oxidants and stochiometric amounts of unstable organometallic reagents among others that limit their overall applicability.

Investigations into the reaction mechanism confirmed the radical nature of the transformation and furthermore in combination with DFT studies were able to suggest the involvement of key diazo reaction intermediates, mechanistically distinguishing the reaction from previously reported photoredox procedures concerning hydrazone substrates. Unfortunately, the reaction does possess a relatively narrow substrate scope as attempts to convert aliphatic substrates (**102w**) and those bearing either redox active or strong electron donating functional groups (**102h, 102t, 102u**) were unsuccessful, limiting the overall utility of the reaction in providing rapid access to potential antibacterial scaffolds. Nevertheless the reaction was capable enough to provide access to numerous aromatic sulfone analogues, medicinally relevant scaffolds frequently highlighted as potential DHDPS inhibitors in the previously conducted *in silico* docking studies (ZINC95080289, ZINC91695738, ZINC57478020, ZINC93714108, ZINC47645776, ZINC289626506, etc) underlining their prospects as key candidates for *in vitro* antimicrobial screening.

2.5. *Continued Synthesis of In Silico Determined Antibacterial Molecular Scaffolds*

The developed photoredox methodology was able to provide several compounds that suitably matched the sulfone pharmacophore scaffold generated from the prior *in silico* docking investigations. Based on straightforward retrosynthetic analysis of the remaining cohort of potential target molecules, it was anticipated that additional compounds representative of the alternative pharmacophores developed could be provided *via* more conventional synthetic methodology. While certain virtual hit structures could be approached as direct targets for construction, more elaborate molecular scaffolds had to be simplified in order to reasonably truncate the expected length of the synthetic effort. Wherever possible features from multiple pharmacophores were amalgamated within a single compound in order to improve its potential utility, while seeking to avoid impairment of the discrete pharmacophore features and maintaining a consideration of the relative ease of the synthetic route.

Due to the incompatibility of the developed photocatalytic procedure with non-aromatic substrates, a longer synthetic sequence starting from ketone **103** employing more robust methodologies was devised to obtain the sulfone derivative **109** (ZINC154138, **Figure**

32). Another sulfone analogue **110** (ZINC153751) identified as a hit structure *in silico* was found to be commercially available. The sulfonamide **115** (ZINC20223890) was expected to be constructed in a straightforward manner *via* a Hinsberg reaction between starting amine **111** and a readily available sulfonyl chloride. The resulting sulfonamide was also selected as a promising synthetic target due to the presence of a *para* situated acetamide group, which could serve as both an auxiliary hydrogen bonding moiety capable of engaging with key residues throughout the active site and as a functional handle for ensuing synthetic transformations.
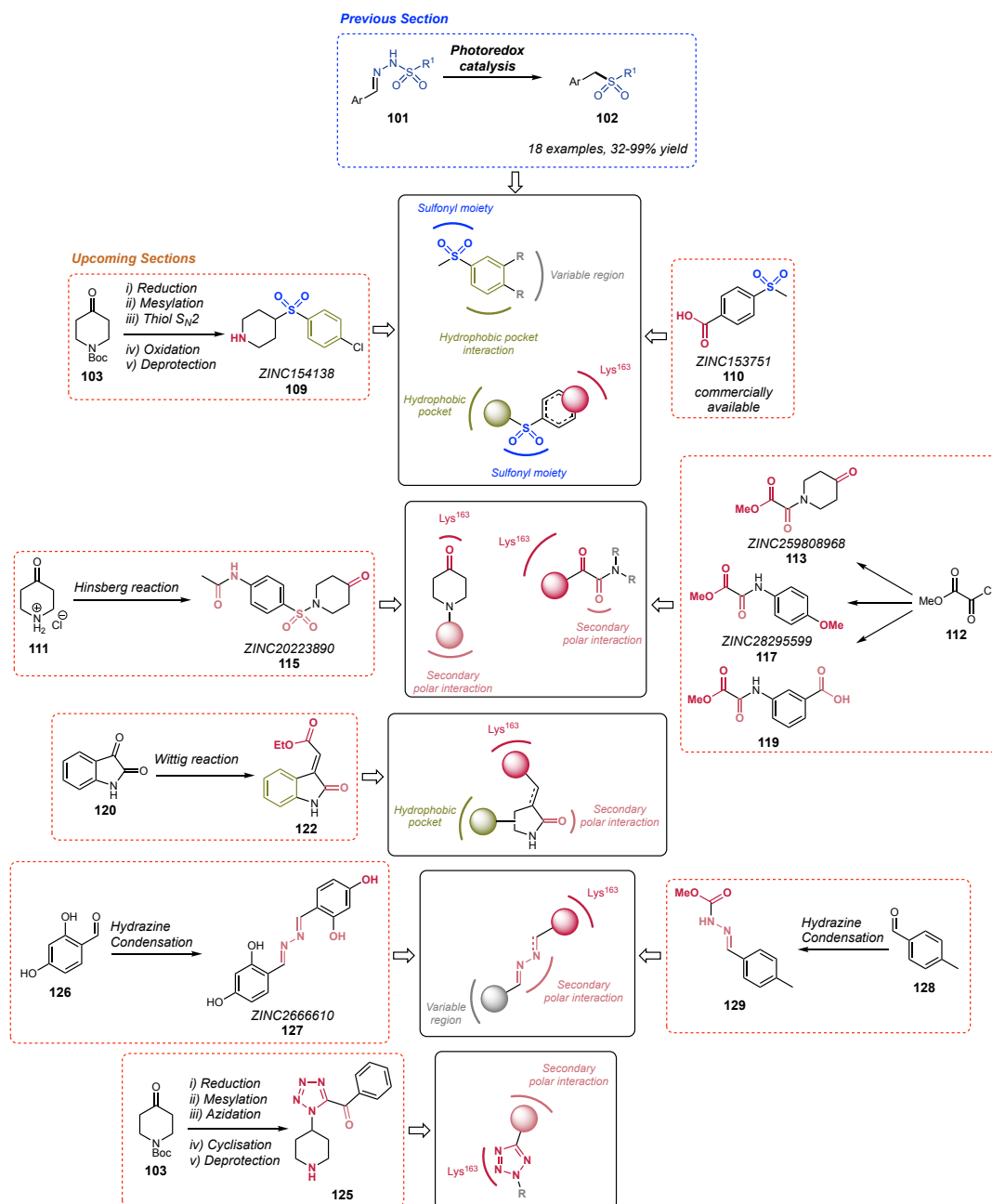
Figure 32. *Overview of the candidate molecules selected as synthetic targets for in vitro antibacterial testing based on the results obtained from the in silico docking and pharmacophore construction process, alongside the proposed synthetic routes.*

The derivative **113** (ZINC259808968) bearing two distinct functional groups capable of engaging with the Lys[163] active site residue, was envisaged to be readily constructed *via* coupling of the aforementioned secondary amine **111** with acid chloride **112**. Meanwhile a similar synthetic procedure was expected to generate the structurally related 1,2-dicarbonyl analogues **117** (ZINC28295599) and **119** *via* reaction of **112** with primary

anilines. In a similar manner to derivative **113** the virtual docking hit structure **117** was prioritised as a synthetic target not only due to its promising behaviour *in silico* but the presence of multiple functional groups within the scaffold purportedly capable of engaging with the key Lys[163] active site residue, as demonstrated by their appearance in other identified pharmacophores. The structurally similar compound **119** was selected on the basis that the introduction of a carboxylic acid group at the *meta* position could facilitate secondary protein–ligand polar interactions involving residues adjacent to the main region of the DHDPS active site. Alternatively, and as outlined in previous target molecules the ancillary potential function of the carboxylic acid moiety of **119** is to engage with the key Lys[163] residue as witnessed in other *in silico* derived hit structures (**110**) due to its established role as a hydrogen bonding pharmacophore feature.

The ethyl ester (**122**) of *in silico* hit compound ZINC71483382 appeared to be obtainable through a Wittig reaction with isatin **120** and a commercially available phosphonium ylide. Condensation of aldehydes **126** and **128** with an appropriate hydrazine species was envisaged as a straightforward route to hydrazone derivatives **127** (ZINC2666610) and a simplified variant of ZINC490675521 (**129**) respectively.

In comparison to the majority of other candidates identified *in silico*, the tetrazole hit compounds possessed relatively complex molecular architectures consisting of highly decorated heterocyclic components. Therefore, the selection of a truncated molecular scaffold as a more readily achievable synthetic target was proposed considering that most of the structural features present in ZINC94726762, ZINC825594726, and ZINC1364039423 appear to be superfluous to their potential binding affinity and yet require numerous synthetic steps to be incorporated into the overall candidate structures. This is of course with the exception of the identified key pharmacophore features centred around the Lys[163] residue binding tetrazole moiety, which were obviously sought to be transposed onto the new derivative either directly or in the form of a more viable bioisostere. Compound **125** was selected as the representative target structure for synthetic efforts, maintaining the tetrazole ring alongside an adjacent carbonyl moiety based on the numerous hydrogen bond acceptors identified *in silico* as engaging in supposed secondary binding interactions within the active site. Furthermore, the incorporation of a piperidine fragment into compound **125** was anticipated to enhance the possibility of inducing antibacterial activity by furnishing alternative modes of binding

within the DHDPS active site. The hydrogen bonding capabilities of the piperidine amine group were identified as a component of other promising candidate structures advocated *via* the virtual docking process such as **109** (ZINC154138). Proliferation of the diversity of key pharmacophore features available within a single scaffold is expected to increase the overall potential ability of **125** to engage in occupation of the active site.

2.5.1. *Acquisition of non-Benzylic Sulfone Derivatives*

Due to the limited substrate scope observed for the prior developed photocatalytic method, a less direct approach employing more routine synthetic processes was undertaken to facilitate access to non-stabilised sulfone analogues. Based on the promising *in silico* behaviour of ZINC154138 in particular alongside other aforementioned sulfone derivatives, compound **109** was selected as an expedient synthetic target (**Scheme 19**). Starting from commercially available *N*-Boc-4-piperidone (**103**) reduction with sodium borohydride provided the corresponding alcohol **104** in 87% yield. Subsequent mesylation (**105**) and nucleophilic substitution with 4-chlorothiophenol under basic conditions rendered the anticipated sulfide **106** in good yield.
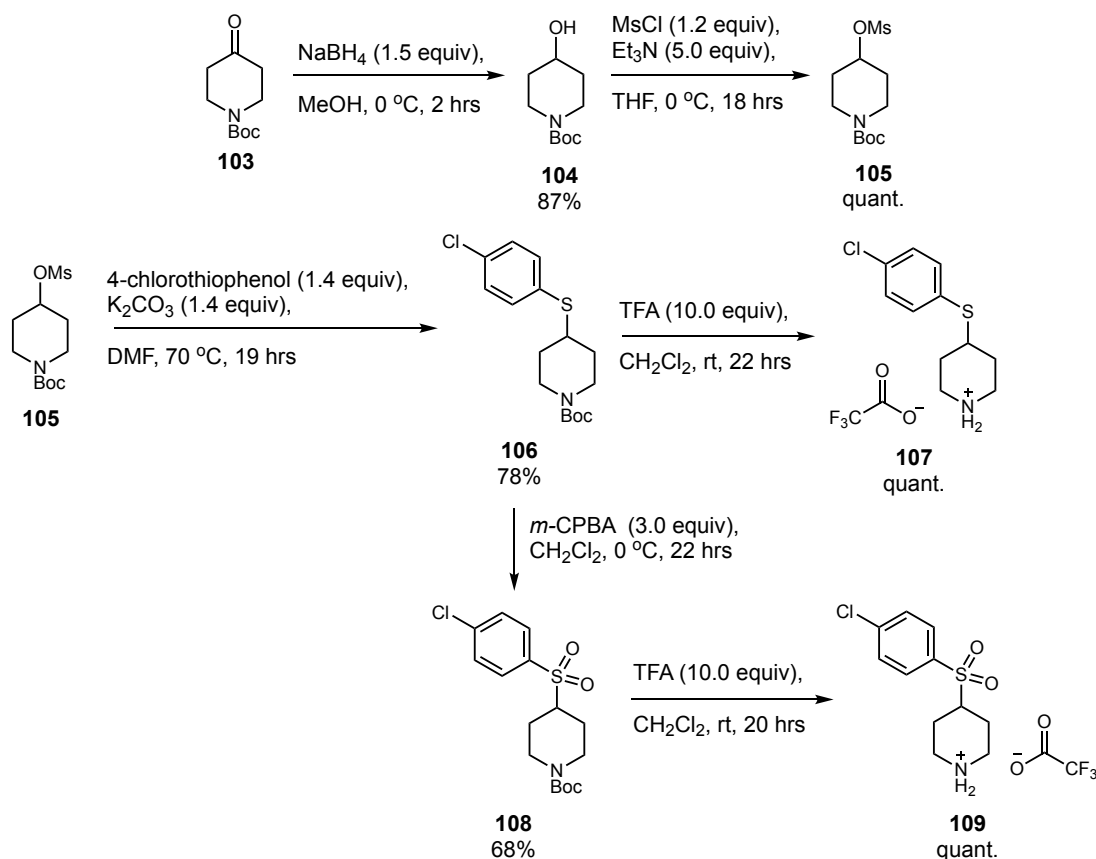
Scheme 19. *Reaction scheme for the five-step synthesis of sulfone **109** from commercially available starting material **103**, alongside the synthesis of closely related sulfide derivative **107**.*

Furthermore it was decided that premature deprotection of the sulfide intermediate should be undertaken, furnishing the triflate salt **107** in quantitative yield. Considering the obvious similarities in skeletal outline compared to the synthetic target **109** punctuated by the presence of an aromatic ring and two hydrogen bond accepting functional groups, the sulfide **107** appeared to be an opportune supplementary analogue suitable for antimicrobial testing based on comparisons with the previously defined pharmacophore features (**Scheme 20**). With the main scaffold of the synthetic target now assembled, all that remained was to oxidise sulfide **106** to the corresponding sulfone (**108**) followed by trivial protecting group removal. Utilising an excess of *m*-CPBA to avoid incomplete oxidation, the desired penultimate intermediate was isolated with a yield of 68%. Subsequent treatment with trifluoroacetic acid facilitated quantitative conversion to the deprotected amine, whereby sulfone **109** was successfully obtained in five steps with an overall yield of 46%. To complete the assemblage of desired sulfone derivatives, *p*-(methylsulfonyl)benzoic acid **110** was purchased for consequent antibacterial testing owing to the promising observations of its *in silico* facsimile ZINC153751 in which the

sulfone moiety was noted to engage in auxiliary binding interactions proximal to the site of the key Lys163 residue.
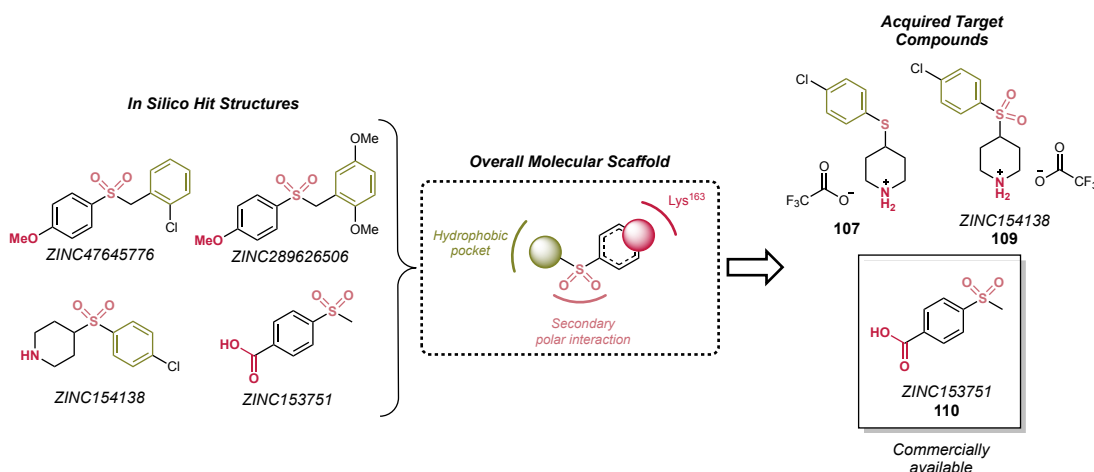
Scheme 20. *Overview of the acquired synthetic targets sulfide **107**, sulfone **109** (ZINC154138) and the commercially available p-(methylsulfonyl)benzoic acid (ZINC153751) **110** showing the parent pharmacophore and the in silico hit compounds on which the antibacterial candidates were based.*

2.5.2. *Synthesis of Piperidinone and 1,2-Dicarbonyl Scaffolds*

With a number of promising sulfone analogues now in hand, the focus of synthetic efforts was diverted towards the construction of piperidinone containing scaffolds. The encouraging *in silico* performance of ZINC259808968 and the sulfonamide ZINC20223890 wherein the piperidinone carbonyl engages in seemingly favourable polar interactions with the key Lys163 residue, provoked their selection as pragmatic synthetic targets. An additional consideration for their selection is the presence of a 1,2-dicarbonyl ester moiety on piperidinone **113** (ZINC259808968) which has been identified as a functional group integral to the promising *in silico* performance of several other candidate structures. Furthermore, based on the observed virtual docking results the *para* situated acetamide group of **115** (ZINC20223890) could engage in secondary ligand–protein binding interactions with residues adjacent to the active site resulting in formation of a more stable complex. Beginning with the synthesis of α-keto ester **113** consultation of the literature provided numerous base promoted approaches towards acylation of the stable hydrochloride salt **111** with methyl chloroglyoxalate (**112**).[179–182] Considering the envisaged importance of this reaction in the construction of further α-keto esters as potential antibacterial agents, a small reaction optimisation screen was conducted to

94

elucidate viable conditions. Employing potassium carbonate as base and dichloromethane as solvent with external cooling resulted in a disappointingly low yield even after leaving the reaction mixture suspension to stir to room temperature overnight (**Table 5**, entry 1**)**. Switching to an organic base with anticipated improved solubility at lower temperatures in the form of Hunig's base resulted in only a minor improvement in overall yield, and the employment of pyridine generated only trace amounts of the desired a-keto ester alongside a complex mixture of unidentified side products (**Table 5**, entry 2 & 3). Considering the relative moisture sensitivity of the oxalyl acid chloride reagent, anhydrous dichloromethane solvent was utilised alongside Hunig's base leading to a further increase in yield to 21% (**Table 5**, entry 4).

Table 5. Optimisation of reaction conditions for the synthesis of 113 via acylation of piperidone 111 with methyl chloroglyoxalate (112).

Entry	Base	Solvent	Yield (%)^a
1	K$_2$CO$_3$	CH$_2$Cl$_2$	8
2	i-Pr$_2$NEt	CH$_2$Cl$_2$	15
3	Pyridine	CH$_2$Cl$_2$	Trace
4	i-Pr$_2$NEt	CH$_2$Cl$_2$^{b}	21
5^c	i-Pr$_2$NEt	CH$_2$Cl$_2$^{b}	9
6^d	i-Pr$_2$NEt	CH$_2$Cl$_2$^{b}	Trace
7	**Et$_3$N**	**CH$_2$Cl$_2$^{b}**	**44^e**
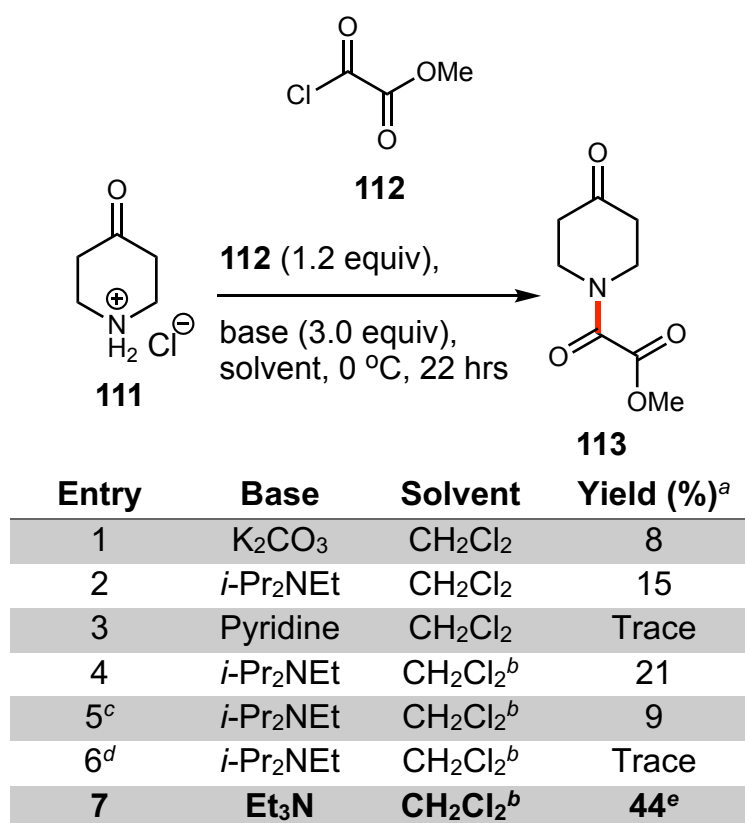
^{a} Yields determined by ^{1}H NMR (±5%). ^{b} Anhydrous solvent employed. ^{c} Reaction time 4 hours. ^{d} Reaction carried out at room temperature. ^{e} Isolated yield.

Still unsatisfied with the poor yield obtained for such an elementary and well documented procedure, the reaction time was shortened to four hours to curtail potential degradation

of the product arising from prolonged exposure to basic conditions at room temperature, however a notable drop in yield was observed (**Table 5**, entry 5). Carrying out the procedure at room temperature resulted in a vigorous reaction upon addition of the acid chloride, after settling the resultant reaction mixture provided the desired product in only trace yields. Having exhausted numerous approaches utilising Hunig's base seemingly without success, it was substituted for triethylamine which pleasingly provided the desired product **113** in an isolated yield of 44% after purification.
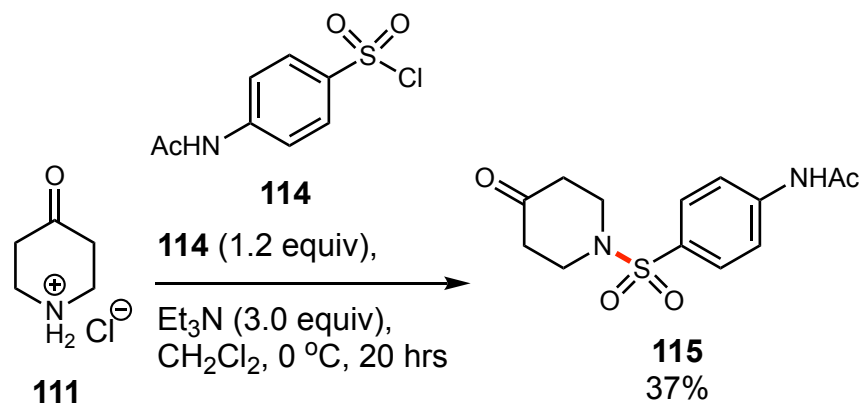
Scheme 21. *Synthesis of sulfonamide **115** from commercially available 4-piperidone hydrochloride **111** and N-acetylsulfanilyl chloride (**114**) under basic conditions.*

Application of the somewhat optimised reaction conditions to **111** in the presence of *N*-acetylsulfanilyl chloride (**114**) furnished the desired sulfonamide **115** in reasonable yield (**Scheme 21**). A similar methodology but employing a lesser excess of triethylamine base was successfully employed towards the synthesis of α-keto esters **117** and **119** furnishing the desired products in excellent and reasonable yields respectively *via* acylation of the corresponding anilines (**Scheme 22**). Similar isolated yields were obtained for the synthesis of **119** when employing 3.0 equivalents of triethylamine base and according to the relatively high amount of product observed within the crude extract, inefficient purification appears to be the culprit for the relatively poor isolated yields obtained.
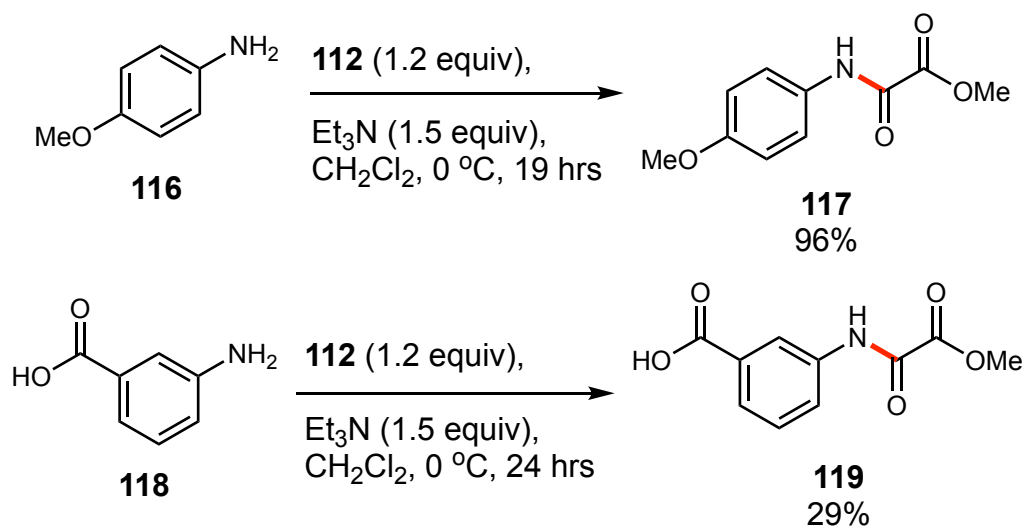
Scheme 22. *Synthesis of in silico determined α-keto ester antibacterial candidates **117** and **119** via acylation of the corresponding anilines **116** and **118** with methyl chloroglyoxalate (**112**).*

As a direct representative of ZINC28295599 **117** represents a promising candidate for antibacterial testing, while the inclusion of a carboxylic acid moiety within the same core scaffold in the case of **119** was conceived as a potential additional source of stabilising polar interactions with key residues situated amongst the DHDPS active site (**Scheme 23**). Furthermore, the *para* situated methoxy group of **117** and the carboxylic acid moiety of **119** both constitute additional functional groups that have exhibited a proficiency to engage with the key Lys163 residue *in silico,* introducing further potential modes of binding to be exploited in pursuit of desired DHDPS inhibition and antimicrobial activity.
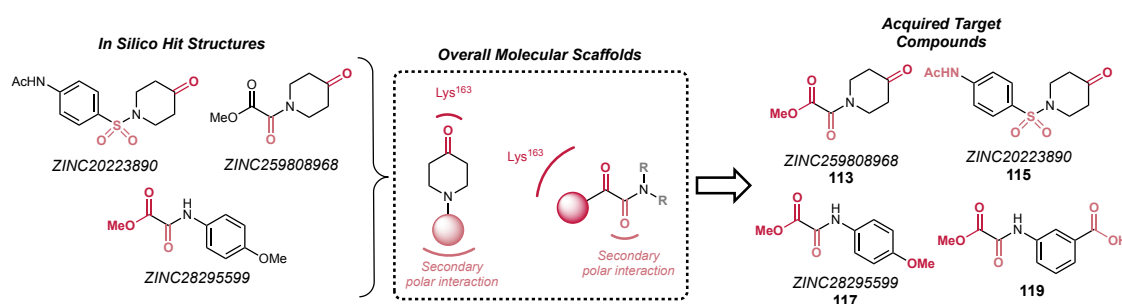
Scheme 23. *Overview of the acquired synthetic targets **113** (ZINC259808968), **115** (ZINC20223890), **117** (ZINC28295599) and **119** showing the in silico hit compounds and the generic molecular templates from which the selected antibacterial candidate structures were derived.*

2.5.3. _Synthesis of Isatin Ethyl Ester_

Isatins such as ZINC71483382 constituted another compound class repeatedly identified as possessing inhibitory potential *via* the virtual docking process. A simplified ethyl ester analogue of ZINC71483382 (**122**) was selected as a synthetic target due to its trivial preparation, potential for additional structural elaboration and high level of structural homology compared to the inspiring carboxylic acid derivative (**Scheme 24**). The coupling of isatin **120** with the stabilised Wittig reagent **121** proceeded at room temperature to provide the desired α,β-unsaturated ester **122** in excellent yield.
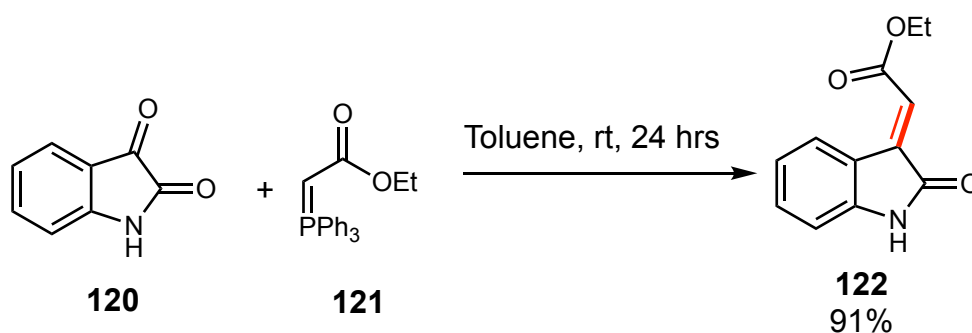
Scheme 24. *Preparation of α,β-unsaturated ester **122** via coupling of isatin **120** and phosphonium ylide **121**.*

Candidate molecule **122** was selected to represent the isatin–based molecular scaffold in proceeding screens for antibacterial activity. Despite being an isolated derivative in comparison to the other groups of compounds investigated it shares several of its structural features with members of other identified pharmacophores, such as an aromatic ring capable of occupying the hydrophobic pocket previously identified *in silico* and a hydrogen bonding array constructed of carbonyl groups that engages in polar interactions with the Lys163 residue and nearby secondary residues within the active site (**Scheme 25**).
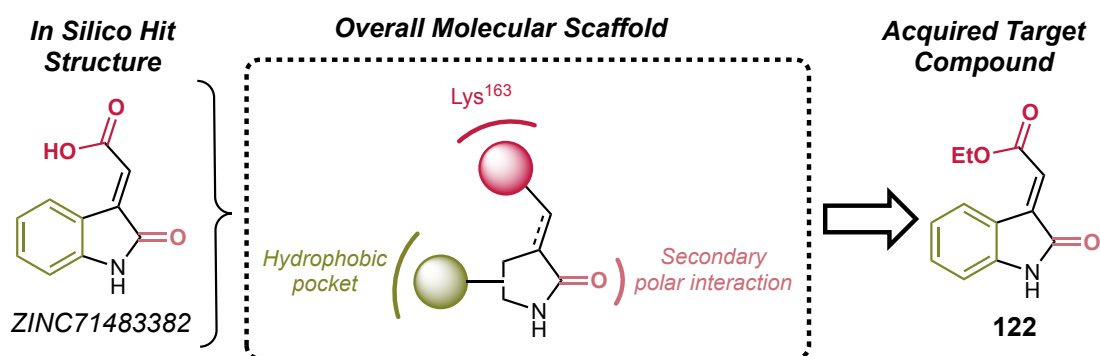
Scheme 25. *The acquired synthetic target **122** showing its structural relationship to the in silico hit compound ZINC71483382 via way of an intermediate molecular scaffold encompassing the key protein–ligand binding features identified.*

2.5.4. *Synthesis of In Silico Derived Tetrazole Analogue*

Continuing with the aim of generating *in silico* determined candidates for antibacterial screening, the tetrazole **125** was selected as the next target of synthetic efforts, based on the promising performance of more densely functionalised tetrazole derivatives such as ZINC94726762, ZINC825594726 and ZINC1364039423 within the virtual docking process (**Scheme 26**). Treatment of the previously synthesised mesylate **105** with sodium azide at elevated temperatures provided the desired product **123** as a yellow oil in quantitative yield (**Scheme 27**).
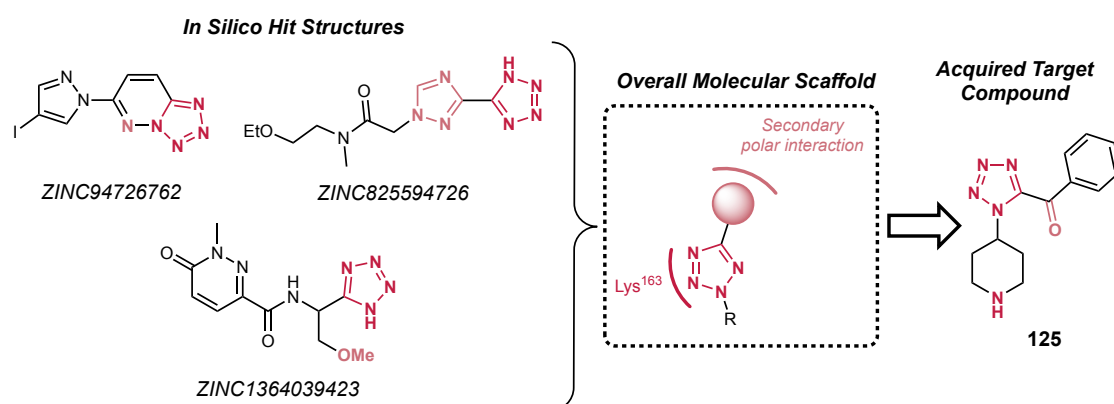
Scheme 26. *The acquired synthetic target **125** showing its structural relationship to the in silico hit compounds ZINC94726762, ZINC825594726 and ZINC1364039423 and the derived pharmacophore.*

An alternative route *via* a Mitsunobu reaction of the corresponding alcohol **104** with sodium azide was also found to provide the product **123** in high yield. However, separation of the product azide from the triphenylphosphine oxide by-product proved problematic hence the more straightforward approach proceeding from intermediate **105** was preferred.
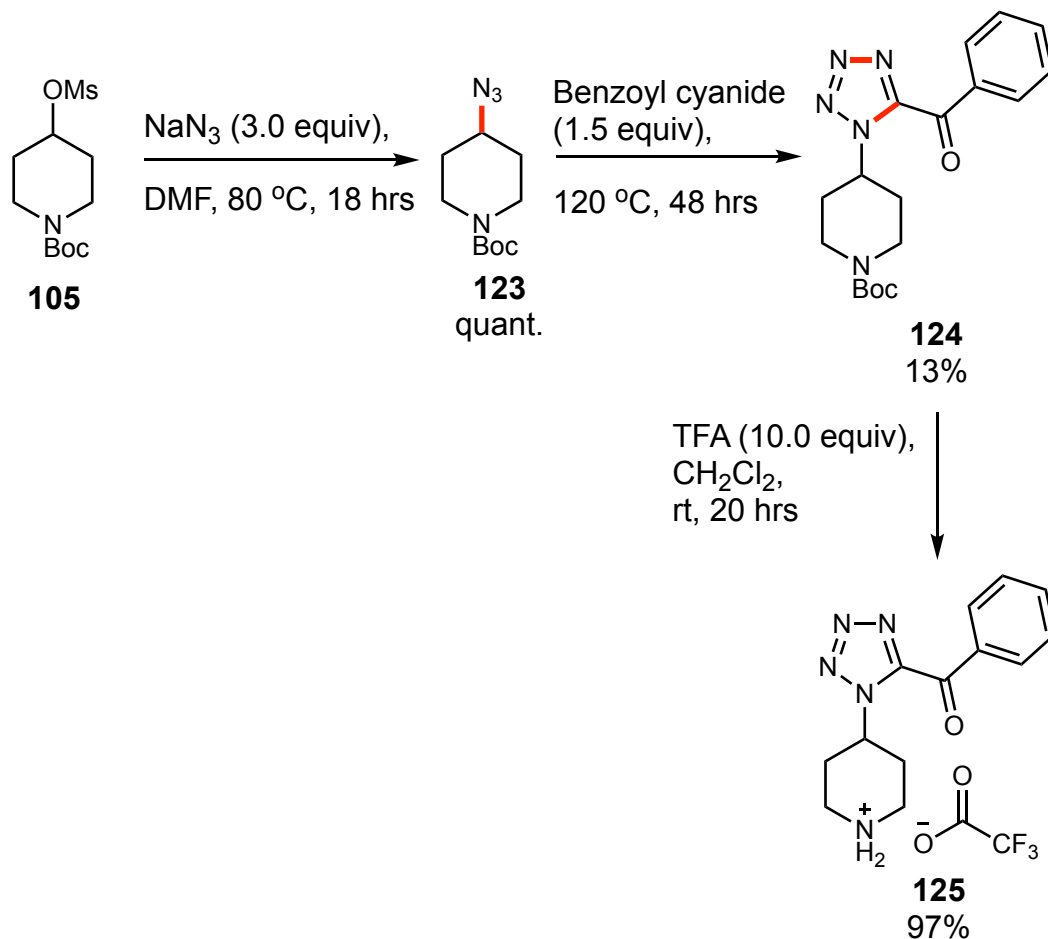
Scheme 27. *Synthesis of tetrazole **125** via azidation of previously utilised mesylate **105** and subsequent cyclisation with benzoyl cyanide to form the precursor **124**, with ultimate deprotection of the amine forming the desired synthetic target.*

Utilising synthetic methodology developed by Demko *et al.* the neat cyclisation of **123** with commercially available benzoyl cyanide was attempted at high temperatures.[183] Although only a low yield of the desired tetrazole **124** was obtained the reaction provided sufficient enough material to be utilised in the upcoming steps, furthermore 40% of the initial azide starting material was recovered following purification. Finally treatment of **124** with an excess of trifluoroacetic acid enabled straightforward deprotection of the piperidine amine, providing the envisaged tetrazole derivative **125** as the trifluoroacetate salt in high yield.

2.5.5. Synthesis of Hydrazone Derivatives and Further Photocatalytic Reaction Development Attempts

Numerous hit structures obtained from the virtual docking process were found to consist of hydrogen bond acceptor/donor components centred around a hydrazone scaffold, supposedly capable of engaging in secondary polar interactions within the DHDPS active site (**Scheme 28**).
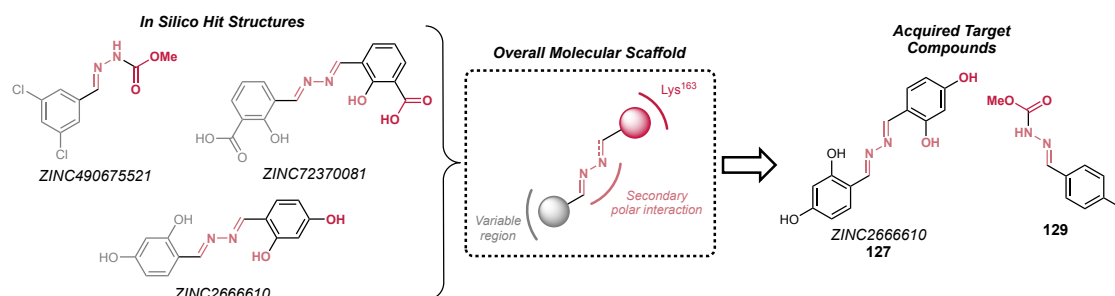
Scheme 28. *The acquired synthetic targets **127** (ZINC2666610) and **129** showing their structural relationship to the in silico hit compounds ZINC490675521, ZINC72370081 and ZINC2666610 and the overarching molecular scaffold.*

Treatment of rudimentary 2,4-dihydroxybenzaldehyde **126** with hydrazine monohydrate generated quantitative amounts of the desired hydrazone dimer **127**, a derivative modelled closely on the structures of ZINC72370081 and ZINC2666610 (**Scheme 29**). In an analogous manner a simplified variant of the virtual hit ZINC490675521 was synthesised *via* condensation of *p*-tolualdehyde (**128**) with methyl hydrazinocarboxylate providing the corresponding hydrazone **129** in excellent yield.
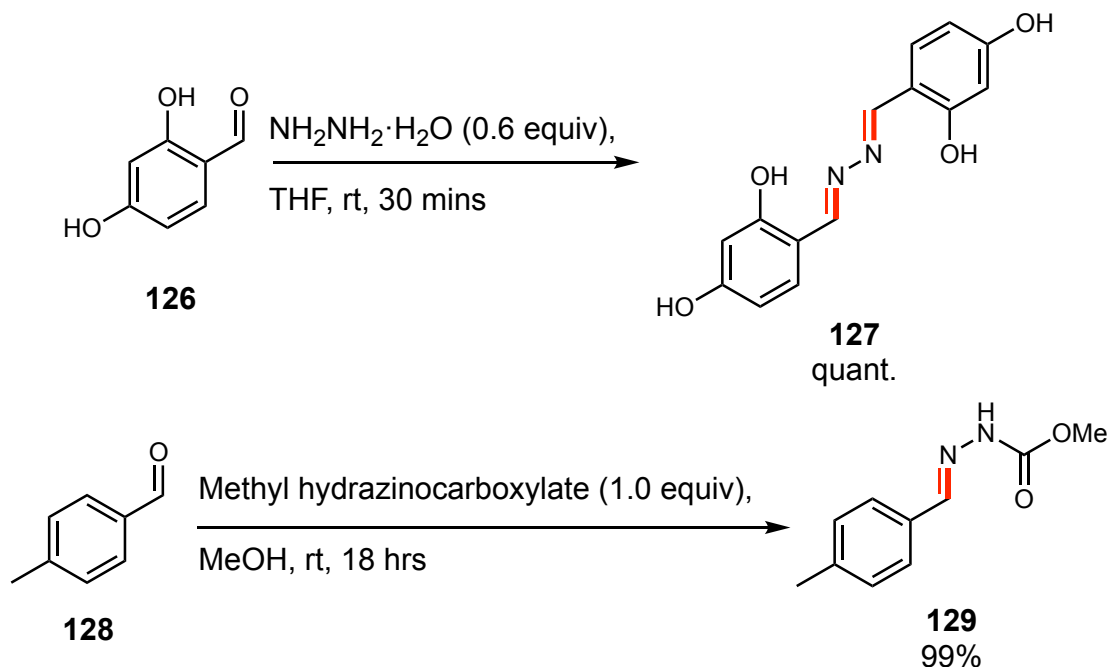
Scheme 29. *Synthesis of hydrazone dimer **127** and hydrazone carboxylate **129** via condensation of the corresponding aldehydes with hydrazine monohydrate and methyl hydrazinocarboxylate respectively.*

As well as a promising candidate for antibacterial testing, hydrazone **129** also appeared to be an apt substrate for exploring photocatalytic transformations due to its homogenous electronic molecular features compared to the previously described sulfonylhydrazone reagents successfully employed in a range of photoredox methodologies.[90,92,184–186] Alongside constituting an unprecedented approach towards carbon-carbon bond formation with wide-ranging potential for organic synthesis applications, the anticipated methyl ester products (**130**) arising from photocatalytic rearrangement of **129** would be of interest to the development of novel DHDPS inhibitors (**Table 6**). The installation of an ester, a hydrogen bond accepting functional group found ubiquitously as a key binding array throughout the structures of both previously reported DHDPS inhibitors and those identified *via* virtual docking procedures, would facilitate the trivial construction of promising analogues as candidates for antibacterial testing.

Table 6. *Attempted optimisation of reaction conditions for photocatalytic rearrangement of hydrazone **129** into methyl ester **130** with undesired formation of aldehyde **128**.[a]*
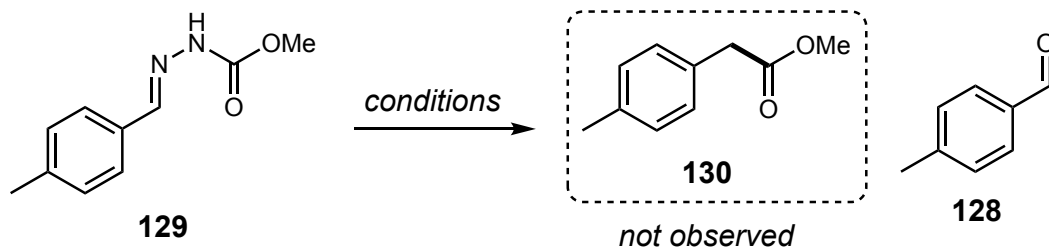
Entry	Base	Photocatalyst	Additive	Solvent	Yield 130 (%)[b]	Yield 128 (%)[b]
1	CsF	Ru(bpy)$_3$Cl$_2$·6H$_2$O	–	DMF	0	0
2	Cs$_2$CO$_3$	Ru(bpy)$_3$Cl$_2$·6H$_2$O	–	DMF	0	0
3	CsF	Ru(bpy)$_3$Cl$_2$·6H$_2$O	1,3-DNB	DMF	0	0
4	CsF	Ru(bpy)$_3$Cl$_2$·6H$_2$O	CBr$_4$	DMF	0	0
5	CsF	Ru(bpy)$_3$Cl$_2$·6H$_2$O	CCl$_3$Br	DMF	0	0
6	Cs$_2$CO$_3$	Ru(bpy)$_3$Cl$_2$·6H$_2$O	1,3-DNB	DMF	0	0
7	KOPiv	Ru(bpy)$_3$Cl$_2$·6H$_2$O	1,3-DNB	DMF	0	0
8	KHCO$_3$	Ru(bpy)$_3$Cl$_2$·6H$_2$O	1,3-DNB	DMF	0	0
9	NaOAc	Ru(bpy)$_3$Cl$_2$·6H$_2$O	1,3-DNB	DMF	0	0
10	CsOH·H$_2$O	Ru(bpy)$_3$Cl$_2$·6H$_2$O	1,3-DNB	DMF	0	0
11	Cs$_2$CO$_3$	*fac*-Ir(ppy)$_3$	CHI$_3$	DMF	0	0
12	Cs$_2$CO$_3$	Eosin Y	1,3-DNB	DMF	0	0
13[c,d]	Cs$_2$CO$_3$	Rose bengal	–	DMF	0	11
14[c]	Cs$_2$CO$_3$	Ru(bpy)$_3$Cl$_2$·6H$_2$O	–	DMF	0	23
15[c]	Cs$_2$CO$_3$	*fac*-Ir(ppy)$_3$	–	DMF	0	8
16[c]	Cs$_2$CO$_3$	Eosin Y	–	DMF	0	9
17[c]	Cs$_2$CO$_3$	5-Aminofluorescein	–	DMF	0	Trace
18[c]	Cs$_2$CO$_3$	Ru(bpy)$_3$Cl$_2$·6H$_2$O	–	CHCl$_3$	0	Trace
19[c]	Cs$_2$CO$_3$	Ru(bpy)$_3$Cl$_2$·6H$_2$O	–	H$_2$O	0	Trace
20[c]	Cs$_2$CO$_3$	Ru(bpy)$_3$Cl$_2$·6H$_2$O	–	1,4-dioxane	0	15
21[c]	Cs$_2$CO$_3$	Ru(bpy)$_3$Cl$_2$·6H$_2$O	–	Toluene	0	11
22[c]	Cs$_2$CO$_3$	Ru(bpy)$_3$Cl$_2$·6H$_2$O	–	MeCN	0	29
23	Cs$_2$CO$_3$	Ru(bpy)$_3$Cl$_2$·6H$_2$O	–	MeCN	0	0
24	Cs$_2$CO$_3$	Ru(bpy)$_3$Cl$_2$·6H$_2$O	1,3-DNB	MeCN	0	0
25	Cs$_2$CO$_3$	Ru(bpy)$_3$Cl$_2$·6H$_2$O	CBr$_4$	MeCN	0	0
26[c]	Cs$_2$CO$_3$	Ru(bpy)$_3$Cl$_2$·6H$_2$O[e]	–	MeCN	0	27
27	–	Ru(bpy)$_3$Cl$_2$·6H$_2$O	–	MeCN	0	23
28	Cs$_2$CO$_3$	–	–	MeCN	0	0
29[f]	Cs$_2$CO$_3$	Ru(bpy)$_3$Cl$_2$·6H$_2$O	–	MeCN	0	0

[a] *Reaction conditions:* **129** *(0.25 mmol), photocatalyst (2.5 μmol), base (0.50 mmol), oxidant (0.375 mmol) sealed tube under inert atmosphere, degassed solvent (5 mL) added dropwise, 38 °C, blue LEDs (~470 nm), 20 hrs.* [b] *Yields determined by* [1]*H NMR (±5%).* [c] *Reaction performed in air.* [d] *Irradiated with green LEDs (~525 nm).* [e] *5.0 μmol photocatalyst employed.* [f] *Reaction conducted in darkness.*

Beginning with the conditions established previously for the conversion of sulfonylhydrazones into sulfones, the substrate was irradiated with blue light in the presence of Ru(bpy)$_3^{2+}$ photocatalyst employing caesium fluoride as base and DMF as solvent. No conversion was observed as only starting material was recovered after work up, switching to a stronger base in the form of caesium carbonate yielded the same result (**Table 6**, entry 1 & 2). In an attempt to accelerate potentially sluggish photocatalytic turnover due to the seemingly reduced reactivity of the substrate the oxidants 1,3-dinitrobenzene, carbon tetrabromide and bromotrichloromethane were screened in conjunction with caesium fluoride as base, however once more no conversion of the starting material was observed (**Table 6**, entry 3–5). Several bases of wide-ranging pK_a and bearing different alkali metal counterions were employed, however no impact on the reaction outcome- or lack of one- was observed even in the presence of 1,3-dinitrobenzene as a reliable oxidant (**Table 6**, entry 6–10).

Considering the lack of consumption of the starting material observed thus far, alternative photocatalysts were employed to explore other routes towards reaction progress. Utilisation of Ir(ppy)$_3$ alongside caesium carbonate as base and known oxidant iodoform once more yielded no conversion of starting material, and a similarly disappointing result was obtained with the employment of Eosin Y (**Table 6**, entry 11 & 12).[187] Continuing with the assessment of organic photocatalysts Rose Bengal was assayed in the presence of air acting as a surreptitious oxidant alongside irradiation with green LEDs, analysis of the crude mixture obtained revealed a small amount of *p*-tolualdehyde **128** was present (**Table 6**, entry 13). The employment of other photocatalysts in the presence of air yielded similar results confirming the premise that the aldehyde was a consequent product of photocatalytic quenching by oxygen, with the initial catalyst Ru(bpy)$_3^{2+}$ generating the highest yield of **128 (Table 6**, entry 13–17).

Suspecting that the oxygenation of **129** could be adapted to potentially facilitate more elaborate radical transformations while also serving as a measure of reaction progress *via* starting material consumption, a small screen of solvents was undertaken in an attempt to discern improved reaction conditions. With chloroform as solvent only trace amounts of **128** were observed, and a similarly poor result was obtained with the implementation of water likely due to poor solubility of the substrate (**Table 6**, entry 18 & 19). The employment of polar aprotic solvents such as 1,4-dioxane and non-polar toluene alike

generated **128** in only low yields, however the use of acetonitrile saw a slight increase in yield to 29% comparable to the yield obtained employing DMF as solvent (**Table 6**, entry 20–22).

Unsurprisingly conducting the reaction in the absence of air led to a complete shutdown in starting material consumption, attempts to rekindle any semblance of reactivity *via* introduction of 1,3-dinitrobenzene and carbon tetrabromide as alternative oxidants under air free conditions were unsuccessful (**Table 6**, entry 23–25). Increasing the amount of photocatalyst employed twofold had no impact upon the yield of **128**, and although subsequent control reactions established the need for photocatalyst and light in facilitating the oxygenation of **129**, it was deemed too inefficient a process for the elaboration of further transformations, and furthermore no formation of the desired methyl ester **130** was observed under the reaction conditions investigated.

2.6. *Evaluation of In Vitro Antibacterial Activity*

Broth microdilution–based assays constitute a relatively straightforward way of determining MIC values of novel antibacterial agents. This is done by determining the lowest concentration of a candidate molecule required to visibly inhibit *in vitro* bacterial growth in comparison to control samples over a specified time period under corresponding conditions. Although unable to distinguish between bactericidal and bacteriostatic antibiotics in isolation, MIC tests are often employed in the early stages of drug discovery programmes to determine the viability of potential antimicrobial agents, acting as a starting point for more in depth biochemical evaluations. MIC assays are incapable of uncovering the mechanism of action through which a particular antibacterial agent functions, nor are they able to confirm or refute the implication of a specific biomolecular target directly.

Although MIC assays are unable to assess DHDPS inhibition among the selected candidate molecules, their purpose is to prematurely establish the presence of *in vitro* antibacterial activity. The previously developed target–based assays for the verification of DHDPS inhibition although reliable and effective, require extensive optimisation and validation efforts due to complications arising from both the underlying dual enzymatic assay setup, and the reported proclivity for errors regarding UV absorbance

measurements. Furthermore, the numerous unsuccessful antibiotic drug discovery campaigns over the previous decades typically over–emphasised the importance of compound potency through initial target–based screening approaches towards drug design.[9,10] These serve as informative warnings of the problems associated with assuming that low inhibitory concentrations guarantee desirable antibacterial activity in subsequent phenotypic screens. To this end the establishment of a compound's *in vitro* activity through phenotypic assays is an essential prerequisite before mechanism of action and target identification studies can be undertaken, and numerous recent antimicrobial drug discovery programmes have returned to phenotypic screening methods in response to the exposed faults of target–based screening methods.[21,56,188]

102b **102c** **102d** **102ea**

102f **102g** **102i** **102j**

102k **102l** *ZINC289626506* **102p** **102q**

102r **107** *ZINC154138* **109** *ZINC153751* **110**

ZINC259808968 **113** *ZINC20223890* **115** *ZINC28295599* **117** **119**

122 **125** *ZINC2666610* **127** **129**
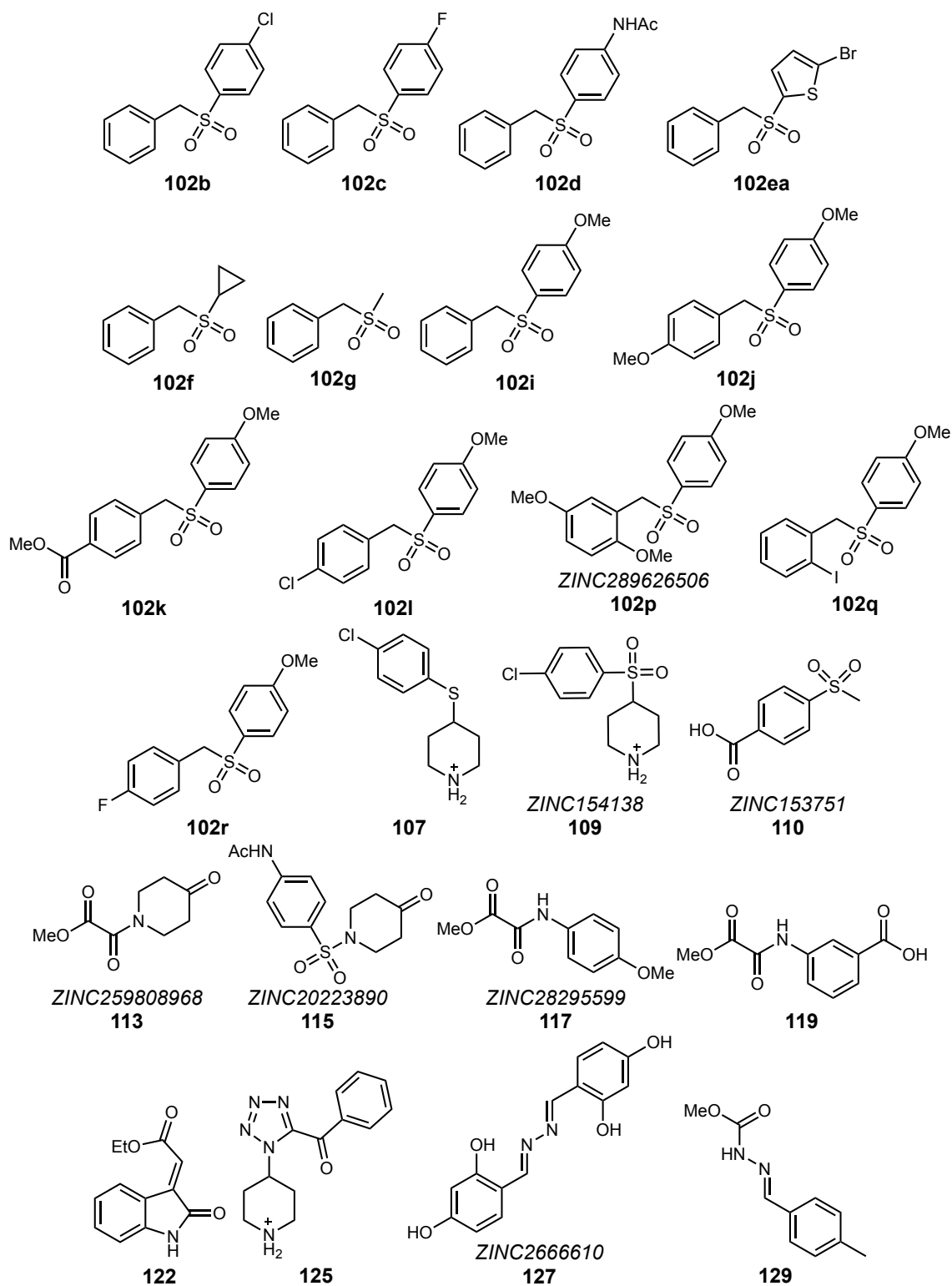
Scheme 29. *Overview of compound structures selected to be tested in vitro for antibacterial activity.*

107

The antibacterial activities of the assembled library of candidate structures were evaluated *via* MIC determination against both gram-negative (*E. coli*) and gram-positive (*S. aureus*) bacterial species (**Scheme 30**). Commencing with the photoredox generated sulfone derivatives, *p*-chlorophenyl sulfone **102b** was found to exhibit identical albeit relatively low antibacterial activity against *E. coli* and *S. aureus* species with an MIC of 0.96 mM (Entry 1, **Table 7**). Further derivatives bearing *para* substituents on the sulfonyl aromatic ring (**102c**, **102d**) performed equally innocuously if not less effective in comparison to **102b** (Entry 2 & 3, **Table 7**). Furthermore, analogues possessing non-phenyl sulfonyl moieties such as bromothiophene **102ea** and aliphatic derivatives **102f** and **102g** also demonstrated poor antibacterial activity (Entry 4–6, **Table 7**).

Pleasingly *para*-substituted phenyl methoxy derivatives **102i** and **102j** showed improved antibacterial activity against *S. aureus* obtaining MIC values of 0.49 mM and 0.44 mM respectively- the most potent derivatives against *S. aureus* found compared to all molecular candidates tested (Entry 7 & 8, **Table 7**). Despite sharing clear and promising structural features with *in silico* determined inhibitors ZINC47645776 and ZINC289626506, both **102i** and **102j** exhibited considerably reduced antimicrobial activity against *E. coli*. This lack of efficacy could be attributed to poor penetration across the hydrophilic outer membrane of the *E. coli* bacterial cell envelope, a common and troublesome obstacle encountered by antibiotic agents attempting to disrupt the cytoplasmic activities of gram-negative strains.[189] Replacement of the benzylic *p*-methoxy group of **102j** with a methyl ester (**102k**) or chloride group (**102l**) led to considerably diminished activity against *S. aureus* and comparatively only a minor improvement in effectiveness against *E. coli* (Entry 9 & 10, **Table 7**). The 2,5-dimethoxy variant **102p** had been identified as a candidate for DHDPS inhibition according to the promising *in silico* behaviour of ZINC289626506 within the virtual screening process. However when facing the realities of phenotypic screening **102p** performed relatively poorly, and contrary to the conduct of the structurally similar **102j** exhibited a pronounced enhancement in antibacterial activity against *E. coli* strains comparative to *S. aureus* (Entry 11, **Table 7**).

The iodinated derivative **102q** displayed the best all-round antibacterial activity of the compounds tested, with an MIC value of 0.66 mM against both species (Entry 12, **Table 7**). While possessing a high level of structural homology with the prominent virtual hit

ZINC47645776 could suggest the desired inhibition of DHDPS as the underlying cause of its antibacterial activity, there remains substantial uncertainty. Considering that several other organo-iodine compounds have been reported to possess broad-spectrum antibacterial activity, the precise mechanism by which **102q** acts cannot be presumed to correspond to DHDPS inhibition based on *in silico* occupation of the binding site alone.[190–192] The *p*–fluoro derivative **102r** also displayed relatively good antibacterial activity against *E. coli* however was considerably less effective against *S. aureus* (Entry 13, **Table 7**).

Table 7. *Minimum inhibitory concentration (MIC) values obtained from in silico derived hit structures against E.coli and S.aureus bacterial strains.*

Entry	Compound	MIC *E.coli* (mM)	MIC *S.aureus* (mM)
1	**102b**	0.96	0.96
2	**102c**	1.02	1.71 ± 0.60
3	**102d**	0.89	0.89
4	**102ea**	0.81	1.08 ± 0.46
5	**102f**	1.3	1.3
6	**102g**	1.5	1.5
7	**102i**	0.98	0.49
8	**102j**	1.17 ± 0.51	0.44
9	**102k**	0.8	1.6
10	**102l**	0.86	1.73
11	**102p**	0.79	1.59
12	**102q**	0.66	0.66
13	**102r**	0.61 ± 0.26	1.22 ± 0.53
14	**107**	0.75	1.00 ± 0.43
15	**109**	0.69	0.91 ± 0.40
16	**110**	1.28	2.56
17	**113**	1.38	1.38
18	**115**	0.58 ± 0.25	1.15 ± 0.50
19	**117**	1.22	1.22
20	**119**	1.53 ± 0.66	1.53 ± 0.66
21	**122**	1.18	0.59
22	**125**	0.69	1.38
23	**127**	1.25 ± 0.54	1.88
24	**129**	1.33	1.33

It is noteworthy that of the benzylic sulfone derivatives tested, the most potent analogues (**102i**, **102j**, **102q** & **102r**) all possess a *p*–methoxyphenyl sulfonyl ring suggesting that this structural feature is essential to antibacterial activity (**Scheme 31**). Of the six non–methoxylated sulfone analogues tested none achieved an MIC value < 0.81 mM, meanwhile of the seven *p*–methoxy sulfone derivatives tested four obtained MIC values < 0.67 mM against at least one of the two bacterial species. Furthermore as previously noted, several hit structures possessing this *p*–methoxy functional group were identified throughout the course of the *in silico* screening programme.
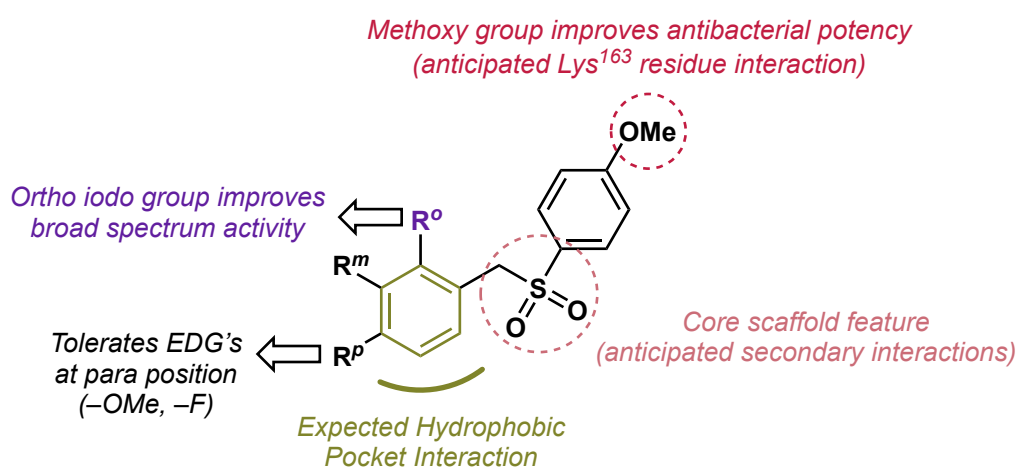
Scheme 31. *Diagram showing SAR of benzylic sulfone analogues determined thus far accounting for the apparent increased antibacterial activity of p–methoxyphenyl sulfonyl derivatives **102i, 102j, 102q** and **102r**.*

Inspection of the *p*–methoxy derivatives tested thus far uncovers some initial SAR features regarding the benzyl ring, a key structural feature anticipated to occupy a hydrophobic pocket within the DHDPS active site according to *in silico* docking results. At the *para* position electron donating groups appear to be well tolerated (**102j** & **102r**) with such analogues providing similar antibacterial activity to sulfone **102i**. By comparison *para* situated electron withdrawing groups (**102k** & **102l**) appear to not be tolerated, resulting in reduced antibacterial activity. It is possible that the relatively improved potency of analogue **102j** could be due to the propensity of the benzylic *p*–methoxy group to engage in additional hydrogen bonding interactions with the suspected DHDPS target. However it is clear that this effect is not reciprocated for derivatives bearing functional groups capable of similar intermolecular interactions (**102k** & **102p**). The *meta* and *ortho* positions of the benzyl ring remain so far underexplored, however the disappointing performance of sulfone **102p** appears to indicate that unlike the *para*

position, methoxy groups are not tolerated at the *meta* and *ortho* positions resulting in diminished antibacterial activity. The incorporation of an iodide group at the *ortho* position (**102q**) is not only tolerated, but also appears to be congruent to obtaining more broad spectrum antibacterial activity considering that sulfone **102q** is the only derivative tested that exhibits relatively good activity against both *E. coli* and *S. aureus* species.

Moving forward the piperidine sulfide **107** and its corresponding sulfone **109**-representing the potential DHDPS inhibitor ZINC154138- were found to be reasonably effective inhibitors of *E. coli* growth (Entry 14 & 15, **Table 7**). Sulfone **109** was determined to be the marginally more potent analogue against both species, however as in several previous cases the antibacterial activity of both derivatives against *S. aureus* was comparatively deficient (**Scheme 32**). Alongside the sulfonyl group, the *in silico* docking results obtained for sulfone **109** suggest the piperidine amine and phenyl ring as the key binding features to be investigated *via* future SAR studies. The commercially available 4-methylsulfonyl benzoic acid (**110**) performed disappointingly, showing low levels of antibacterial activity against both species despite representing the *in silico* derived candidate ZINC153751 that appeared to possess a significant affinity for the DHDPS binding site as suggested by the virtual docking results (Entry 16, **Table 7**).
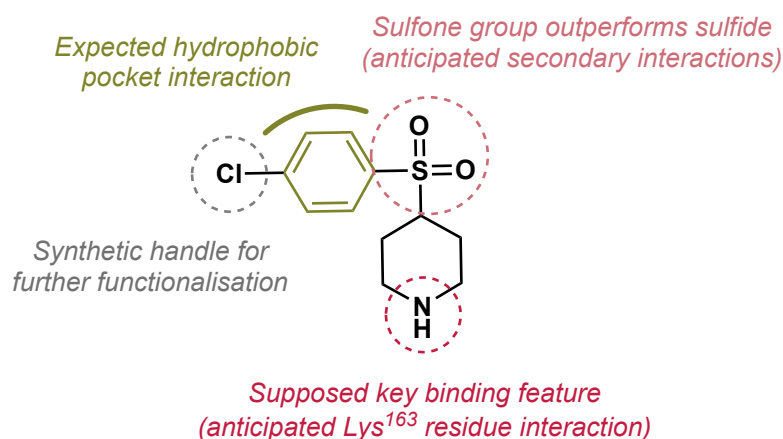
Scheme 32. *Proposed SAR of key functional groups based on binding features identified in silico and the in vitro performance of sulfide **107** and sulfone **109**.*

Another direct representative of a virtual hit structure that performed unsatisfactorily was the piperidone glyoxylate **113** (ZINC259808968), with MIC values of 1.38 mM obtained against both bacterial species (Entry 17, **Table 7**). The structurally related sulfonamide piperidone **115** by comparison was found to exhibit considerably improved antibacterial activity against *E. coli*, obtaining the lowest MIC value observed (0.58 mM) against the gram-negative strain among all candidate structures tested *in vitro* (Entry 18, **Table 7**). However, although the computational homolog of **115** (ZINC20223890) demonstrated significant inhibitory potential as represented within the virtual docking process, *in vitro* the sulfonamide remained unavailing against *S. aureus* (**Scheme 33**). Considering the relatively poor performance of derivative **113** it is unlikely that the piperidone carbonyl functionality present in **115** is an optimal key binding feature, as proposed by the prior *in silico* docking studies. Further SAR studies of the sulfonamide scaffold focusing on elaboration of the acetamide moiety and substitution of the piperidone group are suggested for proceeding investigations. Regarding the remaining synthesised glyoxalates **117** and **119**, both possessed only weak antibacterial activity despite the promise demonstrated *in silico* by ZINC28295599 which served as the motivating structure for both derivatives (Entry 19 & 20, **Table 7**).

Potentially suboptimal binding feature (anticipated Lys^{163} residue interaction)

Synthetic handle with under explored role in potential protein–ligand binding

Core scaffold feature (anticipated secondary binding interactions)
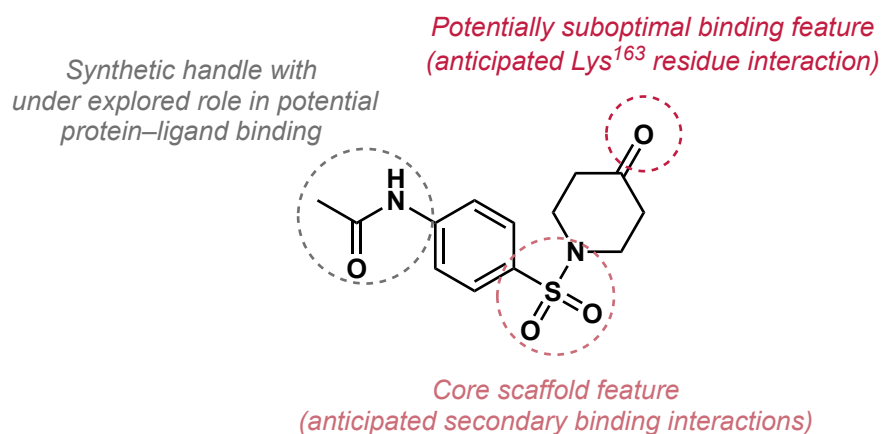
Scheme 33. *Overview of structural features of sulfonamide **115** suspected to considerably influence antibacterial activity based on in silico screening pharmacophore profiles and in vitro activity of derivatives **113** and **115**.*

The isatin **122**- representing the virtual hit ZINC71483382 as the ethyl ester analogue- was found to possess only weak antibacterial activity against *E. coli*, while exhibiting considerably greater potency against *S. aureus* contrary to the majority of compounds tested (Entry 21, **Table 7**). On the basis of the *in silico* docking results obtained for isatin derivative ZINC71483382, straightforward derivatisation of the α,β–unsaturated ester

moiety of analogue **122** appears to be the most direct way of ascertaining the relative importance of this supposed binding feature (**Scheme 34**). The aromatic ring of **122** is anticipated to engage with a hydrophobic pocket contiguous to the active site, and therefore substituent effects are likely to heavily impact binding efficiency as well as the overall stability of the isatin core.
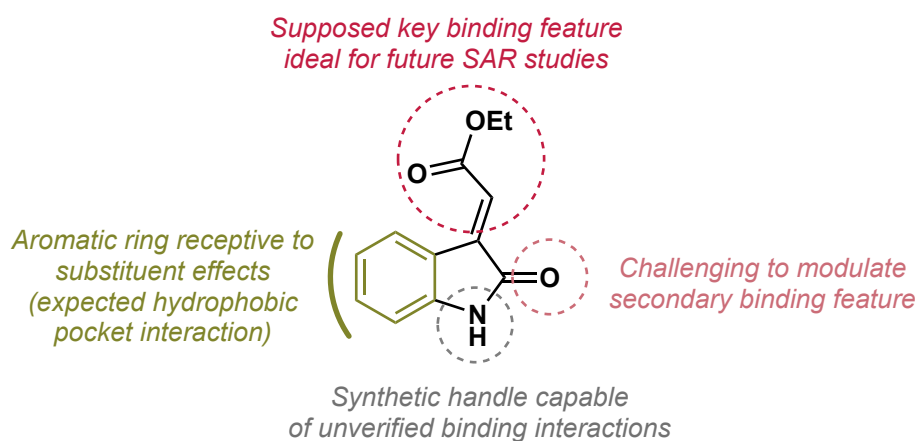
Scheme 34. *Overview of key structural features of isatin **122** to be considered in the proceeding rounds of hit compound design and synthesis.*

Possessing three polar functional groups with widespread representation across the initial pharmacophores, tetrazole **125** showed relatively impressive levels of antibacterial activity against *E. coli* (Entry 22, **Table 7**). However comparable activity against *S. aureus* required significantly elevated concentrations. Considering the relatively impressive performance of other piperidine derivatives (**107** & **109**) future SAR investigations to determine the importance of the secondary amine group of **125** in target binding are likely to be congruent to progress (**Scheme 35**). Furthermore, the carbonyl group and adjacent phenyl ring represent ideal points of variation regarding the design of subsequent analogues. Finally the two hydrazone derivatives tested (**127** & **129**) despite bearing close structural similarities with, ZINC72370081, ZINC2666610 and ZINC490675521 showed very low levels of antibacterial activity against both species (Entry 23–25, **Table 7**).

Aromatic ring receptive to substituent effects

Core scaffold feature (potential Lys^{163} interactions/ secondary interactions)

Synthetic handle potentially capable of secondary binding interactions

Potential key binding feature (anticipated Lys^{163} residue interaction)
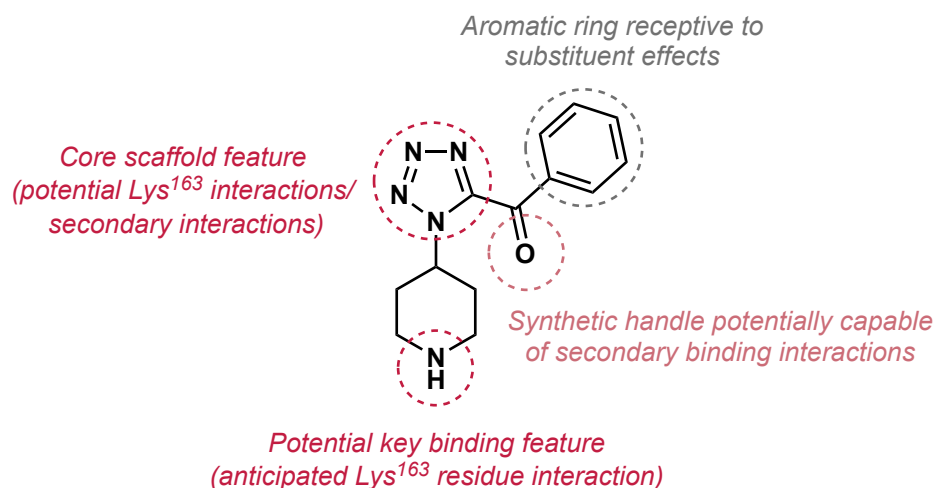
Scheme 35. *Overview of key structural features of tetrazole **125** based on binding features determined in silico and the in vitro activity of other piperidine derivatives tested thus far.*

Despite the promise shown by certain sulfone derivatives (**102i**, **102j**, **102q**, **102r** & **109**) as well as sulfonamide **115**, isatin **122** and tetrazole **125** their level of antibiotic activity remains significantly below the required level to be considered lead candidates worthy of inclusion in further MIC assays and mechanism of action studies. In order to be of potential pre-clinical interest an improvement in potency by at least a factor of a hundred is required, as a benchmark the antibiotic ciprofloxacin has been reported to possess MIC values of 1.81 μM and 48.3 nM against *S.aureus* and *E.coli* strains respectively.[193] Therefore the development of more potent analogues *via* iterative rounds of virtual docking studies, synthesis and antimicrobial testing based around the structural features of the best performing derivatives is necessary before expansion of the project scope can be considered.

2.7. *Conclusions and Future Work*

In summary the aforementioned work describes the implementation of molecular mechanical computational models to conduct *in silico* screening of virtual compound libraries. This consisted of pharmacophore profiling and qualitative assessment of supposed docking interactions between ligands and the crystal structure of the *S.aureus* DHDPS active site, utilising the structure and *in silico* derived binding interactions of known DHDPS inhibitors (**25** & **37**) and pyruvate substrate (**9**) to determine the antibacterial potential of hit compounds.

Once identified as virtual hits, truncated derivatives of the prospective antibacterial scaffolds were outlined as synthetic targets. Towards this end a novel and atom economical photocatalytic transformation of bench-stable sulfonylhydrazone reagents (**101**) into the corresponding benzylic sulfones (**102**) was developed, and subsequent exploration of the substrate scope led to the synthesis of numerous aromatic sulfones often in good to excellent yields. This discovery enabled straightforward access to a molecular scaffold identified as a recurring virtual hit according to the preceding virtual docking studies, and thus of significant interest in the pursuit of novel antibacterial compounds.

Mechanistic studies including radical trap experiments, deuterium labelling studies, nucleophilic crossover experiments and ^{1}H NMR reaction monitoring were undertaken to discern the presence of key reaction intermediates as well as details pertaining to specific steps. Supported by DFT calculations, a chain mechanism involving formation of a diazo radical intermediate *via* dissociation of the sulfonyl group followed by HAT and radical propagation involving another molecule of the hydrazone starting material **101** was proposed.

As elucidated by the prior mechanistic investigations, the narrow substrate scope accessed by the photoredox methodology meant that additional sulfone derivatives of interest such as **109** had to be obtained utilising conventional synthetic approaches. The synthesis of additional *in silico* derived molecular targets including 1,2-dicarbonyl derivatives, (**113**, **117** & **119**) sulfonamide **115**, isatin **122**, tetrazole **125** and hydrazone

derivatives (**127** & **129**) was accomplished using established methodology comprised of 1–5 synthetic steps to afford the desired products in a straightforward fashion. Attempts to employ hydrazone **129** as a substrate for photoredox transformations analogous to those of sulfonylhydrazones were unsuccessful despite extensive attempts at reaction optimisation, only affording the undesired aldehyde **128** in low yield on occasion.

The assembled compound library was subjected to MIC assays against *E.coli* and *S.aureus* strains to evaluate their antibacterial activity. Iodinated derivative **102q** demonstrated the most potent overall activity against both species, while fluorinated sulfone **102r** and sulfonamide **115** displayed the highest level of efficacy against gram-negative *E.coli*. Conversely sulfone **102j** and isatin **122** were found to be the most potent derivatives against gram-positive *S.aureus*, and regarding the benzylic sulfone derivatives (**102**) it was noted that the presence of a *p*-methoxyphenyl sulfonyl group was required in order to obtain antibacterial activity above the norm. Despite the relative promise of these findings, the level of antibacterial activity shown by even the more potent derivatives remains far below the benchmark required to warrant further pursual as lead candidates in their own right.

Regarding potential avenues for future work, further mechanistic studies concerning the photocatalytic rearrangement of sulfonylhydrazones would be pertinent in order to more concretely establish the proposed reaction steps. Actinometry experiments could be conducted to determine the quantum yield of the reaction and thus establish the presence or absence of a chain mechanism, and DFT- ^{1}H NMR calculations could be undertaken to determine beyond doubt the identity of the reaction intermediate corresponding to the observed peak at 5.76 δ/ppm. Additional IR reaction monitoring experiments should be considered to complement the results of the ^{1}H NMR monitoring experiments, aiding to determine the presence and identity of intermediate diazo species. The results of these mechanistic studies could potentially be utilised in the discovery of novel photocatalytic transformations involving hydrazone reagents, demonstrating wider applicability. The current state of the methodology clearly imposes limitations as to the substrate scope available, however sulfonylhydrazones bearing alternative electron–withdrawing groups to phenyl rings are expected to be tolerated. The reaction outcome appears to be considerably less affected by alterations to the sulfonyl fragment of hydrazone **101**, which therefore constitutes the more promising approach for further exploration of the substrate

scope. Furthermore, the employment of dedicated HAT agents is envisaged to potentially broaden the reaction substrate scope by enabling more feasible radical abstraction by the key diazo radical intermediate. Investigation of a wider range of hydrazone substrates may also facilitate the discovery of improved or novel modes of reactivity through manipulation of the dissociation step *via* stereo-electronic effects.

Another aspect of proposed future work concerns the *in silico* screening, synthesis and antimicrobial testing of additional candidates based around the structural features of the most potent compounds discerned thus far. This allows for enhanced understanding of the structure-activity relationships while also progressing towards the attainment of derivatives with improved antibacterial activity. As the most promising candidate regarding broad-spectrum activity, *m*– and *p*–iodo analogues of **102q** should be investigated to see if they possess similar activities to the *o*– structural isomer. In a similar fashion investigation of halide and pseudo-halide functional groups *ortho* to the benzylic carbon in place of the iodide would also liberate valuable information regarding the structure-activity relationships. Amalgamation of the best performing sulfone structures (**102i**, **102j**, **102q** & **102r**) to generate various derivatives bearing different iterations of methoxy, fluorine and iodine substituents would constitute another set of high potential analogues worthy of assessment *via* virtual docking. The investigation of different analogues of sulfone **109** through *in silico* docking procedures, particularly focusing on the introduction of methoxy groups and other hydrogen bonding groups to the aromatic ring as well as amine substitution is likely to uncover key details to inform further SAR studies through *in vitro* testing. In a similar fashion investigation of the chemical space surrounding sulfonamide **115** is commended to provide insight into the underlying structural motifs responsible for the observed antibacterial activity, focusing on the inclusion of bioisosteres and additional hydrogen-bonding groups around the carbonyl moiety as well as different substitution patterns around the aromatic sulfonyl ring. Substitution of the ester moiety of **122** with the corresponding carboxylic acid and related bioisosteres, as well as the inclusion of additional hydrogen bonding groups and synthetic handles as substituents of the aromatic ring is anticipated to provide additional suitable candidates for the proceeding round of virtual docking studies and eventual *in vitro* testing. Utilising the secondary amine and carbonyl group as synthetic handles for further elaboration, analogues of the tetrazole derivative **125** can be achieved in a straightforward manner following *in silico* evaluation.

As the overall process of *in silico* screening, synthesis and phenotypic screening takes the form of an iterative cycle, this provides a straightforward outline for the basis and order of immediate continuing work until compounds of sufficiently improved potency (MIC: < 50 μM) are obtained. Satisfaction of this condition alone would warrant further investigation of the *in vitro* behaviour of the antibacterial candidates through mechanism of action studies, this would include screening satisfactory compounds against the DHDPS/DHDPR dual enzyme assay in order to assess potential DHDPS inhibitory activity. These target–based screening steps would also be accompanied by an expansion of the phenotypic screening process in order to evaluate antibacterial activity against clinically relevant bacterial strains, resistance susceptibility testing and counter–screening assays to monitor the emergence of general cytotoxicity.

Chapter 3

Experimental Materials and Methods

3.1. In Silico Screening Procedures

3.1.1. Pharmacophore Modelling and Searches

All *in silico* procedures were perfomed using a 2013 MacBook Air (1.3 GHz Intel Core i5 processor). Pharmacophore models were constructed and queried using CSD-Crossminer employing point features provided by the Cambridge Structure Database (CSD) with tolerance radii set at 1.50 Å for all features.[95] Pharmacophore searches based on reference structures **9**, **25** and **37** were performed against the ZINC database of compounds (molecular weight: 200–400, LogP: –1–3.5, reactivity: "Anodyne").[96] Additional pharmacophore screening of the commercially available ZINC database was performed using ZINCPharmer employing the same reference structures and point features (molecular weight: 100–500, LogP: –1–5.0, purchasability: "In-Stock").[97]

Compound clustering and diverse set selection was performed using OSIRIS DataWarrior 4.4.4.[99] Compound libraries were segregated based on molecular weight, LogP and Murcko scaffold analysis with structural similarity calculations conducted using the FragFp chemical structure descriptor (similarity limit = >0.8). Diverse compound selection was limited to <1% of the overall library size.

3.1.2. Docking Studies

Structures for docking were modelled using OSIRIS DataWarrior 4.4.4 with conformers generated using a random low energy bias algorithim and energy minimised with MMFF94s force field.[194] The crystal structure model of DHDPS was obtained from the worldwide Protein DataBank (PDB ID: 3DI1).[33,35] Docking studies were performed using CSD GOLD.[100] The active site was defined as a 10.0 Å radius cavity around the bound pyruvate substrate which was removed alongside water molecules situated outside the boundary of the selected cavity, manual corrections to the protonation state were applied. 10 docking poses per ligand were assessed using the ChemPLP fitness function and rescored with GoldScore to optimise pose prediction, employing automatic parameters for docking efficiency.[102] The conformations of completed docking runs were visualised using PyMol 2.01 molecular graphics system (Schrödinger, LLC).

3.2. Chemistry Procedures

3.2.1. General Methods

All reactions were performed using oven dried glassware (100 °C). All solvents were purchased as high performance liquid chromatography (HPLC) grade from Fisher Scientific and used as supplied unless otherwise stated. Anhydrous CH_2Cl_2 was purchased from Sigma-Aldrich and used as supplied. All reagents were used as supplied or purified *via* standard procedures if necessary. All working solutions were aqueous and comprised of deionised water purified using a Millipore Direct Q 8UV purification system unless stated otherwise.

All photochemical experiments were performed using Integral™ 12 V DC constant voltage 50 W max (6 W/m) LED strip light sources with 45 mm path length photoreactors conducted at wavelengths ~470 nm (blue) and ~525 nm (green) as specified.

Flash column chromatography was performed using W.R. Grace Davisil™ silica gel 60Å pore size 40–63 μm particle size purchased from Fisher Scientific under air pressure. Analytical thin layer chromatography (TLC) was performed using silica gel 60 F_{254} pre-coated glass or aluminium backed plates and visualised *via* ultraviolet radiation (254 nm), iodine adsorbed on silica, or potassium permanganate as appropriate.

Quantities are reported to 3 significant figures and are rounded accordingly. Isolated yields are reported to 0 decimal places and "quant." signifies a yield of ≥99.5%.

^{1}H NMR spectra were recorded on Bruker Ultrashield-400 (400 MHz). Chemical shifts are reported in ppm with the resonance resulting from incomplete deuteration of the solvent as the internal standard ($CDCl_3$: 7.26 δ/ppm, CD_3OD: 3.31 δ/ppm, DMSO-d_6: 2.50 δ/ppm). ^{13}C NMR spectra were recorded on Bruker Ultrashield-400 (100 MHz) with complete proton decoupling. Chemical shifts are reported in ppm with the resonance resulting from incomplete deuteration of the solvent as the internal standard ($CDCl_3$: 77.0 δ/ppm t, CD_3OD: 49.0 δ/ppm septet, DMSO-d_6: 39.5 δ/ppm septet). ^{19}F NMR were recorded on Bruker Ultrashield-400 (377 MHz) with complete proton decoupling. Chemical shifts are reported in ppm without reference to an internal standard.

Data is reported as follows: chemical shift δ/ppm (integration (1H only), multiplicity (s = singlet, d = doublet, t = triplet, q = quartet, quint = quintet, sxt = sextet, spt = septet, oct = octet, non = nonet, br = broad, app = apparent, m = multiplet or combinations thereof. ^{13}C signals are singlets unless otherwise stated), coupling constants J Hz, assignment).

Spectra are assigned as fully as possible, using ^{1}H-COSY, ^{13}C-DEPT, HMQC and HMBC where appropriate to facilitate structural determination. Multiple signals arising from diastereotopic or (pseudo-)axial/equatorial positions are suffixed alphabetically (e.g. H1a, H1b). Terminal alkene signals are further designated *cis/trans* according to relative magnitude of the observed $^3J_{HH}$ values where distinguishable. Overlapping signals that cannot be resolved are reported with their assignments denoted in list format (eg. H1, H2 & H3). ^{1}H NMR signals are reported to 2 decimal places and ^{13}C signals to 1 decimal place unless rounding would result in identical values corresponding to different signals, in which case an additional decimal place is reported for both signals concerned.

High resolution mass spectrometry (HRMS) was performed on a Waters XEVO G2-XS QTof using atmospheric pressure chemical ionisation (positive ion mode) conducted with an atmospheric solids analysis probe (ASAP). HRMS signals are reported to 4 decimal places and are within ± 5 ppm of theoretical values.

Infrared (IR) spectra were recorded neat as thin films on a Bruker Alpha Platinum ATR-FTIR and only selected peaks are reported (s = strong, m = medium, w = weak, br = broad).

3.2.2. Synthetic Procedures

2-(allyloxy)benzaldehyde **(57m)**. Prepared according to a known procedure.[195] To a solution of salicylaldehyde (6.11 g, 50.0 mmol, 1.0 equiv), in DMF (25 mL) was added allyl bromide (6.48 mL, 75.0 mmol, 1.5 equiv) dropwise followed by K_2CO_3 (10.4 g, 75.0 mmol, 1.5 equiv). The reaction mixture was stirred at room temperature for 23 hours, diluted with water (100 mL) and partitioned with EtOAc (50 mL). The aqueous layer was extracted with pentane (3 x 50 mL), and the collected organic layers were washed with 5% w/v LiCl solution (6 x 35 mL) and dried over $MgSO_4$. Solvents were removed *in vacuo* to yield the desired compound as a yellow oil (7.54 g, 46.5 mmol, 93%).
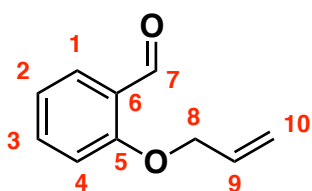
2-(allyloxy)benzaldehyde
Molecular Weight: 162.19

57m

¹H NMR (400 MHz, $CDCl_3$): δ 4.64 (2H, ddd, *J* 5.2, 1.6 Hz, H8), 5.33 (1H, dd, *J* 10.6,1.4 Hz, H10a-*cis*), 5.45 (1H, dd, *J* 17.2, 1.4 Hz, H10b-*trans*), 6.02-6.11 (1H, m, H9), 6.96 (1H, d, *J* 8.7 Hz, H4), 7.01 (1H, dd, *J* 7.6, 7.5 Hz, H2), 7.52 (1H, ddd, *J* 7.4, 6.6, 1.9 Hz, H3), 7.82, (1H, dd, *J* 7.7, 1.8 Hz, H1), 10.52 (1H, s, H7).

¹³C NMR (100 MHz, $CDCl_3$): δ 69.1 (C8), 112.8 (C4), 118.1 (C10), 120.9 (C2), 125.0 (C6), 128.4 (C1), 132.4 (C9), 135.9 (C3), 161.0 (C5), 189.8 (C7).

FTIR (υ_{max}cm⁻¹): 3077 (w, CH_X), 2761-2862 (m, CH, aldehyde), 1682 (s, C=O), 1424-1597 (s, C–C), 1221 (s, C–O).

R$_f$: 0.74 (20:80 EtOAc/hexane).

Data is consistent with a reported example.[195]

General Synthetic Procedure A: Preparation of Sulfonylhydrazides

Compounds were prepared according to a known procedure.[82] To a cooled (0 °C) solution of sulfonyl chloride (1.0 equiv) in THF (0.2 M) was added hydrazine monohydrate (2.5 equiv) dropwise with stirring. The reaction mixture was allowed to reach room temperature and was monitored by TLC until complete conversion was observed, before being partitioned between EtOAc and saturated brine solution. The aqueous layer was extracted with EtOAc (x 3) and the collected organic layers dried over MgSO$_4$. Solvents were removed *in vacuo* to give the title compound without further purification.

4-Chlorobenzenesulfonohydrazide (**58b**). Isolated as a white solid (1.80 g, 8.70 mmol, 87%) according to general procedure A.
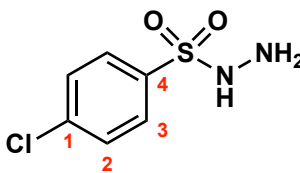
4-chlorobenzenesulfonohydrazide
Molecular Weight: 206.64

58b

^{1}H NMR (400 MHz, DMSO-d_6): δ 4.19 (2H, br, -NH$_2$), 7.68 (2H, d, *J* 8.7 Hz, H2), 7.80 (2H, d, *J* 8.7 Hz, H3), 8.48 (1H, br, -NH).

^{13}C NMR (100 MHz, DMSO-d_6): δ 129.6 (C2), 130.1 (C3), 137.6 (C4), 137.9 (C1).

FTIR (υ_{max}cm^{-1}): 3291 (m, NH), 3085 (w, CH$_x$), 1611 (m, NH), 1474 (m, C–C).

R$_f$: 0.11 (30:70 EtOAc/hexane).

Data is consistent with a reported example.[196]

***4-Fluorobenzenesulfonohydrazide* (58c)**. Isolated as a white solid (1.71 g, 8.97 mmol, 90%) according to general procedure A.
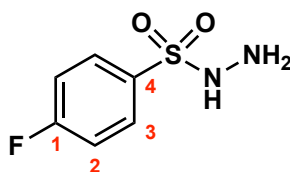
4-fluorobenzenesulfonohydrazide
Molecular Weight: 190.19

58c

^{1}H NMR (400 MHz, CDCl$_3$): δ 3.66 (2H, br, -NH$_2$), 5.83 (1H, br, -NH), 7.29 (2H, m, H2), 7.98 (2H, dd, *J* 9.0, 5.0 Hz, H3).

^{13}C NMR (100 MHz, CDCl$_3$): δ 116.7 (d, *J* 22.7 Hz, C2), 131.1 (d, *J* 9.6 Hz, C3), 132.4 (d, *J* 3.4 Hz, C4), 165.7 (d, *J* 256.3 Hz, C1).

FTIR (υ$_{max}$cm^{-1}): 3290 (m, NH), 3065 (w, CH$_x$), 1612 (m, NH), 1492 (m, C–C).

R$_f$: 0.14 (30:70 EtOAc/hexane).

Data is consistent with a reported example.[196]

***N-(4-(hydrazineylsulfonyl)phenyl)acetamide* (58d)**. Isolated as a white solid (1.88 g, 8.22 mmol, 82%) according to general procedure A.
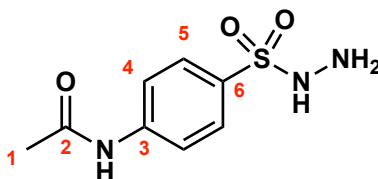
N-(4-(hydrazineylsulfonyl)phenyl)acetamide
Molecular Weight: 229.25

58d

^{1}H NMR (400 MHz, DMSO-*d$_6$*): δ 2.10 (3H, s, H1), 4.01 (2H, br, -NH$_2$), 7.70 (2H, d, *J* 8.9 Hz, H5), 7.82 (2H, d, *J* 8.9 Hz, H4), 8.30 (1H, br, SO$_2$-NH), 10.70 (1H, br, -NH).

^{13}C NMR (100 MHz, DMSO-*d$_6$*): δ 24.1 (C1), 118.5 (C4), 128.7 (C5), 131.5 (C6), 143.2 (C3), 169.2 (C2).

FTIR (υ_{max}cm^{-1}): 3528 (m, NH), 3175-2827 (m, CH$_x$), 1681 (s, C=O), 1608 (m, NH), 1537 (m, C-C).

R$_f$: 0.33 (5:10:80:5 AcOH/*n*-BuOH/EtOAc/H$_2$O).

Data is consistent with a reported example.[197]

5-bromothiophene-2-sulfonohydrazide **(58e)**. Isolated as a pale yellow solid (2.41 g, 9.38 mmol, 94%) according to general procedure A.
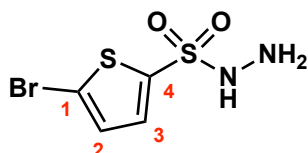
5-bromothiophene-2-sulfonohydrazide
Molecular Weight: 257.12

58e

^{1}H NMR (400 MHz, CDCl$_3$): δ 3.14 (2H, br, -NH$_2$), 5.70 (1H, br, -NH), 7.14 (1H, d, *J* 4.0 Hz, H3), 7.47 (1H, d, *J* 4.0 Hz, H2).

^{13}C NMR (100 MHz, CDCl$_3$): δ 121.7 (C1), 130.8 (C3), 134.4 (C2), 137.5 (C4).

FTIR (υ_{max}cm^{-1}): 3291 (m, NH), 3099 (m, CH$_x$), 1399-1332 (m, C–C).

R$_f$: 0.11 (30:70 EtOAc/hexane).

Data is consistent with a reported example.[198]

Cyclopropanesulfonohydrazide **(58f)**. Isolated as a white solid (1.07 g, 7.83 mmol, 78%) according to general procedure A.
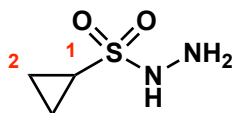
cyclopropanesulfonohydrazide
Molecular Weight: 136.17

58f

¹H NMR (400 MHz, CDCl₃): δ 1.07 (2H, app sxt, *J* 8.0, 7.4, 5.0 Hz, H2a), 1.24 (2H, app sxt, *J* 7.1, 7.2, 5.0 Hz, H2b), 2.46 (1H, app non, *J* 8.0, 4.9 Hz, H1), 3.21 (2H, br, -NH₂), 5.50 (1H, br, -NH).

¹³C DEPT-135 NMR (100 MHz, CDCl₃): δ 5.0 (C2), 27.2 (C1).

FTIR (υ_{max}cm⁻¹): 3349-3248 (m, NH), 3064-2095 (w, CHₓ), 1643 (m, NH), 1435 (m, C–C).

R$_f$: 0.12 (30:70 EtOAc/hexane).

Data is consistent with a reported example.[198]

***Methanesulfonohydrazide* (58g)**. Isolated as a white solid (0.989 g, 8.98 mmol, 90%) according to general procedure A.
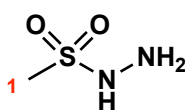
methanesulfonohydrazide
Molecular Weight: 110.13

58g

¹H NMR (400 MHz, DMSO-*d₆*): δ 2.87 (1H, s, H1), 4.36 (2H, br, -NH₂), 7.73 (1H, br, -NH).

¹³C NMR (100 MHz, DMSO-*d₆*): δ 36.4 (C1).

FTIR (υ_{max}cm⁻¹): 3214 (m, NH), 3017-2850 (w, CH₃), 1635 (m, NH), 1420-1317 (m, CH₃).

R$_f$: 0.16 (30:70 EtOAc/hexane).

***4-Nitrobenzenesulfonohydrazide* (58h)**. Isolated as a tan solid (2.11 g, 9.71 mmol, 97%) according to general procedure A.
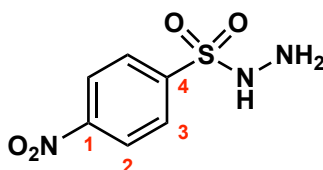
4-nitrobenzenesulfonohydrazide
Molecular Weight: 217.20

(58h)

^{1}H NMR (400 MHz, DMSO-d_6): δ 4.34 (2H, br, -NH$_2$), 8.05 (2H, d, *J* 8.9 Hz, H3), 8.42 (2H, d, *J* 8.9 Hz, H2), 8.77 (1H, br, -NH).

^{13}C NMR (100 MHz, DMSO-d_6): δ 124.3 (C2), 129.3 (C3), 144.2 (C4), 149.7 (C1).

FTIR (υ_{max}cm^{-1}): 3274 (m, NH), 3104 (w, CH$_x$), 1623 (m, NH), 1601 (m, C–C), 1521 (s, N–O).

R$_f$: 0.10 (30:70 EtOAc/hexane).

Data is consistent with a reported example.[196]

***4-Methoxybenzenesulfonohydrazide* (58i)**. Isolated as a white solid (2.02 g, 10.0 mmol, quant.) according to general procedure A.
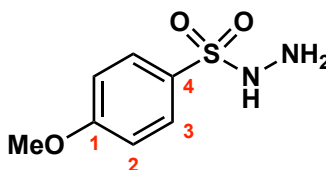
4-methoxybenzenesulfonohydrazide
Molecular Weight: 202.23

58i

^{1}H NMR (400 MHz, CDCl$_3$): δ 3.59 (2H, br, -NH$_2$), 3.89 (3H, s, -OMe), 5.58 (1H, br, -NH), 7.02 (2H, d, *J* 9.0 Hz, H2), 7.85 (2H, d, *J* 9.0 Hz, H3).

^{13}C NMR (100 MHz, CDCl$_3$): δ 55.7 (-OMe), 114.5 (C2), 127.4 (C4), 130.5 (C3), 163.7 (C1).

FTIR (υ_{max}cm^{-1}): 3376-3251 (m, NH), 3096-2048 (w, CH$_x$), 1593 (m, NH), 1575 (m, C–C), 1152 (s, C–O).

R$_f$: 0.15 (30:70 EtOAc/hexane).

Data is consistent with a reported example.[196]

General Synthetic Procedure B: Preparation of Sulfonylhydrazones

Compounds were prepared according to a known procedure.[82] To a solution of sulfonylhydrazide (1.0 equiv) suspended in MeOH (0.3 M) was added aldehyde (1.0 equiv). The reaction mixture was stirred at room temperature until complete conversion was observed by TLC. Solvents were removed *in vacuo* to give the title compound.

(E/Z)-N'-Benzylidene-4-methylbenzenesulfonohydrazide **(101a)**. Isolated as a white solid (2.72 g, 9.92 mmol, 89%) according to general procedure B.
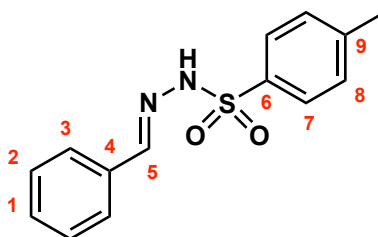
(*E/Z*)-N'-benzylidene-4-methylbenzenesulfonohydrazide
Molecular Weight: 274.34

101a

^{1}H NMR (400 MHz, CDCl$_3$): δ 2.41 (3H, s, H10), 7.31 (2H, d, *J* 8.0 Hz, H8), 7.34-7.38 (3H, m, H1 & H2), 7.57-7.59 (2H, m, H3), 7.75 (1H, s, H5), 7.86 (1H, br, -NH), 7.88 (2H, d, *J* 8.4 Hz, H7).

^{13}C NMR (100 MHz, CDCl$_3$): δ 21.6 (C10), 127.4 (C3), 128.0 (C7), 128.7 (C2), 129.7 (C8), 130.5 (C1), 133.1 (C4), 135.3 (C6), 144.4 (C9), 147.8 (C5).

FTIR (υ$_{max}$cm^{-1}): 3225 (m, NH), 2916-3067 (w, CH$_x$), 1596 (m, NH), 1495 (m, C–C), 1363 (m, S=O).

HRMS (ASAP+): calculated for C$_{14}$H$_{14}$N$_2$O$_2$S [M+H$^+$] 275.0854, found: 275.0851

R$_f$: 0.31 (30:70 EtOAc/hexane).

Data is consistent with a reported example.[82]

(E/Z)-N'-Benzylidene-4-chlorobenzenesulfonohydrazide **(101b)**. Isolated as a white solid (0.734 g, 2.49 mmol, quant.) according to general procedure B.
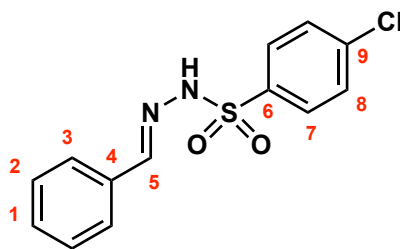
(E/Z)-N'-benzylidene-4-chlorobenzenesulfonohydrazide
Molecular Weight: 294.75

101b

¹H NMR (400 MHz, CDCl$_3$): δ 7.33-7.39 (3H, m, H1 & H2), 7.49 (2H, d, *J* 8.6 Hz, H8), 7.57 (2H, dd, *J* 7.7, 1.8 Hz, H3), 7.78 (1H, s, H5), 7.94 (2H, d, *J* 8.6 Hz, H7), 8.17 (1H, br, -NH).

¹³C NMR (100 MHz, CDCl$_3$): δ 127.4 (C3), 128.8 (C2), 129.4 (C7 & C8), 130.8 (C1), 132.8 (C4), 136.7 (C6), 140.0 (C9), 148.5 (C5).

FTIR (υ$_{max}$cm^{-1}): 3177 (m, NH), 3094 (w, CH$_x$), 1571 (m, NH), 1477 (m, C–C), 1361 (s, S=O).

HRMS (ASAP+): calculated for C$_{13}$H$_{11}$ClN$_2$O$_2$S [M+H$^+$] 295.0308 found: 295.0316

R$_f$: 0.28 (30:70 EtOAc/hexane).

(E/Z)-N'-Benzylidene-4-fluorobenzenesulfonohydrazide **(101c)**. Isolated as a white solid (0.850 g, 3.00 mmol, quant.) according to general procedure B.
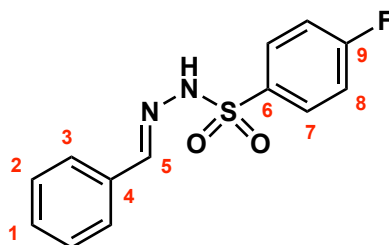
(E/Z)-N'-benzylidene-4-fluorobenzenesulfonohydrazide
Molecular Weight: 278.30

101c

¹H NMR (400 MHz, CDCl$_3$): δ 7.20 (2H, dd, *J* 8.7, 8.1 Hz, H8), 7.33-7.39 (3H, m, H1 & H2), 7.58 (2H, dd, *J* 7.6, 2.4 Hz, H3), 7.78 (1H, s, H5), 8.02 (2H, dd, *J* 9.0, 4.9 Hz, H7), 8.10 (1H, br, -NH).

¹³C NMR (100 MHz, CDCl₃): δ 116.4 (d, *J* 22.7 Hz, C8), 127.4 (C3), 128.8 (C2), 130.7 (C7), 130.8 (C1), 132.9 (C4), 134.2 (d, *J* 3.0 Hz, C6), 148.3 (C5), 165.5 (d, *J* 255.9 Hz, C9).

FTIR (υ_{max}cm⁻¹): 3198 (m, NH), 3083-3062 (w, CHₓ), 1591 (m, NH), 1494 (m, C–C), 1365 (m, S=O).

HRMS (ASAP+): calculated for $C_{13}H_{11}FN_2O_2S$ [M+H⁺] 279.0604 found: 279.0605

R*f*: 0.20 (30:70 EtOAc/hexane).

Data is consistent with a reported example.[199]

(E/Z)-N'-(4-((2-Benzylidenehydrazineyl)sulfonyl)phenyl)acetamide **(101d)**. Isolated as a pale yellow solid (0.636 g 2.00 mmol, 80%) according to general procedure B.
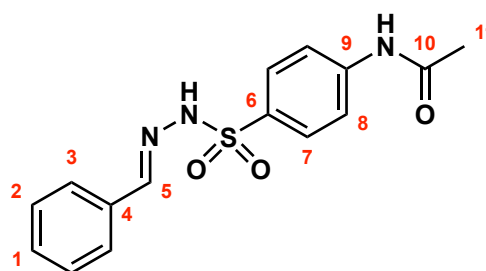
(*E/Z*)-N-(4-((2-benzylidenehydrazineyl)sulfonyl)phenyl)acetamide
Molecular Weight: 317.36

101d

¹H NMR (400 MHz, DMSO-d_6): δ 2.07 (3H, s, H11), 7.38-7.41 (3H, m, H1 & H2), 7.54-7.57 (2H, m, H3), 7.77-7.82 (4H, m, H7 & H8), 7.92 (1H, s, H5), 10.42 (1H, br, C9-NH), 11.43 (1H, br, -NH).

¹³C NMR (100 MHz, DMSO-d_6): δ 24.1 (C11), 118.5 (C8), 126.7 (C3), 128.4 (C2), 128.8 (C7), 130.0 (C1), 132.4 (C6), 133.7 (C4), 143.3 (C9), 146.9 (C5), 169.1 (C10).

FTIR (υ_{max}cm⁻¹): 3327 (m, NH), 3202 (m, NH), 1689 (m, C=O), 1589 (m, NH), 1513 (m, C–C), 1364 (s, S=O).

HRMS (ASAP+): calculated for $C_{15}H_{15}N_3O_3S$ [M+H⁺] 318.0912 found: 318.0910

R*f*: 0.10 (30:70 EtOAc/hexane).

Data is consistent with a reported example.[200]

(E/Z)-N'-Benzylidene-5-bromothiophene-2-sulfonohydrazide **(101e)**. Isolated as a dark yellow solid (0.860 g, 2.49 mmol, quant.) according to general procedure B.
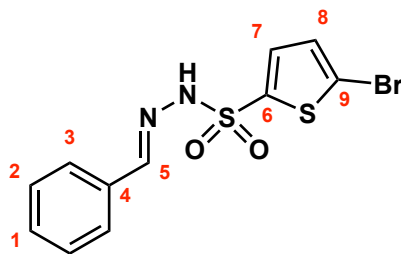
(*E/Z*)-N'-benzylidene-5-bromothiophene-2-sulfonohydrazide
Molecular Weight: 345.23

101e

^{1}H NMR (400 MHz, CDCl$_3$): δ 7.08 (1H, d, *J* 4.0 Hz, H8), 7.38-7.43 (3H, m, H1 & H2), 7.51 (1H, d, *J* 4.0 Hz, H7), 7.63-7.66 (2H, m, H3), 7.82 (1H, s, H5), 7.87 (1H, br, -NH).

^{13}C NMR (100 MHz, CDCl$_3$): δ 121.6 (C9), 127.6 (C3), 128.8 (C2), 130.4 (C8), 130.9 (C1), 132.8 (C4), 133.7 (C7), 138.9 (C6), 149.1 (C5).

FTIR (υ_{max}cm^{-1}): 3180 (m, NH), 3093-2884 (w, CH$_x$), 1682 (w, C=N), 1600 (w, NH), 1445 (m, C–C), 1368 (m, S=O).

HRMS (ASAP+): calculated for C$_{11}$H$_9$BrN$_2$O$_2$S$_2$ [M+H$^+$] 344.9367 found: 344.9376

R$_f$: 0.38 (30:70 EtOAc/hexane).

Data is consistent with a reported example.[174]

E/Z)-N'-Benzylidenecyclopropanesulfonohydrazide **(101f)**. Isolated as a white solid (0.123 g, 0.548 mmol, 61%) according to general procedure B and purified by flash column chromatography (20:80–40:60 EtOAc/hexane).
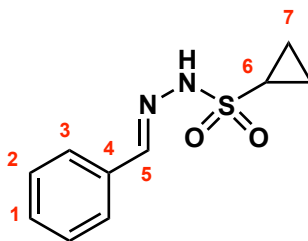
(*E/Z*)-*N'*-benzylidenecyclopropanesulfonohydrazide
Molecular Weight: 224.28

101f

^{1}H NMR (400 MHz, CDCl$_3$): δ 1.07-1.13 (2H, m, H7a), 1.36-1.41 (2H, m, H7b), 2.62-2.69 (1H, m, H6), 7.39-7.42 (3H, m, H1 & H2), 7.65-7.68 (2H, m, H3), 7.73 (1H, br, -NH), 7.83 (1H, s, H5).

¹³C NMR (100 MHz, CDCl₃): δ 5.9 (C7), 29.3 (C6), 127.4 (C3), 128.8 (C2), 130.6 (C1), 133.1 (C4), 147.4 (C5).

FTIR (υ_{max}cm⁻¹): 3144 (m, NH), 1438 (m, C–C), 1323 (s, S=O).

HRMS (ASAP+): calculated for $C_{10}H_{12}N_2O_2S$ [M+H⁺] 225.0698 found: 225.0697

R$_f$: 0.46 (40:60 EtOAc/hexane).

(E/Z)-N'-Benzylidenemethanesulfonohydrazide (**101g**). Isolated as a white solid (0.165 g, 0.830 mmol, quant.) according to general procedure B.
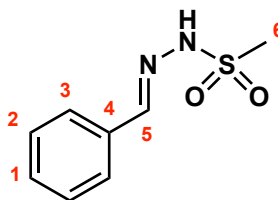
(*E/Z*)-*N*'-benzylidenemethanesulfonohydrazide
Molecular Weight: 198.24

101g

¹H NMR (400 MHz, CDCl₃): δ 3.19 (3H, s, H6), 7.40-7.42 (3H, m, H1 & H2), 7.66-7.69 (3H, m, H3 & -NH), 7.84 (1H, s, H5).

¹³C NMR (100 MHz, CDCl₃): δ 39.0 (C6), 127.5 (C3), 128.8 (C2), 130.8 (C1), 132.9 (C4), 147.9 (C5).

FTIR (υ_{max}cm⁻¹): 3156 (m, NH), 3026-2850 (w, CHₓ), 1686 (w, C=N), 1434 (m, CHₓ), 1349 (s, S=O).

HRMS (ASAP+): calculated for $C_8H_{10}N_2O_2S$ [M+H⁺] 199.0541 found: 199.0554

R$_f$: 0.24 (30:70 EtOAc/hexane).

Data is consistent with a reported example.[201]

(E/Z)-N'-Benzylidene-4-nitrobenzenesulfonohydrazide (**101h**). Isolated as a pale yellow solid (1.52 g, 4.99 mmol, quant.) according to general procedure B.
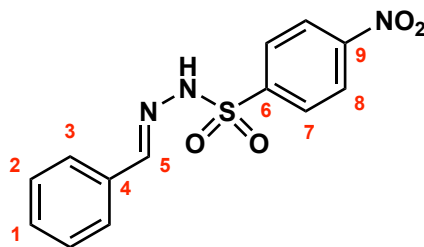
(*E/Z*)-N'-benzylidene-4-nitrobenzenesulfonohydrazide
Molecular Weight: 305.31

101h

^{1}H NMR (400 MHz, CDCl$_3$): δ 7.37-7.42 (3H, m, H1 & H2), 7.58 (2H, dd, *J* 7.8, 2.0, 1.5 Hz, H3), 7.78 (1H, s, H5), 7.95 (1H, br, -NH), 8.20 (2H, d, *J* 9.0 Hz, H7), 8.38 (2H, d, *J* 9.0 Hz, H8).

^{13}C NMR (100 MHz, CDCl$_3$): δ 124.3 (C8), 127.5 (C3), 128.9 (C2), 129.3 (C7), 131.1 (C1), 132.5 (C4), 143.9 (C6), 148.9 (C5).

FTIR (υ$_{max}$cm^{-1}): 3197 (m, NH), 3118-2864 (w, CH$_x$), 1607 (m, NH), 1520 (s, N–O), 1438 (m, C–C), 1364 (s, S=O).

HRMS (ASAP+): calculated for C$_{13}$H$_{11}$N$_3$O$_4$S [M+H$^+$] 306.0549 found: 306.0549

R$_f$: 0.31 (30:70 EtOAc/hexane).

Data is consistent with a reported example.[202]

(E/Z)-N'-Benzylidene-4-methoxybenzenesulfonohydrazide (**101i**). Isolated as a white solid (1.45 g, 4.99 mmol, quant.) according to general procedure B.
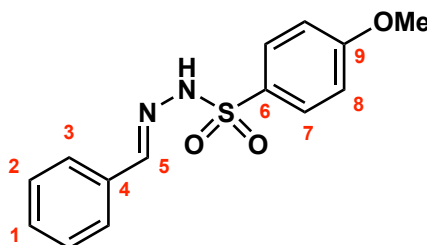
(*E/Z*)-N'-benzylidene-4-methoxybenzenesulfonohydrazide
Molecular Weight: 290.34

101i

^{1}H NMR (400 MHz, CDCl$_3$): δ 3.85 (3H, s, -OMe), 6.98 (2H, d, *J* 9.0 Hz, H8), 7.36 (3H, m, H1 & H2), 7.57-7.59 (2H, m, H3), 7.76 (1H, s, H5), 7.84 (1H, br, -NH), 7.93 (2H, d, *J* 9.0 Hz, H7).

^{13}C NMR (100 MHz, CDCl$_3$): δ 55.6 (-OMe), 114.3 (C8), 127.4 (C3), 128.7 (C2), 129.7 (C6), 130.2 (C7), 130.5 (C1), 133.2 (C4), 147.7 (C5), 163.5 (C9).

FTIR (υ_{max}cm^{-1}): 3195 (m, NH), 3064-2839 (w, CH$_x$), 1593-1575 (m, NH), 1497 (m, C–C), 1361 (s, S=O), 1150 (s, C–O).

HRMS (ASAP+): calculated for C$_{14}$H$_{14}$N$_2$O$_3$S [M+H$^+$] 291.0803 found: 291.0803

R$_f$: 0.26 (30:70 EtOAc/hexane).

Data is consistent with a reported example.[199]

***(E/Z)-4-Methoxy-N'-(4-methoxybenzylidene)benzenesulfonohydrazide* (101j)**. Isolated as a white solid (1.60 g, 5.00 mmol, quant.) according to general procedure B.
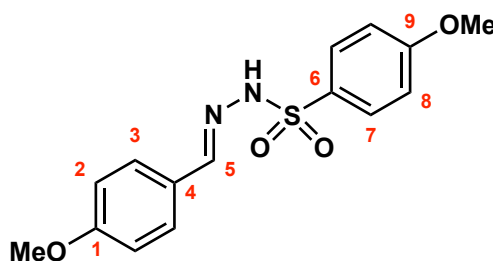
(*E/Z*)-4-methoxy-N'-(4-methoxybenzylidene)benzenesulfonohydrazide
Molecular Weight: 320.36

101j

^{1}H NMR (400 MHz, CDCl$_3$): δ 3.81 (3H, s, C1-OMe), 3.84 (3H, s, C9-OMe), 6.86 (2H, d, *J* 8.8 Hz, H2), 6.96 (2H, d, *J* 9.0 Hz, H8), 7.51 (2H, d, *J* 8.8 Hz, H3), 7.73 (1H, s, H5), 7.92 (2H, d, *J* 9.0 Hz, H7), 7.96 (1H, br, -NH).

^{13}C NMR (100 MHz, CDCl$_3$): δ 55.4 (C1-OMe), 55.6 (C9-OMe), 114.1 (C2), 114.2 (C8), 125.9 (C4), 129.0 (C3), 129.8 (C6), 130.2 (C7), 148.3 (C5), 161.5 (C1), 163.4 (C9).

FTIR (υ_{max}cm^{-1}): 3204 (m, NH), 2975-2842 (w, CH$_x$), 1605 (m, NH), 1595-1496 (m, C–C), 1374 (m, S=O), 1249 (s, C–O).

HRMS (ASAP+): calculated for C$_{15}$H$_{16}$N$_2$O$_4$S [M+H$^+$] 321.0909 found: 321.0908

R$_f$: 0.31 (30:70 EtOAc/hexane).

Methyl (E/Z)-4-((2-((4-methoxyphenyl)sulfonylhydrazineylidene)methyl) benzoate **(101k)**. Isolated as a white solid (0.348 g, 1.00 mmol, quant.) according to general procedure B.
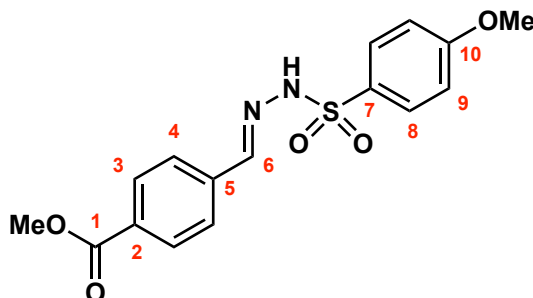
methyl (*E/Z*)-4-((2-((4-methoxyphenyl)sulfonyl)hydrazineylidene)methyl)benzoate
Molecular Weight: 348.37

101k

^{1}H NMR (400 MHz, CDCl$_3$): δ 3.86 (3H, s, C10-OMe), 3.92 (3H, s, C1-OMe), 6.99 (2H, d, *J* 9.0 Hz, H9), 7.64 (2H, d, *J* 8.4 Hz, H4), 7.77 (1H, s, H6), 7.93 (2H, d, *J* 9.0 Hz, H8), 8.02 (2H, d, *J* 8.5 Hz, H3).

^{13}C NMR (100 MHz, CDCl$_3$): δ 52.3 (C1-OMe), 55.7 (C10-OMe), 114.3 (C9), 127.2 (C4), 129.5 (C7), 129.9 (C3), 130.2 (C8), 131.6 (C2), 137.2 (C5), 145.8 (C6), 163.6 (C10), 166.5 (C1).

FTIR (υ_{max}cm^{-1}): 3154 (m, NH), 1688 (s, C=O), 1591-1577 (m, NH), 1496 (m, C–C), 1364 (m, S=O), 1261-1226 (s, C–O).

HRMS (ASAP+): calculated for C$_{16}$H$_{16}$N$_2$O$_5$S [M+H$^+$] 349.0858 found: 349.0856

R$_f$: 0.08 (30:70 EtOAc/hexane).

(E/Z)-N'-(4-Chlorobenzylidene)-4-methoxybenzenesulfonohydrazide **(101l)**. Isolated as a white solid (0.325 g, 1.00 mmol, quant.) according to general procedure B.
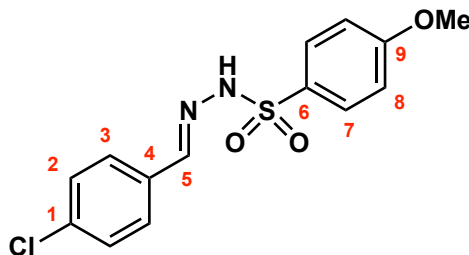
(*E/Z*)-*N'*-(4-chlorobenzylidene)-4-methoxybenzenesulfonohydrazide
Molecular Weight: 324.78

101l

¹H NMR (400 MHz, CDCl₃): δ 3.85 (3H, s, -OMe), 6.98 (2H, d, *J* 9.0 Hz, H8), 7.31 (2H, d, *J* 8.6 Hz, H2), 7.50 (2H, d, *J* 8.6 Hz, H3), 7.73 (1H, s, H5), 7.92 (2H, d, *J* 9.0 Hz, H7), 8.24 (1H, br, -NH).

¹³C NMR (100 MHz, CDCl₃): δ 55.5 (-OMe), 114.3 (C8), 128.5 (C3), 128.9 (C2), 129.6 (C6), 130.1 (C7), 131.8 (C4), 136.3 (C1), 146.3 (C5), 163.5 (C9).

FTIR (υ_{max}cm⁻¹): 3203 (m, NH), 2980-2840 (w, CHₓ), 1595-1581 (m, NH), 1494-1454 (m, C–C), 1357 (m, S=O), 1257 (s, C–O), 821 (s, C–Cl).

HRMS (ASAP+): calculated for C₁₄H₁₃ClN₂O₃S [M+H⁺] 325.0414 found: 325.0434

R*f*: 0.47 (50:50 EtOAc/hexane).

Data is consistent with a reported example.[203]

(E/Z)-N'-(2-(Allyloxy)benzylidene)-4-methoxybenzenesulfonohydrazide **(101m)**.
Isolated as a pale yellow solid (0.350 g, 1.00 mmol, quant.) according to general procedure B.
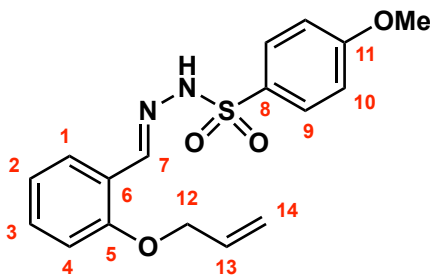
(*E/Z*)-N'-(2-(allyloxy)benzylidene)-4-methoxybenzenesulfonohydrazide
Molecular Weight: 346.40

101m

^{1}H NMR (400 MHz, CDCl$_3$): δ 3.85 (3H, s, -OMe), 4.54 (2H, ddd, *J* 5.3, 1.5 Hz, H12), 5.29 (1H, dd, *J* 10.6, 1.5 Hz, H14a-*cis*), 5.37 (1H, dd, *J* 17.3, 1.5 Hz, H14b-*trans*), 6.02 (1H, ddt, *J* 17.3, 10.5, 5.3 Hz, H13), 6.85 (1H, d, *J* 8.3 Hz, H4), 6.93-6.99 (3H, m, H2 & H10), 7.31 (1H, ddd, *J* 8.3, 7.3, 1.8 Hz, H3), 7.84 (1H, dd, *J* 7.8, 1.8 Hz, H1), 7.92 (2H, d, *J* 9.1 Hz, H9), 8.20 (1H, s, H7).

^{13}C NMR (100 MHz, CDCl$_3$): δ 55.6 (-OMe), 69.2 (C12), 112.3 (C4), 114.2 (C10), 118.1 (C14), 121.1 (C2), 121.7 (C6), 126.9 (C1), 129.8 (C8), 130.2 (C9), 131.9 (C3), 132.7 (C13), 144.3 (C7), 157.0 (C5), 163.4 (C11).

FTIR (υ$_{max}$cm^{-1}): 3155 (m, NH), 3010-2835 (w, CH$_x$), 1595-1579 (m, NH), 1497-1452 (m, C–C), 1357 (m, S=O), 1260-1227 (s, C–O).

HRMS (ASAP+): calculated for C$_{17}$H$_{18}$N$_2$O$_4$S [M+H$^+$] 347.1066 found: 347.1066

R$_f$: 0.16 (30:70 EtOAc/hexane).

(E/Z)-N'-(4-Bromobenzylidene)-4-methoxybenzenesulfonohydrazide **(101n)**. Isolated as a white solid (0.369 g, 1.00 mmol, quant.) according to general procedure B.
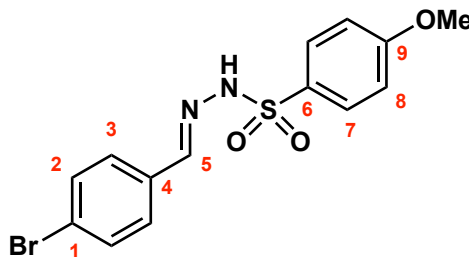
(*E/Z*)-N'-(4-bromobenzylidene)-4-methoxybenzenesulfonohydrazide
Molecular Weight: 369.23

101n

¹H NMR (400 MHz, CDCl₃): δ 3.85 (3H, s, -OMe), 6.98 (2H, d, *J* 9.0 Hz, H8), 7.43-7.50 (4H, m, H2 & H3), 7.70 (1H, s, H5), 7.90-7.93 (3H, m, H7 & -NH).

¹³C NMR (100 MHz, CDCl₃): δ 55.7 (-OMe), 114.3 (C8), 124.8 (C1), 128.7 (C3), 129.6 (C6), 130.2 (C7), 132.0 (C2), 132.1 (C4), 146.2 (C5), 163.6 (C9).

FTIR (υ_{max}cm⁻¹): 3170 (m, NH), 3015-2844 (w, CH$_x$), 1592-1575 (m, NH), 1497 (m, C–C), 1355 (m, S=O), 1264 (s, C–O), 558-534 (s, C–Br).

HRMS (ASAP+): calculated for C₁₄H₁₃BrN₂O₃S [M+H⁺] 368.9909 found: 368.9910

R$_f$: 0.18 (30:70 EtOAc/hexane).

Data is consistent with a reported example.[204]

(E/Z)-4-Methoxy-N'-(2-methylbenzylidene)benzenesulfonohydrazide **(101o)**. Isolated as a white solid (0.305 g, 1.00 mmol, quant.) according to general procedure B.
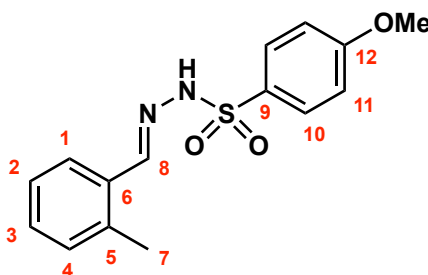
(*E/Z*)-4-methoxy-N'-(2-methylbenzylidene)benzenesulfonohydrazide
Molecular Weight: 304.36

101o

¹H NMR (400 MHz, CDCl₃): δ 2.39 (3H, s, H7), 3.85 (3H, s, -OMe), 6.98 (2H, d, *J* 9.0 Hz, H11), 7.13-7.20 (2H, m, H2 & H4), 7.25 (1H, ddd, *J* 7.9, 7.5, 1.5 Hz, H3), 7.66 (1H, dd, *J* 7.9, 1.3 Hz, H1), 7.89 (1H, br, -NH), 7.93 (2H, d, *J* 9.0 Hz, H10), 8.02 (1H, s, H8).

¹³C NMR (100 MHz, CDCl₃): δ 19.9 (C7), 55.6 (-OMe), 114.2 (C11), 126.2 (C2), 127.4 (C1), 129.7 (C9), 130.1 (C3), 130.2 (C10), 130.9 (C5), 131.2 (C4), 137.1 (C6), 147.0 (C8), 163.5 (C12).

FTIR (υ_{max}cm⁻¹): 3176 (m, NH), 3024-2838 (w, CHₓ), 1592-1576 (m, NH), 1497 (m, C–C), 1358 (m, S=O), 1260 (s, C–O).

HRMS (ASAP+): calculated for C₁₅H₁₆N₂O₃S [M+H⁺] 305.0959 found: 305.0961

R*f*: 0.22 (30:70 EtOAc/hexane).

(E/Z)-N'-(2,5-Dimethoxybenzylidene)-4-methoxybenzenesulfonohydrazide   **(101p)**.

Isolated as a white solid (0.347 g, 0.99 mmol, 99%) according to general procedure B.
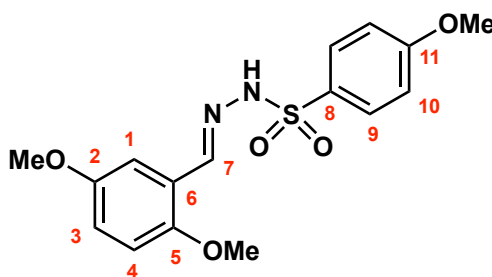
(*E/Z*)-*N'*-(2,5-dimethoxybenzylidene)-4-methoxybenzenesulfonohydrazide
Molecular Weight: 350.39

101p

¹H NMR (400 MHz, CDCl₃): δ 3.77 (3H, s, C5-OMe), 3.79 (3H, s, C2-OMe), 3.85 (3H, s, C11-OMe), 6.80 (1H, d, *J* 9.1 Hz, H4), 6.91 (1H, dd, *J* 9.0, 3.2 Hz, H3), 6.97 (2H, d, *J* 9.0 Hz, H10), 7.36 (1H, d, *J* 3.2 Hz, H1), 7.64 (1H, br, -NH), 7.91 (2H, d, *J* 9.0 Hz, H9), 8.13 (1H, s, H7).

¹³C NMR (100 MHz, CDCl₃): δ 55.6 (C11-OMe), 55.9-56.2 (C2-OMe & C5-OMe), 110.5 (C1), 112.5 (C4), 114.2 (C10), 118.5 (C3), 121.9 (C6), 129.8 (C8), 130.2 (C9), 144.2 (C7), 152.7 (C5), 153.7 (C2), 163.4 (C11).

FTIR (υ_{max}cm⁻¹): 3187 (m, NH), 2998-2835 (w, CHₓ), 1595-1577 (m, NH), 1492 (m, C–C), 1355 (m, S=O), 1260-1218 (s, C–O).

HRMS (ASAP+): calculated for C₁₆H₁₈N₂O₅S [M+H⁺] 351.1015 found: 351.1017

R*f*: 0.10 (30:70 EtOAc/hexane).

(E/Z)-N'-(2-iodobenzylidene)-4-methoxybenzenesulfonohydrazide **(101q)**. Isolated as a white solid (1.04 g, 2.50 mmol, quant.) according to general procedure B.
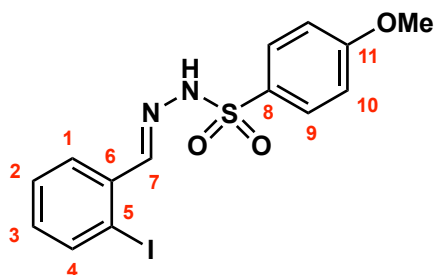
(*E/Z*)-N'-(2-iodobenzylidene)-4-methoxybenzenesulfonohydrazide
Molecular Weight: 416.23

101q

^{1}H NMR (400 MHz, DMSO-d_6): δ 3.82 (3H, s, -OMe), 7.12-7.16 (3H, m, H3 & H10), 7.40 (1H, dd, *J* 7.6 Hz, H2), 7.65 (1H, dd, *J* 7.9, 1.5 Hz, H1), 7.80 (2H, d, *J* 8.9 Hz, H9), 7.87 (1H, d, *J* 7.9 Hz, H4), 8.09 (1H, s, H7), 11.66 (1H, br, -NH).

^{13}C NMR (100 MHz, DMSO-d_6): δ 55.7 (-OMe), 99.7 (C5), 114.5 (C10), 126.7 (C1), 128.6 (C2), 129.4 (C9), 130.5 (C8), 131.8 (C3), 135.1 (C6), 139.6 (C4), 149.4 (C7), 162.7 (C11).

FTIR (υ_{max}cm^{-1}): 3197 (m, NH), 3068-2838 (w, CH$_x$), 1589-1574 (m, NH), 1495 (m, C–C), 1355 (m, S=O), 1257 (s, C–O), 553 (C–I).

HRMS (ASAP+): calculated for C$_{14}$H$_{13}$IN$_2$O$_3$S [M+H$^+$] 416.9770 found: 416.9778

R$_f$: 0.82 (50/50 EtOAc/hexane).

(E/Z)-N'-(4-Fluorobenzylidene)-4-methoxybenzenesulfonohydrazide **(101r)**. Isolated as a white solid (0.770 g, 2.50 mmol, quant.) according to general procedure B.
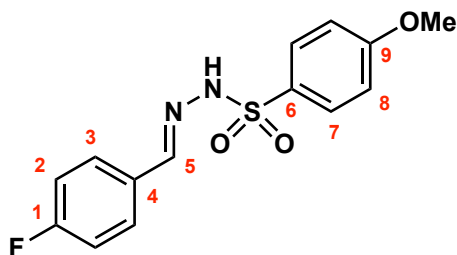
(*E/Z*)-N'-(4-fluorobenzylidene)-4-methoxybenzenesulfonohydrazide
Molecular Weight: 308.33

101r

¹H NMR (400 MHz, CDCl₃): δ 3.86 (3H, s, -OMe), 6.98 (2H, d, *J* 9.0 Hz, H8), 7.05 (2H, dd, *J* 9.0, 8.6 Hz, H2), 7.57 (2H, dd, *J* 7.0, 8.4 Hz, H3), 7.73 (1H, s, H5), 7.80 (1H, br, -NH), 7.92 (2H, d, *J* 8.9 Hz, H7).

¹³C NMR (100 MHz, CDCl₃): δ 55.6 (-OMe), 114.3 (C8), 115.9 (d, *J* 21.9 Hz, C2), 129.3 (d, *J* 9.0 Hz, C3), 129.7 (C6), 130.2 (C7), 132.2 (d, *J* 9.6 Hz, C4), 146.5 (C5), 163.5 (C9), 165.3 (C1).

FTIR (υ_{max}cm⁻¹): 3155 (m, NH), 1597-1581 (m, NH), 1510 (m, C–C), 1368 (m, S=O), 1258 (s, C–O), 1152 (s, C–F).

HRMS (ASAP+): calculated for $C_{14}H_{13}FN_2O_3S$ [M+H⁺] 309.0709 found: 309.0713

R*f*: 0.28 (30:70 EtOAc/hexane).

(E/Z)-4-Methoxy-N'-(4-(trifluoromethyl)benzylidene)benzenesulfonohydrazide **(101s)**.
Isolated as a white solid (0.894 g, 2.50 mmol, quant.) according to procedure B.
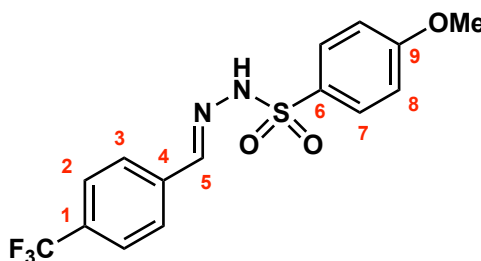
(*E/Z*)-4-methoxy-N'-(4-(trifluoromethyl)benzylidene)benzenesulfonohydrazide
Molecular Weight: 358.34

101s

¹H NMR (400 MHz, DMSO-d₆): δ 3.81 (3H, s, -OMe), 7.12 (2H, d, *J* 9.0 Hz, H8), 7.73-7.79 (4H, m, H2 & H3), 7.81 (2H, d, *J* 9.0 Hz, H7), 7.98 (1H, s, H5), 11.66 (1H, br, -NH).

¹³C NMR (100 MHz, DMSO-d₆): δ 55.7 (-OMe), 114.5 (C8), 124.0 (q, *J* 271.6 Hz, -CF₃), 125.4 (C, 125.8 (q, *J* 3.7 Hz, C2), 127.3 (C3), 130.2 (q *J* 32.2 Hz, C1), 129.8 (C7), 130.4 (C6), 137.6 (C4), 145.0 (C5), 162.7 (C9).

FTIR (υ_{max}cm⁻¹): 3150 (m, NH), 1595-1580 (m, NH), 1498 (m, C–C), 1368 (s, S=O), 1259 (s, C–O), 1151 (s, C–F).

HRMS (ASAP+): calculated for $C_{15}H_{13}F_3N_2O_3S$ [M+H⁺] 359.0677 found: 359.0681

(E/Z)-N'-(4-(Dimethylamino)benzylidene)-4-methoxybenzenesulfonohydrazide (101t). Isolated as an orange solid (0.333 g, 1.00 mmol, quant.) according to general procedure B.
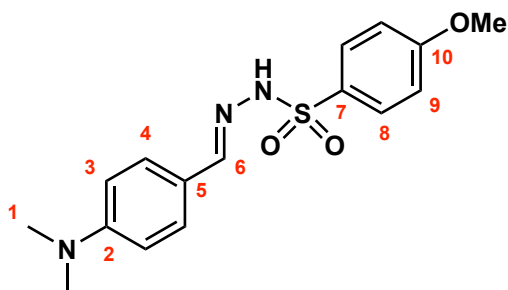
(*E/Z*)-N'-(4-(dimethylamino)benzylidene)-4-methoxybenzenesulfonohydrazide
Molecular Weight: 333.41

101t

¹H NMR (400 MHz, CDCl₃): δ 3.00 (6H, s, H1), 3.84 (3H, s, -OMe), 6.65 (2H, d br, *J* 8.5 Hz, H3), 6.96 (2H, d, *J* 9.0 Hz, H9), 7.46 (2H, d, *J* 8.9 Hz, H4), 7.51 (1H, br, -NH), 7.70 (1H, s, H6), 7.90 (2H, d, *J* 9.0 Hz, H8).

¹³C NMR (100 MHz, CDCl₃): δ 40.3 (C1), 55.6 (-OMe), 111.8 (C3), 114.1 (C9), 129.0 (C4), 130.0 (C7), 130.2 (C8), 150.2 (C6), 163.3 (C10).

FTIR (υ$_{max}$cm^{-1}): 3179 (m, NH), 2898-2803 (w, CH$_x$), 1593-1576 (m, NH), 1553 (m, C–C), 1358 (m, S=O), 1300 (s, C–N), 1262 (s, C–O).

HRMS (ASAP+): calculated for C₁₆H₁₉N₃O₃S [M+H⁺] 334.1225 found: 334.1223

R*f*: 0.10 (30:70 EtOAc/hexane).

(E/Z)-N'-(2-Hydroxybenzylidene)-4-methoxybenzenesulfonohydrazide **(101u)**. Isolated as a white solid (0.306 g, 1.00 mmol, quant.) according to general procedure B.
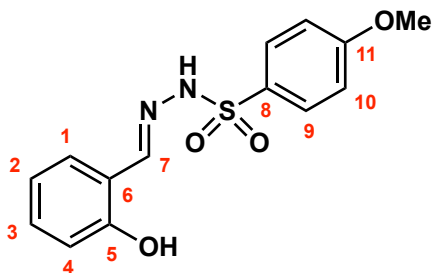
(*E/Z*)-N'-(2-hydroxybenzylidene)-4-methoxybenzenesulfonohydrazide
Molecular Weight: 306.34

101u

¹H NMR (400 MHz, CDCl₃): δ 3.86 (3H, s, -OMe), 6.88 (1H, dd, J 7.5, 7.4 Hz, H2), 6.94 (1H, d, J 8.3 Hz, H4), 7.01 (2H, d, J 9.0 Hz, H10), 7.14 (1H, dd, J 7.8, 1.6 Hz, H1), 7.29 (1H, ddd, J 7.8, 7.6, 1.6 Hz, H3), 7.83 (1H, br, -NH), 7.89 (2H, d, J 9.0 Hz, H9), 7.97 (1H, s, H7).

¹³C NMR (100 MHz, CDCl₃): δ 55.7 (-OMe), 114.7 (C10), 116.9 (C6), 117.1 (C4), 119.6 (C2), 128.7 (C8), 130.2 (C9), 131.2 (C1), 132.3 (C3), 152.7 (C7), 158.1 (C5), 163.9 (C11).

FTIR (υ_{max}cm⁻¹): 3181 (m, NH, OH), 1622-1577 (m, NH), 1498 (m, C–C), 1359 (m, S=O), 1326 (m, OH), 1263 (s, C–O).

HRMS (ASAP+): calculated for C₁₄H₁₄N₂O₄S [M+H⁺] 307.0753 found: 307.0757

R$_f$: 0.15 (30:70 EtOAc/hexane).

Data is consistent with a reported example.[205]

(E/Z)-4-Methoxy-N'-(thiophen-2-ylmethylene)benzenesulfonohydrazide   **(101v)**.

Isolated as a tan solid (0.739 g, 2.49 mmol, quant.) according to general procedure B.
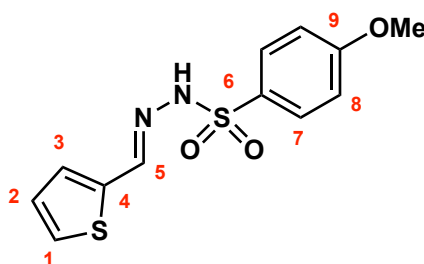
(*E/Z*)-4-methoxy-N'-(thiophen-2-ylmethylene)benzenesulfonohydrazide
Molecular Weight: 296.36

101v

¹H NMR (400 MHz, CDCl₃): δ 3.85 (3H, s, -OMe), 6.97 (2H, d, J 9.0 Hz, H8), 7.00 (1H, dd, J 5.0, 3.7 Hz, H2), 7.19 (1H, dd, J 3.7, 1.0 Hz, H1), 7.35 (1H, d, J 5.0 Hz, H3), 7.88 (1H, br, -NH), 7.90 (2H, d, J 9.0 Hz, H7), 7.99 (1H, s, H5).

¹³C NMR (100 MHz, CDCl₃): δ 55.6 (-OMe), 114.3 (C8), 127.4 (C2), 128.9 (C3), 129.6 (C6), 130.2 (C7), 130.4 (C1), 138.0 (C4), 143.4 (C5), 163.5 (C9).

FTIR (υ_{max}cm⁻¹): 3164 (m, NH), 2968-2838 (w, CHₓ), 1592-1577 (m, NH), 1499 (m, C–C), 1363 (m, S=O), 1262 (s, C–O).

HRMS (ASAP+): calculated for $C_{12}H_{12}N_2O_3S_2$ [M+H$^+$] 297.0368 found: 297.0370

R$_f$: 0.34 (30:70 EtOAc/hexane).

4-Methoxy-N'-(tetrahydro-4H-pyran-4-ylidene)benzenesulfonohydrazide **(101w)**.

Isolated as a white solid (0.284 g, 1.00 mmol, quant.) according to general procedure B.
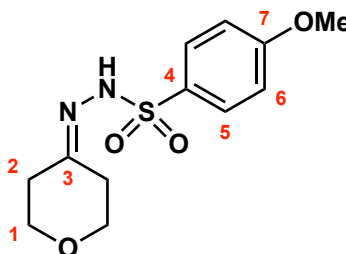
4-methoxy-N'-(tetrahydro-4H-pyran-4-ylidene)benzenesulfonohydrazide
Molecular Weight: 284.33

101w

^{1}H NMR (400 MHz, CDCl$_3$): δ 2.37-2.40 (4H, m br, H2), 3.71 (2H, t, *J* 5.8 Hz, H1a), 3.78 (2H, t, *J* 5.7 Hz, H1b), 3.87 (3H, s, -OMe), 6.99 (2H, d, *J* 9.0 Hz, H6), 7.61 (1H, br, -NH), 7.89 (2H, d, *J* 9.0 Hz, H5).

^{13}C NMR (100 MHz, CDCl$_3$): δ 28.3 (C2a), 35.3 (C2b), 55.7 (-OMe), 66.2 (C1a), 68.1 (C1b), 114.2 (C6), 129.7 (C4), 130.3 (C5), 157.8 (C3), 163.4 (C7).

FTIR (υ_{max}cm^{-1}): 3240-3192 (m, NH), 2864 (w, CH$_x$), 1598-1577 (m, NH), 1496 (m, C–C), 1262 (s, C–O), 1089 (s, C–O).

HRMS (ASAP+): calculated for $C_{12}H_{16}N_2O_4S$ [M+H$^+$] 285.0909 found: 285.0910

R$_f$: 0.27 (30:70 EtOAc/hexane).

Data is consistent with a reported example.[82]

(E/Z)-N'-(2-(Allyloxy)benzylidene)-4-methylbenzenesulfonohydrazide **(101x)**. Isolated as a tan solid (3.29 g, 9.97 mmol, quant.) according to general procedure B.
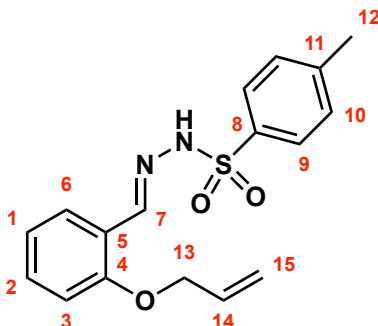
(*E/Z*)-N'-(2-(allyloxy)benzylidene)-4-methylbenzenesulfonohydrazide
Molecular Weight: 330.40

101x

¹H NMR (400 MHz, CDCl₃): δ 2.35 (3H, s, H12), 4.48 (2H, br, H13), 5.23 (1H, d, *J* 10.1 Hz, H15a-*cis*), 5.31 (1H, d, *J* 17.2 Hz, H15b-*trans*), 5.92-5.99 (1H, m, H14), 6.79 (1H, d, *J* 8.0 Hz, H3), 6.89 (1H, dd, *J* 7.4 Hz, H1), 7.21-7.26 (3H, m, H2 & H10), 7.78-7.83 (4H, m, H6, H9 & -NH), 8.15 (1H, s, H7).

¹³C NMR (100 MHz, CDCl₃): δ 21.6 (C12), 69.2 (C13), 112.2 (C3), 118.0 (C15), 121.0 (C1), 121.9 (C5), 126.7 (C6), 128.0 (C10), 129.6 (C9), 131.7 (C2), 132.7 (C14), 135.4 (C8), 143.8 (C7), 144.1 (C11), 156.9 (C4).

**FTIR** (υ_{max}cm⁻¹): 3161 (m, NH), 3067-2888 (w, CH$_x$), 1599 (m, NH), 1487 (m, C–C), 1360 (m, S=O), 1227 (s, C–O).

HRMS (ASAP+): calculated for $C_{17}H_{18}N_2O_3S$ [M+H⁺] 331.1116 found: 331.1118

R$_f$: 0.24 (40:60 EtOAc/hexane).

Data is consistent with a reported example.[174]

General Synthetic Procedure C: Preparation of Sulfones

Sulfonylhydrazone (0.25 mmol, 1.0 equiv), CsF (0.5 mmol, 2.0 equiv), and [Ru(bpy)₃]²⁺Cl₂·6H₂O (2.5 mmol, 0.01 equiv) were placed in an oven-dried tube in vacuo for 20 minutes. The tube was backfilled with nitrogen and evacuated (3 cycles), followed by addition of degassed (freeze-pump-thaw method) DMF (5 mL) dropwise under a nitrogen atmosphere. The tube was sealed and the reaction mixture was left to stir in darkness at room temperature for 15 minutes followed by irradiation with blue LED's

(~470 nm) for 20 hours at 38 °C. After cooling to room temperature the reaction mixture was quenched with saturated NH$_4$Cl solution (20 mL)…

C1: The aqueous layer was extracted with Et$_2$O (3 x 10 mL) and the collected organic layers dried over MgSO$_4$. Volatiles were removed *in vacuo* to give the crude product which was purified *via* flash column chromatography to give the title compounds.

C2: The aqueous layer was extracted with CH$_2$Cl$_2$ (3 x 10 mL) and the collected organic layers washed with 5% w/v LiCl solution (10 x 15 mL) and dried over MgSO$_4$. Volatiles were removed *in vacuo* to give the crude product which was purified *via* flash column chromatography to give the title compounds.

1-(Benzylsulfonyl)-4-methylbenzene **(102a)**. Isolated as a white solid (58.1 mg, 0.236 mmol, 94%) according to general procedure C1 without further purification.
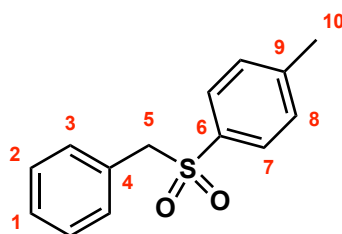
1-(benzylsulfonyl)-4-methylbenzene
Molecular Weight: 246.32
102a

^{1}H NMR (400 MHz, CDCl$_3$): δ 2.43 (3H, s, H10), 4.31 (2H, s, H5), 7.11 (2H, d, *J* 6.9 Hz, H3), 7.24-7.35 (5H, m H1, H2 & H8), 7.52 (2H, d, *J* 8.3 Hz, H7).

^{13}C NMR (100 MHz, CDCl$_3$): δ 21.7 (C10), 62.9 (C5), 128.3 (C4), 128.6 (C7), 128.7 (C1 & C2), 129.5 (C8), 130.8 (C3), 135.0 (C6), 144.7 (C9).

FTIR (υ_{max}cm^{-1}): 3062-2849 (w, CH$_x$), 1594-1454 (m, C–C), 1310 (s, S=O).

HRMS (ASAP+): calculated for C$_{14}$H$_{14}$O$_2$S [M+H$^+$] 247.0793 found: 247.0811

R$_f$: 0.56 (50:50 EtOAc/hexane).

Data is consistent with a reported example.[206]

1-(Benzylsulfonyl)-4-chlorobenzene **(102b)**. Isolated as a white solid (55.0 mg, 0.206 mmol, 83%) according to general procedure C1 without further purification.
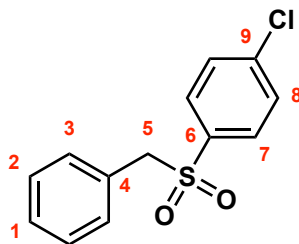
1-(benzylsulfonyl)-4-chlorobenzene
Molecular Weight: 266.74

102b

^{1}H NMR (400 MHz, CDCl$_3$): δ 4.22 (2H, s, H5), 6.99 (2H, d, *J* 7.1 Hz, H3), 7.17-7.24 (3H, m, H1 & H2), 7.32 (2H, d, *J* 8.3 Hz, H8), 7.44 (2H, d, *J* 8.3 Hz, H7).

^{13}C NMR (100 MHz, CDCl$_3$): δ 62.9 (C5), 127.9 (C4), 128.7 (C2), 129.0 (C1), 129.2 (C8), 130.2 (C7), 130.8 (C3), 136.3 (C6), 140.5 (C9).

FTIR (υ_{max}cm^{-1}): 3060-2942 (w, CH$_x$), 1583-1454 (m, C–C), 1326-1313 (s, S=O), 696 (s, C–Cl).

HRMS (ASAP+): calculated for C$_{13}$H$_{11}$ClO$_2$S [M+H$^+$] 267.0247 found: 267.0273

R$_f$: 0.80 (30:70 EtOAc/hexane).

Data is consistent with a reported example.[206]

1-(Benzylsulfonyl)-4-fluorobenzene **(102c)**. Isolated as a white solid (62.1 mg, 0.248 mmol, 99%) according to general procedure C1 without further purification.
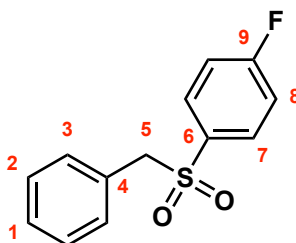
1-(benzylsulfonyl)-4-fluorobenzene
Molecular Weight: 250.29

102c

^{1}H NMR (400 MHz, CDCl$_3$): δ 4.31 (2H, s, H5), 7.06-7.13 (4H, m, H3 & H8), 7.25-7.35 (3H, m, H1 & H2), 7.60 (2H, dd, *J* 8.9, 5.1 Hz, H7).

13C NMR (100 MHz, CDCl$_3$): δ 63.0 (C5), 116.1-116.3 (d, J 22.7 Hz, C8), 128.0 (C4), 128.7 (C2), 128.9 (C1), 130.8 (C3), 131.5-131.6 (d, J 9.6 Hz, C7), 133.7-133.8 (d, J 3.3 Hz, C6), 164.6-167.1 (d, J 256.6 Hz, C9).

FTIR (υ_{max}cm^{-1}): 3061-2941 (w, CH$_x$), 1590-1403 (m, C–C), 1327-1313 (s, S=O), 1229 (s, CF).

HRMS (ASAP+): calculated for C$_{13}$H$_{11}$FO$_2$S [M+H$^+$] 251.0542 found: 251.0532

R$_f$: 0.85 (50:50 EtOAc/hexane).

Data is consistent with a reported example.[206]

***N-(4-(Benzylsulfonyl)phenyl)acetamide* (102d)**. Isolated as a white solid (23.0 mg, 79.5 mmol, 32%) according to general procedure C2 without further purification.
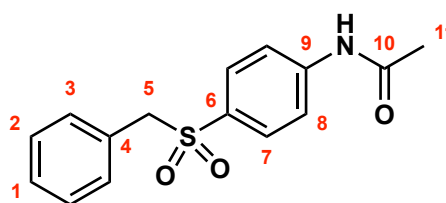
N-(4-(benzylsulfonyl)phenyl)acetamide
Molecular Weight: 289.35

102d

1H NMR (400 MHz, CDCl$_3$): δ 2.20 (3H, s, H11), 4.29 (2H, s, H5), 7.07-7.09 (2H, m, H3), 7.24-7.33 (3H, m, H1 & H2), 7.52-7.54 (3H, m, H7 & -NH), 7.59 (2H, d, J 8.8 Hz, H8)

13C NMR (100 MHz, CDCl$_3$): δ 24.8 (C11), 63.0 (C5), 118.9 (C8), 128.1 (C4), 128.6 (C2), 128.8 (C1), 130.0 (C7), 130.8 (C3), 132.4 (C6), 142.9 (C9), 168.7 (C10).

FTIR (υ_{max}cm^{-1}): 3299 (m, NH), 3060-2948 (w, CH$_x$), 1667 (s, C=O), 1592 (m, NH), 1524-1492 (m, C–C), 1314 (s, S=O).

HRMS (ASAP+): calculated for C$_{15}$H$_{15}$NO$_3$S [M+H$^+$] 290.0851 found: 290.0852

R$_f$: 0.38 (90:10 CH$_2$Cl$_2$/MeOH).

2-(Benzylsulfonyl)-5-bromothiophene **(102ea)**. Isolated as a pale yellow solid (47.9 mg, 0.151 mmol, 61%) according to general procedure C1 and purified *via* flash column chromatography (15:85 EtOAc/hexane).
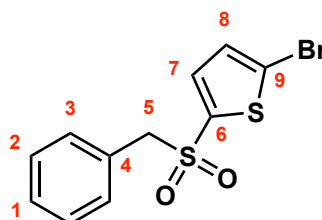
2-(benzylsulfonyl)-5-bromothiophene
Molecular Weight: 317.22

102ea

^{1}H NMR (400 MHz, CDCl$_3$): δ 4.38 (2H, s, H5), 7.02 (1H, d, *J* 4.0 Hz, H8), 7.07 (1H, d, *J* 4.0 Hz, H7), 7.16-7.18 (2H, m, H3), 7.30-7.39 (3H, m, H1 & H2).

^{13}C NMR (100 MHz, CDCl$_3$): δ 63.9 (C5), 122.5 (C9), 127.9 (C4), 128.8 (C2), 129.2 (C1), 130.71 (C7), 130.73 (C3), 135.1 (C8), 139.2 (C6).

FTIR (υ_{max}cm^{-1}): 3088-2852 (w, CH$_x$), 1589-1455 (m, C–C), 1314 (s, S=O), 532 (C–Br).

HRMS (ASAP+): calculated for C$_{11}$H$_9$BrO$_2$S$_2$ [M+H$^+$] 316.9306 found: 316.9321

R$_f$: 0.30 (20:80 EtOAc/hexane).

2-(Benzylsulfonyl)thiophene **(102eb)**. Isolated as a white solid (12.0 mg, 50.0 mmol, 20%) according to general procedure C1 and purified *via* flash column chromatography (15:85 EtOAc/hexane).
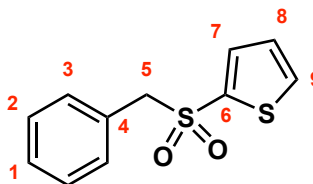
2-(benzylsulfonyl)thiophene
Molecular Weight: 238.32

102eb

¹H NMR (400 MHz, CDCl₃): δ 4.41 (2H, s, H5), 7.05 (1H, dd, J 4.9, 3.8 Hz, H8), 7.13-7.15 (2H, m, H3), 7.27-7.35 (4H, m, H1, H2 & H9), 7.65 (1H, dd, J 4.9, 1.4 Hz, H7).

¹³C NMR (100 MHz, CDCl₃): δ 64.1 (C5), 127.7 (C8), 128.2 (C4), 128.7 (C2), 129.0 (C1), 130.7 (C3), 134.3 (C7), 134.9 (C9), 138.5 (C6).

R$_f$: 0.18 (20:80 EtOAc/hexane).

Data is consistent with a reported example.[207]

((Cyclopropylsulfonyl)methyl)benzene (**102f**). Isolated as a white solid (44.0 mg, 0.224 mmol, 90%) according to general procedure C1 and purified *via* flash column chromatography (15:85 EtOAc/hexane).
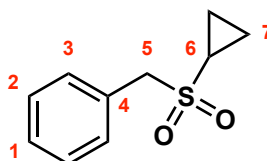
((cyclopropylsulfonyl)methyl)benzene
Molecular Weight: 196.26
102f

¹H NMR (400 MHz, CDCl₃): δ 0.93 (2H, app sxt, J 7.9, 7.5, 5.1 Hz, H7a), 1.13 (2H, app sxt, J 4.8, 7.2, 4.6 Hz, H7b), 2.20 (1H, app non, J 7.9, 4.9 Hz, H6), 4.26 (2H, s, H5), 7.38-7.44 (5H, m, H1, H2 & H3).

¹³C NMR (100 MHz, CDCl₃): δ 4.8 (C7), 28.2 (C6), 60.3 (C5), 128.3 (C4), 128.9 (C1 & C2), 130.8 (C3).

**FTIR** (υ_{max}cm⁻¹): 3050-2851 (w, CH$_x$), 1493-1411 (m, C–C), 1299-1282 (s, S=O).

HRMS (ASAP+): calculated for C₁₀H₁₂O₂S [M+H⁺] 197.0636 found: 197.0638

R$_f$: 0.56 (30:70 EtOAc/hexane).

Data is consistent with a reported example.[208]

***((Methylsulfonyl)methyl)benzene* (102g)**. Isolated as a white solid (35.1 mg, 0.206 mmol, 82%) according to general procedure C1 and purified *via* flash column chromatography (15:85 EtOAc/hexane).
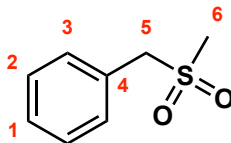
((methylsulfonyl)methyl)benzene
Molecular Weight: 170.23

102g

^{1}H NMR (400 MHz, CDCl$_3$): δ 2.75 (3H, s, H6), 4.25 (2H, s, H5), 7.41 (5H, s, H1, H2 & H3).

^{13}C NMR (100 MHz, CDCl$_3$): δ 39.0 (C6), 61.3 (C5), 128.3 (C4), 129.1 (C1 & C2), 130.5 (C3).

FTIR (υ_{max}cm^{-1}): 3012-2849 (w, CH$_x$), 1495-1412 (m, C–C), 1320-1299 (s, S=O).

HRMS (ASAP+): calculated for C$_8$H$_{10}$O$_2$S [M+H$^+$] 171.0480 found: 171.0507

R$_f$: 0.31 (20:80 EtOAc/hexane).

Data is consistent with a reported example.[209]

***1-(Benzylsulfonyl)-4-methoxybenzene* (102i)**. Isolated as a light brown solid (64.9 mg, 0.248 mmol, 99%) according to general procedure C1 without further purification.
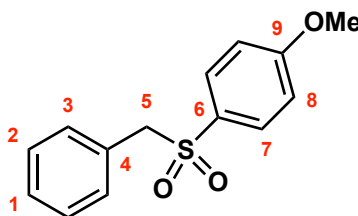
1-(benzylsulfonyl)-4-methoxybenzene
Molecular Weight: 262.32

102i

^{1}H NMR (400 MHz, CDCl$_3$): δ 3.86 (3H, s, -OMe), 4.28 (2H, s, H5), 6.89 (2H, d, *J* 9.0 Hz, H8), 7.07-7.09 (2H, m, H3), 7.24-7.33 (3H, m, H1 & H2), 7.52 (2H, d, *J* 9.0 Hz, H7).

¹³C NMR (100 MHz, CDCl₃): δ 55.7 (-OMe), 63.1 (C5), 114.0 (C8), 128.5 (C4), 128.6 (C2), 128.7 (C1), 129.4 (C6), 130.8 (C3 & C7), 163.7 (C9).

FTIR (υ_{max}cm⁻¹): 3076-2837 (w, CHₓ), 1593-1455 (m, C–C), 1308-1294 (s, S=O), 1241 (s, C–O).

HRMS (ASAP+): calculated for $C_{14}H_{14}O_3S$ [M+H⁺] 263.0742 found: 263.0767

R$_f$: 0.59 (50:50 EtOAc/hexane).

Data is consistent with a reported example.[206]

1-Methoxy-4-((4-methoxybenzyl)sulfonyl)benzene **(102j)**. Isolated as a brown solid (73.1 mg, 0.250 mmol, quant.) according to general procedure C2 without further purification.
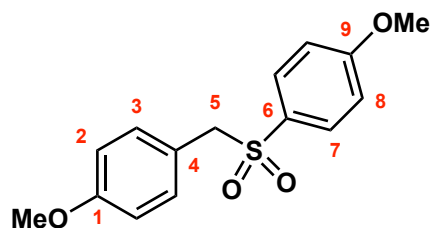
1-methoxy-4-((4-methoxybenzyl)sulfonyl)benzene
Molecular Weight: 292.35

102j

¹H NMR (400 MHz, CDCl₃): δ 3.79 (3H, s, C1-OMe), 3.86 (3H, s, C9-OMe), 4.22 (2H, s, H5), 6.79 (2H, d, *J* 8.7 Hz, H2), 6.90 (2H, d, *J* 9.0 Hz, H8), 6.99 (2H, d, *J* 8.7 Hz, H3), 7.53 (2H, d, *J* 9.0 Hz, H7).

¹³C NMR (100 MHz, CDCl₃): δ 55.3 (C1-OMe), 55.7 (C9-OMe), 62.4 (C5), 113.98 (C2), 114.04 (C8), 120.4 (C4), 129.5 (C6), 130.8 (C7), 132.0 (C3), 159.9 (C1), 163.7 (C9).

FTIR (υ_{max}cm⁻¹): 3077-2835 (w, CHₓ), 1595-1409 (m, C–C), 1322-1309 (s, S=O), 1257-1237 (s, C–O).

HRMS (ASAP+): calculated for $C_{15}H_{16}O_4S$ [M+H⁺] 293.0848 found: 293.0874

R$_f$: 0.47 (50:50 EtOAc/hexane).

Methyl 4-(((4-methoxyphenyl)sulfonyl)methyl)benzoate **(102k).** Isolated as a white solid (51.3 mg, 0.160 mmol, 63%) according to general procedure C1 and purified *via* flash column chromatography (15:85 EtOAc/hexane).
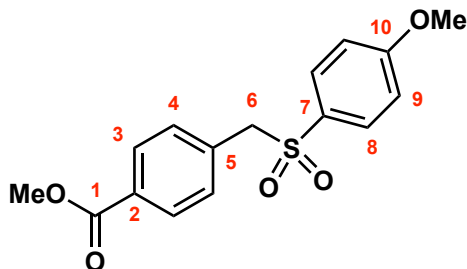
methyl 4-(((4-methoxyphenyl)sulfonyl)methyl)benzoate
Molecular Weight: 320.36

102k

^{1}H NMR (400 MHz, CDCl$_3$): δ 3.85 (3H, s, C10-OMe), 3.91 (3H, s, C1-OMe), 4.33 (2H, s, H6), 6.89 (2H, d, *J* 8.9 Hz, H9), 7.16 (2H, d, *J* 8.2 Hz, H4), 7.51 (2H, d, *J* 8.9 Hz, H8), 7.93 (2H, d, *J* 8.2 Hz, H3).

^{13}C NMR (100 MHz, CDCl$_3$): δ 52.2 (C1-OMe), 55.6 (C10-OMe), 62.8 (C6), 114.1 (C9), 129.1 (C7), 129.7 (C3), 130.3 (C2), 130.7 (C8), 130.8 (C4), 133.5 (C5), 163.8 (C10), 166.5 (C1).

FTIR (υ_{max}cm^{-1}): 3080-2843 (CH$_x$), 1713 (s, C=O), 1595-1415 (m, C–C), 1312 (m, S=O), 1278-1251 (s, C–O).

HRMS (ASAP+): calculated for C$_{16}$H$_{16}$O$_5$S [M+H$^+$] 321.0797 found: 321.0795

R$_f$: 0.68 (50:50 EtOAc/hexane).

Data is consistent with a reported example.[210]

***1-Chloro-4-(((4-methoxyphenyl)sulfonyl)methyl)benzene* (102l)**. Isolated as a light brown solid (61.1 mg, 0.206 mmol, 82%) according to general procedure C1 without further purification.
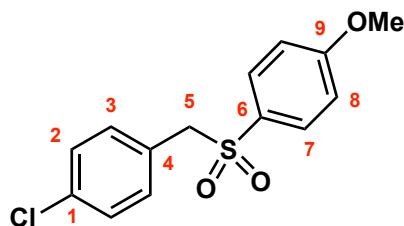
1-chloro-4-(((4-methoxyphenyl)sulfonyl)methyl)benzene
Molecular Weight: 296.77

102I

¹H NMR (400 MHz, CDCl₃): δ 3.87 (3H, s, -OMe), 4.24 (2H, s, H5), 6.92 (2H, d, *J* 9.0 Hz, H8), 7.02 (2H, d, *J* 8.5 Hz, H3), 7.25 (2H, d, *J* 8.5 Hz, H2), 7.54 (2H, d, *J* 9.0 Hz, H7).

¹³C NMR (100 MHz, CDCl₃): δ 55.7 (-OMe), 62.4 (C5), 114.2 (C8), 127.1 (C4), 128.8 (C2), 129.2 (C6), 130.8 (C7), 132.1 (C3), 135.0 (C1), 163.9 (C9).

FTIR (υ_{max}cm⁻¹): 3077-2838 (w, CH$_x$), 1593-1410 (m, C–C), 1311 (s, S=O), 1260 (s, C–O), 571 (C–Cl).

HRMS (ASAP+): calculated for $C_{14}H_{13}ClO_3S$ [M+H⁺] 297.0352 found: 297.0376

R$_f$: 0.58 (50/50 EtOAc/hexane).

Data is consistent with a reported example.[211]

1-(Allyloxy)-2-(((4-methoxyphenyl)sulfonyl)methyl)benzene **(102m)**. Isolated as a yellow oil (71.0 mg, 0.223 mmol, 89%) according to general procedure C1 without further purification.
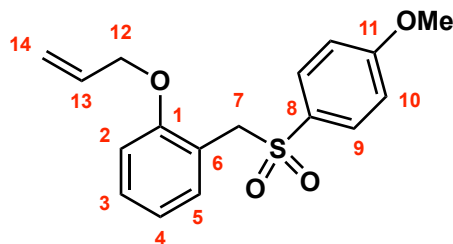
1-(allyloxy)-2-(((4-methoxyphenyl)sulfonyl)methyl)benzene
Molecular Weight: 318.39

102m

^{1}H NMR (400 MHz, CDCl$_3$): δ 3.83 (3H, s, -OMe), 4.12 (2H, ddd, *J* 5.2, 1.6 Hz, H12), 4.46 (2H, s, H7), 5.18-5.25 (2H, m, H14), 5.77 (1H, ddt, *J* 17.2, 10.5, 5.2 Hz, H13), 6.66 (1H, d, *J* 8.3 Hz, H2), 6.83 (2H, d, *J* 9.0 Hz, H10), 6.94 (1H, ddd, *J* 7.5, 1.0 Hz, H4), 7.25 (1H, ddd, *J* 7.5, 1.8 Hz, H3), 7.33 (1H, dd, *J* 7.5, 1.7 Hz, H5), 7.48 (2H, d, *J* 9.0 Hz, H9).

^{13}C NMR (100 MHz, CDCl$_3$): δ 55.6 (-OMe), 56.6 (C7), 68.7 (C12), 111.5 (C2), 113.6 (C10), 117.3 (C6 & C14), 120.8 (C4), 130.2 (C3), 130.3 (C8), 130.9 (C9), 132.5 (C5), 132.8 (C13), 156.5 (C1), 163.5 (C11).

FTIR (υ_{max}cm^{-1}): 3075-2842 (w, CH$_x$), 1594-1412 (m, C–C), 1317 (s, S=O), 1247 (s, C–O).

HRMS (ASAP+): calculated for C$_{17}$H$_{18}$O$_4$S [M+H$^+$] 319.1004 found: 319.1000

R$_f$: 0.60 (50:50 EtOAc/hexane).

1-Bromo-4-(((4-methoxyphenyl)sulfonyl)methyl)benzene **(102n)**. Isolated as a white solid (73.0 mg, 0.214 mmol, 86%) according to general procedure C1 without further purification.
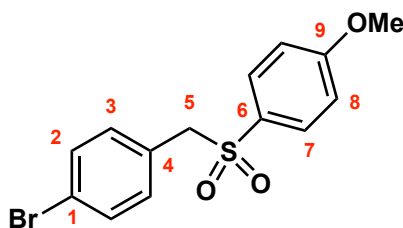
1-bromo-4-(((4-methoxyphenyl)sulfonyl)methyl)benzene
Molecular Weight: 341.22

102n

^{1}H NMR (400 MHz, CDCl$_3$): δ 3.87 (3H, s, -OMe), 4.23 (2H, s, H5), 6.92 (2H, d, *J* 9.0 Hz, H8), 6.96 (2H, d, *J* 8.4 Hz, H3), 7.40 (2H, d, *J* 8.4 Hz, H2), 7.54 (2H, d, *J* 8.9 Hz, H7).

^{13}C NMR (100 MHz, CDCl$_3$): δ 55.7 (-OMe), 62.4 (C5), 114.2 (C8), 123.2 (C1), 127.6 (C4), 129.1 (C6), 130.8 (C7), 131.8 (C2), 132.4 (C3), 163.9 (C9).

FTIR (υ_{max}cm^{-1}): 3076-2836 (w, CH$_x$), 1593-1409 (m, C–C), 1309 (s, S=O), 1258 (s, C–O), 565 (C–Br).

HRMS (ASAP+): calculated for C$_{14}$H$_{13}$BrO$_3$S [M+H$^+$] 340.9847 found: 340.9848

R$_f$: 0.56 (50:50 EtOAc/hexane).

Data is consistent with a reported example.[210]

1-(((4-Methoxyphenyl)sulfonyl)methyl)-2-methylbenzene **(102o)**. Isolated as a brown solid (64.9 mg, 0.235 mmol, 94%) according to general procedure C1 without further purification.
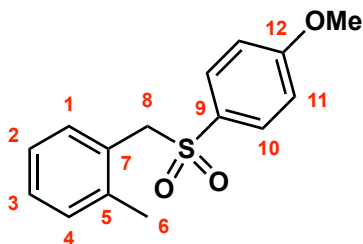
1-(((4-methoxyphenyl)sulfonyl)methyl)-2-methylbenzene
Molecular Weight: 276.35

102o

^{1}H NMR (400 MHz, CDCl$_3$): δ 2.12 (3H, s, H6), 3.86 (3H, s, -OMe), 4.35 (2H, s, H8), 6.90 (2H, d, *J* 9.0 Hz, H11), 7.02 (1H, d, *J* 7.7 Hz, H1), 7.08-7.13 (2H, m, H2 & H4), 7.22 (1H, ddd, *J* 7.5, 1.5 Hz, H3), 7.54 (2H, d, *J* 9.0 Hz, H10).

^{13}C NMR (100 MHz, CDCl$_3$): δ 19.4 (C6), 55.7 (-OMe), 60.2 (C8), 114.1 (C11), 126.0 (C2), 126.9 (C7), 128.9 (C3), 129.8 (C9), 130.6 (C4), 130.8 (C10), 131.9 (C1), 138.3 (C5), 163.8 (C12).

FTIR (υ_{max}cm^{-1}): 3078-2842 (w, CH$_x$), 1592-1412 (m, C–C), 1317-1308 (s, S=O), 1261-1241 (s, C–O).

HRMS (ASAP+): calculated for C$_{15}$H$_{16}$O$_3$S [M+H$^+$] 277.0898 found: 277.0925

R$_f$: 0.62 (50:50 EtOAc/hexane).

1,4-Dimethoxy-2-(((4-methoxyphenyl)sulfonyl)methyl)benzene **(102p)**. Isolated as a colourless solid (54.1 mg, 0.168 mmol, 67%) according to general procedure C2 and purified *via* flash column chromatography (20:80-30:70 EtOAc/hexane).
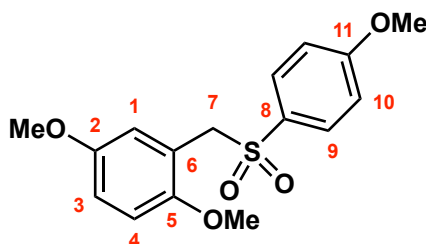
1,4-dimethoxy-2-(((4-methoxyphenyl)sulfonyl)methyl)benzene
Molecular Weight: 322.38

102p

^{1}H NMR (400 MHz, CDCl$_3$): δ 3.37 (3H, s, C5-OMe), 3.75 (3H, s, C2-OMe), 3.84 (3H, s, C11-OMe), 4.39 (2H, s, H7), 6.60 (1H, d, *J* 8.9 Hz, H4), 6.80 (1H, dd, *J* 8.9, 3.1 Hz, H3), 6.85-6.88 (3H, m, H1 & H10), 7.54 (2H, d, *J* 8.9 Hz, H9).

^{13}C NMR (100 MHz, CDCl$_3$): δ 55.8-56.0 (C2-OMe, C5-OMe & C11-OMe), 56.9 (C7), 111.6 (C4), 113.7 (C10), 115.8 (C3), 117.5 (C1), 118.0 (C6), 130.5 (C8), 131.1 (C9), 152.0 (C5), 153.5 (C2), 163.7 (C11).

FTIR (υ$_{max}$cm^{-1}): 2998-2914 (w, CH$_x$), 1436-1407 (m, C–C), 1312 (m, S=O), 1017 (s, C–O).

HRMS (ASAP+): calculated for C$_{16}$H$_{18}$O$_5$S [M+H$^+$] 323.0953 found: 323.0938

R$_f$: 0.22 (30:70 EtOAc/hexane).

1-Iodo-2-(((4-methoxyphenyl)sulfonyl)methyl)benzene **(102q)**. Isolated as a white solid (64.1 mg, 0.165 mmol, 66%) according to general procedure C1 and purified *via* flash column chromatography (15:85-20:80 EtOAc/hexane).
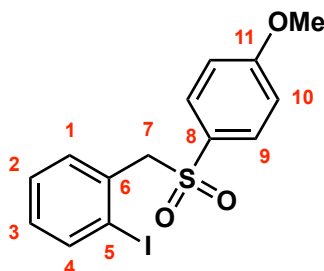
1-iodo-2-(((4-methoxyphenyl)sulfonyl)methyl)benzene
Molecular Weight: 388.22

102q

¹H NMR (400 MHz, CDCl₃): δ 3.87 (3H, s, -OMe), 4.57 (2H, s, H7), 6.90 (2H, d, *J* 9.0 Hz, H10), 7.01 (1H, ddd, *J* 7.8, 7.8, 1.7 Hz, H2), 7.36 (1H, ddd, *J* 7.6, 7.6, 1.2 Hz, H3), 7.50-7.56 (3H, m, H1 & H9), 7.74 (1H, dd, *J* 8.0, 1.2 Hz, H4).

¹³C NMR (100 MHz, CDCl₃): δ 55.7 (-OMe), 66.3 (C7), 102.3 (C5), 114.2 (C10), 128.5 (C3), 129.7 (C8), 130.3 (C2), 131.2 (C9), 132.2 (C1 & C6), 139.8 (C4), 164.1 (C11).

FTIR (υ_{max}cm⁻¹): 2980-2919 (w, CHₓ), 1592-1413 (m, C–C), 1318-1306 (m, S=O), 1263-1244 (s, C–O), 551 (s, C–I).

HRMS (ASAP+): calculated for C₁₄H₁₃IO₃S [M+H⁺] 388.9708 found: 388.9730

R*f*: 0.38 (20:80 EtOAc/hexane).

***1-Fluoro-4-(((4-methoxyphenyl)sulfonyl)methyl)benzene* (102r)**. Isolated as a white solid (69.4 mg, 0.248 mmol, 99%) according to general procedure C1 without further purification.
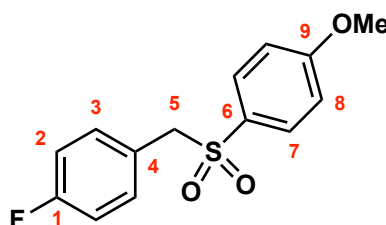
1-fluoro-4-(((4-methoxyphenyl)sulfonyl)methyl)benzene
Molecular Weight: 280.31

102r

¹H NMR (400 MHz, CDCl₃): δ 3.86 (3H, s, -OMe), 4.25 (2H, s, H5), 6.91 (2H, d, *J* 8.9 Hz, H8), 6.96 (2H, dd, *J* 8.6 Hz, H2), 7.04-7.08 (2H, m, H3), 7.53 (2H, d, *J* 9.0 Hz, H7).

¹³C NMR (100 MHz, CDCl₃): δ 55.7 (-OMe), 62.2 (C5), 114.1 (C8), 115.5-115.8 (d, *J* 21.7 Hz, C2), 124.39-124.43 (d, *J* 3.3 Hz, C4), 129.2 (C6), 130.8 (C7), 132.5-132.6 (d, *J* 8.4 Hz, C3), 161.8-164.2 (d, *J* 248.4 Hz, C1), 163.8 (C9).

FTIR (υ_{max}cm⁻¹): 3069-2838 (w, CHₓ), 1596-1413 (m, C–C), 1313 (s, S=O), 1263 (s, C–O), 1144 (s, C–F).

HRMS (ASAP+): calculated for C₁₄H₁₃FO₃S [M+H⁺] 281.0648 found: 281.0674

R*f*: 0.47 (30:70 EtOAc/hexane).

Data is consistent with a reported example.[210]

1-Methoxy-4-((4-(trifluoromethyl)benzyl)sulfonyl)benzene **(102s)**. Isolated as a white solid (59.1 mg, 0.179 mmol, 72%) according to general procedure C1 and purified *via* flash column chromatography (15:85 EtOAc/hexane).
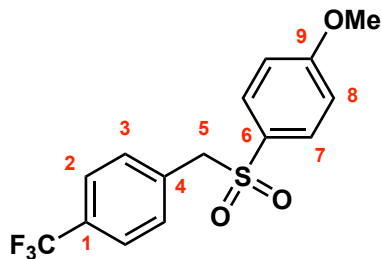
1-methoxy-4-((4-(trifluoromethyl)benzyl)sulfonyl)benzene
Molecular Weight: 330.32

102s

^{1}H NMR (400 MHz, CDCl$_3$): δ 3.87 (3H, s, -OMe), 4.33 (2H, s, H5), 6.92 (2H, d, *J* 9.0 Hz, H8), 7.23 (2H, d, *J* 8.1 Hz, H3), 7.53-7.57 (4H, m, H2 & H7).

^{13}C NMR (100 MHz, CDCl$_3$): δ 55.7 (-OMe), 62.6 (C5), 114.3 (C8), 125.5 (q, *J* 3.7 Hz, C2), 129.1 (C6), 130.8 (C7), 131.2 (C3), 132.5 (C4), 164.0 (C9).

^{19}F{^{1}H} NMR (377 MHz, CDCl$_3$): δ –62.7 (-CF$_3$).

FTIR (υ$_{max}$cm^{-1}): 3296-2845 (w, CH$_x$), 1597-1412 (m, C–C), 1335-1313 (s, S=O), 1265 (s, C–O), 1148-1116 (s, C–F).

HRMS (ASAP+): calculated for C$_{15}$H$_{13}$F$_3$O$_3$S [M+H$^+$] 331.0616 found: 331.0619

R$_f$: 0.15 (20:80 EtOAc/hexane).

Data is consistent with a reported example.[210]

Tert-butyl 4-hydroxypiperidine-1-carboxylate **(104)**. A flask containing 3.99 g of N-Boc-4-piperidone (**103**, 20.0 mmol, 1.0 equiv) was subjected to vacuum and backfilled with nitrogen (3 cycles). MeOH (25 mL) was added dropwise and the reaction mixture cooled to 0 °C. NaBH$_4$ (1.14 g, 30.0 mmol, 1.5 equiv) was added portionwise and reaction progress monitored *via* TLC. After 2 hours the reaction mixture was quenched with saturated NH$_4$Cl solution (60 mL) with continued cooling. Volatiles were removed *in vacuo* and the remaining aqueous layer was extracted with EtOAc (3 x 50 mL). The collected organic layers were dried over MgSO$_4$ and the solvent removed *in vacuo* to yield a colourless oil which was purified *via* flash column chromatography (90:10 CH$_2$Cl$_2$/acetone) to afford the desired product **104** as a colourless oil (3.49 g, 17.33 mmol, 87%).
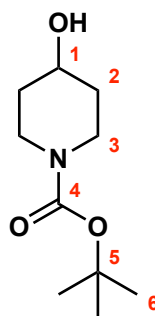
tert-butyl 4-hydroxypiperidine-1-carboxylate
Molecular Weight: 201.27

104

¹H NMR (400 MHz, CDCl₃): δ 1.40-1.49 (11H, m, H2a & H6), 1.82-1.86 (3H, m, H2b & -OH), 3.01 (2H, ddd, *J* 13.4, 9.9, 3.3 Hz, H3a), 3.79-3.85 (3H, m, H1 & H3b).

¹³C NMR (100 MHz, CDCl₃): δ 28.4 (C6), 34.2 (C2), 41.4 (C3), 67.7 (C1), 79.6 (C5), 154.8 (C4).

FTIR (υ_{max}cm⁻¹): 3457 (s, OH), 3004–2860 (w, CHₓ), 1657 (s, C=O).

HRMS (ASAP+): calculated for C₁₀H₁₉NO₃ [M+H⁺] 202.1443 found: 202.1456

R*f*: 0.68 (90:10 CH₂Cl₂/MeOH).

Data is consistent with a reported example.[212]

***Tert-butyl-((methylsulfonyl)oxy)piperidine-1-carboxylate* (105)**. Prepared according to a known procedure.[213] A flask containing 3.50 g of alcohol **104** (17.40 mmol, 1.0 equiv) was subjected to vacuum and backfilled with nitrogen (3 cycles). THF (20 mL) was added dropwise and the reaction mixture cooled to 0 °C. Et₃N (12 mL, 87.0 mmol, 5.0 equiv), was introduced dropwise followed by addition of mesyl chloride (1.6 mL, 20.88 mmol, 1.2 equiv) dropwise. The reaction mixture was allowed to stir to room temperature for 18 hours and monitored *via* TLC. Upon completion the reaction mixture was partitioned with water (60 mL) and the aqueous layer was extracted with EtOAc (3 x 60 mL). The collected organic layers were dried over MgSO₄ and the solvent removed *in vacuo* to obtain the product **105** as a pale yellow solid (4.70 g, 16.83 mmol, 97%) without further purification.
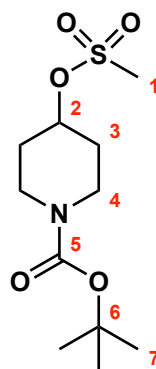
tert-butyl 4-((methylsulfonyl)oxy)piperidine-1-carboxylate
Molecular Weight: 279.35

105

¹H NMR (400 MHz, CDCl₃): δ 1.46 (9H, s, H7), 1.77-1.85 (2H, m, H3a), 1.93-2.00 (2H, m, H3b), 3.04 (3H, s, H1), 3.30 (2H, oct, *J* 13.7, 8.1, 3.8 Hz, H4a), 3.70 (2H, oct, *J* 13.7, 6.9, 4.0 Hz, H4b), 4.88 (1H, spt, *J* 7.8, 3.7 Hz, H2).

¹³C NMR (100 MHz, CDCl₃): δ 28.4 (C7), 31.7 (C3), 38.9 (C1), 40.5 (C4), 77.6 (C2), 80.0 (C6), 154.6 (C5).

FTIR (υₘₐₓcm⁻¹): 3337–2852 (w, CHₓ), 1692–1679 (s, C=O).

HRMS (ASAP+): calculated for C₁₁H₂₁NO₅S [M+H⁺] 280.1219 found: 280.1221

R_f: 0.10 (20:80 EtOAc/hexane).

Data is consistent with a reported example.[213]

***Tert-butyl 4-((4-chlorophenyl)thio)piperidine-1-carboxylate* (106)**. A flask containing mesylate **105** (2.30 g, 8.23 mmol, 1.0 equiv), 4-chlorothiophenol (1.67 g, 11.52 mmol, 1.4 equiv) and K₂CO₃ (1.59 g, 11.52 mmol, 1.4 equiv) was subjected to vacuum and backfilled with nitrogen (3 cycles). DMF (35 mL) was added dropwise and the subsequent reaction mixture heated to 70 ºC with stirring, and reaction progress was monitored *via* TLC. After 19 hours the reaction mixture was cooled to room temperature and partitioned with water (160 mL), and the aqueous layer extracted with EtOAc (3 x 80 mL). The combined organic layers were dried over Na₂SO₄ and the solvent removed *in vacuo* to afford a yellow oil which was purified *via* flash column chromatography (5:95 EtOAc/hexane) to provide the desired product **106** as a colourless oil (2.10 g, 6.41 mmol, 78%).
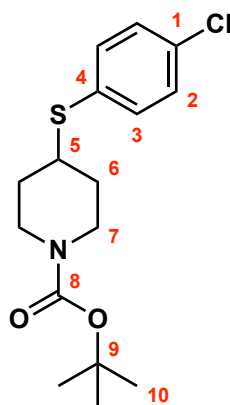
tert-butyl 4-((4-chlorophenyl)thio)piperidine-1-carboxylate
Molecular Weight: 327.87

106

^{1}H NMR (400 MHz, CDCl$_3$): δ 1.37-1.47 (11H, m, H6a & H10), 1.80-1.85 (2H, m, H6b), 2.84 (2H, t, *J* 12.2 Hz, H7a), 3.10 (1H, tt, *J* 10.3, 3.9 Hz, H5), 3.88 (2H, br, H7b), 7.20 (2H, d, *J* 8.6 Hz, H3), 7.27 (2H, d, *J* 8.6 Hz, H2).

^{13}C NMR (100 MHz, CDCl$_3$): δ 28.4 (C10), 32.0 (C6), 43.2 (C7), 44.8 (C5), 79.6 (C9), 129.1 (C3), 132.2 (C1), 133.5 (C4), 134.0 (C2), 154.6 (C8).

FTIR (υ_{max}cm^{-1}): 2975–2854 (w, CH$_x$), 1687 (s, C=O), 1573–1418 (m, C–C), 820 (s, C–Cl).

HRMS (ASAP+): calculated for C$_{16}$H$_{22}$ClNO$_2$S [M+H$^+$] 328.1138 found: 328.1090

R$_f$: 0.27 (10:90 EtOAc/hexane).

Data is consistent with a reported example.[214]

4-((4-Chlorophenyl)thio)piperidin-1-ium 2,2,2-trifluoroacetate (**107**). To a solution of sulfide **106** (0.490 g, 1.50 mmol, 1.0 equiv) in CH$_2$Cl$_2$ (15 mL) was added TFA (1.25 mL, 16.3 mmol, 10.9 equiv) dropwise at room temperature with stirring, and reaction progress was monitored *via* TLC. After 22 hours the reaction mixture was concentrated *in vacuo* and the resulting oil suspended in water (15 mL) to form a precipitate isolated *via* filtration. The obtained solids were washed with Et$_2$O (5 x 20 mL) and dried *in vacuo* to afford the desired product **107** as a white solid (0.512 g, 1.50 mmol, quant.).
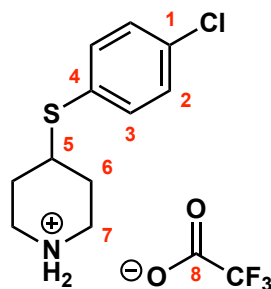
4-((4-chlorophenyl)thio)piperidin-1-ium 2,2,2-trifluoroacetate
Molecular Weight: 341.77

107

^{1}H NMR (400 MHz, CDCl$_3$): δ 1.83-1.92 (2H, m, H6a), 2.15-2.21 (2H, m, H6b), 2.99 (2H, br, H7a), 3.30-3.38 (3H, m, H5 & H7b), 7.30 (2H, d, *J* 8.7 Hz, H3), 7.36 (2H, d, *J* 8.7 Hz, H2), 9.48 (2H, br, -NH$_2$).

^{13}C NMR (100 MHz, CDCl$_3$): δ 28.2 (C6), 41.9 (C5), 42.1 (C7), 129.5 (C3), 130.9 (C1), 134.4 (C2), 143.7 (C4).

^{19}F{^{1}H} NMR (377 MHz, CDCl$_3$): δ -75.7 (-CF$_3$).

FTIR (υ$_{max}$cm^{-1}): 2963–2503 (br, NH), 1675 (s, C=O), 1474–1433 (m, C–C), 1180–1077 (s, C–F), 792 (s, C–Cl).

HRMS (ASAP+): calculated for C$_{11}$H$_{14}$ClNS [M+H$^+$] 228.0614 found: 228.0565

R$_f$: 0.33 (90:10 CH$_2$Cl$_2$/MeOH).

***Tert-butyl-4-((4-chlorophenyl)sulfonyl)piperidine-1-carboxylate* (108)**. To a solution of sulfide **106** (1.00 g, 3.05 mmol, 1.0 equiv) in CH$_2$Cl$_2$ (60 mL) cooled to 0 °C was added ≤77% *m*–CPBA (2.02 g, 9.00 mmol, 3.0 equiv). The reaction mixture was left to stir to room temperature and monitored *via* TLC. After 22 hours the reaction mixture was quenched with saturated NaHCO$_3$ solution (60 mL) and left to stir at room temperature for a further 15 minutes. The aqueous layer was removed and the remaining organic layer was washed consecutively with 1.0 M NaOH solution (30 mL), water (30 mL) and saturated brine solution (30 mL) before drying over Na$_2$SO$_4$. The solvent was removed *in vacuo* to afford a white solid which was purified *via* flash column chromatography (40:60 EtOAc/hexane) to provide the desired product **108** as a white solid (0.736 g, 2.05 mmol, 68%).
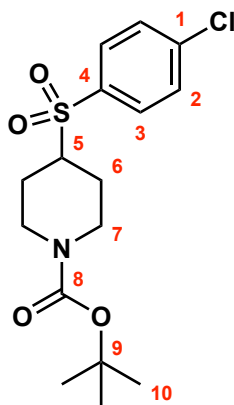
tert-butyl 4-((4-chlorophenyl)sulfonyl)piperidine-1-carboxylate
Molecular Weight: 359.87

108

¹H NMR (400 MHz, CDCl₃): δ 1.43 (9H, s, H10), 1.59 (2H, dddd, *J* 12.8, 12.5, 4.6 Hz, H6a), 1.97 (2H, d br, *J* 12.4 Hz, H6b), 2.65 (2H, br, H7a), 3.02 (1H, tt, *J* 12.1, 3.7 Hz, H5), 4.23 (2H, br, H7b), 7.56 (2H, d, *J* 8.7 Hz, H2), 7.80 (2H, d, *J* 8.7 Hz, H3).

¹³C NMR (100 MHz, CDCl₃): δ 25.0 (C6), 28.4 (C10), 42.8 (C7), 61.9 (C5), 80.2 (C9), 129.6 (C2), 130.6 (C3), 135.1 (C4), 140.9 (C1), 154.3 (C8).

FTIR (υ_{max}cm⁻¹): 3090–2868 (w, CH$_x$), 1683 (s, C=O), 1581–1423 (m, C–C), 1306 (s, S=O), 821 (s, C–Cl).

HRMS (ASAP+): calculated for C₁₆H₂₂ClNO₄S [M+H⁺] 360.1036 found: 360.1007

R$_f$: 0.83 (20:80 EtOAc/hexane).

***4-((4-Chlorophenyl)sulfonyl)piperidin-1-ium 2,2,2-trifluoroacetate* (109)**. To a solution of sulfone **108** (0.360 g, 1.00 mmol, 1.0 equiv) in CH₂Cl₂ (10 mL) was added TFA (770 μL, 10.0 mmol, 10.0 equiv) dropwise at room temperature with stirring, and reaction progress was monitored *via* TLC. After 20 hours the reaction mixture was concentrated *in vacuo* and the resulting brown oil was suspended in Et₂O (10 mL) to form a precipitate isolated *via* filtration. The obtained solids were washed with Et₂O (3 x 10 mL) and dried *in vacuo* to afford the desired product **109** as a white solid (0.372 g, 0.995 mmol, quant.).
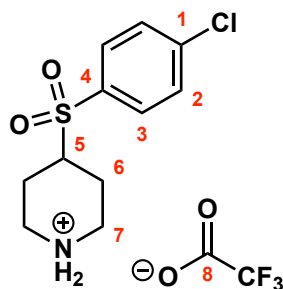
4-((4-chlorophenyl)sulfonyl)piperidin-1-ium 2,2,2-trifluoroacetate
Molecular Weight: 373.77

109

^{1}H NMR (400 MHz, CD$_3$OD): δ 1.83-1.94 (2H, m, H6a), 2.20 (2H, d br, *J* 14.8 Hz, H6b), 3.00 (2H, ddd, *J* 13.0, 3.2 Hz, H7a), 3.47-3.57 (3H, m, H5 & H7b), 7.72 (2H, d, *J* 8.8 Hz, H2), 7.91 (2H, d, *J* 8.8 Hz, H3).

^{13}C NMR (100 MHz, CD$_3$OD): δ 23.4 (C6), 43.7 (C7), 58.7 (C5), 131.0 (C2), 131.9 (C3), 136.4 (C4), 142.2 (C1).

^{19}F{^{1}H} NMR (377 MHz, CD$_3$OD): δ -76.9 (-CF$_3$).

FTIR (υ$_{max}$cm^{-1}): 3077–2930 (w, CH$_x$), 2201–1923 (m, NH), 1665 (s, C=O), 1583–1433 (m, C–C), 1322–1308 (m, S=O), 1035–1123 (s, C–F), 632 (s, C–Cl).

HRMS (ASAP+): calculated for C$_{11}$H$_{14}$ClNO$_2$S [M+H$^+$] 260.0512 found: 260.0546

R$_f$: 0.35 (90:10 CH$_2$Cl$_2$/MeOH).
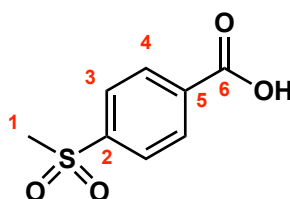
4-(methylsulfonyl)benzoic acid
Molecular Weight: 200.21

110

^{1}H NMR (400 MHz, DMSO-*d$_6$*): δ 3.28 (3H, s, H1), 8.05 (2H, d, *J* 8.6 Hz, H3), 8.17 (2H, d, *J* 8.6 Hz, H4), 13.56 (1H, br, -COOH).

^{13}C NMR (100 MHz, DMSO-*d$_6$*): δ 43.2 (C1), 127.3 (C3), 130.2 (C4), 135.2 (C5), 144.3 (C2), 166.2 (C6).

FTIR (υ$_{max}$cm^{-1}): 3104–2540 (br, OH), 1689 (s, C=O), 1574–1425 (m, C–C), 1320 (s, S=O).

HRMS (ASAP+): calculated for $C_8H_8O_4S$ [M+H$^+$] 201.0222 found: 201.0241

R$_f$: 0.38 (70:30 EtOAc/MeOH).

Methyl 2-oxo-2-(4-oxopiperidin-1-yl)acetate **(113)**. Prepared according to a modified known procedure.[215] A flask containing 3.07 g of 4-piperidone hydrochloride monohydrate (**111**, 20.0 mmol, 1.0 equiv) was subjected to vacuum and backfilled with nitrogen (3 cycles). Anhydrous CH_2Cl_2 (80 mL) was added dropwise and the resulting solution cooled to 0 °C. Et_3N (8.4 mL, 60.0 mmol, 3.0 equiv) was introduced dropwise followed by the addition of methyl chloroglyoxalate (**112**, 2.2 mL, 24.0 mmol, 1.2 equiv) over a five-minute interval, accompanied by evolution of colourless gas. The reaction mixture was left to stir to room temperature and monitored *via* TLC. After 22 hours the reaction mixture was partitioned with water (100 mL) and the aqueous layer extracted with a 3:1 $CHCl_3$/*i*-PrOH mixture (3 x 100 mL). The collected organic layers were washed with aqueous 10% w/v $CuSO_4$ solution (3 x 100 mL) and dried over $MgSO_4$. The solvents were removed *in vacuo* to afford the crude product, which was purified *via* flash column chromatography (90:10 CH_2Cl_2/MeOH) to give the desired product **113** as a brown oil (1.64 g, 8.86 mmol, 44%).
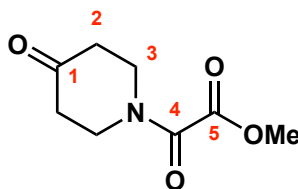
methyl 2-oxo-2-(4-oxopiperidin-1-yl)acetate
Molecular Weight: 185.18

113

^{1}H NMR (400 MHz, CDCl$_3$): δ 2.5-2.56 (4H, m, H2), 3.73 (2H, t, *J* 6.3 Hz, H3a), 3.88-3.91 (5H, m, H3b & -OMe).

^{13}C NMR (100 MHz, CDCl$_3$): δ 40.4 (C2a), 40.6 (C2b), 41.1 (C3a), 44.7 (C3b), 52.9 (-OMe), 160.0 (C4), 162.6 (C5), 205.3 (C1).

FTIR (υ_{max}cm^{-1}): 2959 (w, CH$_x$), 1733–1650 (s, C=O).

HRMS (ASAP+): calculated for $C_8H_{11}NO_4$ [M+H$^+$] 186.0766 found: 186.0764

R$_f$: 0.75 (80:10:5:5 EtOAc/*n*-BuOH/AcOH/H$_2$O).

N-(4-((4-oxopiperin-1-yl)sulfonyl)phenyl)acetamide (**115**). Prepared according to a modified known procedure.[215] A flask containing 3.07 g of 4-piperidone hydrochloride monohydrate (**111**, 20.0 mmol, 1.0 equiv) and 5.61 g of N-acetylsulfanilyl chloride (**114**, 24.0 mmol, 1.2 equiv) was subjected to vacuum and backfilled with nitrogen (3 cycles). Anhydrous CH_2Cl_2 (80 mL) was added dropwise and the resulting solution cooled to 0 °C. Et_3N (8.4 mL, 60.0 mmol, 3.0 equiv) was introduced dropwise and the reaction mixture was left to stir to room temperature and monitored *via* TLC. After 20 hours the reaction mixture was partitioned with water (75 mL) and the aqueous layer extracted with CH_2Cl_2 (3 x 100 mL). The collected organic layers were washed with aqueous 10% w/v $CuSO_4$ solution (3 x 100 mL) and dried over Na_2SO_4. The solvent was removed *in vacuo* to provide the crude product, which was purified *via* flash column chromatography (90:10 CH_2Cl_2/MeOH) to afford the desired product **115** as a white solid (2.20 g, 7.42 mmol, 37%).
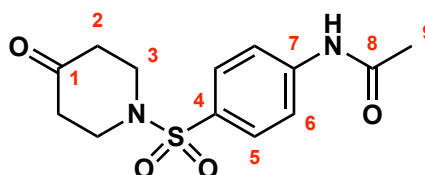
N-(4-((4-oxopiperidin-1-yl)sulfonyl)phenyl)acetamide
Molecular Weight: 296.34

115

¹H NMR (400 MHz, DMSO-d_6): δ 2.09 (3H, s, H9), 2.41 (4H, t, *J* 6.2 Hz, H2), 3.27 (4H, t, *J* 6.2 Hz, H3), 7.73 (2H, d, *J* 8.9 Hz, H5), 7.82 (2H, d, *J* 8.9 Hz, H6), 10.39 (1H, br, -NH).

¹³C NMR (100 MHz, DMSO-d_6): 24.2 (C9), 39.8 (C2), 45.1 (C3), 118.7 (C6), 128.6 (C4), 129.3 (C5), 143.6 (C7), 169.1 (C8), 205.6 (C1).

FTIR (υ_{max}cm^{-1}): 3334 (m, NH), 3113–2852 (w, CH$_x$), 1714–1691 (C=O), 1589–1473 (m, C–C).

HRMS (ASAP+): calculated for $C_{13}H_{16}N_2O_4S$ [M+H$^+$] 297.0909 found: 297.0911

R$_f$: 0.64 (10:90 MeOH/CH_2Cl_2).

Methyl 2-((4-methoxyphenyl)amino)-2-oxoacetate (**117**). Prepared according to a modified known procedure.[215] A flask containing 2.46 g of *p*–anisidine (**116**, 20.0 mmol, 1.0 equiv) was subjected to vacuum and backfilled with nitrogen (3 cycles). Anhydrous CH_2Cl_2 (80 mL) was added dropwise and the resulting solution cooled to 0 °C. Et_3N (4.2

mL, 30.0 mmol, 1.5 equiv) was introduced dropwise followed by the addition of methyl chloroglyoxalate (**112**, 2.2 mL, 24.0 mmol, 1.2 equiv) over a five-minute interval, accompanied by evolution of colourless gas. The reaction mixture was left to stir to room temperature and monitored *via* TLC. After 19 hours the reaction mixture was partitioned with water (75 mL) and the aqueous layer extracted with CH_2Cl_2 (3 x 50 mL). The collected organic layers were washed with saturated brine (3 x 50 mL) and aqueous 10% w/v $CuSO_4$ solution (3 x 100 mL) sequentially and dried over $MgSO_4$. Removal of the solvent *in vacuo* gave the desired product **117** as a grey solid (4.0 g, 14.12 mmol, 96% yield) without further purification.
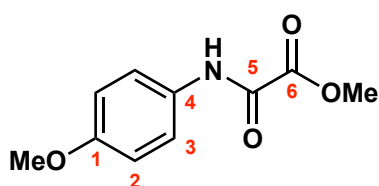
methyl 2-((4-methoxyphenyl)amino)-2-oxoacetate
Molecular Weight: 209.20

117

¹H NMR (400 MHz, CDCl₃): δ 3.80 (3H, s, C1-OMe), 3.96 (3H, s, C6-OMe), 6.90 (2H, d, *J* 9.1 Hz, H2), 7.56 (2H, d, *J* 9.1 Hz, H3), 8.79 (1H, br, -NH).

¹³C NMR (100 MHz, CDCl₃): δ 54.0 (C6-OMe), 55.5 (C1-OMe), 114.4 (C2), 121.4 (C3), 129.4 (C4), 153.4 (C5), 157.2 (C1), 161.7 (C6).

FTIR (υ_{max}cm⁻¹): 3351–3326 (m, NH), 3005–2837 (w, CH$_x$), 1729–1694 (s, C=O), 1546–1445 (m, C–C).

HRMS (ASAP+): calculated for $C_{10}H_{11}NO_4$ [M+H⁺] 210.0766 found: 210.0767

R$_f$: 0.90 (90:10 CH_2Cl_2/MeOH).

Data is consistent with a reported example.[215]

***3-(2-methoxy-2-oxoacetamido)benzoic acid* (119)**. Prepared according to a modified known procedure.[215] A flask containing 2.74 g of 3-aminobenzoic acid (**118**, 20.0 mmol, 1.0 equiv) was subjected to vacuum and backfilled with nitrogen (3 cycles). Anhydrous CH_2Cl_2 (80 mL) was added dropwise and the resulting solution cooled to 0 °C. Et₃N (4.2 mL, 30.0 mmol, 1.5 equiv) was introduced dropwise followed by the addition of methyl chloroglyoxalate (**112**, 2.2 mL, 24.0 mmol, 1.2 equiv) over a five-minute interval, accompanied by evolution of colourless gas. The reaction mixture was left to stir to room

temperature and monitored *via* TLC. After 24 hours the reaction mixture was partitioned with water (75 mL) and the aqueous layer extracted with CH$_2$Cl$_2$ (3 x 50 mL). The collected organic layers were washed with saturated brine (3 x 50 mL) and aqueous 10% w/v CuSO$_4$ solution (3 x 100 mL) sequentially and dried over MgSO$_4$. The solvent was removed *in vacuo* to obtain the crude product, which was purified *via* flash column chromatography (100:0–90:10 CH$_2$Cl$_2$/MeOH) to give the desired product **119** as a white solid (1.30 g, 5.83 mmol, 29%).
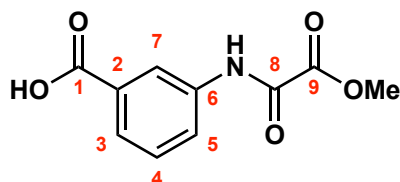
3-(2-methoxy-2-oxoacetamido)benzoic acid
Molecular Weight: 223.18

119

^{1}H NMR (400 MHz, DMSO-d_6): δ 3.86 (3H, s, -OMe), 7.48 (1H, dd, *J* 7.9 Hz, H4), 7.73 (1H, ddd, *J* 7.8, 1.3 Hz, H3), 7.95 (1H, ddd, *J* 8.1, 2.2, 1.0 Hz, H5), 8.41 (1H, dd, *J* 1.8 Hz, H7), 10.99 (1H, s, -NH), 13.06 (1H, br, -COOH).

^{13}C NMR (100 MHz, DMSO-d_6): δ 53.3 (-OMe), 121.3 (C7), 124.7 (C5), 125.6 (C3), 129.1 (C4), 131.5 (C2), 137.8 (C6), 155.5 (C8), 160.9 (C9), 167.1 (C1).

FTIR (υ_{max}cm^{-1}): 3350 (m, NH), 2962–2562 (br, OH), 1703–1683 (s, C=O), 1552–1445 (m, C–C).

HRMS (ASAP+): calculated for C$_{10}$H$_9$NO$_5$ [M+H$^+$] 224.0559 found: 224.0561

R$_f$: 0.31 (90:10 CH$_2$Cl$_2$/MeOH).

***Ethyl (E)-2-(2-oxoindolin-3-ylidene)acetate* (122)**. Prepared according to a known procedure.[216] A solution of isatin (**120**, 2.94 g, 20.0 mmol, 1.0 equiv) and (carbethoxymethylene)triphenylphosphorane (**121**, 7.66 g, 22.0 mmol, 1.1 equiv) in toluene (60 mL) was stirred at room temperature for 24 hours and monitored by TLC. Upon completion the resulting suspension was left to stand for 1 hour. The accumulated precipitate was filtered off and washed with hexane (3 x 70 mL). Cooling of the filtrate to 5 °C for 17 hours produced a second crop of solids that were isolated *via* filtration, recrystallised from boiling hexane (100 mL) and washed with cold hexane (3 x 100 mL).

The combined crops of precipitate were dried *in vacuo* to afford the desired product **122** as a bright orange solid (3.95 g, 18.20 mmol, 91%).
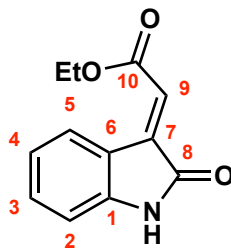
ethyl (E)-2-(2-oxoindolin-3-ylidene)acetate
Molecular Weight: 217.22

122

¹H NMR (400 MHz, CDCl₃): δ 1.38 (3H, t, *J* 7.2 Hz, -OEt), 4.34 (2H, q, *J* 7.1 Hz, -OEt), 6.86 (1H, d, *J* 7.8 Hz, H2), 6.88 (1H, s, H9), 7.05 (1H, ddd, *J* 7.8, 1.0 Hz, H4), 7.32 (1H, ddd, *J* 7.7, 1.2 Hz, H3), 8.28 (1H, br, -NH), 8.55 (1H, d, *J* 7.8 Hz, H5).

¹³C NMR (100 MHz, CDCl₃): δ 14.2 (-OEt), 61.3 (-OEt), 110.1 (C2), 120.4 (C6), 122.7 (C9), 122.9 (C4), 129.1 (C5), 132.6 (C3), 138.0 (C7), 143.22 (C1), 165.6 (C10), 169.1 (C8).

FTIR (υ_{max}cm⁻¹): 3186, (m, NH), 3159–2825 (w, CHₓ), 1706 (s, C=O), 1584–1409 (m, C–C).

HRMS (ASAP+): calculated for C₁₂H₁₁NO₃ [M+H⁺] 218.0817 found: 218.0818

R$_f$: 0.18 (CH₂Cl₂).

Data is consistent with a reported example.[216]

***Tert*-butyl 4-azidopiperidine-1-carboxylate** (**123**). Prepared according to a known procedure.[217] A flask containing mesylate **105** (2.30 g, 8.23 mmol, 1.0 equiv) and sodium azide (1.61 g, 24.69 mmol, 3.0 equiv) was subjected to vacuum and backfilled with nitrogen (3 cycles). DMF (15 mL) was added dropwise with stirring and the reaction mixture heated to 80 °C for 18 hours. Upon completion according to TLC the reaction mixture was cooled to room temperature and partitioned with water (160 mL), and the aqueous layer extracted with EtOAc (3 x 80 mL). The combined organic layers were dried over Na₂SO₄ and the solvent removed *in vacuo* to provide the desired product **123** as a yellow oil (1.86 g, 8.21 mmol, quant.) without further purification.
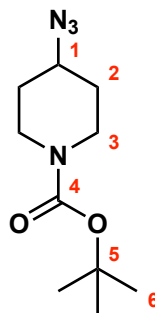
tert-butyl 4-azidopiperidine-1-carboxylate
Molecular Weight: 226.28

123

¹H NMR (400 MHz, CDCl₃): δ 1.36 (9H, s, H6), 1.40-1.49 (2H, m, H2a), 1.75-1.79 (2H, m br, H2b), 3.00 (2H, spt, *J* 13.7, 9.5, 3.4 Hz, H3a), 3.49 (1H, spt, *J* 9.1, 3.9 Hz, H1), 3.70-3.74 (2H, m br, H3b).

¹³C NMR (100 MHz, CDCl₃): δ 28.3 (C6), 30.5 (C2), 41.4 (C3), 57.5 (C1), 79.7 (C5), 154.5 (C4).

FTIR (υ_{max}cm^{-1}): 2977–2864 (w, CH$_x$), 2091 (s, N₃), 1684 (s, C=O).

HRMS (ASAP+): calculated for $C_{10}H_{18}N_4O_2$ [M+H⁺] 227.1508 found: 227.1501

R$_f$: 0.11 (20:80 EtOAc/hexane).

Data is consistent with a reported example.[218]

***Tert*-butyl 4-(5-benzoyl-1H-tetrazol-1-ylpiperidine-1-carboxylate** **(124)**. Prepared according to a known procedure.[183] A vial containing benzoyl cyanide (0.787 g, 6.00 mmol, 1.5 equiv) was evacuated and backfilled with nitrogen (3 cycles). Azide **123** (0.905 g, 4.00 mmol, 1.0 equiv) was added dropwise at room temperature under a nitrogen atmosphere. The vial was sealed and the reaction mixture heated to reflux at 120 °C. After 48 hours the reaction mixture was cooled to room temperature suspended in EtOAc (15 mL) and quenched with 10% w/v Na₂CO₃ solution (50 mL). The resulting aqueous layer was extracted with EtOAc (3 x 15 mL) and the collected organic layers dried over Na₂SO₄. The dried solution was filtered through a silica plug and rinsed through with hexane (50 mL) and EtOAc (50 mL). The organic phase was concentrated *in vacuo* to a brown oil which was purified *via* flash column chromatography (20:80 EtOAc/hexane) to afford the desired product **124** as a white solid (0.180 g, 0.504 mmol, 13%).
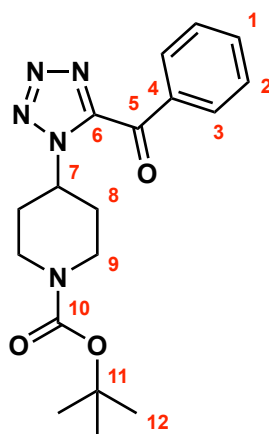
tert-butyl 4-(5-benzoyl-1H-tetrazol-1-yl)piperidine-1-carboxylate
Molecular Weight: 357.41

124

¹H NMR (400 MHz, CDCl₃): δ 1.49 (9H, s, H12), 2.13-2.28 (4H, m, H8), 2.94 (2H, br, H9a), 4.31 (2H, br, H9b), 5.14 (1H, tt, *J* 11.1, 4.4 Hz, H7), 7.57 (2H, dd, *J* 7.9 Hz, H2), 7.73 (1H, ddd, *J* 7.4, 1.3 Hz, H1), 8.39 (2H, dd, *J* 8.5, 1.3 Hz, H3).

¹³C NMR (100 MHz, CDCl₃): δ 28.4 (C12), 32.0 (C8), 42.8 (C9), 58.4 (C7), 80.2 (C11), 128.9 (C2), 131.1 (C3), 135.0 (C4), 135.4 (C1), 149.1 (C6), 154.5 (C10), 182.1 (C5).

FTIR (υ_{max}cm⁻¹): 3059–2847 (w, CH$_x$), 1675 (s, C=O), 1579–1414 (m, C–C).

HRMS (ASAP+): calculated for $C_{18}H_{23}N_5O_3$ [M+H⁺] 358.1879 found: 358.1873

R$_f$: 0.21 (20:80 EtOAc/hexane).

***4-(5-Benzoyl-1H-tetrazol-1-yl)piperidin-1-ium 2,2,2-trifluoroacetate* (125)**. To a solution of tetrazole **124** (0.140 g, 0.390 mmol, 1.0 equiv) in CH₂Cl₂ (5 mL) was added TFA (300 μL, 3.90 mmol, 10.0 equiv) dropwise at room temperature with stirring, and reaction progress was monitored *via* TLC. After 20 hours the reaction mixture was concentrated *in vacuo* and the resulting residue was washed with Et₂O (3 x 5 mL) and dried *in vacuo* to afford the desired product **125** as a pale yellow solid (0.140 g, 0.378 mmol, 97%).
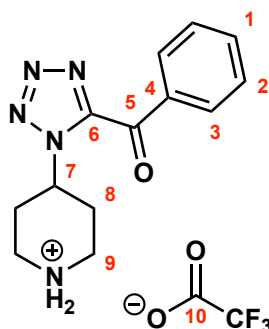
4-(5-benzoyl-1H-tetrazol-1-yl)piperidin-1-ium 2,2,2-trifluoroacetate
Molecular Weight: 371.32

125

¹H NMR (400 MHz, CD₃OD): δ 2.42-2.55 (4H, m, H8), 3.27-3.34 (2H, m, H9a), 3.65 (2H, ddd, *J* 13.5, 3.7 Hz, H9b), 5.39 (1H, tt, *J* 9.9, 5.0 Hz, H7), 7.62 (2H, dd, *J* 8.0 Hz, H2), 7.78 (1H, ddd, *J* 7.5, 1.3 Hz, H1), 8.37 (2H, dd, *J* 8.5, 1.3 Hz, H3).

¹³C NMR (100 MHz, CD₃OD): δ 29.9 (C8), 44.0 (C9), 56.0 (C7), 129.9 (C2), 132.1 (C3), 136.3 (C1), 136.5 (C4), 151.1 (C6), 183.1 (C5).

¹⁹F{¹H} NMR (377 MHz, CD₃OD): δ -76.9 (-CF₃).

FTIR (υ$_{max}$cm⁻¹): 2925–2520 (br, NH), 1664 (s, C=O), 1594–1427 (m, C–C), 1126–1169 (s, C–F).

HRMS (ASAP+): calculated for C₁₃H₁₅N₅O [M+H⁺] 258.1355 found: 258.1349

R*$_f$*: 0.36 (90:10 CH₂Cl₂/MeOH).

4,4'-((1E/Z,   1'E/Z)-hydrazine-1,2-diylidenebis(methaneylylidene))bis(benzene-1,3-diol) (127). To a solution of 2,4-dihydroxybenzaldehyde (**126**, 1.11 g, 8.00 mmol, 1.0 equiv) in THF (8 mL) was added hydrazine monohydrate (560 μL, 4.80 mmol, 0.6 equiv) dropwise at room temperature with stirring, and reaction progress monitored *via* TLC. After 30 minutes a precipitate was seen to form and isolated *via* filtration. The obtained solids were washed with water (5 x 10 mL) suspended in MeOH (30 mL) and all volatiles removed *in vacuo* to afford the desired product **127** as a pale yellow solid (1.09 g, 3.99 mmol, quant.).
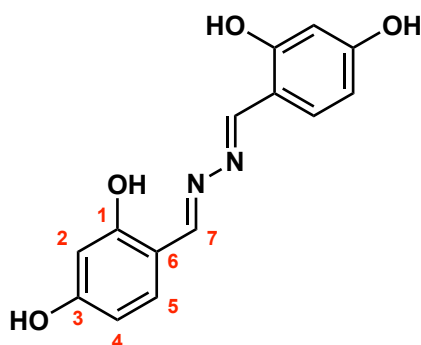
4,4'-((1*E/Z*,1'*E/Z*)-hydrazine-1,2-diylidenebis(methaneylylidene))bis(benzene-1,3-diol)
Molecular Weight: 272.26

127

^{1}H NMR (400 MHz, DMSO-d_6): δ 6.34 (2H, d, *J* 2.2 Hz, H2), 6.40 (2H, dd, *J* 8.5, 2.2 Hz, H4), 7.41 (2H, d, *J* 8.6 Hz, H5), 8.76 (2H, s, H7).

^{13}C NMR (100 MHz, DMSO-d_6): δ 102.5 (C2), 108.3 (C4), 110.3 (C6), 132.9 (C5), 160.7 (C7), 161.7 (C1), 162.2 (C3).

FTIR (υ_{max}cm^{-1}): 3462–3185 (br, OH), 1612 (s, C=N), 1585–1443 (m, C–C).

HRMS (ASAP+): calculated for $C_{14}H_{12}N_2O_4$ [M+H$^+$] 273.0875 found: 273.0875

R$_f$: 0.51 (90:10 CH$_2$Cl$_2$/MeOH).

Data is consistent with a reported example.[219]

***Methyl (E/Z)-(4-methylbenzylidene)hydrazine-1-carboxylate* (129)**. Prepared according to a known procedure.[220] To a solution of *p*–tolualdehyde (**128**, 2.40 g, 20.0 mmol, 1.0 equiv) in MeOH (80 mL) was added methyl carbazate (1.80 g, 20.0 mmol, 1.0 equiv) at room temperature with stirring, and reaction progress was monitored *via* TLC. After 18 hours the reaction mixture was concentrated and dried *in vacuo* to obtain the desired product **129** as a white solid (3.80 g, 19.77 mmol, 99%).
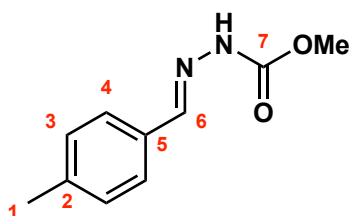
methyl (*E/Z*)-2-(4-methylbenzylidene)hydrazine-1-carboxylate
Molecular Weight: 192.22

129

^{1}H NMR (400 MHz, CDCl$_3$): δ 2.35 (3H, s, H1), 3.85 (3H, s, -OMe), 7.16 (2H, d, *J* 7.77 Hz, H), 7.56 (2H, d, *J* 7.79 Hz, H), 7.84 (1H, s, H6), 8.40 (1H, br, -NH).

^{13}C NMR (100 MHz, CDCl$_3$): δ 21.6 (C1), 53.2 (-OMe), 127.4 (C4), 129.5 (C3), 131.0 (C5), 140.5 (C2), 145.1 (C6), 154.6 (C7).

FTIR (υ_{max}cm^{-1}): 3165 (m, NH), 3049–2848 (w, CH$_x$), 1713–1694 (s, C=O), 1560–1438 (m, C–C).

HRMS (ASAP+): calculated for C$_{10}$H$_{12}$N$_2$O$_2$ [M+H$^+$] 193.0977 found: 193.1028

R$_f$: 0.27 (30:70 EtOAc/hexane).

Data is consistent with a reported example.[220]

3.2.3. DFT Methodology

All DFT calculations were performed by Dr. Alex Hamilton (Sheffield Hallam University, UK). DFT calculations were undertaken using ORCA 4.2 computational software.[221]

Optimisations were performed at the RI B97-D3 def2-TZVP level of theory and single point energies and solvation corrections calculated with a double-hybrid DFT functional RIJK RI-PWPB95 D3BJ/def2-TZVPP utilising unrelaxed MP2 densities and default settings for integration grid.[222–227] The effective core potential (ECP) generated by

Andrae *et al.* was used for the Ru atom as specified within the Ahlrichs def2 family of basis sets.[228]

Solvation corrected linear response (LR) time-dependent DFT calculations of the Ru(bpy)$_3^{2+}$ photocatalyst excited states were performed at the RIJCOSX RI-PWPB95 D3BJ def2-TZVPP level of theory employing the Tamm-Dancoff approximation, calculating 25 excitation roots with a max dimension of 5 to determine the Davidson correction for excited state energies.[222–225,227,229]

Frequencies calculations approximated the ZPE correction and entropic contributions to the free energy term as well as confirming all intermediates were true with no imaginary modes and all transition states had the correct critical frequency of decomposition. D3BJ dispersion corrections were employed for all single-point energy and excited state calculations.[223] Solvation corrections for all calculations were implemented using the CPCM model for DMF (ε = 36.7).[230] Graphical visualisation using Gabedit 2.4.8 and Avogadro 1.2.0 programs.[231,232]

3.3. Biological Procedures

3.3.1. In Vitro Antibacterial Testing

All working solutions were autoclaved (121 °C, 15 psi, 15 minutes) and cooled to room temperature under sterile conditions prior to use. Molecular biology grade DMSO was purchased from Sigma-Aldrich. *E.coli* JM109 and *S.aureus* SH1000 strains were cultured on Mueller-Hinton agar plates statically for 24 hours at 37 °C and stored at <5 °C prior to use. Mueller-Hinton broth solutions were prepared at concentrations of 21.0 g/L (regular) and 42.0 g/L (double-strength) in deionised water. Stock solutions were prepared of the test compounds at concentrations of 0.512 g/L, 1.02 g/L and 2.05 g/L in DMSO. All compounds were assayed in triplicate.

10 mL aliquots of regular Mueller-Hinton broth were inoculated with either *E.coli* or *S.aureus* and incubated for 24 hours (37 °C, 100 rpm). The incubated solutions were analysed *via* UV/Vis spectrophotometry and aliquots diluted to OD$_{600}$: 0.008 in 20 mL of regular Mueller-Hinton broth. To column 1 of a clear flat-bottomed 48 well plate was

added 150 μL of double-strength Mueller-Hinton broth and 150 μL of the test compound in DMSO. To columns 2–8 was added 150 μL of regular Mueller-Hinton broth and 150 μL of the column 1 mixture was serially diluted across columns 2–7. 150 μL of the prepared bacterial solutions were added to each well of columns 2–8, and the positive control wells (column 8) were seeded with 75.0 μL of DMSO to account for activity of the solvent. Plates were incubated (37 ºC, 100 rpm) for 24 hours and the minimum inhibitory concentration (MIC) values determined by comparison of bacterial growth within treated wells to both positive and negative controls.

Appendix I

DFT Calculated Structures

Cartesian Co-ordinates (Å) of Calculated Structures

CsF

```
F    -0.462857  -0.452191   0.000051
Cs    1.019674   1.099894  -1.091990
```

DMF

```
N     0.149369   0.041223   0.007077
C     1.476909   0.348487   0.022843
O     1.999468   1.254132   0.654374
H     2.060392  -0.340155  -0.626916
C    -0.800317   0.816960   0.789255
H    -0.247263   1.596620   1.314844
H    -1.313563   0.180019   1.521028
H    -1.552487   1.281256   0.138667
C    -0.336149  -1.075298  -0.798946
H    -1.418045  -1.152053  -0.674055
H     0.109679  -2.026208  -0.482983
H    -0.127992  -0.924983  -1.865186
```

Intermediate A (Ru(bpy)$_3^{2+}$)

```
Ru    3.700282   2.544216   0.053208
N     2.229292   3.506053  -1.063141
N     3.579489   4.384257   1.019489
N     5.337853   3.281779  -0.999388
N     5.287490   1.782689   1.164089
N     3.587901   0.705804  -0.917255
N     2.176643   1.603545   1.115881
C     1.573962   2.972074  -2.112446
C     0.585799   3.658530  -2.805442
C     0.253135   4.950982  -2.399789
C     0.922928   5.506190  -1.314834
C     1.910672   4.770322  -0.653486
C     2.674951   5.266040   0.497879
C     2.517438   6.538826   1.054207
C     3.287471   6.918405   2.148262
C     4.209535   6.010275   2.668695
C     4.325661   4.759478   2.077069
C     5.271774   4.061876  -2.096149
C     6.403254   4.538713  -2.744449
C     7.659814   4.201421  -2.241411
C     7.734694   3.399732  -1.107534
C     6.562834   2.946921  -0.494331
C     6.534855   2.097686   0.702933
C     7.676889   1.626667   1.357360
C     7.549055   0.827218   2.488101
C     6.270222   0.510545   2.946369
```

```
C    5.170165    1.004744    2.258182
C    4.366114    0.319902   -1.947530
C    4.253851   -0.929378   -2.543079
C    3.301285   -1.824417   -2.055985
C    2.497955   -1.433756   -0.990137
C    2.653159   -0.163076   -0.428385
C    1.855148    0.343734    0.694890
C    0.833808   -0.377737    1.320066
C    0.133000    0.187505    2.379955
C    0.469074    1.475284    2.797464
C    1.491467    2.147239    2.140859
H    1.865044    1.966724   -2.394093
H    0.089441    3.183384   -3.645094
H   -0.515018    5.516381   -2.917782
H    0.675570    6.507933   -0.983518
H    1.798039    7.232072    0.634359
H    3.170781    7.905031    2.585299
H    4.833347    6.261894    3.519984
H    5.027627    4.022869    2.450614
H    4.276060    4.297543   -2.453696
H    6.294923    5.162838   -3.625292
H    8.565486    4.557156   -2.722321
H    8.702322    3.130019   -0.700980
H    8.662452    1.880774    0.985215
H    8.431300    0.457477    3.000935
H    6.120743   -0.110912    3.823067
H    4.158872    0.785183    2.580482
H    5.090966    1.046735   -2.295614
H    4.904096   -1.189973   -3.371588
H    3.186601   -2.809501   -2.497011
H    1.754447   -2.116800   -0.596392
H    0.584427   -1.376071    0.980100
H   -0.661456   -0.366643    2.869658
H    1.786589    3.148421    2.432975
H   -0.050657    1.957869    3.618527
```

Intermediate B- singlet state (Ru(bpy)$_3$$^{2+*}$)

```
Ru   3.700282    2.544216    0.053208
N    2.229292    3.506053   -1.063141
N    3.579489    4.384257    1.019489
N    5.337853    3.281779   -0.999388
N    5.287490    1.782689    1.164089
N    3.587901    0.705804   -0.917255
N    2.176643    1.603545    1.115881
C    1.573962    2.972074   -2.112446
C    0.585799    3.658530   -2.805442
C    0.253135    4.950982   -2.399789
C    0.922928    5.506190   -1.314834
```

```
C    1.910672   4.770322  -0.653486
C    2.674951   5.266040   0.497879
C    2.517438   6.538826   1.054207
C    3.287471   6.918405   2.148262
C    4.209535   6.010275   2.668695
C    4.325661   4.759478   2.077069
C    5.271774   4.061876  -2.096149
C    6.403254   4.538713  -2.744449
C    7.659814   4.201421  -2.241411
C    7.734694   3.399732  -1.107534
C    6.562834   2.946921  -0.494331
C    6.534855   2.097686   0.702933
C    7.676889   1.626667   1.357360
C    7.549055   0.827218   2.488101
C    6.270222   0.510545   2.946369
C    5.170165   1.004744   2.258182
C    4.366114   0.319902  -1.947530
C    4.253851  -0.929378  -2.543079
C    3.301285  -1.824417  -2.055985
C    2.497955  -1.433756  -0.990137
C    2.653159  -0.163076  -0.428385
C    1.855148   0.343734   0.694890
C    0.833808  -0.377737   1.320066
C    0.133000   0.187505   2.379955
C    0.469074   1.475284   2.797464
C    1.491467   2.147239   2.140859
H    1.865044   1.966724  -2.394093
H    0.089441   3.183384  -3.645094
H   -0.515018   5.516381  -2.917782
H    0.675570   6.507933  -0.983518
H    1.798039   7.232072   0.634359
H    3.170781   7.905031   2.585299
H    4.833347   6.261894   3.519984
H    5.027627   4.022869   2.450614
H    4.276060   4.297543  -2.453696
H    6.294923   5.162838  -3.625292
H    8.565486   4.557156  -2.722321
H    8.702322   3.130019  -0.700980
H    8.662452   1.880774   0.985215
H    8.431300   0.457477   3.000935
H    6.120743  -0.110912   3.823067
H    4.158872   0.785183   2.580482
H    5.090966   1.046735  -2.295614
H    4.904096  -1.189973  -3.371588
H    3.186601  -2.809501  -2.497011
H    1.754447  -2.116800  -0.596392
H    0.584427  -1.376071   0.980100
H   -0.661456  -0.366643   2.869658
```

```
H     1.786589   3.148421   2.432975
H    -0.050657   1.957869   3.618527
```

Intermediate B- triplet state (Ru(bpy)₃²⁺*)

```
Ru    3.688371   2.565444   0.052872
N     2.178836   3.524947  -1.046110
N     3.589475   4.436607   0.997995
N     5.341715   3.349427  -0.929637
N     5.240926   1.766699   1.177650
N     3.625791   0.737064  -0.930733
N     2.120453   1.629175   1.043063
C     1.454437   2.944210  -2.023225
C     0.394095   3.586590  -2.640279
C     0.044191   4.874595  -2.209824
C     0.774586   5.470057  -1.193129
C     1.856445   4.788987  -0.614510
C     2.688670   5.319527   0.452942
C     2.630281   6.639398   0.925594
C     3.468204   7.045817   1.952457
C     4.375668   6.127186   2.499662
C     4.413742   4.842308   1.984460
C     5.294431   4.246219  -1.936556
C     6.435045   4.708889  -2.568359
C     7.685098   4.235795  -2.136227
C     7.742275   3.334462  -1.085991
C     6.559095   2.894871  -0.470158
C     6.501443   2.005499   0.671503
C     7.619410   1.408572   1.279359
C     7.456958   0.601309   2.391846
C     6.165207   0.381705   2.898871
C     5.090355   0.969885   2.256167
C     4.435101   0.372083  -1.946828
C     4.412823  -0.899410  -2.491936
C     3.534181  -1.851304  -1.948061
C     2.708147  -1.488333  -0.898453
C     2.746927  -0.178260  -0.390793
C     1.903109   0.318507   0.676413
C     0.888230  -0.420049   1.306406
C     0.097807   0.173269   2.276899
C     0.317790   1.519051   2.613821
C     1.331022   2.208245   1.971388
H     1.755938   1.942944  -2.309976
H    -0.147551   3.089143  -3.437347
H    -0.793443   5.398227  -2.659646
H     0.502250   6.456778  -0.836694
H     1.938575   7.344387   0.479253
H     3.425992   8.065959   2.320830
H     5.043068   6.403564   3.308576
```

```
H     5.106342   4.099305   2.363942
H     4.305476   4.571762  -2.239727
H     6.349348   5.418687  -3.383743
H     8.598333   4.577711  -2.612786
H     8.701994   2.976116  -0.732182
H     8.610237   1.580853   0.875406
H     8.319604   0.142172   2.864237
H     5.997029  -0.239112   3.771863
H     4.073002   0.818554   2.599426
H     5.106087   1.137219  -2.321146
H     5.071211  -1.142885  -3.318415
H     3.503155  -2.861641  -2.343508
H     2.030022  -2.215099  -0.466575
H     0.716106  -1.452620   1.025424
H    -0.687755  -0.395436   2.764204
H     1.548510   3.244991   2.203138
H    -0.282947   2.020070   3.364904
```

Intermediate C (Ru(bpy)₃⁺)

```
Ru    3.698864   2.543325   0.053906
N     2.264225   3.487298  -1.070392
N     3.576010   4.343968   1.032445
N     5.302477   3.260490  -1.007936
N     5.253574   1.803889   1.171936
N     3.585167   0.744381  -0.929136
N     2.211128   1.620307   1.125624
C     1.627717   2.954699  -2.139969
C     0.666626   3.650492  -2.869623
C     0.340874   4.967915  -2.482020
C     0.981420   5.520528  -1.376495
C     1.941587   4.768371  -0.662941
C     2.662791   5.240241   0.508629
C     2.479419   6.503790   1.114142
C     3.231757   6.860480   2.229770
C     4.175262   5.941499   2.736909
C     4.310661   4.704520   2.110954
C     5.228257   4.021983  -2.124806
C     6.355947   4.471430  -2.807902
C     7.632216   4.118504  -2.319575
C     7.719394   3.345155  -1.165353
C     6.544575   2.923665  -0.502845
C     6.517403   2.123767   0.711650
C     7.661983   1.686498   1.415557
C     7.523115   0.914399   2.565568
C     6.225555   0.578721   3.007780
C     5.129193   1.043416   2.285062
C     4.353198   0.372852  -1.980321
C     4.221877  -0.861794  -2.611744
```
5

```
C    3.246485   -1.766287   -2.140131
C    2.459409   -1.398355   -1.052474
C    2.639854   -0.137907   -0.439682
C    1.883564    0.344723    0.705101
C    0.885774   -0.392412    1.381754
C    0.213610    0.169708    2.463470
C    0.545875    1.481434    2.864562
C    1.544260    2.162249    2.171773
H    1.918135    1.934745   -2.408854
H    0.183270    3.169915   -3.725634
H   -0.403689    5.547298   -3.037964
H    0.743894    6.538723   -1.056481
H    1.743928    7.200334    0.702511
H    3.092876    7.838618    2.702097
H    4.796476    6.180050    3.605544
H    5.023177    3.958121    2.474524
H    4.219137    4.263763   -2.471533
H    6.236650    5.085349   -3.705791
H    8.540074    4.447098   -2.836251
H    8.697474    3.060846   -0.767733
H    8.657367    1.957549    1.053248
H    8.407367    0.573565    3.114260
H    6.065954   -0.033566    3.900515
H    4.105082    0.815389    2.595258
H    5.089862    1.108386   -2.316932
H    4.870724   -1.109693   -3.457253
H    3.110002   -2.742079   -2.617980
H    1.698802   -2.083662   -0.668558
H    0.643909   -1.406448    1.051959
H   -0.560297   -0.397981    2.990656
H    1.840727    3.177283    2.452466
H    0.038915    1.969143    3.702699
```

Intermediate D (101i)
```
C   -2.714179   -1.842183    0.167222
C   -1.572978   -1.344306   -0.483712
C   -1.021413   -2.087921   -1.543363
C   -1.599853   -3.289332   -1.934021
C   -2.737043   -3.775778   -1.279108
C   -3.292002   -3.047457   -0.226875
H   -3.148638   -1.273083    0.986638
H   -0.139462   -1.706703   -2.048606
H   -1.165036   -3.854497   -2.754717
H   -3.185359   -4.715959   -1.589438
H   -4.175934   -3.417268    0.286421
C   -1.006271   -0.075955   -0.031869
H   -1.513260    0.406519    0.805536
N    0.028184    0.432250   -0.606763
```

6

```
N     0.592562   1.578539  -0.153896
H     1.257263   1.987636  -0.799878
S    -0.059421   2.766596   0.882102
O    -1.467466   2.958765   0.619315
O     0.890534   3.849326   0.750141
C     0.105059   2.014433   2.475243
C     1.381639   1.689475   2.954357
C     1.517969   1.109164   4.202410
C     0.380898   0.851025   4.991292
C    -0.893485   1.184299   4.510778
C    -1.024697   1.764509   3.249650
H     2.256387   1.894135   2.345579
H     2.495207   0.845153   4.594601
H    -1.782044   0.999032   5.102511
H    -2.005021   2.027948   2.866656
O     0.623248   0.278472   6.197933
C    -0.489084  -0.004982   7.049678
H    -0.064030  -0.451641   7.949698
H    -1.029059   0.913329   7.313469
H    -1.178811  -0.715310   6.576099
```

Intermediate E
```
C    -2.885624  -1.579844   0.150730
C    -1.624277  -1.174355  -0.342149
C    -0.898760  -2.115793  -1.111024
C    -1.413159  -3.379672  -1.369580
C    -2.666568  -3.764724  -0.872893
C    -3.396262  -2.848956  -0.109571
H    -3.463625  -0.874639   0.746353
H     0.073291  -1.818263  -1.493444
H    -0.831288  -4.081934  -1.965696
H    -3.062951  -4.757085  -1.077011
H    -4.372306  -3.127089   0.286179
C    -1.128388   0.154430  -0.043734
H    -1.780764   0.800077   0.547293
N     0.032752   0.550213  -0.502037
N     0.636759   1.707434  -0.280025
S    -0.022501   2.849199   0.754328
O    -1.441917   3.169588   0.564099
O     0.925616   3.956462   0.759890
C     0.111912   2.075778   2.379284
C     1.386133   1.821292   2.902413
C     1.525582   1.163874   4.116195
C     0.387466   0.747215   4.824850
C    -0.886380   1.001054   4.309784
C    -1.013179   1.662687   3.082860
H     2.258783   2.141770   2.341978
H     2.506721   0.955464   4.535054
```

H	-1.780386	0.686562	4.837554
H	-1.996130	1.868196	2.670601
O	0.631025	0.096707	6.014795
C	-0.490677	-0.382046	6.739610
H	-0.087276	-0.878495	7.626173
H	-1.152426	0.439405	7.052035
H	-1.074053	-1.103918	6.150065

HF

H	0.000000	0.000000	0.037044
F	0.000000	0.000000	0.962956

Intermediate F

C	-2.632350	-1.029834	-0.798605
C	-1.268368	-0.698781	-0.719257
C	-0.481111	-1.285623	0.290156
C	-1.048242	-2.179566	1.188514
C	-2.407655	-2.502591	1.101542
C	-3.197262	-1.924666	0.106726
H	-3.245927	-0.576158	-1.573463
H	0.572640	-1.029221	0.352345
H	-0.432879	-2.629707	1.963111
H	-2.846729	-3.202182	1.807773
H	-4.253034	-2.171752	0.035863
C	-0.721710	0.255950	-1.667332
H	-1.388963	0.698476	-2.411023
N	0.525571	0.593475	-1.666632
N	1.170268	1.455964	-2.368268
S	0.746427	3.123074	-2.040136
O	-0.697662	3.206706	-1.910555
O	1.462401	3.877989	-3.037743
C	1.475832	3.384992	-0.455866
C	0.744028	3.089733	0.702931
C	1.342075	3.234005	1.943300
C	2.675165	3.672811	2.040039
C	3.402118	3.968238	0.876228
C	2.799348	3.817286	-0.369944
H	-0.286886	2.763046	0.621095
H	0.796164	3.019409	2.856936
H	4.427941	4.313273	0.929161
H	3.349893	4.040555	-1.277801
O	3.166885	3.780903	3.301463
C	4.514895	4.225649	3.468388
H	4.690208	4.234940	4.545217
H	5.221160	3.538063	2.985758
H	4.650924	5.236876	3.064173

TS_{F-G}

C	-3.082234	-1.191389	-0.805203

8

C	-1.686380	-1.000138	-0.881718
C	-0.840431	-1.976897	-0.312172
C	-1.376666	-3.098178	0.306185
C	-2.762978	-3.276181	0.377137
C	-3.610315	-2.316417	-0.182189
H	-3.744881	-0.445292	-1.237186
H	0.237220	-1.847009	-0.368303
H	-0.711877	-3.842946	0.736305
H	-3.176853	-4.155917	0.861970
H	-4.688168	-2.447329	-0.133014
C	-1.179410	0.189398	-1.517773
H	-1.850210	0.925919	-1.956563
N	0.101043	0.444332	-1.612933
N	1.068556	1.096104	-1.790264
S	0.590855	3.283621	-1.451466
O	-0.824590	3.276807	-1.064253
O	1.074110	4.081784	-2.576882
C	1.571150	3.658550	-0.016104
C	1.079365	3.337874	1.255942
C	1.873436	3.560395	2.368407
C	3.167856	4.091070	2.220044
C	3.656922	4.398912	0.941058
C	2.856475	4.173495	-0.176857
H	0.076782	2.936464	1.361568
H	1.513537	3.335658	3.367851
H	4.649044	4.813144	0.805351
H	3.220802	4.410456	-1.171078
O	3.864233	4.268948	3.372782
C	5.187029	4.803309	3.290606
H	5.843112	4.147866	2.703627
H	5.181333	5.808577	2.850109
H	5.547295	4.856339	4.319109

Intermediate G

C	-1.297035	0.351460	-0.240023
C	0.115073	0.561017	-0.305394
C	1.001021	-0.405458	0.258957
C	0.485298	-1.531542	0.861738
C	-0.909697	-1.727197	0.920126
C	-1.793619	-0.782265	0.367628
H	-1.967869	1.089156	-0.670671
H	2.075969	-0.256566	0.215034
H	1.152598	-2.270841	1.293152
H	-1.305865	-2.618700	1.397704
H	-2.865231	-0.946206	0.419976
C	0.568050	1.739494	-0.938909
H	-0.085658	2.489768	-1.375482
N	1.867092	2.028265	-1.051961

N	2.959873	2.279617	-1.151876

PMP-SO₂⁻

S	0.871103	3.023215	-2.824644
O	0.430724	4.423130	-3.180541
O	2.259202	2.668366	-3.303126
C	1.160077	3.190773	-0.964273
C	0.323241	3.994016	-0.184715
C	0.480495	4.062471	1.197775
C	1.486918	3.312969	1.821876
C	2.335539	2.508079	1.054255
C	2.158012	2.454546	-0.335223
H	-0.434172	4.593185	-0.688038
H	-0.154588	4.697147	1.813864
H	3.133473	1.933253	1.516618
H	2.824862	1.858336	-0.956664
O	1.566093	3.441320	3.202111
C	2.583856	2.714324	3.861427
H	2.483555	2.946227	4.926281
H	2.472476	1.628635	3.714483
H	3.587108	3.011248	3.518382

Intermediate H+D

C	-4.661793	-0.442097	-0.440837
C	-3.532467	-0.617701	-1.279999
C	-3.606817	-0.204924	-2.632084
C	-4.780199	0.341449	-3.122627
C	-5.895550	0.500405	-2.288718
C	-5.829919	0.102359	-0.948584
H	-4.610507	-0.759753	0.597345
H	-2.737730	-0.294957	-3.275828
H	-4.831386	0.660136	-4.159116
H	-6.806790	0.941195	-2.679754
H	-6.693823	0.225759	-0.302783
C	-2.354817	-1.190903	-0.709868
H	-2.263066	-1.455120	0.337921
N	-1.320771	-1.560526	-1.447768
N	-0.438635	-1.879538	-2.075848
H	-1.579703	1.779799	0.689256
C	-5.955720	3.574415	-0.348290
C	-4.774981	3.298156	-1.069648
C	-4.727009	3.600021	-2.450732
C	-5.826613	4.166041	-3.078107
C	-6.992834	4.434529	-2.350826
C	-7.054583	4.135657	-0.985090
H	-5.998530	3.344809	0.713692
H	-3.818359	3.385664	-3.002800
H	-5.782688	4.403536	-4.137173

H	-7.850676	4.879733	-2.846788
H	-7.958811	4.348190	-0.422437
C	-3.656242	2.705547	-0.381125
H	-3.764217	2.510982	0.694047
N	-2.557483	2.401635	-1.009754
N	-1.581818	1.814708	-0.334690
S	-0.032580	1.616119	-1.084088
O	-0.331668	1.222299	-2.434517
O	0.632112	0.750068	-0.142330
C	0.676232	3.211140	-1.063346
C	0.348158	4.124862	-2.080104
C	0.892904	5.393135	-2.050306
C	1.772606	5.766968	-1.011068
C	2.095500	4.844370	0.002306
C	1.542178	3.570910	-0.024261
H	-0.313099	3.825227	-2.885564
H	0.668786	6.118314	-2.826038
H	2.779218	5.108011	0.800068
H	1.796465	2.847770	0.743458
O	2.251071	7.020631	-1.082256
C	3.171346	7.477819	-0.076440
H	3.415403	8.503246	-0.353106
H	2.703526	7.460798	0.914615
H	4.080404	6.865798	-0.076012

TS_{H-I}

C	-4.858134	-0.469284	-0.345964
C	-3.624821	-0.416760	-1.008655
C	-3.568390	-0.091515	-2.371779
C	-4.745501	0.178952	-3.062825
C	-5.974950	0.140546	-2.400937
C	-6.029098	-0.185530	-1.044462
H	-4.900016	-0.725827	0.709608
H	-2.611666	-0.012802	-2.881315
H	-4.700695	0.435034	-4.116984
H	-6.889401	0.366679	-2.940978
H	-6.984442	-0.222403	-0.529486
C	-2.365989	-0.570475	-0.214113
H	-2.482415	-0.854795	0.834090
N	-1.427136	-1.401080	-0.787600
N	-0.609692	-1.947995	-1.315510
H	-1.811197	0.662469	-0.212808
C	-5.927710	3.329429	-0.375788
C	-4.718110	3.292765	-1.110725
C	-4.698516	3.794822	-2.436960
C	-5.852053	4.316969	-2.995136
C	-7.042771	4.349348	-2.253724
C	-7.077210	3.855037	-0.943824

11

H	-5.944741	2.938660	0.638226
H	-3.771628	3.755097	-2.998984
H	-5.837445	4.702995	-4.010114
H	-7.943971	4.762263	-2.698307
H	-8.001982	3.885369	-0.375597
C	-3.564255	2.706347	-0.508880
H	-3.657511	2.284864	0.496916
N	-2.409507	2.638978	-1.152467
N	-1.471691	1.923155	-0.586823
S	-0.005148	1.791041	-1.543733
O	-0.383788	1.576908	-2.921160
O	0.725433	0.787137	-0.802578
C	0.719893	3.364230	-1.338576
C	0.424718	4.390168	-2.253232
C	0.993521	5.635149	-2.076776
C	1.862147	5.873358	-0.988043
C	2.149429	4.839254	-0.074843
C	1.573534	3.589853	-0.250413
H	-0.228667	4.191272	-3.095228
H	0.798363	6.446192	-2.770941
H	2.820979	5.001999	0.759302
H	1.795745	2.781378	0.437800
O	2.365857	7.115385	-0.914011
C	3.278934	7.442598	0.148943
H	3.547013	8.486301	-0.012822
H	2.793716	7.328790	1.124867
H	4.174990	6.814372	0.095348

Intermediate I+F

C	-4.822217	-0.693376	-0.367899
C	-3.586998	-0.432191	-0.968812
C	-3.514962	0.048074	-2.281285
C	-4.692566	0.274405	-2.988018
C	-5.930392	0.037337	-2.386832
C	-5.995324	-0.444616	-1.079084
H	-4.871198	-1.069734	0.650801
H	-2.557431	0.282572	-2.738400
H	-4.641512	0.654047	-4.003586
H	-6.845772	0.232826	-2.937268
H	-6.957130	-0.630653	-0.610819
C	-2.335998	-0.553518	-0.134027
H	-2.500322	-0.985398	0.857705
N	-1.362673	-1.406222	-0.769453
N	-0.596386	-1.950139	-1.353264
H	-1.807862	0.438219	-0.035822
C	-6.092919	3.415322	-0.404309
C	-4.886563	3.391750	-1.146118
C	-4.913811	3.755749	-2.517386

C	-6.107449	4.124898	-3.112486
C	-7.295138	4.138560	-2.365894
C	-7.283496	3.783497	-1.011194
H	-6.075019	3.137468	0.646497
H	-3.988094	3.734035	-3.082350
H	-6.126039	4.407119	-4.161209
H	-8.227980	4.431115	-2.839735
H	-8.205137	3.801155	-0.437134
C	-3.690016	2.951939	-0.507508
H	-3.723751	2.655356	0.546281
N	-2.550464	2.834602	-1.186782
N	-1.579755	2.258322	-0.549441
S	-0.171565	2.013025	-1.553125
O	-0.569967	1.846431	-2.935194
O	0.486086	0.923560	-0.850243
C	0.720738	3.498156	-1.341635
C	0.517393	4.559275	-2.241360
C	1.197490	5.745433	-2.052712
C	2.084407	5.892242	-0.963615
C	2.277302	4.826407	-0.063434
C	1.590705	3.635299	-0.252475
H	-0.154279	4.432141	-3.083236
H	1.074144	6.578732	-2.736991
H	2.959406	4.918780	0.772989
H	1.737667	2.803370	0.427829
O	2.697646	7.084993	-0.875520
C	3.630044	7.316281	0.194119
H	3.990288	8.334373	0.047910
H	3.132780	7.233120	1.167240
H	4.468111	6.612554	0.136283

N₂

N	0.000000	0.000000	0.075587
N	0.000000	0.000000	1.174413

Intermediate J

C	-0.960566	1.246426	0.972198
C	-0.814002	0.178019	0.014570
C	-0.172447	-1.049848	0.415879
C	0.291516	-1.190175	1.702611
C	0.133068	-0.127153	2.615352
C	-0.489354	1.085334	2.253846
H	-1.445774	2.168324	0.663690
H	-0.064558	-1.850251	-0.310868
H	0.776136	-2.107615	2.020635
H	0.502906	-0.246283	3.631136
H	-0.591538	1.879483	2.986374

```
C   -1.279966   0.327798  -1.265997
H   -1.766486   1.246114  -1.588296
H   -1.178547  -0.467603  -2.001537
```

102i

```
C   -2.091587  -1.028829  -2.637673
C   -2.237540   0.318738  -2.286425
C   -3.077662   1.136377  -3.052219
C   -3.772275   0.611775  -4.140398
C   -3.629550  -0.735037  -4.478565
C   -2.786236  -1.553823  -3.725822
H   -1.422004  -1.661426  -2.061041
H   -3.175036   2.188560  -2.798486
H   -4.422520   1.255382  -4.727082
H   -4.171581  -1.144319  -5.327124
H   -2.666478  -2.601636  -3.988548
C   -1.463772   0.889952  -1.139595
H   -1.225898   0.143451  -0.376897
S    0.156640   1.533006  -1.711127
O   -0.101612   2.655919  -2.594462
O    0.947693   0.400896  -2.159340
C    0.867075   2.155149  -0.202242
C    0.603012   3.470094   0.200434
C    1.136683   3.945940   1.387439
C    1.940481   3.112289   2.185112
C    2.206863   1.796925   1.775572
C    1.665413   1.324106   0.581152
H   -0.001155   4.113680  -0.431174
H    0.954217   4.964322   1.716911
H    2.834097   1.141700   2.368524
H    1.878289   0.314160   0.244934
O    2.415755   3.673252   3.328228
C    3.248088   2.880385   4.176587
H    3.507433   3.523506   5.018990
H    2.712730   1.994169   4.541165
H    4.162766   2.569246   3.655785
H   -1.966020   1.742209  -0.673635
```

Intermediate D (101w)

```
C   -1.201489  -2.473639   0.345963
C    0.120601  -1.811117   0.056855
C    1.304075  -2.669502   0.404243
C    1.162173  -3.147481   1.861160
O   -0.081084  -3.815820   2.074038
C   -1.185875  -2.963762   1.811946
N    0.350150  -0.602479  -0.314835
N   -0.711562   0.238198  -0.598645
H   -1.647072  -0.116529  -0.380787
```

```
S    -0.561641   1.769492   0.149049
O    -1.872796   2.352590  -0.020571
O     0.632795   2.392930  -0.350610
C    -0.319976   1.344270   1.854755
C     0.973460   1.098539   2.331680
C     1.152383   0.649719   3.630599
C     0.042491   0.434689   4.465659
C    -1.251968   0.685937   3.985025
C    -1.426031   1.137462   2.677432
H     1.822760   1.258318   1.676876
H     2.145629   0.455279   4.023890
H    -2.121469   0.540923   4.615416
H    -2.422914   1.339917   2.298069
O     0.324851  -0.018073   5.715703
C    -0.763181  -0.265467   6.607951
H    -0.309603  -0.623181   7.533499
H    -1.329688   0.653343   6.806721
H    -1.436774  -1.034094   6.207198
H     1.243475  -2.282503   2.540534
H     1.943511  -3.869814   2.114881
H     1.339401  -3.551561  -0.249583
H     2.227936  -2.098375   0.274678
H    -1.160568  -2.087336   2.481993
H    -2.084986  -3.548304   2.029818
H    -1.331926  -3.340021  -0.314789
H    -2.069549  -1.822115   0.199971
```

101w Intermediate F

```
C    -1.429993  -2.043580   0.575396
C    -0.064674  -1.751933   0.019005
C     0.940760  -2.850313   0.171914
C     0.929227  -3.328581   1.639551
O    -0.381737  -3.693447   2.057695
C    -1.277778  -2.586555   2.009637
N     0.290015  -0.610920  -0.451403
N    -0.464179   0.411222  -0.733131
S    -0.043257   1.832148   0.151266
O    -1.190047   2.691718  -0.012047
O     1.279820   2.254751  -0.248984
C     0.020262   1.258856   1.829066
C     1.217183   0.748694   2.348640
C     1.250031   0.256301   3.643573
C     0.086979   0.263794   4.433339
C    -1.110343   0.775693   3.908923
C    -1.137840   1.268108   2.605433
H     2.111602   0.754847   1.734959
H     2.167034  -0.137983   4.070892
H    -2.016338   0.799572   4.502979
```
15

H	-2.055595	1.672752	2.190822
O	0.222267	-0.248680	5.683705
C	-0.925847	-0.272405	6.534931
H	-0.588796	-0.720617	7.470662
H	-1.298492	0.742100	6.725108
H	-1.727059	-0.884438	6.101083
H	1.323926	-2.529619	2.288188
H	1.550402	-4.220850	1.758987
H	0.661343	-3.698321	-0.468059
H	1.937356	-2.504597	-0.118075
H	-0.921983	-1.780716	2.669273
H	-2.237769	-2.951726	2.386291
H	-1.908587	-2.816578	-0.041214
H	-2.051537	-1.144299	0.560493

101w TS$_{F-G}$

C	-1.543469	-2.869848	-0.166666
C	-0.363531	-1.973260	0.120660
C	0.655040	-2.509095	1.089117
C	-0.072559	-3.076489	2.321003
O	-1.077732	-4.017682	1.951184
C	-2.098148	-3.414014	1.160782
N	-0.277536	-0.791896	-0.377923
N	-0.448030	0.182834	-1.048564
S	0.059254	1.985025	0.006519
O	-1.138762	2.808101	-0.054049
O	1.344221	2.467456	-0.487061
C	0.273555	1.357092	1.657502
C	1.551910	1.008325	2.110376
C	1.698567	0.411331	3.352704
C	0.569155	0.138180	4.144037
C	-0.710218	0.486199	3.682572
C	-0.852853	1.087981	2.434563
H	2.416277	1.220484	1.489517
H	2.679250	0.141890	3.733242
H	-1.592593	0.291046	4.280600
H	-1.836756	1.360991	2.066106
O	0.816466	-0.475563	5.330354
C	-0.293663	-0.796339	6.172368
H	0.134277	-1.280442	7.051321
H	-0.834051	0.108971	6.476539
H	-0.983395	-1.487185	5.670625
H	-0.526121	-2.248513	2.888832
H	0.624905	-3.612315	2.972441
H	1.224491	-3.324017	0.618374
H	1.355267	-1.726291	1.391144
H	-2.571825	-2.591967	1.725320
H	-2.845675	-4.192549	0.980029

```
H    -1.217042  -3.720153  -0.784378
H    -2.321140  -2.328502  -0.714324
```

101w Intermediate G

```
C    -1.316850  -3.211771  -0.383705
C     0.017574  -2.627061  -0.127799
C     1.214186  -3.260698  -0.724210
C     1.131706  -4.805886  -0.365529
O    -0.118941  -5.308853  -0.761215
C    -1.200729  -4.761125  -0.052095
N     0.168786  -1.761538   0.869538
N     0.293159  -0.976767   1.675338
H     1.299978  -4.934758   0.712129
H     1.897330  -5.336170  -0.935182
H     1.163018  -3.185250  -1.815713
H     2.154222  -2.834878  -0.367761
H    -1.083415  -4.888711   1.032430
H    -2.109028  -5.259057  -0.396932
H    -1.553163  -3.132836  -1.450306
H    -2.112538  -2.753041   0.206725
```

101w Intermediate H+D

```
C     2.251506   0.322080  -5.893497
C     1.180011   1.326157  -5.625227
C    -0.212695   1.003380  -6.030872
C    -0.531456  -0.451987  -5.574520
O     0.479763  -1.349996  -5.995808
C     1.735638  -1.066111  -5.410381
N     1.400252   2.291301  -4.753694
N     1.593843   3.155152  -4.044755
H     3.197073   0.582322  -5.411472
H     2.404248   0.259978  -6.976650
H     1.670399  -1.078101  -4.311699
H     2.425506  -1.847863  -5.737734
H    -0.256462   1.048942  -7.129284
H    -0.933551   1.715754  -5.627270
H    -1.462942  -0.782283  -6.039854
H    -0.643373  -0.479795  -4.479864
C     2.574081   2.206472 -10.673290
C     1.299875   1.786412 -10.002280
C     0.381945   0.995434 -10.878711
C     0.153543   1.785910 -12.192008
O     1.389185   2.099081 -12.818562
C     2.203735   2.919477 -12.005246
N     0.857216   2.143526  -8.839178
N     1.665424   2.863172  -7.993634
H     2.639089   3.001139  -8.281814
S     1.015579   4.379431  -7.450160
```

```
O    2.129340   4.936756  -6.723619
O   -0.236759   4.061737  -6.815889
C    0.732546   5.256546  -8.939825
C   -0.476870   5.077439  -9.630656
C   -0.666975   5.714106 -10.842664
C    0.344827   6.537294 -11.382264
C    1.554563   6.710602 -10.682254
C    1.745407   6.065463  -9.466238
H   -1.255376   4.454505  -9.204584
H   -1.596432   5.606717 -11.392822
H    2.336828   7.351514 -11.070604
H    2.668390   6.205776  -8.912648
O    0.057291   7.108285 -12.563953
C    1.020025   7.988088 -13.170887
H    0.556982   8.327395 -14.097072
H    1.224754   8.845612 -12.520239
H    1.949538   7.451761 -13.394397
H   -0.406746   2.708173 -11.970344
H   -0.415315   1.184008 -12.904354
H    0.842903   0.034169 -11.137783
H   -0.568104   0.810432 -10.370235
H    1.695542   3.868590 -11.773681
H    3.110780   3.131228 -12.576804
H    3.171518   1.320072 -10.916742
H    3.195133   2.882168 -10.076908
```

101w TS_{H-I}
```
C    2.404978   0.240221  -5.955599
C    1.337546   1.332401  -5.846038
C   -0.096962   0.801038  -5.900175
C   -0.247332  -0.428046  -4.991702
O    0.737880  -1.411316  -5.282347
C    2.053531  -0.941505  -5.034895
N    1.548179   2.192952  -4.806908
N    1.711664   2.998269  -4.044058
H    3.401853   0.633719  -5.733622
H    2.397804  -0.098835  -6.997605
H    2.161606  -0.638000  -3.979337
H    2.727083  -1.781587  -5.224837
H   -0.276538   0.515296  -6.942988
H   -0.814934   1.584757  -5.644523
H   -1.218277  -0.902853  -5.155277
H   -0.181232  -0.124345  -3.932901
C    2.354067   2.480767 -10.887764
C    1.173922   1.817350 -10.240847
C    0.357920   0.937051 -11.130309
C    0.042935   1.709241 -12.436253
O    1.232374   2.186559 -13.043723
```

```
C    1.908068   3.124044  -12.221897
N    0.801078   2.015869   -9.026943
N    1.418445   2.747751   -8.113931
H    1.505233   2.132149   -7.001492
S    0.559937   4.244018   -7.638507
O    1.487616   4.794021   -6.681328
O   -0.780018   3.863170   -7.260075
C    0.540836   5.161529   -9.120455
C   -0.595659   5.122554   -9.946563
C   -0.611617   5.867315  -11.110102
C    0.504198   6.654615  -11.468159
C    1.640732   6.682598  -10.634685
C    1.654848   5.937494   -9.463892
H   -1.456483   4.531003   -9.654660
H   -1.479649   5.870947  -11.761529
H    2.500811   7.291358  -10.885613
H    2.515509   5.970766   -8.803763
O    0.386201   7.335445  -12.617765
C    1.465420   8.186642  -13.046170
H    1.128884   8.627669  -13.983889
H    1.651801   8.974916  -12.308566
H    2.376451   7.601454  -13.215477
H   -0.640381   2.545082  -12.216003
H   -0.435266   1.043364  -13.158139
H    0.950351   0.052662  -11.397932
H   -0.558598   0.613320  -10.630050
H    1.262056   3.988661  -12.013407
H    2.782775   3.462659  -12.782700
H    3.092908   1.701441  -11.116435
H    2.806671   3.219768  -10.223092
```

Table A1. *Energy components of the calculated structures.*

DFT Model	G RI-PWPB95 def2-TZVP (E_h)
CsF	-120.0498637
DMF	-248.3652423
$Ru(bpy)_3^{2+}$ (A)	-1579.950108
$Ru(bpy)_3^{2+}$ (B^S)	-1579.878436
$Ru(bpy)_3^{2+}$ (B^T)	-1579.870109
$Ru(bpy)_3^{+}$ (C)	-1580.055915
101i (D)	-1274.719065
101i (Intermediate E)	-1274.255132
HF	-100.4578322
101i (Intermediate F)	-1274.085081
101i (TS_{F-G})	-1274.063513
101i (Intermediate G)	-379.390747
$PMP–SO_2^-$	-894.6766384
101i (Intermediate H+D)	-1654.099504
101i (TS_{H-I})	-1654.071316
101i (Intermediate I+F)	-1654.086649
N_2	-109.5231969
101i (Intermediate J)	-270.5324601
102i	-1165.290307
101w (Intermediate D)	-1274.92762
101w (Intermediate F)	-1274.29784
101w (TS_{F-G})	-1274.26295
101w (Intermediate G)	-379.590193
101w (Intermediate H+D)	-1654.50316
101w (TS_{H-I})	-1654.47899

Appendix II

References

Appendix 2: References

1   L. Morrison and T. R. Zembower, *Gastrointest. Endosc. Clin. N. Am.*, 2020, **30**, 619–635.
2   World Economic Forum, Global Risks Report 2013, http://reports.weforum.org/global-risks-2013/, (accessed 4 February 2022).
3   L. L. Silver, *Antibiotics: Targets, Mechanisms and Resistance*, Wiley-VCH, Singapore, 1st edn., 2014.
4   F. Sams-Dodd, *Drug Discov. Today*, 2005, **10**, 139–147.
5   B. Booth and R. Zemmel, *Nat. Rev. Drug Discov.*, 2004, **3**, 451–456.
6   J. W. Scannell, A. Blanckley, H. Boldon and B. Warrington, *Nat. Rev. Drug Discov.*, 2012, **11**, 191–200.
7   R. W. Barker and J. W. Scannell, *Ther. Innov. Regul. Sci.*, 2014, **49**, 415–424.
8   T. Kodadek, *Chem. Commun.*, 2011, **47**, 9757.
9   R. De La Fuente, N. D. Sonawane, D. Arumainayagam and A. S. Verkman, *Br. J. Pharmacol.*, 2006, **149**, 551–559.
10   D. J. Payne, M. N. Gwynn, D. J. Holmes and D. L. Pompliano, *Nat. Rev. Drug Discov.*, 2007, **6**, 29–40.
11   D. N. Gilbert, R. J. Guidos, H. W. Boucher, G. H. Talbot, B. Spellberg, J. E. Edwards, W. Michael Scheld, J. S. Bradley and J. G. Bartlett As, *Clin. Infect. Dis.*, 2010, **50**, 1081–1083.
12   T. A. Keating, J. V. Newman, N. B. Olivier, L. G. Otterson, B. Andrews, P. A. Boriack-Sjodin, J. N. Breen, P. Doig, J. Dumas, E. Gangl, O. M. Green, S. Y. Guler, M. F. Hentemann, D. Joseph-Mccarthy, S. Kawatkar, A. Kutschke, J. T. Loch, A. R. McKenzie, S. Pradeepan, S. Prasad and G. Martínez-Botella, *ACS Chem. Biol.*, 2012, **7**, 1866–1872.
13   S. D. Mills, A. E. Eakin, E. T. Buurman, J. V. Newman, N. Gao, H. Huynh, K. D. Johnson, S. Lahiri, A. B. Shapiro, G. K. Walkup, W. Yang and S. S. Stokes, *Antimicrob. Agents Chemother.*, 2011, **55**, 1088–1096.
14   D. Häbich and F. Von Nussbaum, *ChemMedChem*, 2006, **1**, 951–954.
15   H. Brötz-Oesterhelt, D. Beyer, H. P. Kroll, R. Endermann, C. Ladel, W. Schroeder, B. Hinzen, S. Raddatz, H. Paulsen, K. Henninger, J. E. Bandow, H. G. Sahl and H. Labischinski, *Nat. Med.*, 2005, **11**, 1082–1087.
16   L. L. Ling, T. Schneider, A. J. Peoples, A. L. Spoering, I. Engels, B. P. Conlon, A. Mueller, T. F. Schäberle, D. E. Hughes, S. Epstein, M. Jones, L. Lazarides, V. A. Steadman, D. R. Cohen, C. R. Felix, K. A. Fetterman, W. P. Millett, A. G. Nitti, A. M. Zullo, C. Chen and K. Lewis, *Nature*, 2015, **517**, 455–459.
17   P. H. Mygind, R. L. Fischer, K. M. Schnorr, M. T. Hansen, C. P. Sönksen, S. Ludvigsen, D. Raventós, S. Buskov, B. Christensen, L. De Maria, O. Taboureau, D. Yaver, S. G. Elvig-Jørgensen, M. V Sørensen, B. E. Christensen, S. Kjærulff, N. Frimodt-Moller, R. I. Lehrer, M. Zasloff and H.-H. Kristensen, *Nature*, 2005, **437**, 975–980.
18   D. J. Haydon, N. R. Stokes, R. Ure, G. Galbraith, J. M. Bennett, D. R. Brown, P. J. Baker, V. V Barynin, D. W. Rice, S. E. Sedelnikova, J. R. Heal, J. M. Sheridan, S. T. Aiwale, P. K. Chauhan, A. Srivastava, A. Taneja, I. Collins, J. Errington and L. G. Czaplewski, *Science (80-.).*, 2008, **321**, 1673–1675.

19 K. Andries, P. Verhasselt, J. Guillemont, H. W. H. Göhlmann, J. M. Neefs, H. Winkler, J. Van Gestel, P. Timmerman, M. Zhu, E. Lee, P. Williams, D. De Chaffoy, E. Huitric, S. Hoffner, E. Cambau, C. Truffot-Pernot, N. Lounis and V. Jarlier, *Science (80-.).*, 2005, **307**, 223–227.

20 D. Sehnal, S. Bittrich, M. Deshpande, R. Svobodová, K. Berka, V. Bazgier, S. Velankar, S. K. Burley, J. Koča and A. S. Rose, *Nucleic Acids Res.*, 2021, **49**, W431–W437.

21 R. Tommasi, D. G. Brown, G. K. Walkup, J. I. Manchester and A. A. Miller, *Nat. Rev. Drug Discov.*, 2015, **14**, 529–542.

22 A. Barker, J. G. Kettle, T. Nowak and J. E. Pease, *Drug Discov. Today*, 2013, **18**, 298–304.

23 S. D. Roughley and A. M. Jordan, *J. Med. Chem.*, 2011, **54**, 3451–3479.

24 R. O'Shea and H. E. Moser, *J. Med. Chem.*, 2008, **51**, 2871–2878.

25 R. H. Baltz, *Curr. Opin. Pharmacol.*, 2008, **8**, 557–563.

26 R. M. Christoff, C. K. Gardhi, T. P. Soares Da Costa, M. A. Perugini and B. M. Abbott, *Medchemcomm*, 2019, **10**, 1581–1588.

27 S. Blickling, C. Renner, B. Laber, H. D. Pohlenz, T. A. Holak and R. Huber, *Biochemistry*, 1997, **36**, 24–33.

28 A. M. Velasco, J. I. Leguina and A. Lazcano, *J. Mol. Evol.*, 2002, **55**, 445–459.

29 Y. Yugari and C. Gilvarg, *J. Biol. Chem.*, 1965, **240**, 4710–4716.

30 S. Desbois, U. P. John and M. A. Perugini, *Biochimie*, 2018, **152**, 73–84.

31 S. C. Atkinson, C. Dogovski, M. T. Downton, F. G. Pearce, C. F. Reboul, A. M. Buckle, J. A. Gerrard, R. C. J. Dobson, J. Wagner and M. A. Perugini, *PLoS One*, 2012, **7**, 1–9.

32 J. A. Dobson, R. C. J., Griffin, M. D. W., Jameson, G. B. & Gerrard, *Acta Cryst. D*, 2005, **61**, 1116–1124.

33 T. S. Girish, E. Sharma and B. Gopal, *FEBS Lett.*, 2008, **582**, 2923–2930.

34 T. P. Soares da Costa, C. J. Hall, S. Panjikar, J. A. Wyllie, R. M. Christoff, S. Bayat, M. D. Hulett, B. M. Abbott, A. R. Gendall and M. A. Perugini, *Elife*, 2021, **10**, 1–17.

35 H. Berman, K. Henrick and H. Nakamura, *Nat. Struct. Biol.*, 2003, **10**, 980.

36 V. Mitsakos, R. C. J. Dobson, F. G. Pearce, S. R. Devenish, G. L. Evans, B. R. Burgess, M. A. Perugini, J. A. Gerrard and C. A. Hutton, *Bioorganic Med. Chem. Lett.*, 2008, **18**, 842–844.

37 T. J. Riedel, L. C. Johnson, J. Knight, R. R. Hantgan, R. P. Holmes and W. T. Lowther, *PLoS One*, , DOI:10.1371/journal.pone.0026021.

38 R. E. Impey, S. Panjikar, C. J. Hall, L. J. Bock, J. M. Sutton, M. A. Perugini and T. P. Soares da Costa, *FEBS J.*, 2020, **287**, 386–400.

39 B. Laber, F. X. Gomis-Ruth, M. J. Romao and R. Huber, *Biochem. J.*, 1992, **288**, 691–695.

40 W. E. Karsten, *Biochemistry*, 1997, **36**, 1730–1739.

41 P. Shrivastava, V. Navratna, Y. Silla, R. P. Dewangan, A. Pramanik, S. Chaudhary, G. Rayasam, A. Kumar, B. Gopal and S. Ramachandran, *Sci. Rep.*, 2016, **6**, 1–17.

42 C. V. Coulter, J. A. Gerrard, J. A. E. Kraunsoe and A. J. Pratt, *Pestic. Sci.*, 1999, **55**, 887–895.

43 Y. V. Skovpen, C. J. T. Conly, D. A. R. Sanders and D. R. J. Palmer, *J. Am. Chem. Soc.*, 2016, **138**, 2014–2020.

44 M. M. Heravi and V. Zadsirjan, *RSC Adv.*, 2020, **10**, 44247–44311.

45   E. J. T. C. Lynda Couper, John E. McKendrick, David J. Robins, *Bioorg. Med. Chem. Lett.*, 1994, **4**, 2267–2272.

46   J. J. Turner, J. A. Gerrard and C. A. Hutton, *Bioorganic Med. Chem.*, 2005, **13**, 2133–2140.

47   J. J. Turner, J. P. Healy, R. C. J. Dobson, J. A. Gerrard and C. A. Hutton, *Bioorganic Med. Chem. Lett.*, 2005, **15**, 995–998.

48   B. A. Boughton, L. Hor, J. A. Gerrard and C. A. Hutton, *Bioorganic Med. Chem.*, 2012, **20**, 2419–2426.

49   S. Ekins, J. Mestres and B. Testa, *Br. J. Pharmacol.*, 2007, **152**, 9–20.

50   G. Klebe, *Drug Discov. Today*, 2006, **11**, 580–594.

51   H. Willems, S. De Cesco and F. Svensson, *J. Med. Chem.*, 2020, **63**, 10158–10169.

52   S. Ekins, J. Mestres and B. Testa, *Br. J. Pharmacol.*, 2007, **152**, 21–37.

53   M. Brvar, A. Perdih, M. Oblak, L. P. Mašič and T. Solmajer, *Bioorganic Med. Chem. Lett.*, 2010, **20**, 958–962.

54   A. Perdih, M. Hrast, H. Barreteau, S. Gobec, G. Wolber and T. Solmajer, *Bioorganic Med. Chem.*, 2014, **22**, 4124–4134.

55   F. Y. Chan, N. Sun, M. A. C. Neves, P. C. H. Lam, W. H. Chung, L. K. Wong, H. Y. Chow, D. L. Ma, P. H. Chan, Y. C. Leung, T. H. Chan, R. Abagyan and K. Y. Wong, *J. Chem. Inf. Model.*, 2013, **53**, 2131–2140.

56   J. Sun, W. He, H. Y. Liu, J. Qin and C. L. Ye, *Bioorg. Chem.*, 2019, **88**, 102958.

57   A. Garg, R. Tewari and G. P. S. Raghava, *BMC Bioinformatics*, 2010, **11**, 1–9.

58   G. Kefala, G. L. Evans, M. D. W. Griffin, S. R. A. Devenish, F. G. Pearce, M. A. Perugini, J. A. Gerrard, M. S. Weiss and R. C. J. Dobson, *Biochem. J.*, 2008, **411**, 351–360.

59   A. Rehman, S. Akhtar, M. H. Siddiqui, U. Sayeed, S. S. Ahmad, J. M. Arif and M. K. A. Khan, *Bioinformation*, 2016, **12**, 400–407.

60   S. P. Singh, B. K. Konwar, R. L. Bezbaruah and T. C. Bora, *Med. Chem. Res.*, 2013, **22**, 4755–4765.

61   J. Boruwa, B. Kalita, N. C. Barua, J. C. Borah, S. Mazumder, D. Thakur, D. K. Gogoi and T. C. Bora, *Bioorganic Med. Chem. Lett.*, 2004, **14**, 3571–3574.

62   D. J. C. Constable, P. J. Dunn, J. D. Hayler, G. R. Humphrey, J. L. Leazer, R. J. Linderman, K. Lorenz, J. Manley, B. A. Pearlman, A. Wells, A. Zaks and T. Y. Zhang, *Green Chem.*, 2007, **9**, 411–42.

63   T. Cernak, K. D. Dykstra, S. Tyagarajan, P. Vachal and S. W. Krska, *Chem. Soc. Rev.*, 2016, **45**, 546–576.

64   T. W. J. Cooper, I. B. Campbell and S. J. F. MacDonald, *Angew. Chemie - Int. Ed.*, 2010, **49**, 8082–8091.

65   M. H. Shaw, J. Twilton and D. W. C. MacMillan, *J. Org. Chem.*, 2016, **81**, 6898–6926.

66   N. A. Romero and D. A. Nicewicz, *Chem. Rev.*, 2016, **116**, 10075–10166.

67   L. Marzo, S. K. Pagire, O. Reiser and B. König, *Angew. Chemie - Int. Ed.*, 2018, **57**, 10034–10072.

68   D. A. Nicewicz and D. W. C. Macmillan, *Science (80-.).*, 2008, **322**, 77–80.

69   M. A. Ischay, M. E. Anzovino, J. Du and T. P. Yoon, *J. Am. Chem. Soc.*, 2008, **130**, 12886–12887.

70   J. M. R. Narayanam, J. W. Tucker and C. R. J. Stephenson, *J. Am.*

Chem. Soc., 2009, **131**, 8756–8757.

71   A. Juris, V. Balzani, F. Barigelletti, S. Campagna, P. Belser and A. von Zelewsky, *Coord. Chem. Rev.*, 1988, **84**, 85–277.

72   D. W. Thompson, A. Ito and T. J. Meyer, *Pure Appl. Chem.*, 2013, **85**, 1257–1305.

73   T. P. Yoon, *Acc. Chem. Res.*, 2016, **49**, 2307–2315.

74   D. M. Schultz and T. P. Yoon, *Science (80-.).*, 2014, **343**, 985–993.

75   J. J. Douglas, M. J. Sevrin and C. R. J. Stephenson, *Org. Process Res. Dev.*, 2016, **20**, 1134–1147.

76   J. M. R. Narayanam and C. R. J. Stephenson, *Chem. Soc. Rev.*, 2011, **40**, 102–113.

77   T. P. Nicholls, D. Leonori and A. C. Bissember, *Nat. Prod. Rep.*, 2016, **33**, 1248–1254.

78   J. R. Fulton, V. K. Aggarwal and J. De Vicente, *European J. Org. Chem.*, 2005, 1479–1492.

79   Q. Xiao, Y. A. N. Zhang and J. Wang, *Acc. Chem. Res.*, 2013, **46**, 236–247.

80   Y. Xia and J. Wang, *Chem. Soc. Rev.*, 2017, **46**, 2306–2362.

81   D. M. Allwood, D. C. Blakemore and S. V. Ley, *Org. Lett.*, 2014, **16**, 3064–3067.

82   D. M. Allwood, D. C. Blakemore, A. D. Brown and S. V. Ley, *J. Org. Chem.*, 2014, **79**, 328–338.

83   R. R. Merchant, D. M. Allwood, D. C. Blakemore and S. V. Ley, *J. Org. Chem.*, 2014, **79**, 8800–8811.

84   J. Barluenga and C. Valdés, *Angew. Chemie - Int. Ed.*, 2011, **50**, 7486–7500.

85   J. Barluenga, N. Quiñones, M. Tomás-Gamasa and M. P. Cabal, *European J. Org. Chem.*, 2012, 2312–2317.

86   J. Barluenga, M. Tomás-Gamasa, F. Aznar and C. Valdé, *Angew. Chemie - Int. Ed.*, 2010, **49**, 4993–4996.

87   J. Barluenga, M. Tomás-Gamasa, F. Aznar and C. Valdés, *Nat. Chem.*, 2009, **1**, 494–499.

88   M. Majek and A. Jacobi Von Wangelin, *Acc. Chem. Res.*, 2016, **49**, 2316–2327.

89   L. Buzzetti, G. E. M. Crisenza and P. Melchiorre, *Angew. Chemie - Int. Ed.*, 2019, **58**, 3730–3747.

90   X. Hu, J. Chen, Q. Wei, F. Liu, Q. Deng, A. M. Beauchemin and W. Xiao, 2014, 12163–12167.

91   X.-Q. Hu, X. Qi, J.-R. Chen, Q.-Q. Zhao, Q. Wei, Y. Lan and W.-J. Xiao, *Nat. Commun.*, 2016, **7**, 11188.

92   Q. Zhao, X. Hu, M. Yang and J. Chen, *Chem. Commun.*, 2016, **52**, 12749–12752.

93   S. Parisotto, G. Garreffa, C. Canepa, E. Diana, F. Pellegrino, E. Priola, C. Prandi, V. Maurino and A. Deagostino, *ChemPhotoChem*, 2017, **1**, 56–59.

94   S. Wang, B. Y. Cheng, M. Sršen and B. König, *J. Am. Chem. Soc.*, 2020, **142**, 7524–7531.

95   O. Korb, B. Kuhn, J. Hert, N. Taylor, J. Cole, C. Groom and M. Stahl, *J. Med. Chem.*, 2016, **59**, 4257–4266.

96   T. Sterling and J. J. Irwin, *J. Chem. Inf. Model.*, 2015, **55**, 2324–2337.

97   D. R. Koes and C. J. Camacho, *Nucleic Acids Res.*, 2012, **40**, 409–414.

98   P. F. Wheat, *J. Antimicrob. Chemother.*, 2001, **48**, 1–4.

99   T. Sander, J. Freyss, M. Von Korff and C. Rufener, *J. Chem. Inf. Model.*, 2015, **55**, 460–473.

100   G. Jones, P. Willett, R. C. Glen, A. R. Leach and R. Taylor, *J. Mol. Biol.*, 1997, **267**, 727–748.

101   G. Jones, P. Willett and R. C. Glen, *J. Mol. Biol.*, 1995, **245**, 43–53.

102   M. L. Verdonk, J. C. Cole, M. J. Hartshorn, C. W. Murray and R. D. Taylor, *Proteins Struct. Funct. Genet.*, 2003, **52**, 609–623.

103   O. Korb, T. Stützle and T. E. Exner, *J. Chem. Inf. Model.*, 2009, **49**, 84–96.

104   H. Y. Liao and S. Y. Chu, *New J. Chem.*, 2003, **27**, 421–424.

105   A. El-Awa, M. N. Noshi, X. M. D. Jourdin and P. L. Fuchs, *Chem. Rev.*, 2009, **109**, 6920–6921.

106   D. Kaiser, I. Klose, R. Oost, J. Neuhaus and N. Maulide, *Chem. Rev.*, 2019, **119**, 8701–8780.

107   M. Feng, B. Tang, S. H. Liang and X. Jiang, *Sulfur Containing Scaffolds in Drugs: Synthesis and Application in Medicinal Chemistry*, 2016, vol. 16.

108   B. S. Patil, G. Krishnamurthy, H. B. Naik, P. R. Latthe and M. Ghate, *Eur. J. Med. Chem.*, 2010, **45**, 3329–3334.

109   P. Li, D. Hu, D. Xie, J. Chen, L. Jin and B. Song, *J. Agric. Food Chem.*, 2018, **66**, 3093–3100.

110   Y. I. Zhu and M. J. Stiller, *J. Am. Acad. Dermatol.*, 2001, **45**, 420–434.

111   B. M. Trost, N. R. Schmuff and M. J. Miller, *J. Am. Chem. Soc.*, 1980, **102**, 5979–5981.

112   C. Y. Meyers, R. Chan-Yu-King, D. H. Hua, V. M. Kolb, W. S. Matthews, T. E. Parady, T. Horii, P. B. Sandrock, Y. Hou and S. Xie, *J. Org. Chem.*, 2003, **68**, 500–511.

113   R. Scholz, G. Hellmann, S. Rohs, D. Özdemir, G. Raabe, C. Vermeeren and H. J. Gais, *European J. Org. Chem.*, 2010, 4588–4616.

114   G. Hellmann, A. Hack, E. Thiemermann, O. Luche, G. Raabe and H. J. Gais, *Chem. - A Eur. J.*, 2013, **19**, 3869–3897.

115   S. Nakamura, N. Hirata, R. Yamada, T. Kita, N. Shibata and T. Toru, *Chem. - A Eur. J.*, 2008, **14**, 5519–5527.

116   J. Chen, C. Yi, S. Wang, S. Wu, S. Li, D. Hu and B. Song, *Bioorganic Med. Chem. Lett.*, 2019, **29**, 1203–1210.

117   A. A. Dar, N. Enjamuri, M. Shadab, N. Ali and A. T. Khan, *ACS Comb. Sci.*, 2015, **17**, 671–681.

118   A. R. Usera, P. Dolan, T. W. Kensler and G. H. Posner, *Bioorganic Med. Chem.*, 2009, **17**, 5627–5631.

119   E. Block and D. Putman, *J. Am. Chem. Soc.*, 1990, **112**, 4072–4074.

120   S. Imamura, T. Ichikawa, Y. Nishikawa, N. Kanzaki, K. Takashima, S. Niwa, Y. Iizawa, M. Baba and Y. Sugihara, *J. Med. Chem.*, 2006, **49**, 2784–2793.

121   K. C. Nicolaou, P. Maligres, T. Suzuki, S. V. Wendeborn, W. M. Dai and R. K. Chadha, *J. Am. Chem. Soc.*, 1992, **114**, 8890–8907.

122   J. F. Hartwig, *Acc. Chem. Res.*, 2008, **41**, 1534–1544.

123   H. Woolven, C. González-Rodríguez, I. Marco, A. L. Thompson and M. C. Willis, *Org. Lett.*, 2011, **13**, 4876–4878.

124   E. J. Emmett and M. C. Willis, *Asian J. Org. Chem.*, 2015, **4**, 602–611.

125   A. Shavnya, S. B. Coffey, A. C. Smith and V. Mascitti, *Org. Lett.*, 2013, **15**, 6226–6229.

126 E. J. Emmett, B. R. Hayter and M. C. Willis, *Angew. Chemie - Int. Ed.*, 2013, **52**, 12679–12683.

127 N. Margraf and G. Manolikakes, *J. Org. Chem.*, 2015, **80**, 2582–2600.

128 N. Umierski and G. Manolikakes, *Org. Lett.*, 2013, **15**, 4972–4975.

129 N. Umierski and G. Manolikakes, *Org. Lett.*, 2013, **15**, 188–191.

130 D. Zheng, M. Chen, L. Yao and J. Wu, *Org. Chem. Front.*, 2016, **3**, 985–988.

131 D. Zheng, R. Mao, Z. Li and J. Wu, *Org. Chem. Front.*, 2016, **3**, 359–363.

132 B. N. Rocke, K. B. Bahnck, M. Herr, S. Lavergne, V. Mascitti, C. Perreault, J. Polivkova and A. Shavnya, *Org. Lett.*, 2014, **16**, 154–157.

133 E. Deruer, V. Hamel, S. Blais and S. Canesi, *Beilstein J. Org. Chem.*, 2018, **14**, 1203–1207.

134 G. L. Patrick, in *An Introduction to Medicinal Chemistry*, Oxford University Press, Lavis, 5th edn., 2013, pp. 416–420.

135 L. Bock, K. J. Schaper, J. K. Seydel and G. H. Miller, *J. Med. Chem.*, 1974, **17**, 23–28.

136 H. Gilman and R. E. Fothergill, *J. Am. Chem. Soc.*, 1929, **51**, 3501–3508.

137 S. S. Labadie, *J. Org. Chem.*, 1989, **54**, 2496–2498.

138 S. Li, P. Wu, J. E. Moses and K. B. Sharpless, *Angew. Chemie Int. Ed.*, 2017, 2903–2908.

139 J. J. Krutak, R. D. Burpitt, W. H. Moore and J. A. Hyatt, *J. Org. Chem.*, 1979, **44**, 3847–3858.

140 W. E. Truce and C. W. Vriesen, *J. Am. Chem. Soc.*, 1953, **75**, 5032–5036.

141 W. E. Truce and J. P. Milionis, *J. Am. Chem. Soc.*, 1952, **74**, 974–977.

142 S. Répichet, C. Le Roux, P. Hernandez, J. Dubac and J. R. Desmurs, *J. Org. Chem.*, 1999, **64**, 6479–6482.

143 B. P. Bandgar, S. V. Bettigeri and J. Phopase, *Org. Lett.*, 2004, **6**, 2105–2108.

144 J. Wei, J. Jiang, X. Xiao, D. Lin, Y. Deng, Z. Ke, H. Jiang and W. Zeng, *J. Org. Chem.*, 2016, **81**, 946–955.

145 M. H. Shaw, J. Twilton and D. W. C. MacMillan, *J. Org. Chem.*, 2016, **81**, 6898–6926.

146 D. B. Bagal, G. Kachkovskyi, M. Knorn, T. Rawner, B. M. Bhanage and O. Reiser, *Angew. Chemie - Int. Ed.*, 2015, **54**, 6999–7002.

147 S. K. Pagire, S. Paria and O. Reiser, *Org. Lett.*, 2016, **18**, 2106–2109.

148 T. C. Johnson, B. L. Elbert, A. J. M. Farley, T. W. Gorman, C. Genicot, B. Lallemand, P. Pasau, J. Flasz, J. L. Castro, M. Maccoss, D. J. Dixon, R. S. Paton, C. J. Schofield, M. D. Smith and M. C. Willis, *Chem. Sci.*, 2018, **9**, 629–633.

149 M. Ratushnyy, M. Kamenova and V. Gevorgyan, *Chem. Sci.*, 2018, **9**, 7193–7197.

150 N. W. Liu, Z. Chen, A. Herbert, H. Ren and G. Manolikakes, *European J. Org. Chem.*, 2018, **2018**, 5725–5734.

151 B. Ni, B. Zhang, J. Han, B. Peng, Y. Shan and T. Niu, *Org. Lett.*, 2020, **22**, 670–674.

152 S. Yang, L. Wang, L. Wang and H. Li, *J. Org. Chem.*, 2020, **85**, 564–573.

153 J. J. Wang and W. Yu, *Org. Lett.*, 2019, **21**, 9236–9240.

154 X. Wang, H. Li, G. Qiu and J. Wu, *Chem. Commun.*, 2019, **55**, 2062–2065.

155 A. U. Meyer, S. Jäger, D. Prasad Hari and B. König, *Adv. Synth. Catal.*,

2015, **357**, 2050–2054.

156 J. L. Zhang, P. W. Hong Chan and C. M. Che, *Tetrahedron Lett.*, 2003, **44**, 8733–8737.

157 J. Barluenga, M. Tomás-Gamasa, F. Aznar and C. Valdés, *European J. Org. Chem.*, 2011, 1520–1526.

158 X. W. Feng, J. Wang, J. Zhang, J. Yang, N. Wang and X. Q. Yu, *Org. Lett.*, 2010, **12**, 4408–4411.

159 C. R. Bock, T. J. Meyer and D. G. Whitten, *J. Am. Chem. Soc.*, 1975, **97**, 2909–2911.

160 Y. Du, F. Yao, Y. Tuo and M. Cai, *J. Chem. Res.*, 2017, **41**, 725–729.

161 H. Jiang and A. Studer, *CCS Chem.*, 2019, 38–49.

162 K. U. Ingold and D. A. Pratt, *Chem. Rev.*, 2014, **114**, 9022–9046.

163 W. Ding, L. Q. Lu, J. Liu, D. Liu, H. T. Song and W. J. Xiao, *J. Org. Chem.*, 2016, **81**, 7237–7243.

164 S. Ye, Y. Li, J. Wu and Z. Li, *Chem. Commun.*, 2019, **55**, 2489–2492.

165 X. Zhong, J. Lv and S. Luo, *Org. Lett.*, 2016, **18**, 3150–3153.

166 J. M. Bakke, *Acta Chem. Scand. Ser. B Org. Chem. Biochem.*, 1982, **B36**, 127–129.

167 D. C. Moebius and J. S. Kingsbury, *J. Am. Chem. Soc.*, 2009, **131**, 878–879.

168 M. Basato, C. Tubaro, A. Biffis, M. Bonato, G. Buscemi, F. Lighezzolo, P. Lunardi, C. Yianini, F. Benetollo and A. Del Zotto, *Chem. - A Eur. J.*, 2009, **15**, 1516–1526.

169 X. Creary, *Org. Synth.*, 1986, **64**, 207.

170 C. G. Overberger and J.-P. Anselme, *J. Org. Chem.*, 1963, **28**, 592–593.

171 C. Ramsden and H. Rose, *Synlett*, 1997, **1**, 27–28.

172

173 F. Neese, *Wiley Interdiscip. Rev. Comput. Mol. Sci.*, 2012, **2**, 73–78.

174 D. Choudhary, V. Khatri and A. K. Basak, *Org. Lett.*, 2018, **20**, 1703–1706.

175 L. Chen, J. Liang, Z. yu Chen, J. Chen, M. Yan and X. jing Zhang, *Adv. Synth. Catal.*, 2019, **361**, 956–960.

176 S. Kozuch and S. Shaik, *Acc. Chem. Res.*, 2011, **44**, 101–110.

177 M. Majek and A. Jacobi Von Wangelin, *Acc. Chem. Res.*, 2016, **49**, 2316–2327.

178 D. Ravelli, S. Protti and M. Fagnoni, *Chem. Rev.*, 2016, **116**, 9850–9913.

179 I. L. Jones, D. J. Schofield, R. R. Strevens, P. N. Horton, M. B. Hursthouse and N. C. O. Tomkinson, *Tetrahedron Lett.*, 2007, **48**, 521–525.

180 M. Jukič, J. Ilaš, M. Brvar, D. Kikelj, J. Cesar and M. Anderluh, *Eur. J. Med. Chem.*, 2017, **125**, 500–514.

181 N. Gruber, J. E. Díaz and L. R. Orelli, *Beilstein J. Org. Chem.*, 2018, **14**, 2510–2519.

182 R. J. Watson, P. Bamborough, H. Barnett, C. W. Chung, R. Davis, L. Gordon, P. Grandi, M. Petretich, A. Phillipou, R. K. Prinjha, I. Rioja, P. Soden, T. Werner and E. H. Demont, *J. Med. Chem.*, 2020, **63**, 9045–9069.

183 Z. P. Demko and K. B. Sharpless, *Angew. Chemie - Int. Ed.*, 2002, **41**, 2110–2113.

184 X. Q. Hu, J. Chen, J. R. Chen, D. M. Yan and W. J. Xiao, *Chem. - A Eur. J.*, 2016, **22**, 14141–14146.

185 X. Y. Duan, N. N. Zhou, R. Fang, X. L. Yang, W. Yu and B. Han, *Angew. Chemie - Int. Ed.*, 2014, **53**, 3158–3162.

186 Q. Q. Zhao, J. Chen, D. M. Yan, J. R. Chen and W. J. Xiao, *Org. Lett.*, 2017, **19**, 3620–3623.

187 S. Y. Chow, M. Y. Stevens, L. Åkerbladh, S. Bergman and L. R. Odell, *Chem. - A Eur. J.*, 2016, **22**, 9155–9161.

188 M. Lakemeyer, W. Zhao, F. A. Mandl, P. Hammann and S. A. Sieber, *Angew. Chemie - Int. Ed.*, 2018, **57**, 14440–14475.

189 K. Lewis, *Cell*, 2020, **181**, 29–45.

190 L. Lefrada, R. Köhn, S. Malki, W. Mazouz, A. Bouchemma and M. Hadjem, 2017, **8**, 82–84.

191 C. Sareena and S. Tharamel, *Microb. Pathog.*, 2020, **147**, 104387.

192 S. Shui and X. Road, 2010, **58**, 3–7.

193 A. A. Firsov, S. N. Vostrov, A. A. Shevchenko, S. H. Zinner, G. Cornaglia and Y. A. Portnoy, 1998, **42**, 2848–2852.

194 T. A. Halgren, *J. Comput. Chem.*, 1999, **20**, 720–729.

195 F. Miege, C. Meyer and J. Cossy, *Angew. Chemie - Int. Ed.*, 2011, **50**, 5932–5937.

196 S. Das, S. Roy, A. Bhowmik, W. Sarkar, I. Mondal, A. Mishra, S. J. Saha, S. Karmakar and I. Deb, *Chem. Commun.*, 2022, **58**, 2902–2905.

197 G. Zhang, Q. Fan, H. Wang, Y. Zhao and C. Ding, *Adv. Synth. Catal.*, 2021, **363**, 833–837.

198 L. Deng, A. W. Kleij and W. Yang, *Chem. - A Eur. J.*, 2018, **24**, 19156–19161.

199 J. Jin, C. Li, R. Wang, Z. Xia, Q. Yan, W. Wang, S. X. Gu, H. Wang and F. Chen, *Org. Lett.*, 2023, **25**, 6012–6017.

200 B. Tian, M. He, S. Tang, I. Hewlett, Z. Tan, J. Li, Y. Jin and M. Yang, *Bioorganic Med. Chem. Lett.*, 2009, **19**, 2162–2167.

201 Q. Zhang, M. Tang, S. Zhang and Z. Wei, *Org. Lett.*, 2020, **22**, 5182–5186.

202 B. Mondal, R. Maiti, X. Yang, J. Xu, W. Tian, J. Yan, X. Li and Y. R. Chi, 2021, 8778–8783.

203 Q. Yang, W. Hao, Y. He, Q. Zhang, X. Yu, Y. Hua and O. Access, 2019, 152–156.

204 S. Pandey, V. K. Sharma, A. Biswas, M. Lahiri and S. Basu, *RSC Med. Chem.*, 2021, **12**, 1604–1611.

205 G. L. Backes, D. M. Neumann and B. S. Jursic, *Bioorganic Med. Chem.*, 2014, **22**, 4629–4636.

206 P. K. Shyam and H. Y. Jang, *J. Org. Chem.*, 2017, **82**, 1761–1767.

207 A. S. Deeming, C. J. Russell, A. J. Hennessy and M. C. Willis, *Org. Lett.*, 2014, **16**, 150–153.

208 F. Xiao, Y. Hu, H. Huang, F. Xu and G. J. Deng, *Org. Biomol. Chem.*, 2020, **18**, 3527–3535.

209 Y. Fu, Q. S. Xu, Q. Z. Li, Z. Du, K. H. Wang, D. Huang and Y. Hu, *Org. Biomol. Chem.*, 2017, **15**, 2841–2845.

210 H. Zhu, Y. Shen, Q. Deng, J. Chen and T. Tu, *ACS Catal.*, 2017, **7**, 4655–4659.

211 B. D. Gupta, M. Roy, S. Roy, M. Kumar and I. Das, *J. Chem. Soc. Perkin Trans. 2*, 1990, **7**, 537–543.

212 V. Soulard, G. Villa, D. P. Vollmar and P. Renaud, *J. Am. Chem. Soc.*, 2018, **140**, 155–158.

213   S. Kuhne, A. J. Kooistra, R. Bosma, A. Bortolato, M. Wijtmans, H. F. Vischer, J. S. Mason, C. De Graaf, I. J. P. De Esch and R. Leurs, *J. Med. Chem.*, 2016, **59**, 9047–9061.

214   Y. P. Cai, F. Y. Nie and Q. H. Song, *J. Org. Chem.*, 2021, **86**, 12419–12426.

215   Q. F. Bai, C. Jin, J. Y. He and G. Feng, *Org. Lett.*, 2018, **20**, 2172–2175.

216   S. H. Cao, X. C. Zhang, Y. Wei and M. Shi, *European J. Org. Chem.*, 2011, 2668–2672.

217   A. Divakaran, S. K. Talluri, A. M. Ayoub, N. K. Mishra, H. Cui, J. C. Widen, N. Berndt, J. Y. Zhu, A. S. Carlson, J. J. Topczewski, E. K. Schonbrunn, D. A. Harki and W. C. K. Pomerantz, *J. Med. Chem.*, 2018, **61**, 9316–9334.

218   K. W. Moore, K. Bonner, E. A. Jones, F. Emms, P. D. Leeson, R. Marwood, S. Patel, S. Patel, M. Rowley, S. Thomas and R. W. Carling, *Bioorganic Med. Chem. Lett.*, 1999, **9**, 1285–1290.

219   M. G. Mohamed, R. C. Lin, J. H. Tu, F. H. Lu, J. L. Hong, K. U. Jeong, C. F. Wang and S. W. Kuo, *RSC Adv.*, 2015, **5**, 65635–65645.

220   K. Sugimoto, S. Kosuge, T. Sugita, Y. Miura, K. Tsuge and Y. Matsuya, *Org. Lett.*, 2021, **23**, 3981–3985.

221   F. Neese, F. Wennmohs, U. Becker and C. Riplinger, *J. Chem. Phys.*

222   S. Grimme, J. Antony and S. Ehrlich, *J. Chem. Phys.*, 2010, **132**, 1–19.

223   S. Grimme, S. Ehrlich and L. Goerigk, *J. Comput. Chem.*, 2011, **32**, 1456–1465.

224   F. Weigend and R. Ahlrichs, *Phys. Chem. Chem. Phys*, 2005, **7**, 3297–3305.

225   F. Weigend, *Phys. Chem. Chem. Phys*, 2006, **8**, 1057–1065.

226   S. Grimme, *J. Comput. Chem.*, 2006, **27**, 1787–1799.

227   L. Goerigk and S. Grimme, *Phys. Chem. Chem. Phys*, 2011, **13**, 6670–6688.

228   D. Andrae, U. H, M. Dolg, H. Stoll and H. Preub, *Theor. Chim. Acta.*, 1990, **77**, 123–141.

229   A. Hellweg, C. Hättig, S. Höfener and W. Klopper, *Theor. Chem. Acc.*, 2007, **117**, 587–597.

230   V. Barone and M. Cossi, *J. Phys. Chem. A*, 1998, **102**, 1995–2001.

231   A. Allouche, D. Lyon and F.- Lyon, *J. Comput. Chem.*, 2011, **32**, 174–182.

232   M. D. Hanwell, D. E. Curtis, D. C. Lonie, T. Vandermeersch, E. Zurek and G. R. Hutchison, *J. Cheminform.*, 2012, **4**, 1–17.